Functional Cylindrical Polymer Brushes and Their Hybrids with Inorganic Nanoparticles

DISSERTATION

zur Erlangung des akademischen Grades eines

Doktors der Naturwissenschaften (Dr. rer. nat.)

im Fach Chemie der Fakultät für Biologie, Chemie und Geowissenschaften

der Universität Bayreuth

vorgelegt von

Youyong Xu

Geboren in Jiangsu/China

Bayreuth, 2008

Die vorliegende Arbeit wurde in der Zeit von April 2004 bis Spetember 2008 in Bayreuth am Lehrstuhl Makromolekulare Chemie II unter Betreuung von Herrn Prof. Dr. Axel H. E. Müller angefertigt.

Vollständiger Abdruck der von Fakultät für Biologie, Chemie und Geowissenschaften der Universität Bayreuth genehmigten Dissertation zur Erlangung des akademischen Grades eines Doktors der Naturwissenschaften (Dr. rer. Nat.).

Dissertation eingereicht am: 06.10.2008

Zulassung durch die Promotionskommission: 15.10.2008

Wissenschaftliches Kolloquium: 16.12.2008

Amtierender Dekan: Prof. Dr. Axel H. E. Müller

Prüfungsausschuß:

Prof. Dr. A. H. E. Müller (Erstgutachter)

Prof. Dr. A. Böker (Zweitgutachter)

Prof. Dr. K. Seifert (Vorsitzender)

Prof. Dr. H. G. Alt

To my parents and Jiazhen

TABLE OF CONTENTS

Summary

Various cylindrical polymer brushes were synthesized via a grafting-from strategy. Very long poly(2-hydroxylethyl methacrylate) backbones of the brushes were prepared by anionic polymerization (DP_n=1500), esterified with an ATRP initiator, and subsequently the side-chains were grafted by atom transfer radical polymerizations (ATRP). Cylindrical brushes with different architectures, such as brushes of single component, double-grafted brushes and core-shell brushes, were built according to the need of applications. A number of functional monomers were involved in the preparations of the brushes, providing possibilities for further functionalizations and uses. Nano-hybrids comprising organic cylindrical brushes and inorganic nanoparticles such as magnetite and polyhedral oligomeric silsesquioxane (POSS) were fabricated through non-covalent inclusion and covalent attachment respectively.

Double-grafted poly(lauryl methacrylate) brushes carry side-chains containing dodecyl short grafts. The long alkyl chains provided good solubility in hydro-carbon solvents like *n*-hexane and paraffin oil. DSC measurements revealed that they undergo side-chain crystallizations.

Grafting of N,N-dimethylaminoethyl methacrylate (DMAEMA) to the macro-initiator by ATRP yielded weak polyelectrolyte cylindrical brushes. They showed responsiveness to pH and salinity in solution. Strong cationic polyelectrolyte brushes were obtained by further quaternization of the PDMAEMA brushes. Their responses to counterions of different valencies were investigated. The addition of a sufficient amount of mono-valent salt induced the collapse of these brushes. When di- and tri-valent counterions were added, helical transition morphologies were recorded before the brushes collapsed into sphere-like structures. Special trivalent counterions, which can change valency through photo-aquation reactions, allowed switching the morphologies of the cationic brushes from worms to globules and back to worms.

The morphologies of the cationic brushes could also be tuned by forming ionic complexes with the anionic surfactant sodium dedecyl sulfonate (SDS) and supramolecular inclusion complexes between cyclodextrins (CDs) and SDS. The brushes underwent transitions from worms, over pearl-necklace structures to totally collapsed

spheres when SDS was added. Introducing α- or β-cyclodextrins could bring the collapsed spheres back to worms. Adamantyl ammonium chloride, a more competitive inclusion agent, deprived SDS of CDs, and re-induced the spherical collapse of the brushes.

The morphologies of the cationic brushes could be regulated in a similar way by forming inter-polyelectrolyte complexes (IPECs) with anionic linear poly(sodium styrene sulfonate) (PSS) in highly diluted solutions. Worm-to-sphere switching with helix-like transition states was also observed.

A new strategy for the direct preparation of strong anionic polyelectrolyte cylindrical brushes without protection was introduced by forming supramolecular complexes between the monomer potassium sulfopropyl methacrylate (SPMA) and crown ether 18-crown-6 in DMSO using ATRP for the grafting-from processes. Well-defined worm-like morphologies were proven by atomic force microscopy (AFM) and cryogenic transmission microscopy (cryo-TEM).

Water soluble double-hydrophilic core-shell cylindrical brushes were prepared and showed pH responsiveness. Magnetic hybrid cylinders were formed by introducing magnetite nanoparticles into the core. They could be aligned on a large scale on the substrates by applying magnetic fields.

Finally, single-molecular hybrid cylinders were created by covalently attaching thiol-functionalized polyhedral oligomeric silsequioxane (POSS) to poly(glycidyl methacrylate) brushes. Their pyrolysis in air resulted in porous silica materials.

Zusammenfassung

Verschiedene zylindrische Polymerbürsten wurden mit der “grafting-from” Strategie synthetisiert. Zu diesem Zweck wurde ein sehr langes Poly(2-hydroxylethyl methacrylat) Polymerrückgrat (DP_n = 1500), welches über anionische Polymerisation hergestellt wurde, mit einem ATRP (Atom Transfer Radical Polymerisation) Initiator verestert und anschließend wurden unterschiedliche Monomer mittels ATRP polymerisiert. Verschiedene Polymerbürstenarchitekturen, wie z.B. homogene oder Kern-Schale Bürsten, wurden entsprechend dem Verwendungszweck hergestellt. Mehrere funktionelle Monomere wurden für die Synthese eingesetzt um die Möglichkeit für weiterführende Funktionalisierungen und Anwendungen zu ermöglichen. Nanoskopische Hybridmaterialien wurden aus organischen Bürsten und anorganischen Nanopartikeln, wie Magnetit oder polyhedralen Silsesquioxanen (POSS), über nicht-kovalente und kovalente Anknüpfungen dargestellt.

Doppelt gepfropfte Poly(laurylmethacrylat)bürsten mit Seitenketten, die über zusätzliche kurze Alkylseitenketten verfügen, wurde synthetisiert. Die Alkylseitenketten sorgten für eine exzellente Löslichkeit in unpolaren Lösungsmitteln (*n*-Hexan, Paraffin) und die Kristallisierbarkeit der Seitenketten wurde mittels DSC gezeigt.

Die ATRP vermittelte Pfropfung von N,N-Dimethylaminoethylmethacrylat (DMAEMA) führte zu zylindrischen, schwachen Polyelektrolytbürsten. Diese zeigten pH-Schaltbarkeit in wässriger Lösung. Starke Polyelektrolytbürsten konnten durch eine Quarternisierungsreaktion hergestellt werden. Deren Verhalten in Gegenwart verschieden geladener Gegenionen wurde untersucht. Bei ausreichender Zugabe monovalenten Salzes zeigte sich ein Kollaps der zylindrischen in eine globuläre Struktur. Bei Zugabe von zwei- und dreiwertigen Gegenionen konnten helikale Übergangszustände vor dem Kollaps gefunden werden. Spezielle photoschaltbare Gegenionen, welche Photoaquation zeigen, erlaubten ein Schalten der Struktur von wurmartigen Partikeln zu sphärischen und zurück zu wurmartigen Bürsten.

Die Morphologien der kationischen Polymerbürsten konnten auch über eine ionische Komplexbildung mit anionischen Tensiden (Natriumdodecylsufat, SDS) und über supramolekulare Einschlussverbindungen von Cyclodextrinen und SDS verändert werden.

Die Bürsten zeigten einen Übergang von wurmartigen zu sphärischen Partikeln mit einer perlkettenartigen Übergangsstruktur bei Zugabe von SDS. Anschließendes Zugeben von α- oder β-Cyclodextrinen erlaubte eine Erholung der Struktur von kollabierten Sphären zu wurmartigen Molekülen. Adamantylammoniumchlorid, welches eine stärkere Einschlussverbindung mit SDS bildet, führte zur erneuten Freisetzung von SDS und zu einem wiederholten Kollaps der Struktur.

Die Interpolyelektrolytkomplexbildung (IPEC) mit linearem Poly(Natriumstyrolsulfonat) (PSS) erlaubte eine Regulierung der Polymerbürstenstruktur in ähnlicher Weise. Übergänge von wurmartigen zu sphärischen Strukturen, mit helixartigen Zwischenzuständen, wurden ebenfalls gefunden.

Eine neue Strategie zur direkten Herstellung von starken anionischen Polyelektrolytbürsten mittels ATRP von Kaliumsulfopropylmethacrylat in DMSO, in dem das Kaliumion durch Kronenether komplexiert ist, wurde entwickelt. Wohldefinierte wurmartige Morphologien wurden mittels Rasterkraftmikroskopie und kryogener Transmissionselektronenmikroskopie gezeigt.

Zudem wurden bis-hydrophile Kern-Schale Polymerbürsten hergestellt, die pH-Schaltbarkeit zeigten. Magnetische Hybridzylinder wurden durch Einlagerung von Magnetitnanopartikeln hergestellt. Diese konnten großflächig durch externe Magnetfelder orientiert werden.

In einem letzten Teil wurden anorganisch-organisch Hybridzylinder über die kovalente Anbindung von thiolfunktionalisierten POSS Molekülen an Glycidylmethacrylatbürsten realisiert. Deren Pyrolyse an Luft resultierte in porösem Silica Material.

1. Introduction

With the rapid development of nanotechnology, tremendous research works have been focused on the preparation of various nanostructures[1, 2]. For different purposes of applications, different nanostructures are required[3, 4]. Nanoparticles (NPs)[5], nanowires (NWs)[6], nanotubes (NTs)[7] and other nanostructures have been successfully prepared. Due to their various architectures and functionalities, soft materials like polymers have been playing extremely important roles for the templated synthesis, surface protection, surface functionalizations of nanostructures[8]. Recent progress in living/controlled polymerization techniques has enabled the preparation of polymers with various well-defined topologies. Scheme 1-1 summarizes the general polymer architectures.

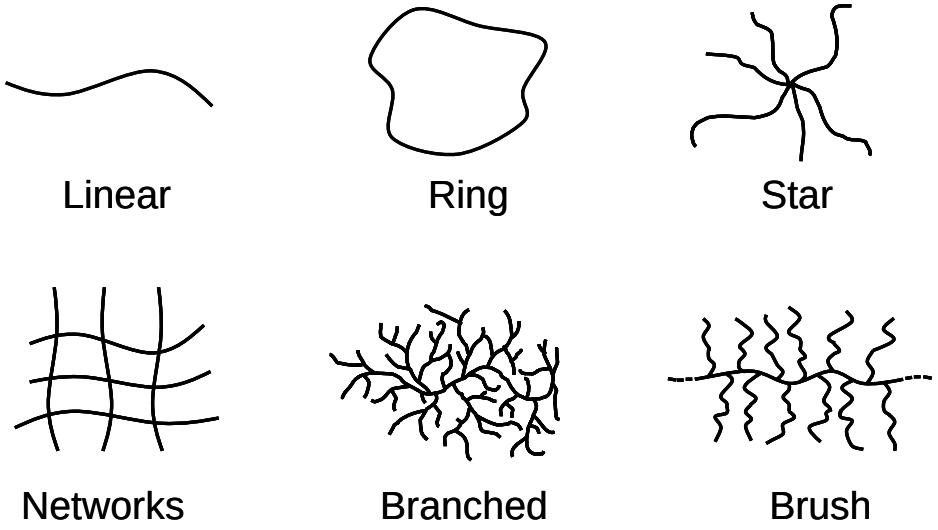

Scheme 1-1. General topologies of polymers.

Polymer brushes

When the grafting density of polymer chains tethered to other polymer chains, spherical, or planar substrates is high enough, polymer brushes are formed[9]. According to the substrates to which the polymers are grafted, polymer brushes can be classified as planar polymer brushes (PPBs)[10], spherical polymer brushes (SPBs)[11] and cylindrical polymer brushes (CPBs)[12, 13]. Scheme 1-2 shows these three different topologies. Due to the high grafting densities and the great steric repulsion, these grafted polymer chains

generally adopt quite stretched conformations, leading to special properties and related applications, either in solutions or on surfaces.

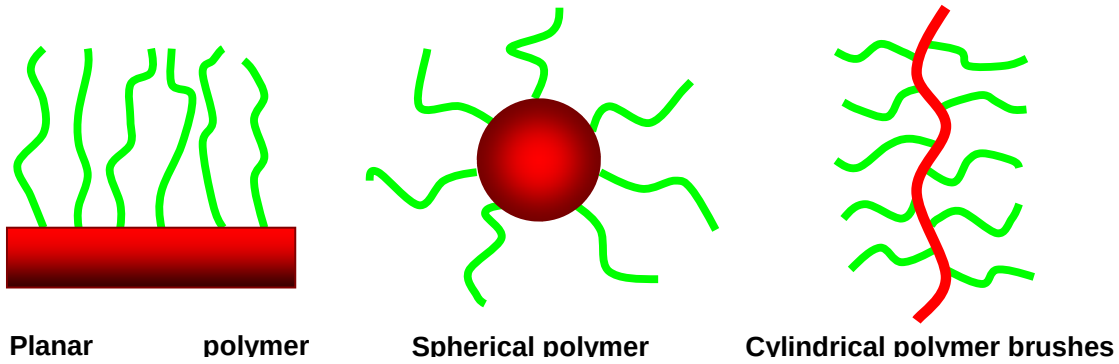

Scheme 1-2. Possible architectures of polymer brushes.

Cylindrical polymer brushes

When a linear polymer is grafted with a large number of relatively short side-chains, cylindrical polymer brushes are formed[9, 12, 13]. Due to their anisotropic nature in topology, they have attracted more and more research interest in their synthesis, bulk, or solution properties, as well as the applications of such polymers. They are also denoted as "bottle brushes" or "molecular brushes".

Three main strategies have been successfully developed for the synthesis of CPBs: grafting through, grafting to, and grafting from. Scheme 1-3 shows the processes for each preparation strategy. In the following, the advantages and disadvantages of each strategy are described in detail.

Grafting through. CPBs can be prepared by the polymerization of the preformed macromonomers[14-16]. This was the first pioneering method in the synthesis of CPBs. For the first time, Tsukahara et al successfully obtained CPBs by the radical polymerization of macromonomers[14]. Short polymeric macromonomers with polymerizable vinyl chain end were first made by anionic polymerization and sequential end-functionalizations. Further radical polymerizations of the pre-made macromonomers yielded CPBs with uniform side chains. This method was then further employed by Schmidt et al[15, 16] and Ishizu et al[17, 18] to prepare CPBs with different functionalities and architectures. The most obvious merit of this method lies in the high grafting density of the side-chains. Unfortunately, inevitable disadvantages are also associated with this method. Generally,

due to the great steric hindrance caused by the macromonomers, it is difficult to get very long CPBs. Conventional radical polymerizations can only afford CPBs with a rather broad distribution of the backbone length. More importantly, it is very difficult to obtain complete conversions of the macromonomers, which results in a more difficult purification process. In order to remove the residual macromonomers from the reaction mixtures, fractionations are generally required. These, in combination, have limited the use of this strategy for the preparation of CPBs with well-defined structures.

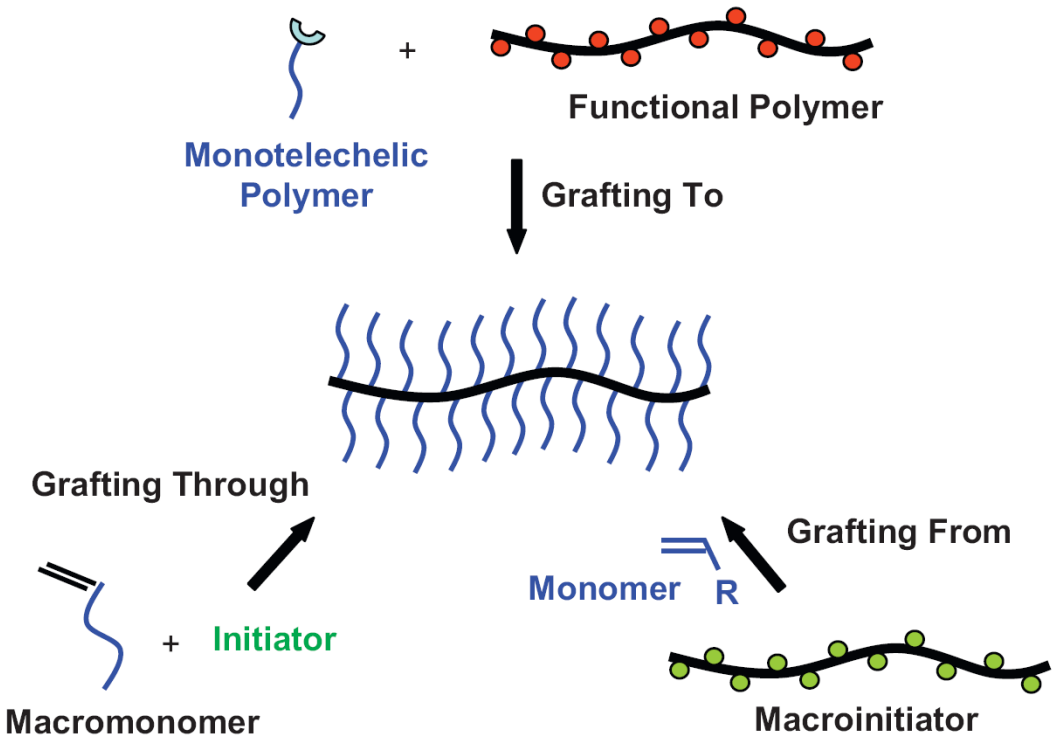

Scheme 1-3. Three different strategies for the preparation of CPBs[13].

Grafting to. CPBs can also be built by coupling reactions between the pre-formed monotelechelic polymers and preformed multi-functionalized long backbones[19-21], as shown in Scheme 1-3. The advantage of this technique is that both backbone and side-chain can be well-defined since they are prepared separately. For example, Matyjaszewski et al prepared both backbones and grafts by using atom transfer radical polymerizations (ATRP) and recently well-developed click chemistry for the coupling reactions[21]. Scheme 1-4 displays the process for the preparation.

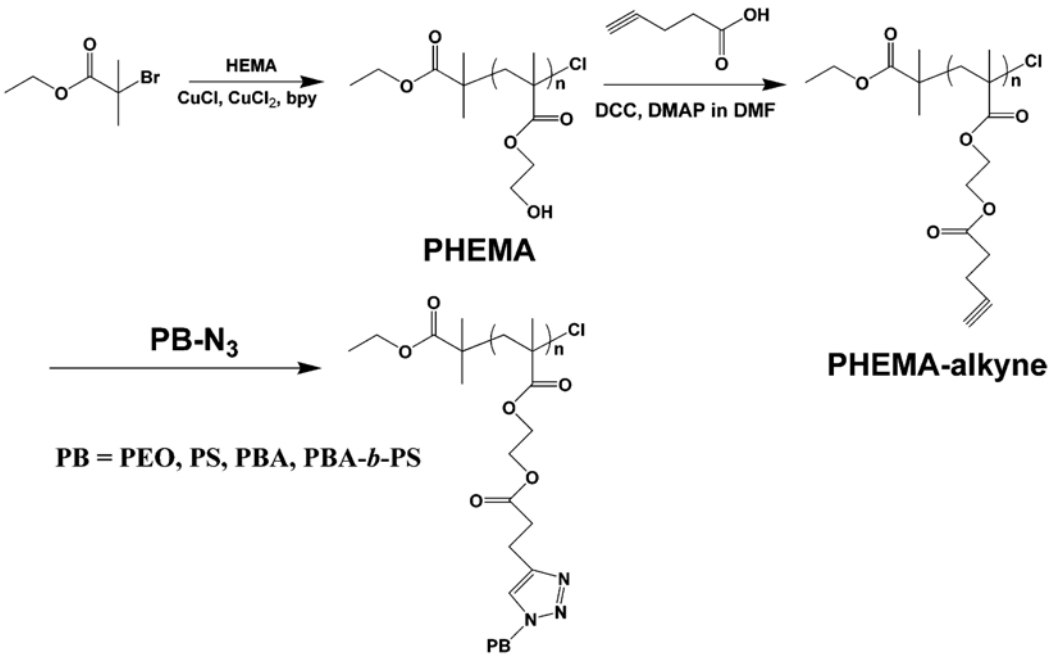

Scheme 1-4. Preparation of CPBs by combination of ATRP and click chemistry[21].

However, low grafting densities are always associated with the grafting to method because of the high steric hindrance, which lead to the relative short brushes caused by the insufficient crowding of the side-chains. Unavoidably, incomplete coupling reactions between the side-chains and backbones cause more problems for the purification procedures, compared to the grafting through method.

Grafting from. Created one decade ago by Matyjaszewski et al[22], the grafting from method has been successful in the syntheses of different CPBs with both well-defined backbones and side-chains[22-24]. In this method, a narrowly distributed long backbone is first prepared via living polymerization techniques, followed by functionalization to attach initiating groups to the backbone for the further grafting polymerizations.

The backbone polymers determine the length and distribution of the CPBs. In order to obtain very long functional backbones, different living polymerizations, such as anionic polymerizations[25], ATRP[22] and reversible addition-fragmentation chain transfer radical polymerizations (RAFT)[26] have been employed. For example, in our group[25], anionic polymerizations of protected 2-hydroxylethyl methacrylate and further esterification

reactions produced extremely long macroinitiators with DP_n up to 3200, as shown in scheme 1-5.

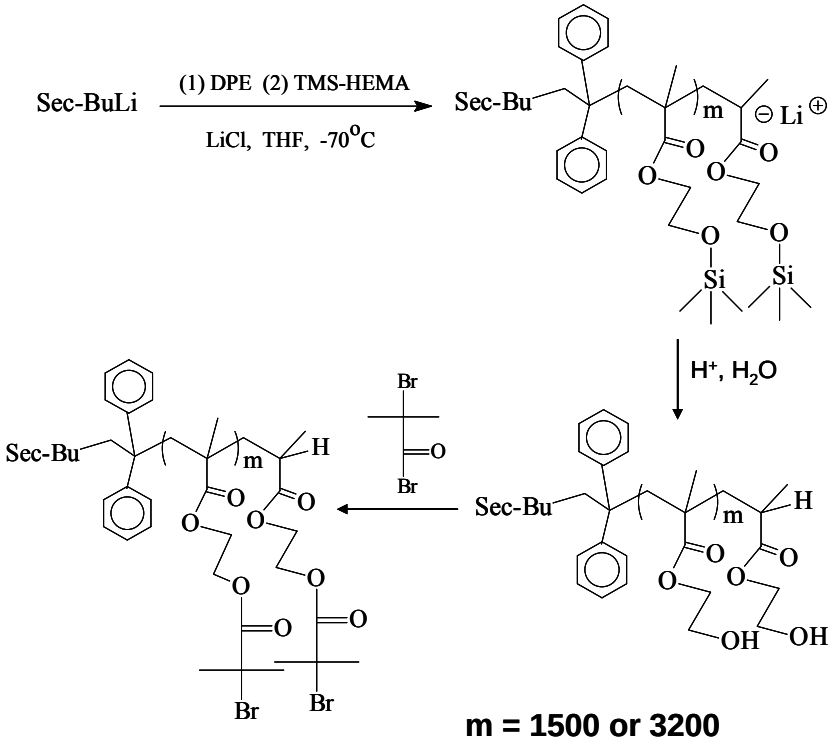

Scheme 1-5. Preparation of macroinitiators by anionic polymerizations and further functionalizations[25].

For the grafting of side-chains, different controlled polymerization techniques were also applied. In addition to the rare cases of ring-opening polymerizations (ROP)[27] and nitroxide mediated radical polymerizations (NMRP)[28], ATRP has been the dominating technique for the preparation of most of the side-chains[22-25].

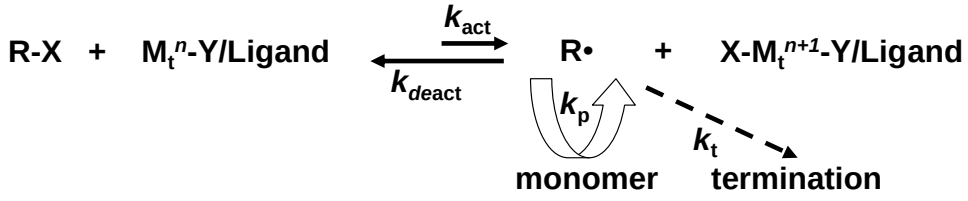

Scheme 1-6. Mechanism of the ATRP technique[29].

As illustrated in scheme 1-6, activation and deactivation processes are involved in the ATRP process and very low concentrations of radicals are generated to give rise to the

controlled growth of the polymer chains[29]. Many aspects, such as monomer, initiator structure, catalyst, ligand, solvent, and temperature, have great impacts on this polymerization technique. When it comes to macroinitiators, the situation is more complicated. Due to the very high local concentration of radicals around the linear macroinitiators, the rate of polymerization is normally higher than that for the ATRP initiated by small initiators. The concentration of the catalyst/ligand complex should be kept low to avoid inter- or intra-molecular coupling reactions[22]. Although few CPBs made by ATRP showed high initiating efficiency[24], low initiating efficiencies were commonly reported[30-33], due to the steric hindrance and slower initiating process compared to the rate of propagation. To improve the initiating efficiency, a lot of measures can be taken. For example, Matyjaszewski et al reported on the improvement of the initiating efficiency by a lower monomer concentration, a higher concentration of the catalyst with adding Cu (II), and halogen exchange[31].

So far, the grafting from strategy has proven to be the most successful one for the preparation of CPBs. Well-defined backbones and side-chains with relatively high grafting density can be prepared.

Cylindrical polymer brushes of different topologies

Based on the strategies described above, CPBs with various topologies have been prepared. Scheme 1-7 shows the possible CPBs of different topologies, as was summarized by Sheiko et al[13].

Some rare examples of CPBs with stiff backbones were also reported[34, 35]. In most cases, the CPBs were prepared from flexible backbones. For the homo-polymer CPBs, brushes with gradient grafting were reported by Matyjaszewski et al[36, 37]. Interesting block copolymer brushes, such as core-shell brushes[23, 24], AB type block copolymer brushes[38, 39] and hetero-grafted (or mixed) brushes[40-44], have attracted people for their possible self-assembly behaviors in solutions or in the bulk. Grafting from the star-like macroinitiators resulted in the star-shaped brushes[45]. Double-grafted (graft-on-graft) CPBs have been successfully synthesized by growing oligomeric macromonomers from the macroinitiators[32, 46]. Matyjaszewski et al reported that the crosslinked CPBs showed

interesting super-soft elastomer properties[47]. Very lately, Deffieux et al even prepared more complicated ring-shaped brushes by grafting to methods[48]. By using suitable backbones, the rings could be opened afterwards to give rise to the common CPBs. In general, these CPBs with different topologies can be regarded as special soft building blocks, nano-templates and novel molecular materials.

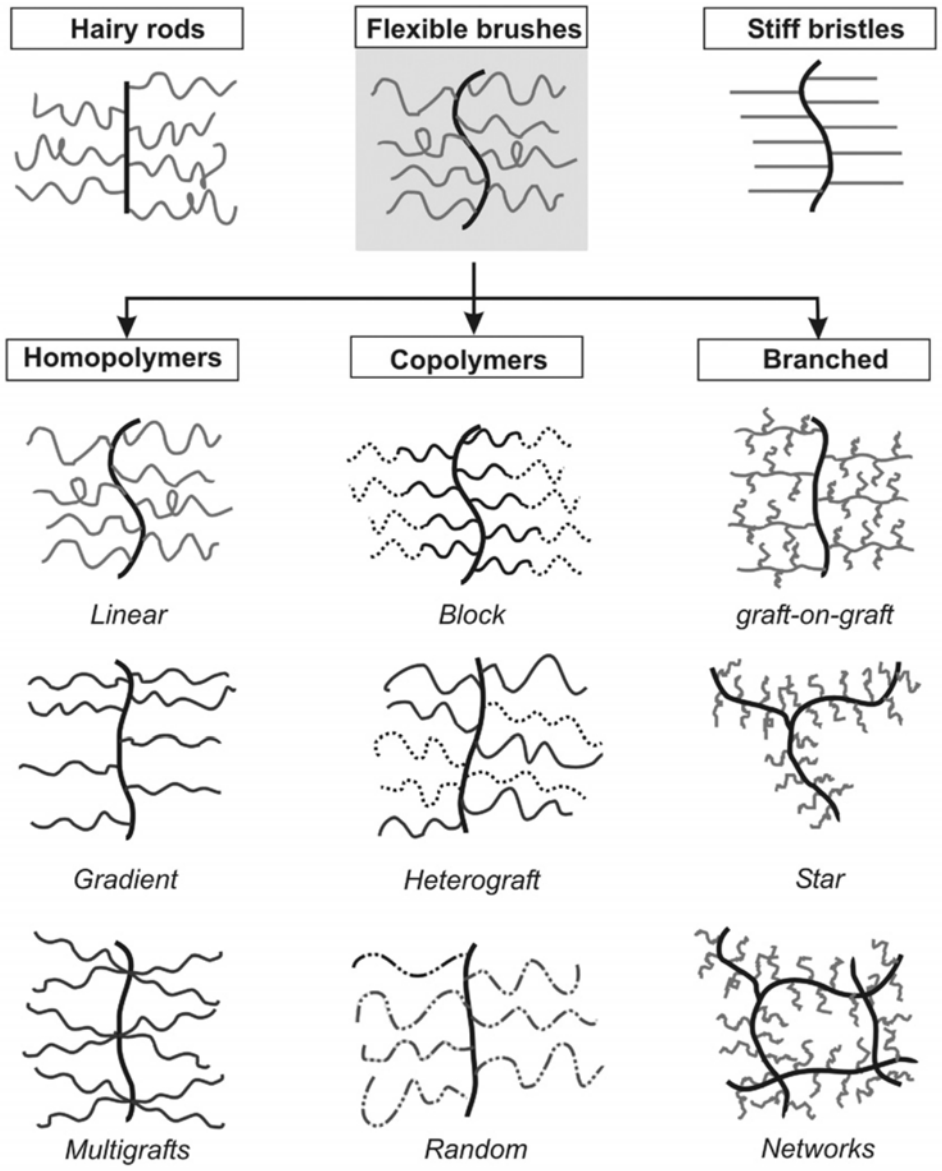

Scheme 1-7. Cylindrical polymer brushes of different topologies[13].

Cylindrical polymer brushes of different functionalities

Thanks to the progress in the living/controlled polymerization techniques, CPBs with diverse functionalities have been prepared.

Müller et al successfully obtained well-defined sugar-containing CPBs by grafting sugar-carrying polymers from long macroinitiators[49]. Cylindrical polypeptide brushes were also reported by grafting through and grafting from methods by Schmidt et al[50]. These bio-compatible nano-cylinders may find their applications in the related fields.

Weak or strong polyelectrolyte CPBs with special solution properties have been prepared by different methods[51-54]. Researches on their solution behavior and ionic complexes with surfactants, oppositely charged polyelectrolytes and nanoparticles are hot topics at present.

Furthermore, a lot of attention has been paid to CPBs with response to external stimuli like pH, temperature, or light, since they might serve as single-molecular nano-actuators or nano-devices. For the first time, Schmidt et al prepared thermal sensitive CPBs with poly(N-isopropylacrylamide) (PNIPAAm) side-chains by grafting from using ATRP[55]. Interesting single-molecular morphology transitions from worm-like structures into spheres were observed when the temperature is higher than the lower critical soluble temperature (LCST). In a similar manner, CPBs with conducting poly(thiophene) backbones and PNIPAAm side-chains were also reported by McCarley et al[56]. Matyjaszewski et al. also successfully prepared photo-tunable temperature responsive core-shell type cylindrical brushes by the grafting from method via ATRP[57].

Properties of cylindrical polymer brushes

So far, there have been intensive studies on the properties of CPBs concerning their properties in the bulk, in solution and on surfaces.

A lot of investigations were carried out to understand the solution properties of the side-chains and the backbones. It is found that the persistence length of CPBs increases monotonously with increasing side chain length, and the contour length per monomer unit in the backbone approaches the limiting value, 0.25 nm, with long side-chains[58-60]. Thus the backbones adopt quite rigid and stretched conformations, while the side-chains

have limited flexibilities due to their tethering to the backbone and the repulsion occurring from the neighbouring side-chains. It was also found that the persistent lengths of the CPBs dramatically decrease in bad solvents[61].

Besides the investigations on the solution properties, interesting bulk properties were also found for the CPBs. If the grafting of the CPBs is dense enough, and the aspect ratio of the length to diameter exceeds a value of 10, so called lyotropic phases appear, resulting from the strong molecular anisotropy of the polymer brushes[62, 63].

More recently, people became interested in the single-molecular morphologies of the CPBs either in solution or on substrates. When the backbone of the CPBs is flexible, it provides another degree of freedom for the worm-like polymers. Responding to different internal or external forces and stimuli, flexible CPBs can undergo morphology transitions from worm-like structures to sphere-like objects. Even helical intermediate transition states have been observed. Scheme 1-8 shows the typical conformation transition processes.

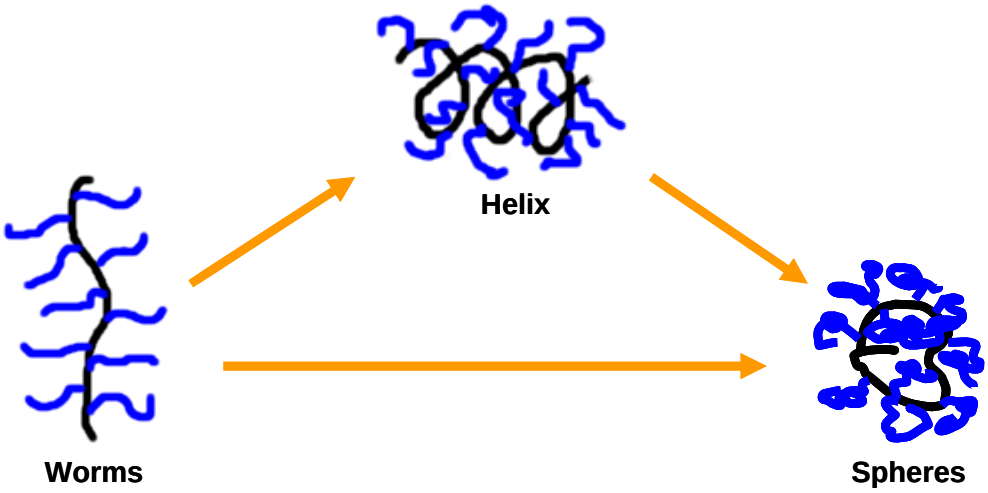

Scheme 1-7. Possible morphological transitions of CPBs.

As pointed out above, CPBs with thermo-sensitive side-chains and flexible backbones showed worm-to-sphere transitions above the critical temperatures[55]. Lately, Schmidt et al showed interesting worm-to-helix and worm-to-sphere transitions of cationic polypeptide brushes by their interaction with the anionic surfactant SDS[64].

Similar worm-to-sphere transitions were also found for the CPBs deposited on the substrates by responding to pressure[65] and the vapor of poor solvents[66-68].

Sheiko et al even found that extremely long CPBs break into smaller pieces simply due to the adsorption on a substrate, which provided some cautions for the use of the brushes on the substrates, and also some opportunities to use this feature deliberately[69].

The single-molecular morphology transitions observed for CPBs give rise to their potential applications in nano-scale devices, such as nano-actuators and nano-sensors.

Nanocomposites of cylindrical polymer brushes

Through the combination of the outstanding mechanical, optical, electric and magnetic properties of inorganic materials with the excellent processability, functionality and biocompatibility of soft organic materials, nano-composites have demonstrated their advanced performances. These often exceed the simple addition of their every single component's characteristics, due to the special surface and quantum effects on the nano-scale[70, 71]. Polymer based nano-composites have been widely investigated and a large category of inorganic materials, such as carbon materials, ceramics, clays, metals, metal oxides and silica, have been incorporated into different polymeric materials[72].

Two general strategies for the preparation of polymer-based nano-composites have been applied. The easiest way is the non-covalent dispersing of the nanometer-sized inorganic materials into the polymer by mechanical blending, melting or solution treatments. The other method is to prepare the nano-composites via covalent linking, either by direct polymerization of functional monomers bearing inorganic groups, or by post-polymerization reactions. The strong covalent linking of the inorganic part to the organic polymer chains is supposed to result in better performances of these materials.

Recent progress has been made for the preparation of nano-composite materials on the molecular level. Suitable nano-structured polymer matrices are greatly demanded for the building the molecular nano-composites. Spherically-shaped polymers like star polymers, dendrimer and hyperbranched polymers can meet the requirements to some extent. Demands on anisotropic polymer molecules are increasing, owing to their interesting properties and potential applications. One-dimensional nano-structured CPBs may play

the roles, owing to their various topologies, functionalities and special properties described previously.

Based on the non-covalent and covalent strategies for the building of nano-composites, single-molecular hybrid materials have been prepared by incorporating inorganic nanoparticles into CPBs.

In most cases, non-covalent hybrid materials from CPBs and inorganic nanoparticles were generated *in situ* in the cavities of core-shell CPBs. Schmidt et al prepared gold nanoparticles and nanowires in the core of CPBs with a poly(vinyl pyridine) core and a poly(styrene) shell[73]. In Müller's group, semi-conducting[74] and supraparamagnetic[75] nanoparticles were also made within amphiphilic core-shell brushes. Scheme 1-8 shows the structures of these hybrids.

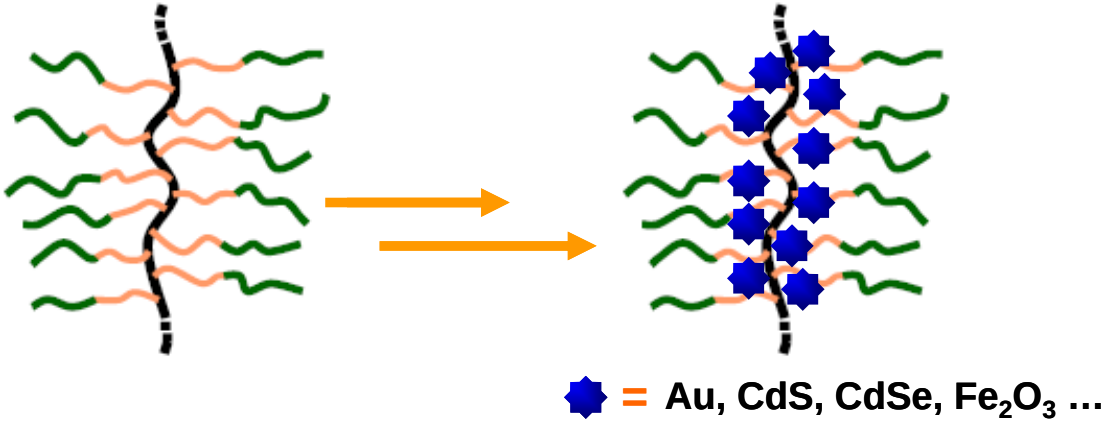

Scheme 1-8. Hybrids with inorganic nanoparticles in the shell of core-shell CPBs.

Hybrids with inorganic nanoparticles covalently linked to the CPBs can be formed by grafting functional monomers with inorganic precursors onto previously formed CPBs. Matyjaszewski et al reported on the synthesis of multi-block copolymer brushes with poly(acrylonitrile) as the core by ATRP[76]. Pyrolysis of the brushes resulted in novel carbon nanomaterials. Very recently, Müller et al have reported the preparation of CPBs with silsesquioxanes as the cores and poly(oligoethyleneglycol methacrylate) (POEGMA) as the water soluble shells, by consecutive ATRP grafting of a siloxane containing monomer and OEGMA, and subsequent sol-gel process[77]. These rigid core-crosslinked nano-cylinders showed typical lyotropic behavior, and could be turned into silica nanowires by pyrolysis on a suitable substrate.

These one-dimensional hybrid materials are ideal candidates as precursors for nanowires, nano-sensors, and catalyst carriers. Wide applications are forthcoming with the creating of more sophisticated hybrid systems with different functional CPBs and nanoparticles.

Objectives of this thesis

The main objective of this thesis is to explore new possibilities of CPBs with different architectures and functionalites. Furthermore, the response of suitable CPBs towards external stimuli in terms of solubility or conformation shall be exploited. Finally, their hybrids with inorganic nanoparticles will be also investigated.

For a specific application in the field of magnetorheology of a ferrofluid-polymer hybrid system[78], CPBs with a good solubility in the very hydrophobic and viscous solvent paraffin oil are needed. CPBs with side-chains carrying long alkyl groups were prepared to meet those requirements.

Due to the wide interests in polyelectrolyte CPBs, novel monomers are used for the preparation of CPBs with different natures. Conventional synthetic methods for polyelectrolyte CPBs require tedious protection and de-protection processes. Within this thesis, a novel method is applied, providing a one-pot procedure, which involves supramolecular complexes.

CPBs grafted from a flexible backbone have one more degree of freedom. Different morphologies could result from the conformational changes of the backbones, caused by the interactions between the side-chains and external stimuli. To broaden the possibilities and understandings of the single-molecular conformation transitions, CPBs which show responses to different stimuli, such as pH, counterions of different valencies, surfactant and oppositely charged linear polyelectrolytes, are widely investigated in this thesis. The responsiveness of the CPB-magnetic nanoparticles hybrid system in magnetic fields was also studied. The corresponding morphology transitions/switches and alignments made them good candidate for sensors or devices on the nano-scale[79].

References

1. Goddard, W. A., III; Brenner, D. W.; Lyshevski, S. E.; Iafrate, G. J.; Eds., *Handbook of Nanoscience, Engineering, and Technology*. CRC Press: Boca Raton, 2003.

2. Whitesides, G. M. *Small* **2005,** 1, 172-179.

3. Klabunde, K. J.; Eds., *Nanoscale Materials in Chemistry*. John Wiley & Sons: New York, 2001.

4. Gleiter, H. *Adv. Mater.* **1992,** 4, 474-481.

5. Schmid, G.; Eds., *Nanoparticles: From Theory to Application*. Wiley-VCH: Weinheim, 2004.

6. Schwarz, J. A.; Contescu, C. I.; Putyera, K., *Dekker Encyclopedia of Nanoscience and Nanotechnology-5 Volume Set*. Marcel Dekker: New York, 2004.

7. Xia, Y.; Yang, P.; Sun, Y.; Wu, Y.; Mayers, B.; Gates, B.; Yin, Y.; Kim, F.; Yan, H. *Adv. Mater.* **2003,** 15, 353-389.

8. Hamley, I. W. *Angew. Chem. Int. Ed.* **2003,** 42, 1692-712.

9. Advincula, R. C.; Brittain, W. J.; Caster, K. C.; Rühe, J., *Polymer Brushes*. Wiley VCH: Weinheim, 2004.

10. Zhao, B.; Brittain, W. J. *Prog. Polym. Sci.* **2000,** 25, 677-710.

11. Pyun, J.; Kowalewski, T.; Matyjaszewski, K. *Macromol. Rapid Comm.* **2003,** 24, 1043-1059.

12. Zhang, M.; Müller, A. H. E. *J. Polym. Sci. Polym. Chem.* **2005,** 43, 3461-3481.

13. Sheiko, S. S.; Sumerlin, B. S.; Matyjaszewski, K. *Prog. Polym. Sci.* **2008,** 33, 759-785.

14. Tsukahara, Y.; Mizuno, K.; Segawa, A.; Yamashita, Y. *Macromolecules* **1989,** 22, 1546-1552.

15. Wintermantel, M.; Gerle, M.; Fischer, K.; Schmidt, M.; Wataoka, I.; Urakawa, H.; Kajiwara, K.; Tsukahara, Y. *Macromolecules* **1996,** 29, 978-983.

16. Dziezok, P.; Sheiko, S. S.; Fischer, K.; Schmidt, M.; Möller, M. *Angew. Chem. Int. Ed.* **1997,** 36, 2812-2815.

17. Tsubaki, K.; Ishizu, K. *Polymer* **2001,** 42, 8387-8393.

18. Ishizu, K. *Polymer Journal* **2004,** 36, 775-792.

19. Deffieux, A.; Schappacher, M. *Macromolecules* **1999,** 32, 1797-1802.

20. Ryu, S. W.; Hirao, A. *Macromolecules* **2000,** 33, 4765-4771.

21. Gao, H.; Matyjaszewski, K. *J. Am. Chem. Soc.* **2007,** 129, 6633-6639.

22. Beers, K. L.; Gaynor, S. G.; Matyjaszewski, K.; Sheiko, S. S.; Möller, M. *Macromolecules* **1998,** 31, 9413-9415.

23. Börner, H. G.; Beers, K.; Matyjaszewski, K.; Sheiko, S. S.; Möller, M. *Macromolecules* **2001,** 34, 4375-4383.

24. Cheng, G.; Böker, A.; Zhang, M.; Krausch, G.; Müller, A. H. E. *Macromolecules* **2001,** 34, 6883-6888.

25. Zhang, M.; Breiner, T.; Mori, H.; Müller, A. H. E. *Polymer* **2003,** 44, 1449-1458.

26. Qin, S.; Börner, H. G.; Matyjaszewski, K.; Sheiko, S. S. *Polym. prepr.* **2002,** 43, (2), 237-238.

27. Lee, H.; Jakubowski, W.; Matyjaszewski, K.; Yu, S.; Sheiko, S. S. *Macromolecules* **2006,** 39, 4983-4989.

28. Cheng, C.; Qi, K.; Khoshdel, E.; Wooley, K. L. *J. Am. Chem. Soc.* **2006,** 128, 6808-6809.

29. Matyjaszewski, K.; Xia, J. *Chem. Rev.* **2001,** 101, 2921-2990.

30. Neugebauer, D.; Sumerlin, B. S.; Matyjaszewski, K.; Goodhart, B.; Sheiko, S. S. *Polymer* **2004,** 45, 8173-8179.

31. Sumerlin, B. S.; Neugebauer, D.; Matyjaszewski, K. *Macromolecules* **2005,** 38, 702-708.

32. Xu, Y.; Becker, H.; Yuan, J.; Burkhardt, M.; Zhang, Y.; Walther, A.; Bolisetty, S.; Ballauff, M.; Müller, A. H. E. *Macromol. Chem. Phys.* **2007,** 208, 1666-1675.

33. Xu, Y.; Bolisetty, S.; Drechsler, M.; Fang, B.; Yuan, J.; Ballauff, M.; Müller, A. H. E. *Polymer* **2008,** 49, 3957-3964.

34. Zhang, W.; Shiotsuki, M.; Masuda, T.; Kumaki, J.; Yashima, E. *Macromolecules* **2007,** 40, 178-185.

35. Zhang, W.; Shiotsuki, M.; Masuda, T. *Polymer* **2007,** 48, 2548-2553.

36. Lee, H.-I.; Matyjaszewski, K.; Yu, S.; Sheiko, S. S. *Macromolecules* **2005,** 38, 8264-8271.

37. Börner, H. G.; Duran, D.; Matyjaszewski, K.; da Silva, M.; Sheiko, S. S. *Macromolecules* **2002,** 35, 3387-3394.

38. Ishizu, K.; Satoh, J.; Toyoda, K.; Sogabe, A. *J. Mater. Sc.* **2004,** 39, 4295-4300.

39. Lee, H.-i.; Matyjaszewski, K.; Yu-Su, S.; Sheiko, S. S. *Macromolecules* **2008,** 41, 6073-6080.

40. Stephan, T.; Muth, S.; Schmidt, M. *Macromolecules* **2002,** 35, 9857-9860.

41. Neugebauer, D.; Zhang, Y.; Pakula, T.; Matyjaszewski, K. *Polymer* **2003,** 44, 6863-6871.

42. Neugebauer, D.; Zhang, Y.; Pakula, T.; Matyjaszewski, K. *Macromolecules* **2005,** 38, 8687-8693.

43. Neugebauer, D.; Theis, M.; Pakula, T.; Wegner, G.; Matyjaszewski, K. *Macromolecules* **2006,** 39, 584-593.

44. Hans, M.; Keul, H.; Heise, A.; Möller, M. *Macromolecules* **2007,** 40, 8872-8880.

45. Matyjaszewski, K.; Qin, S.; Boyce, J. R.; Shirvanyants, D.; Sheiko, S. S. *Macromolecules* **2003,** 36, 1843-1849.

46. Neugebauer, D.; Zhang, Y.; Pakula, T.; Sheiko, S. S.; Matyjaszewski, K. *Macromolecules* **2003,** 36, 6746-6755.

47. Pakula, T.; Zhang, Y.; Matyjaszewski, K.; Lee, H.-i.; Boerner, H.; Qin, S.; Berry, G. C. *Polymer* **2006,** 47, 7198-7206.

48. Schappacher, M.; Deffieux, A. *Science* **2008,** 319, 1512-1515.

49. Muthukrishnan, S.; Zhang, M.; Burkhardt, M.; Drechsler, M.; Mori, H.; Müller, A. H. E. *Macromolecules* **2005,** 38, 7926-7934.

50. Zhang, B.; Fischer, K.; Schmidt, M. *Macromol. Chem. Phys.* **2005,** 206, 157-162.

51. Rühe, J.; Ballauff, M.; Biesalski, M.; Dziezok, P.; Gröhn, F.; Johannsmann, D.; Houbenov, N.; Hugenberg, N.; Konradi, R.; Minko, S.; Motornov, M.; Netz, R. R.; Schmidt, M.; Seidel, C.; Stamm, M.; Stephan, T.; Usov, D.; Zhang, H. *Adv. Polym. Sci.* **2004,** 165, 79-150.

52. Hua, F.; Kita, R.; Wegner, G.; Meyer, W. *ChemPhysChem* **2005,** 6, 336-343.

53. Lienkamp, K.; Ruthard, C.; Lieser, G.; Berger, R.; Groehn, F.; Wegner, G. *Macromol. Chem. Phys.* **2006,** 207, 2050-2065.

54. Lienkamp, K.; Noe, L.; Breniaux, M.-H.; Lieberwirth, I.; Gröhn, F.; Wegner, G. *Macromolecules* **2007,** 40, 2486-2502.

55. Li, C.; Gunari, N.; Fischer, K.; Janshoff, A.; Schmidt, M. *Angew. Chem. Int. Ed.* **2004,** 43, 1101-1104.

56. Balamurugan, S. S.; Bantchev, G. B.; Yang, Y.; McCarley, R. L. *Angew. Chem. Int. Ed.* **2005,** 44, 4872-4876.

57. Lee, H.-i.; Pietrasik, J.; Matyjaszewski, K. *Macromolecules* **2006,** 39, 3914-3920.

58. Terao, K.; Takeo, Y.; Tazaki, M.; Nakamura, Y.; Norisuye, T. *Polym. J.* **1999,** 31, 193-198.

59. Terao, K.; Nakamura, Y.; Norisuye, T. *Macromolecules* **1999,** 32, 711-716.

60. Terao, K.; Hokajo, T.; Nakamura, Y.; Norisuye, T. *Macromolecules* **1999,** 32, 3690-3694.

61. Fischer, K.; Schmidt, M. *Macromol. Rapid Comm.* **2001,** 22, 787-791.

62. Wintermantel, M.; Fischer, K.; Gerle, M.; Ries, R.; Schmidt, M.; Kajiwara, K.; Urakawa, H.; Wataoka, I. *Angew. Chem. Int. Ed.* **1995,** 34, 1472-1474.

63. Saariaho, M.; Ikkala, O.; Szleifer, I.; Erukhimovich, I.; ten Brinke, G. *J. Chem. Phys* **1997,** 107, 3267-3276.

64. Gunari, N.; Cong, Y.; Zhang, B.; Fischer, K.; Janshoff, A.; Schmidt, M. *Macromol. Rapid Comm.* **2008,** 29, 821-825.

65. Xu, H.; Sun, F. C.; Shirvanyants, D. G.; Rubinstein, M.; Shabratov, D.; Beers, K. L.; Matyjaszewski, K.; Sheiko, S. S. *Adv. Mater.* **2007,** 19, 2930-2934.

66. Sun, F.; Sheiko, S. S.; Moeller, M.; Beers, K.; Matyjaszewski, K. *J. Phys. Chem. A* **2004,** 108, 9682-9686.

67. Sheiko, S. S.; Borisov, O. V.; Prokhorova, S. A.; Moeller, M. *Eur. Phys. J. E* **2004,** 13, 125-131.

68. Gallyamov, M. O.; Tartsch, B.; Mela, P.; Potemkin, I. I.; Sheiko, S. S.; Borner, H.; Matyjaszewski, K.; Khokhlov, A. R.; Moller, M. *J. Polym. Sci. Polym. Phys.* **2007,** 45, 2368-2379.

69. Sheiko, S. S.; Sun, F. C.; Randall, A.; Shirvanyants, D.; Rubinstein, M.; Lee, H.-i.; Matyjaszewski, K. *Nature* **2006,** 440, 191-194.

70. Gross, M., *Springer Handbook of Nanotechnology*. Springer-Verlag: Berlin, 2005.

71. Schaefer, D. W.; Justice, R. S. *Macromolecules* **2007,** 40, 8501-8517.

72. Paul, D. R.; Robeson, L. M. *Polymer* **2008,** 49, 3187-3204.

73. Djalali, R.; Li, S. Y.; Schmidt, M. *Macromolecules* **2002,** 35, 4282-4288.

74. Zhang, M.; Drechsler, M.; Müller, A. H. E. *Chem. Mater.* **2004,** 16, 537-543.

75. Zhang, M.; Estournes, C.; Bietsch, W.; Müller, A. H. E. *Adv. Funct. Mater.* **2004,** 14, 871-882.

76. Tang, C.; Dufour, B.; Kowalewski, T.; Matyjaszewski, K. *Macromolecules* **2007,** 40, 6199-6205.

77. Yuan, J.; Xu, Y.; Walther, A.; Bolisetty, S.; Schumacher, M.; Schmalz, H.; Ballauff, M.; Müller, A. H. E. *Nat. Mater.* **2008,** 7, 718-722.

78. Saldivar-Guerrero, R.; Richter, R.; Rehberg, I.; Aksel, N.; Heymann, L.; Rodriguez-Fernández, O. *Magnetohydrodynamics* **2005,** 41, 385-390.

79. Dai, L., *Intelligent Macromolecules for Smart Devices: From Materials Synthesis to Device Applications*. Springer-Verlag: London, 2003.

2. Overview of this Thesis

The research presented in this thesis is dealing with cylindrical polymer brushes (CPBs) with various topologies, functionalities and their hybrids with inorganic nanoparticles. In general, these chapters can be divided into three categories: in chapter 3 brushes with a novel topology are presented; chapter 4 to 8 focus on the synthesis, characterization, and morphological transitions of cationic and anionic CPBs; finally, chapter 9 and 10 highlight the hybrid materials created from inorganic nanoparticles and these CPBs. This thesis provides new insights into the responsiveness of CPBs and their hybrids with inorganic nanoparticles, which may lead to their applications as devices or sensors on nano-scale.

In the following, a brief summary of the main results is presented.

Double-grafted cylindrical polymer brushes

To improve the solubility of CPBs in very hydrophobic solvents such as paraffin oil, poly(lauryl methacrylate) (PLMA) brushes with dodecyl side chains were prepared by grafting LMA monomers from linear macro-initiators poly(2-(2-bromoisobutyryloxy)-ethyl methacrylate) (PBIEM) by atom transfer radical polymerizations (ATRP) at 70 ^{o}C. Considering the bulky nature of the LMA monomer, a low initiating efficiency was expected. In order to increase the initiating efficiency, a halide exchange reaction with CuCl was used. Also, 50 wt% solutions of monomer in anisole were used which considerably decreased the viscosity of the reaction solution. The ligand also plays a key role in the ATRP process. Dinonylbipyridine (dNbpy) was selected since the long alkyl chains of the dNbpy ligand are much better compatible with the LMA monomer and the solvent. The chelating efficiency of dNbpy with Cu(I) halides is lower than that of PMDETA and therefore the polymerization rate decreased dramatically. However, this initiator/ligand combination drastically improved the controlled nature of the ATRP process. Figure 1 shows the ^{1}H NMR spectra of the macro-initiator and PLMA brushes. The peaks assigned in Figure 1 confirmed the successful grafting process. Conventional GPC measurements were conducted for the brushes. They showed shifts to higher molecular weights compared to the macro-initiators.

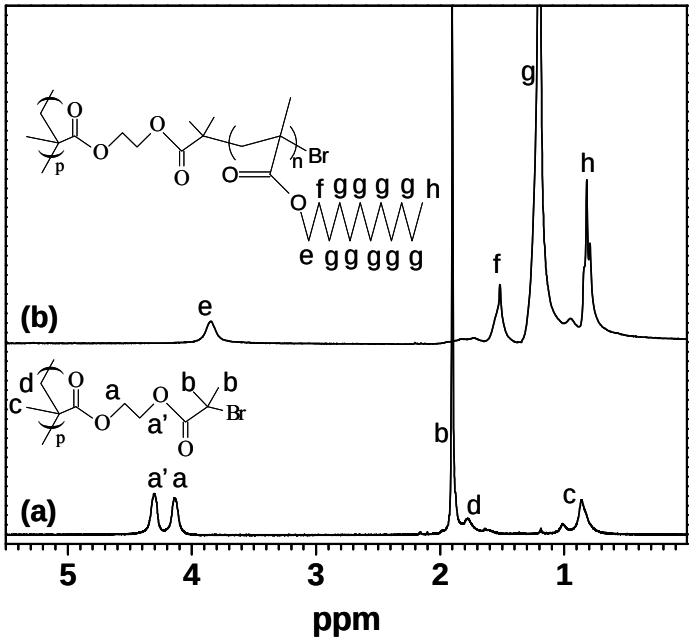

Figure 1. ^{1}H NMR spectra of the macro-initiator PBIEM (a) and the PLMA brushes (b).

True molecular weights and sizes of the brushes were obtained by both dynamic and static light scattering measurements. The obtained values are comparable to the ones calculated from the monomer conversions. The values of R_g/R_h are all around 1.3, indicating the semi-flexible nature of these brushes.

The initiating efficiencies were determined by cleaving the PLMA side-chains from the brushes through a trans-esterification reaction under basic conditions. The molecular weights of the cleaved side-chains then were compared with the theoretical values from the monomer conversions. It was found that the initiating efficiencies were quite low (between 34% and 67%), probably due to the bulky nature of the LMA monomer.

The morphologies of the brushes were directly visualized by atomic force microscopy (AFM). Figure 2 shows the AFM height and phase images of PLMA brushes with a long backbone ($DP_{n,\,backbone}$ = 1500). According to the statistical analysis, the number-average length is L_n =151 nm, which corresponds to around 40% of the calculated contour length for the fully extended backbone (375 nm). This is mainly attributed to the rather low grafting density of the side chains.

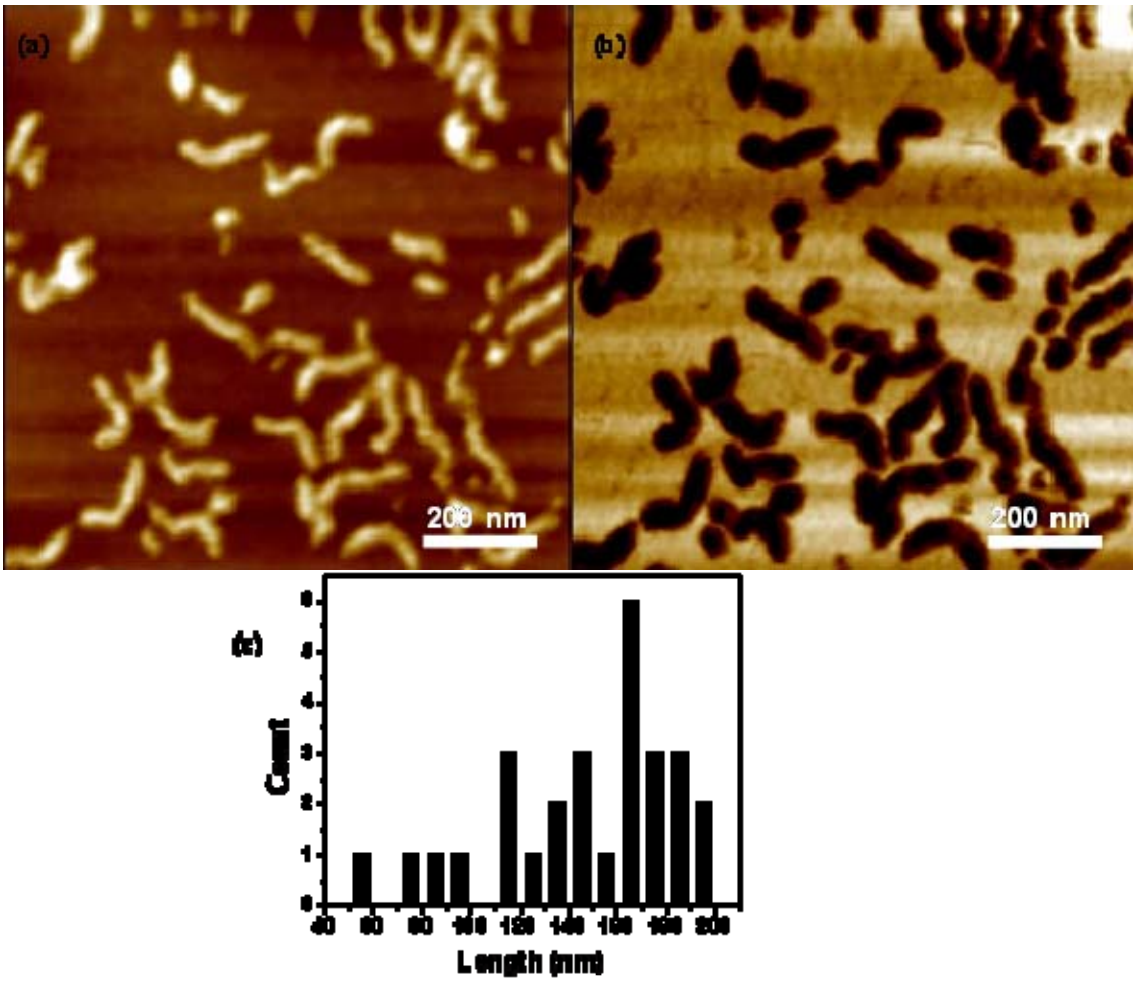

Figure 2. AFM of PLMA brushes: (a) height image (z-range 6 nm), (b) phase image (z range 12°) and (c) histogram of the contour length for 30 molecules.

DSC measurements of the brushes showed that they retained the crystalline properties of the original PLMA side-chains. These brushes are well-soluble in hydro-carbon solvents like *n*-hexane and paraffin oil. Thus, the highly hydrophobic worm-like PLMA brushes can be dispersed in paraffin oil based ferrofluids for further magneto-rheological applications.

Synthesis of cationic polyelectrolyte brushes

The grafting-from strategy was also employed to prepare poly(N,N-dimethylaminoethyl methacrylate) (PDMAEMA) cylindrical brushes by ATRP from PBIEM macroinitiators. Due to the highly active monomer DMAEMA, the

polymerizations were carried out at room temperature. The formation of the weak polyelectrolyte PDMAEMA brushes was demonstrated by ^{1}H NMR, GPC and SLS measurements. Their worm-like structure was visualized by AFM measurements. Due to the weak polyelectrolyte nature, they showed response to pH-changes in solution. Figure 3 shows their apparent hydrodynamic radii changes with increasing pH. A steady decrease was observed, indicating the collapse of the PDMAEMA brushes at high pH. This was also evidenced by the cryo-TEM measurements at different pH values.

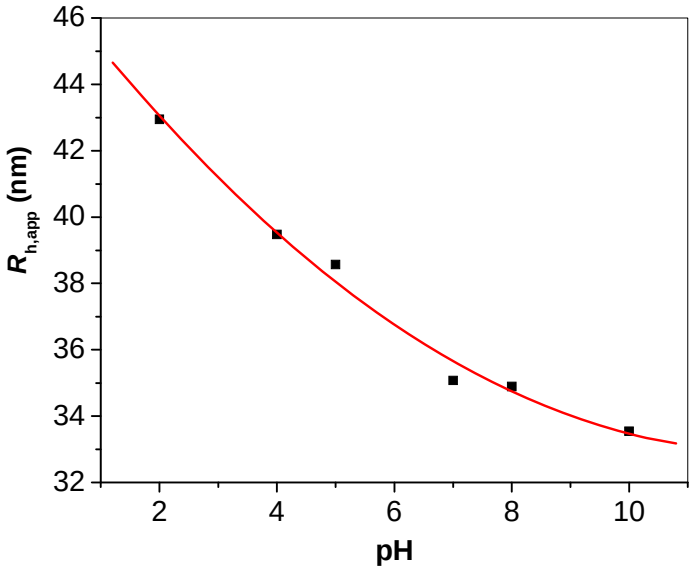

Figure 3. Apparent hydrodynamic radii of PDMAEMA brushes in 0.2 g/L aqueous solution at different pH values.

Strong polyelectrolyte poly{[2-(methacryloyloxy)ethyl] trimethylammonium iodide} (PMETAI) brushes were obtained by further quaternization of the PDMAEMA brushes with methyl iodide. By treating the PMETAI brushes with a strong base, the side-chains of the brushes were detached. Molecular analysis and calculations showed that the initiating efficiencies for the CPBs with grafted PDMAEMA side-chains were around 50%.

Due to the strong Coulombic repulsion of the charged chains, the strong polyelectrolyte PMETAI brushes show a rather elongated conformation. Worm-like morphologies were also observed for the PMETAI brushes, as shown by AFM and cryo-TEM images in Figure 4.

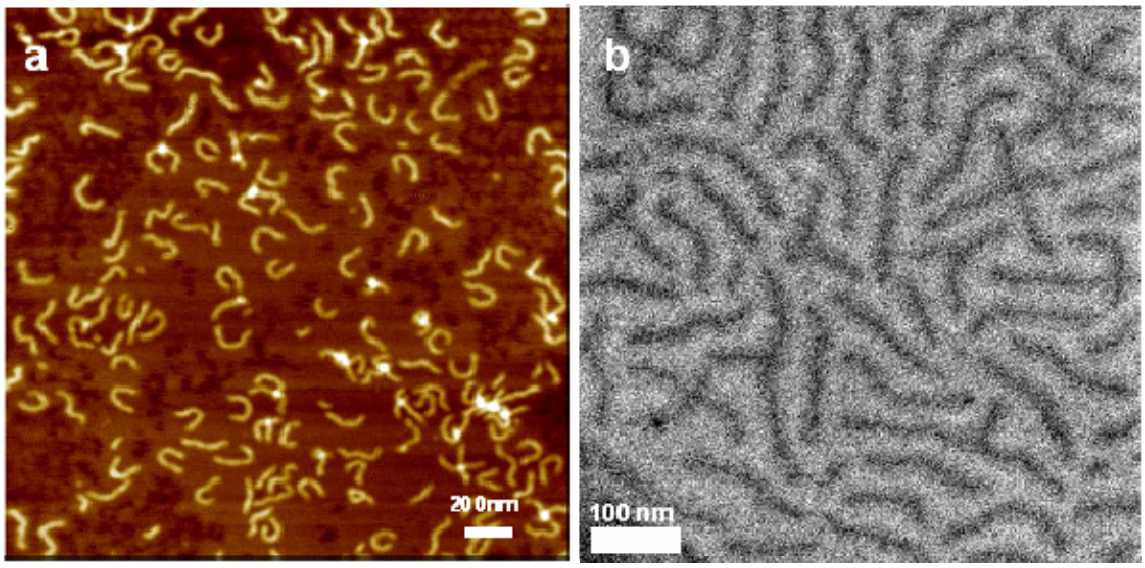

Figure 4. (a) AFM height image (Z range 7 nm) and (b) cryo-TEM image of PMETAI brushes

Addition of salt to the solution will screen the electrostatic interaction within the polyelectrolyte brushes. Thus, the stretching of the polyelectrolyte chains should diminish, resulting in a more collapsed conformation. DLS measurements of the PMETAI brush with different NaBr concentrations confirmed this. Increasing the NaBr concentration from 0 M to 1 M leads to a remarkable decrease of the apparent R_h. When the salt concentration is higher than 1 M, the apparent R_h increases again. A possible explanation is that the bromine ions interact with the cationic polyelectrolyte chains. The collapsed nature of the CPBs was clearly seen in the AFM images for the PMETAI brushes from 0.5 M NaBr solution.

Helical morphologies induced by multi-valent counterions

The response of the PMETAI brushes to counterions of different valences was investigated. At high concentrations of the CPBs, aggregation or precipitation occurred upon addition of di- or trivalent counterions, even at very low salt concentrations. The di- and trivalent salts were potassium tetracyanonickelate(II) $K_2[Ni(CN)_4]$ and potassium hexacyanocobaltate(III) $K_3[Co(CN)_6]$, respectively. In order to observe the single-molecular morphologies of the brushes, very low concentration of brushes (0.02 g/L)

were prepared. For the divalent counterions and a charge ratio $Z_{-/+}$ (the ratio between the negative charges from the counterions and the positive charges carried by the brushes) of 1, the brushes displayed a transition from a worm- to a sphere-like conformation. Interestingly, helical morphologies were obtained before the collapse into sphere-like structures at $Z_{-/+}$ = 0.75. Similar phenomena were also observed for the trivalent counterions at $Z_{-/+}$ of 1, as shown in Figure 5. We believe that this helix-formation is driven by a contraction of the CPBs along their long axis initiated by the presence of the multivalent counter-ions.

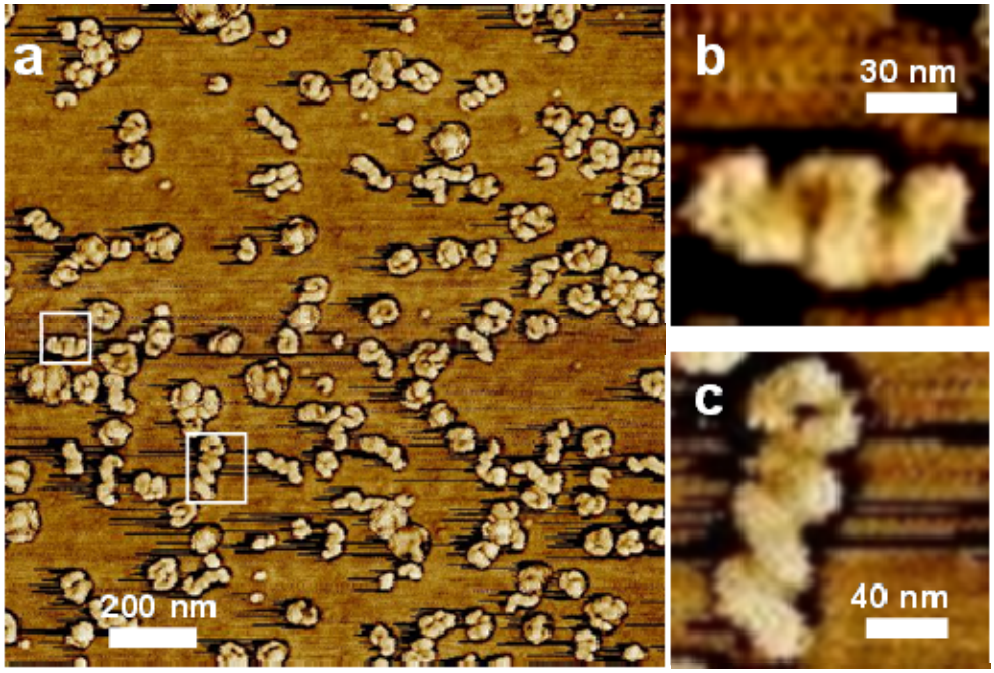

Figure 5. (a) AFM height image of PMETAI brushes with added trivalent salt spin-coated onto mica, $Z_{-/+}$ = 1, z range 12 nm, brush concentration 0.02 g/L, and the trivalent salt concentration 2.2×10^{-2} mM; (b) and (c) show a typical right- and left-handed helix, respectively.

Initial experiments showed that at $Z_{-/+}$ = 0.66 for the divalent counterions, the brushes still exhibited a worm-like morphology. The trivalent counterion employed, $[Co(CN)_6]^{3-}$, is able to undergo photo-aquation upon UV irradiation, resulting in a mixture of mono- and divalent ions. This enabled us to change both charge ratio and the CPB conformation reversibly by UV. Starting from a charge ratio of 1 and trivalent counter-ions, irradiation results in a mixture of mono- and di-valent counterions and a charge ratio of around 0.66.

Thus, we could switch the morphologies of the cationic CPBs between extended structures and collapsed spherical states. The whole process is illustrated in Scheme 1.

Scheme 1. Morphological transition processes by the switching of the counterion valency via UV irradiation.

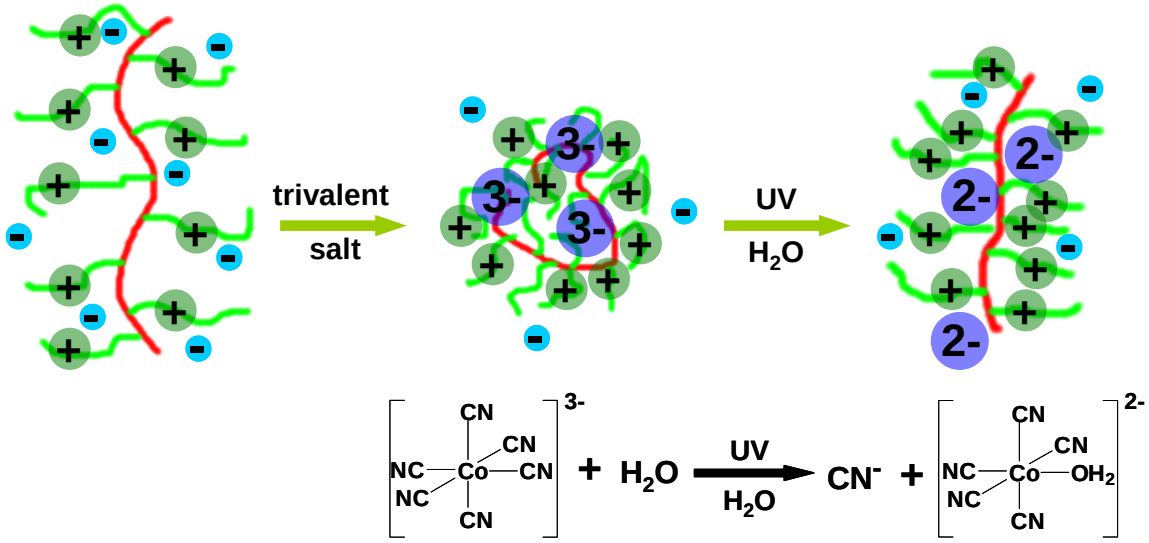

Morphological switching of cationic cylindrical brushes

The morphology of cationic cylindrical polymer brushes' (CCPB) can also be tuned by forming complexes with the anionically charged surfactant sodium dedecyl sulfonate (SDS). At high concentrations of the brushes, aggregation or precipitation occurs. In order to see the single-molecular morphology changes, AFM measurements were carried out at brush concentration of 0.02 g/L. Upon addition of SDS, the brushes showed a collapse from worms to spheres with an intermediate pearl-necklace structure. The addition of α- or β-cyclodextrins (CDs) results in a re-formation of the worm-like structures, through the formation of soluble supramolecular inclusion complexes between CDs and SDS. Further addition of adamantyl ammonium chloride (AdAC), a more competitive inclusion agent, can release SDS from the CD. The release of SDS results in a re-collapse of the CPBs to spherical morphologies. Figure 6 shows the morphology switches of the PMETAI brushes by interacting with SDS, CDs and AdAC. The

reversible morphological transitions of the cationic brushes might be of use as surfactant-responsive sensors or devices on the nano-scale.

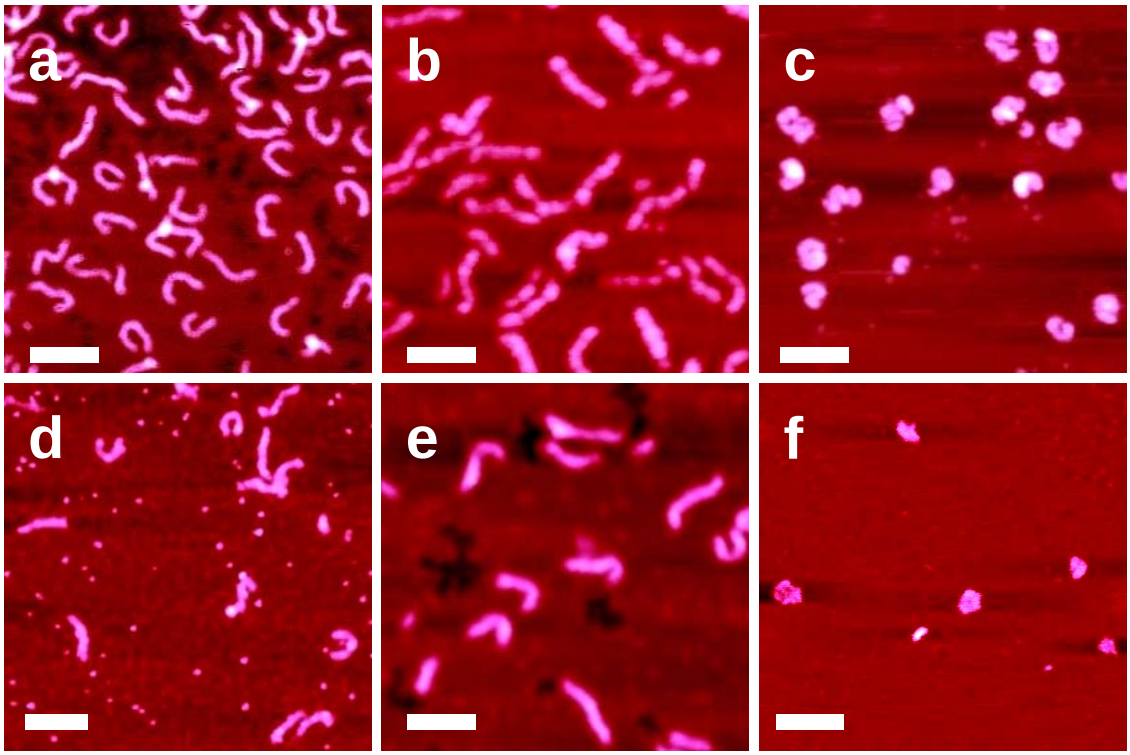

Figure 6. AFM height images of (a) pure CCPB; (b) CCPB with SDS, with $Z_{-/+} = 0.5$; (c) CCPB with SDS, $Z_{-/+} = 1$; (d) CCPB/SDS $Z_{-/+} = 1$ with added α-CD (equimolar with SDS); (e) same, but with added β-CD; (f) sample with β-CD after addition of AdAC (equimolar with β-CD). The scale bars represent 200 nm and the brush concentration is 0.02 g/L. Samples were spin-coated to a freshly cleaved mica surface. AFM height ranges are 5 nm, 12nm, 8nm, 8nm, 8nm, and 4 nm, respectively.

Inter-polyelectrolyte complexes with cationic polymer brushes

The formation of inter-polyelectrolyte complexes (IPECs) of the cationic CPBs with anionic linear poly(sodium styrene sulfonate) (PSS) in highly diluted solutions is another possibility to tune the morphology of the brushes. Similarly, all the experiments were conducted at very low concentrations of the brushes (0.02 g/L) to avoid inter-molecular aggregation. The AFM measurements were mainly carried out for all the following samples. It was found that the charge ratio $Z_{-/+}$ plays a key role in the morphology

transitions of the cationic brushes. When short PSS was employed for the IPECs, at low charge ratios, the brushes only became straighter and the diameter increased (see figure 7). Intermediated helix-like morphologies were observed at a $Z_{-/+}$ of 0.75. Globular collapsed structures of the brushes were detected at a $Z_{-/+}$ of 1.

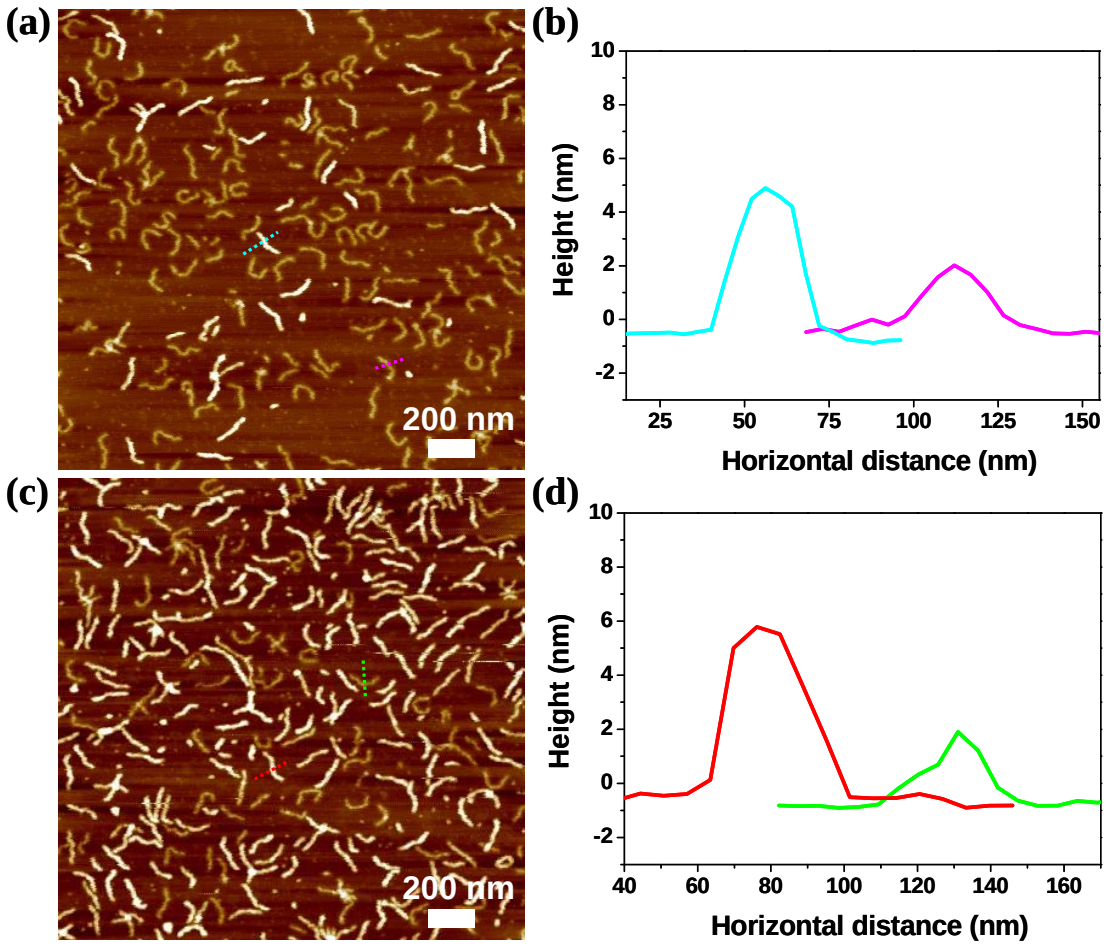

Figure 7. (a) AFM height image of IPECs by PMETAI brushes and short PSS, charge ratio $Z_{-/+}$ 0.1, AFM Z range 10 nm; (b) Section analyses of the cursors displayed in (a); (c) AFM height image of IPECs by PMETAI brushes and short PSS, charge ratio $Z_{-/+}$ 0.5, AFM Z range 10 nm; (d) Section analyses of the cursors displayed in (c).

Extremely long linear PSS was also used for comparison. It can induce the spherical collapse of the brushes at very low $Z_{-/+}$ ratios without other transition states. Full collapse of the brushes was demonstrated at lower charge ratios ($Z_{-/+}$ = 0.5), attributed to the large number of negative charges carried by the long PSS.

In conclusion, the morphologies of the cationic brushes could be tuned by IPEC formation with linear anionic polyelectrolyte chains, PSS. These results could provide a better understanding of the IPECs formed by polyelectrolytes or bio-macromolecules, and might be useful for the building of smart nano-sensors.

Direct preparation of anionic polyelectrolyte brushes

A new strategy for the direct preparation of strong anionic polyelectrolyte cylindrical brushes (BSPMA) without protection is demonstrated by the formation of supramolecular complexes between the monomer potassium sulfopropyl methacrylate (SPMA) and crown ether 18-crown-6 in DMSO using ATRP for the grafting-from processes. The synthetic procedure is shown in scheme 2. DLS and SLS measurements for the size and the absolute molecular weight of the CPBs indicated a good control of the polymerization reaction.

By the treatment with a strong base, the side-chains of the BSPMA brushes were cleaved and transformed into poly(methacrylic acid) (PMAA). Further characterizations yielded that the initiating efficiency was 35%.

Scheme 2. Synthetic procedure for anionic BSPMA.

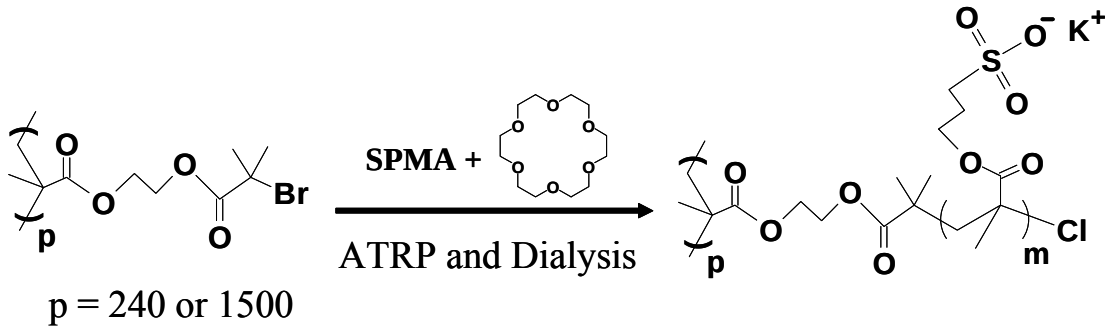

Well-defined worm-like morphologies were directly obtained through AFM and cryo-TEM measurements. Figure 8 displays the cryo-TEM images of BSPMA brushes in 1 g/L solutions with 0.1 M CsCl. Through the addition of heavy counter-ions (Cs^+), even the corona of the CPBs is visible in the cryo-TEM micrographs.

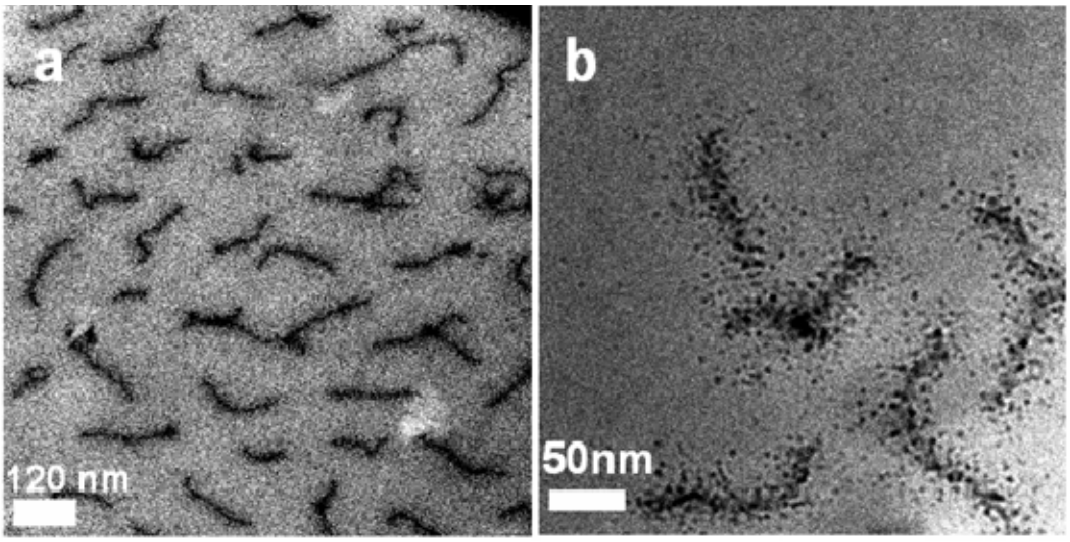

Figure 8. Cryo-TEM images of BSPMA (1g/L) in 0.1 M CsCl solutions: (a) in a large scale; and (b) at a higher magnification.

Magnetic hybrid nano-cylinders

To improve the magnetic response of hybrid nano-cylinders formed by cylindrical brushes and magnetic nanoparticles, we employed a new strategy for their preparation. Water soluble double-hydrophilic core-shell cylindrical brushes were prepared, with PMAA as the core and poly(oligoethyleneglycol methacrylate) (POEGMA) as the protecting shell. They showed interesting pH responsiveness. As displayed in Figure 9, obvious pearl-necklace structures are obtained at pH 4 due to the low solubility of PMAA. At pH 7, however, these structures disappeared, caused by the ionization of PMAA.

Magnetic hybrid cylinders were formed by introducing pre-formed 10 nm sized magnetite nanoparticles into the double-hydrophilic core-shell brushes. The formation of the hybrid cylinders was investigated by AFM and TEM measurements. It could be shown that the hybrid cylinders still exhibited the superparamagnetic properties of the single magnetite nanoparticles.

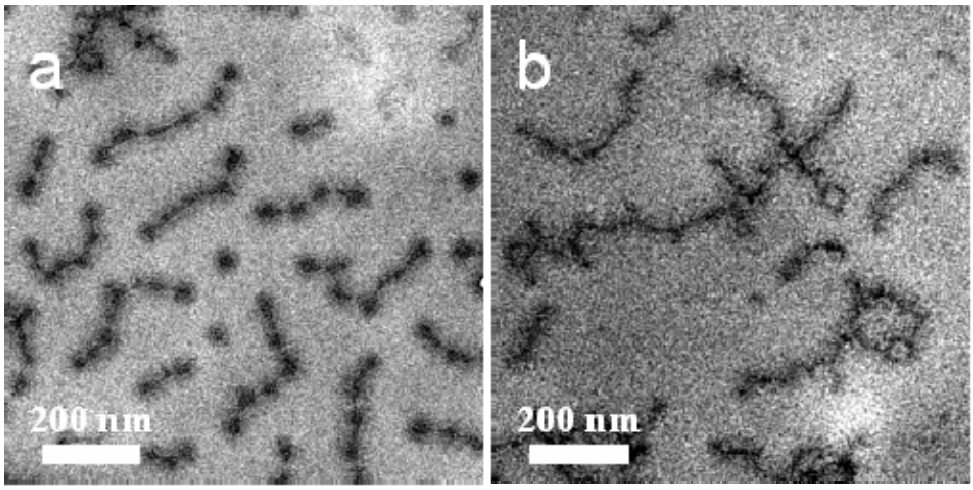

Figure 9. cryo-TEM images of BMO brush at a) pH=4 and b) pH=7.

These hybrid materials could be aligned on a large scale on the substrates by applying magnetic fields during the drying process, as demonstrated in Figure 10. Similar experiments were also performed and visualized by non-stained TEM, leading to comparable results.

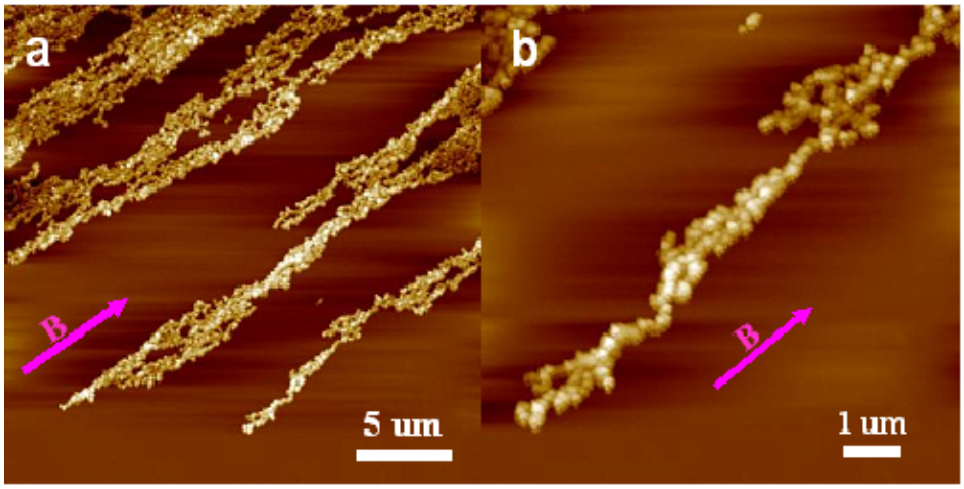

Figure 10. a) AFM height image of the aligned magnetic hybrid on mica surface in a magnetic field of 40 mT, Z range 50 nm; and b) Magnification of one aligned chain of the magnetic hybrid cylinders.

Single-molecular hybrid nano-cylinders

Single-molecular hybrid nano-cylinders were fabricated by covalently attaching a thiol-functionalized polyhedral oligomeric silsesquioxane (POSS) to poly(glycidyl methacrylate) brushes (BGMA). First, BGMA brushes, which carry a large number of epoxy groups, were prepared by the grafting-from strategy using ATRP technique in a similar way as described above for the other brushes. Scheme 1 shows the synthetic procedure. GPC, NMR, and light scattering results indicate a successful synthesis. Typical worm-like structures were observed by AFM measurements from anisole solutions, as is displayed in Figure 11.

Scheme 3. Synthetic procedure for BGMA brushes by ATRP.

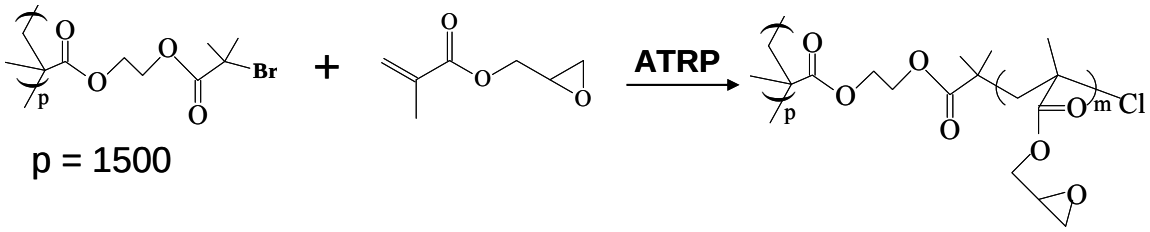

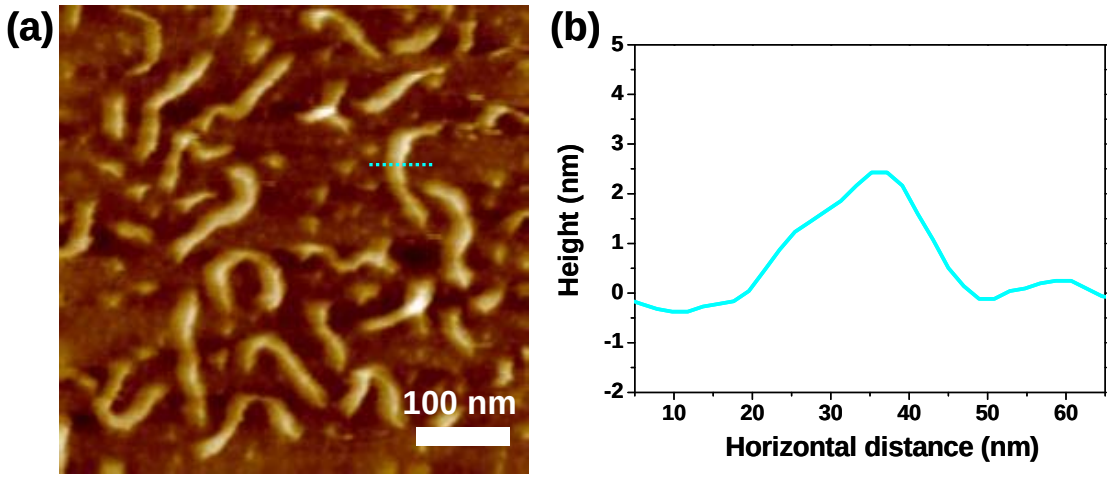

Figure 11. (a) AFM height image of BGMA on mica in anisole, Z rang 7 nm; and (b) section analysis of the cursor shown in (a).

Hybrid BGMA-POSS materials were prepared by reacting the epoxy groups of BGMA with the thiol groups in the POSS under basic conditions at 65°C. Scheme 2 depicts the preparation process for the hybrid cylinders. FTIR was employed to prove the formation of the hybrid. From the molecular weight increase in SLS, the attaching efficiency of the

POSS nanoparticles was estimated to be only around 20%, probably due to the high steric hindrance. Significant contrast increase in the non-stained TEM measurements gave direct proof of the formation of BGMA-POSS, as shown in Figure 12. EDX and TGA were also employed for the characterization of the hybrid materials.

Scheme 4. Procedure for the preparation of nano-hybrid BGMA-POSS.

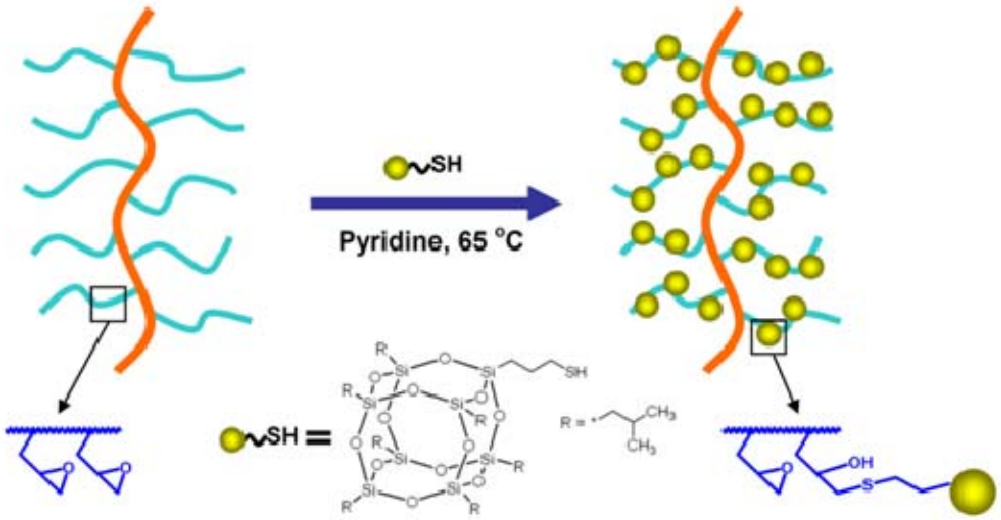

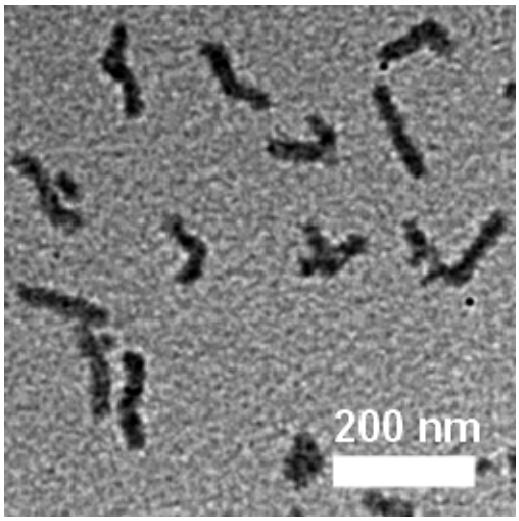

Figure 12. Non-stained TEM image of BGMA-POSS on carbon-coated TEM grid.

Pyrolysis of the hybrid materials at high temperature resulted in porous silica materials, which might find their applications in fields like catalyst carrier or molecular sieves.

Individual Contributions to Joint Publications

In the following, the contributions of each author to the related publications are indicated. The asterisks indicate the corresponding authors.

Chapter 3

This work has been published in *Macromolecular Chemistry and Physics* (2007, 208, 1666-1675) under the title:

Double-grafted Cylindrical Brushes: Synthesis and Characterization of Poly(lauryl methacrylate) Brushes

by Youyong Xu, Harald Becker, Jiayin Yuan, Markus Burkhardt, Yong Zhang, Andreas Walther, Sreenath Bolisetty, Matthias Ballauff, Axel H. E. Müller*

I conducted most of the experiments and wrote the manuscript. Harald Becker provided the PLMA calibration for GPC. Jiayin Yuan measured DSC. Markus Burkhardt and Yong Zhang performed the SLS and DLS measurements, respectively. Andreas Walther did the GPC-MALS measurements. Sreenath Bolisetty measured DDLS for the brushes. Prof. Dr. Matthias Ballauff and Prof. Dr. Axel H. E. Müller were involved the scientific discussions and corrected the manuscript.

Chapter 4

This work has been published in *Polymer* (2008, 49, 3957-3964) under the title:

pH and Salt Responsive Poly(N,N-dimethylaminoethyl methacrylate) Cylindrical Brushes and their Quaternized Derivatives

by Youyong Xu, Sreenath Bolisetty, Markus Drechsler, Bing Fang, Jiayin Yuan, Matthias Ballauff, Axel H. E. Müller*

I conducted most of the experiments and wrote the paper. Sreenath Bolisetty measured DLS for the brushes. Markus Drechsler measured the cryo-TEM. Bing Fang performed the SLS measurements. Jiayin Yuan was involved in the scientific discussions. Prof. Dr. Matthias Ballauff and Prof. Dr. Axel H. E. Müller read and corrected the manuscript.

Chapter 5

This work has been accepted by *Soft Matter* under the title:

Manipulating Cylindrical Polyelectrolyte Brushes on the Nanoscale by Counterions: Collapse Transition to Helical Structures

by Youyong Xu, Sreenath Bolisetty, Markus Drechsler, Bing Fang, Jiayin Yuan, Ludger Harnau, Matthias Ballauff*, Axel H. E. Müller*

I conducted most of the experiments and wrote most part of the paper. Sreenath Bolisetty measured DLS for the brushes. Markus Drechsler measured the cryo-TEM. Bing Fang and Jiayin Yuan were involved in the scientific discussions. Ludger Harnau wrote the theoretical part of the paper. Prof. Dr. Matthias Ballauff wrote part of the paper. Prof. Dr. Matthias Ballauff and Prof. Dr. Axel H. E. Müller read and corrected the manuscript.

Chapter 6

This work has been submitted to *Journal of the American Chemical Society* under the title:

Switching the Morphologies of Cylindrical Polycation Brushes by Ionic and Supramolecular Inclusion Complexes

by Youyong Xu, Sreenath Bolisetty, Matthias Ballauff, Axel H. E. Müller*

I carried out most of the experiments and wrote part of the paper. Sreenath Bolisetty measured DLS. Prof. Dr. Matthias Ballauff and Prof. Dr. Axel H. E. Müller read and corrected the manuscript.

Chapter 7

This work is written in the form of a manuscript to be submitted under the title:

Manipulating the morphologies of Cylindrical Polyelectrolyte Brushes by Forming Inter-Polyelectrolyte Complexes with Oppositely Charged Linear Polyelectrolytes: An AFM Study

by Youyong Xu, Axel H. E. Müller*

I carried out all the experiments and wrote the paper. Prof. Dr. Axel H. E. Müller was involved in the scientific discussions and corrected the manuscript.

Chapter 8

This work is written in the form of a manuscript to be submitted under the title:

Direct Synthesis of Poly(potassium 3-sulfopropyl methacrylate) Cylindrical Polymer Brushes via ATRP using Supramolecular Complex with Crown Ether

by Youyong Xu, Andreas Walther, Sreenath Bolisetty, Matthias Ballauff, Axel H. E. Müller*

I conducted most of the experiments and wrote the paper. Andreas Walther performed the cryo-TEM measurements. Sreenath Bolisetty measured some DLS. Prof. Dr. Matthias Ballauff and Prof. Dr. Axel H. E. Müller read and corrected the manuscript.

Chapter 9

This work is written in the form of a manuscript to be submitted under the title:

Hybrids of Magnetic Nanoparticles with Double-hydrophilic Core-shell Cylindrical Polymer Brushes and their Alignment in Magnetic Field

by Youyong Xu, Jiayin Yuan, Bing Fang, Markus Drechsler, Sreenath Bolisetty, Matthias Ballauff, Axel H. E. Müller*

I did most of the experiments and wrote the paper. Jiayin Yuan and Bing Fang measured TEM. Markus Drechsler conducted cryo-TEM. Sreenath Bolisetty performed the DLS measurements. Prof. Dr. Matthias Ballauff and Prof. Dr. Axel H. E. Müller were involved in the scientific discussions and corrected the manuscript.

Chapter 10

This work is written in the form of a manuscript to be submitted under the title:

Single-molecular Hybrid Nano-cylinders: Attaching Polyhedral Oligomeric Silsesquioxane Covalently to Poly(glycidyl methacrylate) Cylindrical Brushes

by Youyong Xu, Jiayin Yuan, Axel H. E. Müller*

I did most of the experiments and wrote the paper. Jiayin Yuan measured TEM. Prof. Dr. Axel H. E. Müller was involved in the scientific discussions and corrected the manuscript.

3. Double-grafted Cylindrical Brushes: Synthesis and Characterization of Poly(lauryl methacrylate) Brushes

Youyong Xu[a], Harald Becker[a], Jiayin Yuan[a], Markus Burkhardt[a], Yong Zhang[a], Andreas Walther[a], Sreenath Bolisetty[b], Matthias Ballauff[b], Axel H. E. Müller[a,*]

[a]*Makromolekulare Chemie II* , [b]*Physikalische Chemie I, and Bayreuther Zentrum für Kolloide und Grenzflächen, Universität Bayreuth, D-95440 Bayreuth, Germany*

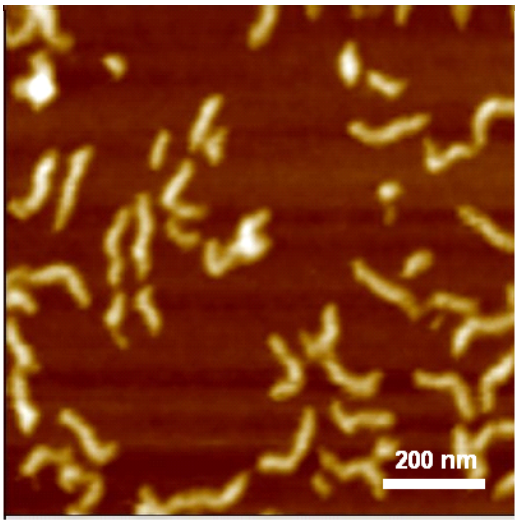

Published in *Macromolecular Chemistry and Physics* **2007**, 208, 1666-1675

Abstract

Double-grafted cylindrical brushes with poly(lauryl methacrylate) (PLMA) as the side chains were synthesized using the grafting-from strategy via atom transfer radical polymerization (ATRP). The polyinitiator poly(2-(2-bromoisobutyryloxy)ethyl methacrylate) (PBIEM) with DP_n = 240 and 1500 served as the backbone. The PLMA side chains of the brushes carry long alkyl chains. GPC and ^{1}H NMR measurements confirmed the successful formation of the PLMA cylindrical brushes. The side chains were cleaved from the cylindrical brushes by transesterification. GPC and ^{1}H NMR results indicate that the initiating efficiency of the bromoester groups on the backbone for the bulky monomer was in the range of $0.34 \leq f \leq 0.67$. Static and dynamic light scattering show that the ratio of the radius of gyration to the hydrodynamic radius, R_g/R_h, is in the range of 1.2 to 1.3, indicating that the LMA cylindrical brushes are semiflexible in solution. Atomic force microscopy (AFM) measurements show that short PLMA brushes exhibit a spherical morphology while the long brushes exhibit a worm-like structure. Differential scanning calorimetry displayed melting peaks at around -30 °C, indicating the alkyl side chains of the PLMA chains in the double-grafted cylindrical brushes are crystallizable.

Keywords: Poly(lauryl methacylate), cylindrical brushes, double-grafted, ATRP

Introduction

With the rapid development of nanotechnology, intense research has been focused on the preparation of various nanostructures[1, 2]. For various purposes of applications, different nanostructures are required[3, 4]. Hence, nanoparticles[5], nanowires[6], nanotubes[7] and other nanostructures have been successfully prepared. Soft materials like polymers play an important role for the templated synthesis, surface protection, surface functionalizations of nanostructures[8], since polymers can show diverse architectures, e.g. linear, star-like[9-11], comb-shaped[12], and dendritic[13, 14] topologies.

When the side chains of the comb-shaped polymers are grafted densely enough, cylindrical polymer brushes are formed[15, 16]. The stretched and anisotropic nature of such comb-like polymers has gained vast experimental and theoretical interest. They exhibit different solution and bulk properties since the backbones are more stretched by the repulsion of the relatively short but dense side chains.

The grafting-onto, grafting-through, and grafting-from strategies have proven very successful to obtain cylindral polymer brushes. Controlled/living polymerizations like atom transfer radical polymerization (ATRP)[17-20], nitroxide mediated radical polymerization (NMRP)[21] and ring opening polymerization (ROP)[22] have been used successfully used to attain well-defined materials.

Based on the strategies described above, cylindrical polymer brushes with various architectures have been prepared. Core-shell cylindrical brushes[18-22], brushes with a grafting density gradient, [23, 24], hetero-grafted brushes[25-27], brush block copolymers[28], star brushes[29, 30], ring brushes[31] and double-grafted brushes[32] have been prepared. Cylindrical brushes with different functionalities were also available. Cylindrical polyelectrolyte brushes[33], thermal responsive brushes[34], photo-responsive brushes[22], sugar-containing brushes[35] and polypeptide brushes[36] were reported.

Neugebauer et al.[32] reported the synthesis of double-grafted poly(poly(ethylene oxide) methacrylate) (PPEOMA) cylindrical brushes using the grafting-through strategy via ATRP, which was the first example of double-grafted cylindrical brushes. While double-grafted brushes with short PEO segments were amorphous, while ones with longer PEO segments in the macromonomer were crystalline. However, during attempts to synthesize

PPEOMA chains with high molecular weight, crosslinked materials were obtained and the resulting double-grafted brushes could serve as a new type of elastomeric materials.

Here we present the synthesis and characterization of cylindrical brushes containing poly(lauryl methacrylate) (PLMA) side chains. The long alkyl side-chains can be regarded as grafts on a poly(methyl methacrylate) backbone, thus giving the double-grafte character. Linear PLMA is an interesting material since the long alkyl side chains can crystallize[37]. The alkyl chains has also lead to a very low a very low glass transition temperature, T_g, ABA block copolymers of LMA and methyl methacrylate (MMA) show typical properties of thermoplastic elastomers[38]. The alkyl side chains also make PLMA very hydrophobic, which may lead to applications such as oil-soluble drag reducers[39] and oil absorbency agents[40, 41]. PLMA is also used as a viscosity modifier for motor oils. The controlled synthesis of PLMA has been achieved by anionic polymerization[42], group transfer polymerization (GTP)[43] and ATRP. [44-46].

Here we present the synthesis of double-grafted cylindrical brushes with PLMA as the side chains using the grafting-from strategy via ATRP. Polyinitiators poly(2-(2-bromoisobutyryloxy)ethyl methacrylate) (PBIEM) with DP_n = 240 and 1500 acted as the backbones. Scheme 1 presents the synthesis of these polymers.

Scheme 1. Synthetic procedures of PLMA cylindrical brushes

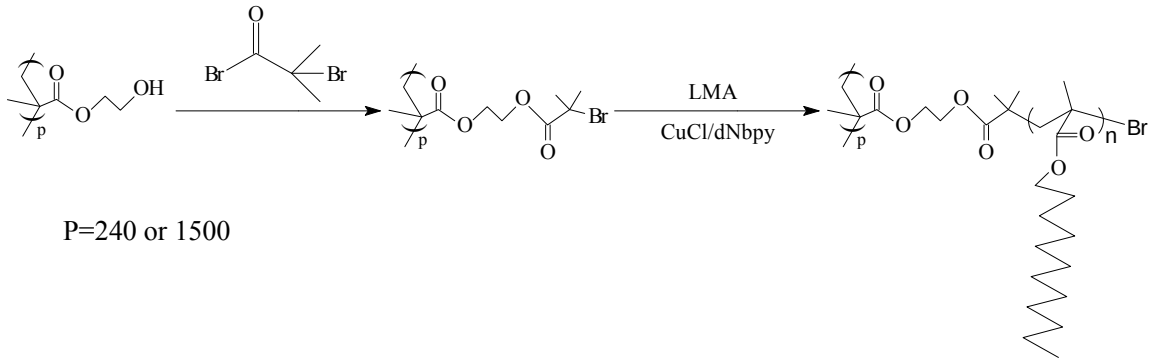

Because of the long alkyl sidechains, these bottlebrush polymers are expected to exhibit a good solubility in apolar solvents as paraffin oil. Hence, these bottlebrush

polymers could be used in inverse magnetorheological fluids,[47] serving as cylindrical holes in a magnetic quasi-continuum.[48]

Experimental

Materials. CuCl (97%, Aldrich) was purified by stirring with acetic acid overnight. After filtration, it was washed with ethanol and ether and then dried in vacuum oven. N,N,N′,N″,N″-pentamethyldiethylenetriamine (PMDETA, Aldrich) was distilled before use. 4,4′-Dinonyl-2,2′-dipyridyl (dNbpy) was purchased from Aldrich and used without further purification. Sodium methoxide (25% in methanol, Aldrich) was used as received. Lauryl methacrylate (LMA; mixture of 72% n-dodecyl methacrylate and 28% n-tetradecyl methacrylate) was kindly donated by RohMax Additives GmbH (Darmstadt, Germany) and was purified by passing through basic alumina columns before polymerizations. Polyinitiators poly(2-(2-bromoisobutyryloxy)ethyl methacrylate) PBIEM-I (DP_n = 240, PDI = 1.16) and PBIEM-II (DP_n = 1500, PDI = 1.08) used for the synthesis of the PLMA brushes were reported previously[20]. All the other solvents and chemicals were used as received.

Polymerizations. All polymerizations were carried out in a round-bottom flask sealed with a rubber septum. A typical example of the synthesis of a PLMA cylindrical brush is described as follows: PBIEM-I (55.8 mg, 0.2 mmol of initiating α-bromoester groups) and dinonylbipyridyl (dNbpy) (81.7 mg, 0.2 mmol) were dissolved in anisole (25.4 g) in a pear-shaped flask and stirred overnight to assure the complete dissolution of the high molecular weight polyinitiator. Then the monomer LMA (25.4 g, 0.1 mol) was injected via a syringe and stirred for 15 min. The flask was purged with argon for 15 min. About 0.5 mL of solution was taken out with an argon-purged syringe as an initial sample for conversion measurement by ^{1}H NMR. A round-bottom flask with CuCl (10 mg, 0.1 mmol) was also deoxygenated by argon flow. Then the solution in the pear-shaped flask was transferred into the round-bottom flask by a cannula. The solution immediately turned orange. The round-bottom flask was then inserted into an oil-bath heated at a 70 °C. Small samples were taken out at intervals to check the monomer conversion. After 17 hours, the conversion determined by ^{1}H NMR reached 14.5%. The round-bottom flask

was then cooled to room temperature and opened to air. Dichloromethane was added to dilute the solution and the color of the solution turned green. After passing through a basic alumina column, the colorless solution was concentrated by a rotary evaporator. Afterwards, it was precipitated into cold methanol to remove the residual monomer and other impurities. The precipitation procedure was repeated three times from THF solution into large amounts of cold methanol to make sure the viscous monomer was removed. The viscous crude product was then dried in a vacuum oven at 100 °C for two days. A transparent and viscous polymer was obtained. The polymer is soluble in THF, hexane, toluene and chloroform, but insoluble in methanol, acetone, and water.

Cleavage of the side chains from the PLMA brushes: The cleavage of the side chains from the PLMA brushes was carried out by base catalyzed transesterfication reactions. One typical reaction is described as follows: The PLMA brush (0.1 g) was dissolved in 5 mL THF in a 20 mL bottle. Methanol was added until the solution became turbid. Sodium methoxide solution (10 drops) was then added. The tube was capped tightly and put in an oil bath and kept at 90 °C for 10 days. Then, the solution was cooled and stirred overnight in the presence of cationic ion-exchange resin (Dowex MSC-1). The solution was filtered and evaporated. The resulting product was analyzed by ^{1}H NMR and conventional GPC with a linear PLMA calibration.

Characterizations. ^{1}H NMR was measured on a Bruker AC-250 instrument at room temperature with $CDCl_3$ as the solvent.

The apparent molecular weights of the brushes were characterized by conventional GPC using THF as eluent at a flow rate of 1.0 mL/min at room temperature. Column set: 5 μm p SDV gel, 10^2, 10^3, 10^4, and 10^5 Å, 30 cm each (PSS, Mainz). Detectors used are RI and UV operated at 254 nm. Polystyrene standards (PSS, Mainz) with narrow molecular weight distribution were used for the calibration of the column set. The molecular weights of the cleaved side chains from the PLMA cylindrical brushes were also determined by the same instrument set-up, but with PLMA standards made by ATRP and characterized by GPC-MALS.

GPC with a multi-angle light scattering detector (GPC-MALS) was used to determine the absolute molecular weights of the PLMA cylindrical brushes. THF was used as eluent

at a flow rate of 1.0 mL/min. Column set: 5 μm PSS SDV gel, 10^3, 10^5, and 10^6 Å, 30 cm each. Detectors: An RI detector and a Wyatt DAWN DSP-F MALS detector equipped with a He-Ne laser (λ = 632.8 nm) were used.

The refractive index increment of the PLMA cylindrical brush solution in THF at 25 °C was measured to be dn/dc = 0.080 mL/mg using a PSS DnDc-2010/620 differential refractometer.

Static light scattering (SLS) was measured on a Sofica goniometer using a He-Ne laser (λ = 632.8 nm). Prior to the light scattering measurements, the sample solutions were filtered 3 times by using Millipore Teflon filters with a pore size of 0.45 μm. Five concentrations of the PLMA cylindrical brush solutions in THF were measured at angles in the range from 30 ^{o} to 150 ^{o}. Absolute weight-average molecular weights, M_w, radii of gyration, R_g, and second virial coefficient, A_2 , of the PLMA brushes were obtained by the analysis of the Zimm-plots.

Dynamic light scattering (DLS) was carried out on an ALV DLS/SLS-SP 5022F compact goniometer system with an ALV 5000/E correlator and a He-Ne laser (λ = 632.8 nm) at five different angles. Before the light scattering measurements, the sample solutions were filtered 3 times by using Millipore Teflon filters with a pore size of 0.45 μm. A CONTIN analysis was taken for the measured intensity correlation functions. Apparent hydrodynamic radii, R_h, of the PLMA cylindrical brushes were calculated according to the Stokes-Einstein equation. For depolarized dynamic light scattering (DDLS), the horizontal polarized scattered intensity, I_{VH}, was measured by applying a Glan-Thomson prism in front of the detector. All the measurements were carried out at 25°C.The measurements were performed at scattering angles ranging from 40° to 140° with an angular step of 10°.

Atomic force microscopy (AFM) measurements were performed on a Digital Instruments Dimension 3100 microscope operated in tapping mode. The micro-cantilever used for the AFM measurements were from Olympus with resonant frequency between 284.3 kHz and 386.0 kHz, and spring constant ranging from 35.9 to 92.0 N/m. Carbon-coated mica substrates were prepared using a Balzers MED 010 minideposition system. Carbon with a thickness of approximately 10 nm was deposited on the freshly cleaved

mica surfaces by evaporation. The samples were prepared by dip-coating from very dilute (0.01 g/L) THF solutions of PLMA brushes onto freshly cleaved mica surfaces or carbon coated mica surfaces.

Differential scanning calorimetry (DSC) measurements were performed on a Perkin Elmer Pyris-1 instrument. The samples were first heated up to 120 °C and kept for 5 min. Then the samples were subjected to a cooling process from 120 °C to -80 °C with a cooling rate of 10 K/min. They were kept at -80 °C for another 5 min. Finally, the samples were reheated to 120 °C from -80 °C with a heating rate of 10 K/min.

Results and discussion

1. Synthesis and molecular characterization of LMA brushes. The synthesis of cylindrical brushes using the grafting-from strategy requires linear polyinitiators, which determine the length and length distribution of the cylindrical brushes., The synthesis of PBIEM polyinitiators by both ATRP and anionic polymerization was previously reported by our group[20]. The PBIEM-I polyinitiator synthesized by ATRP had a DP_n = 240 and relatively broad MWD (M_w/M_n = 1.16), while PBIEM-II prepared by anionic polymerization had DPn = 1500 and very narrow MWD (M_w/M_n = 1.08). Short and long double-grafted PLMA cylindrical brushes were prepared by growing PLMA side chains from the two polyinitiators.

For the grafting-from process using ATRP, high local concentration of radicals in one polyinitiator molecule may cause intra- or even intermolecular radical coupling reactions.[17]. To suppress these coupling reactions the catalyst-to-initiator molar ratio was 0.5, which is much lower than normal ATRP processes for linear polymers.

Considering the bulky nature of the LMA monomer, a low initiating efficiency was expected. In order to increase the initiating efficiency, a halide exchange reaction with CuCl was used.[49] Sumerlin et al.[50] proved that high dilution could improve the initiating efficiency of ATRP for cylindrical brushes. Thus, a 50 wt% solution of monomer in anisole was used, which considerably decreased the viscosity of the reaction solution.

Table 1. Synthesis and molecular characterization of PLMA cylindrical brushes[a]

Brush	Initiator	DP_n of back-bone	time (h)	conv(%) [b]	$10^{-6}M_{n,GPC}$ [c]	PDI [c]	$10^{-6}M_{n,calc}$ [d]	$10^{-6}M_{w,}$ GPC-MALS
1	PBIEM-I	240	18	14.5	0.28	1.17	4.62	1.69±0.08
2	PBIEM-I	240	42	21.7	0.43	1.13	6.89	6.74±0.33
3	PBIEM-II	1500	17	11.3	0.84	1.28	22.40	10.1±0.50
4	PBIEM-II	1500	40	24.9	0.88	1.31	49.00	19.5±7.8

[a]50 wt % solutions in anisole; ATRP at 70 °C with constant ratio of $[M]_0/[I]_0/[CuCl]_0/[dNbpy]_0 = 500:1:0.5:1$. [b] Monomer conversion determined by ^{1}H NMR. [c]Apparent values determined by conventional GPC with a polystyrene standard calibration. [d]M_n calculated from conversion by ^{1}H NMR. $M_{n,calc} = (262 \times \text{Conversion} + 280) \times DP_{n,backbone}$.

The ligand also plays a very important role in the ATRP process. PMDETA was used for the first experiments. A very fast polymerization rate was observed, the conversion reaching over 20% within 15 min and the final product showing bimodal MWD. Then dinonylbipyridine (dNbpy) was used. The long alkyl chains of the dNbpy ligand are much better compatible with the LMA monomer and the solvent. Since the chelating efficiency of dNbpy with Cu(I) halides is lower than that of PMDETA, the rate of polymerizations decreased dramatically, but with better control of the reaction.

Table 1 lists the results of of the characterization of the PLMA cylindrical brushes obtained. The MWDs of the brushes are quite narrow, indicating a good control of the ATRP process. However, the PDI of the long brushes are significantly higher than those of the long backbones, indicating a polydispersity in the number of side chains.

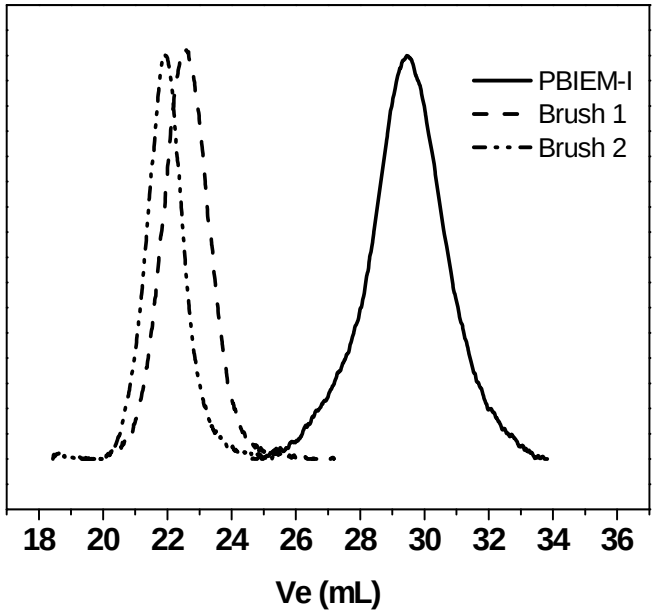

Figure 1. GPC traces of PBIEM-I and corresponding short PLMA cylindrical brushes.

Figures 1 and **2** show the GPC traces of the polyinitiators and corresponding short and long PLMA cylindrical brushes. Monomodal eluograms were observed for all the PLMA cylindrical brushes. The molecular weights of the PLMA cylindrical brushes were first characterized by conventional GPC, using a polystyrene calibration. True molecular weights were determined by GPC-MALS. The true molecular weights are several times

higher than those from conventional GPC, typical for highly branched systems and also partially due to the inappropriate calibration standards. It is also found that the molecular weight determined by GPC-MALS is always lower than the ones calculated from ^{1}H NMR conversion. For the calculation of the M_n, the ^{1}H NMR conversion values have to be multiplied by huge numbers (see **Table 1**). So, small deviations or errors will cause huge differences of the molecular weight. At the same time, NMR itself has around 5% error. According to the values in Table 1, some GPC-MALS results also have errors up to 40%. This could be the cause of the mismatch of the calculated molecular weight values and experimental values.

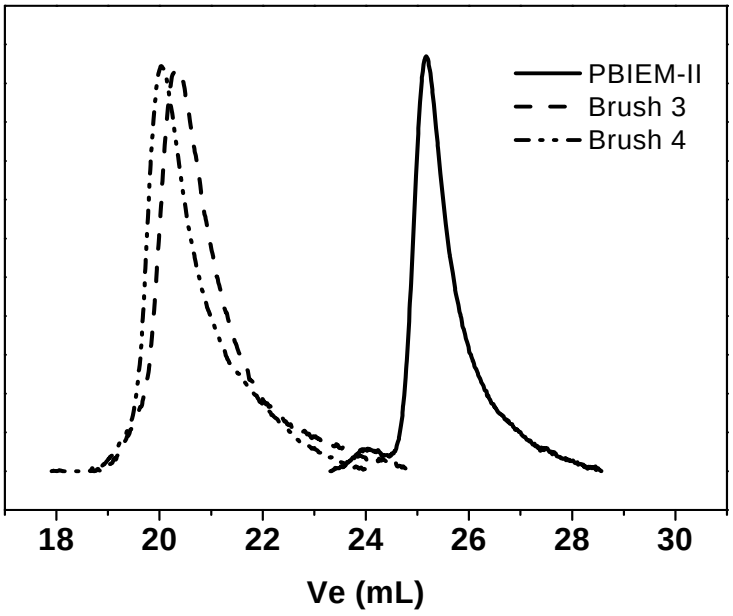

Figure 2. GPC traces of PBIEM-II and corresponding long PLMA cylindrical brushes.

Figure 3 shows the NMR spectra of the polyinitiator and the PLMA cylindrical brushes. The two peaks at 4.12 ppm (a) and 4.3 ppm (a′) are assigned to the methylene protons between two ester groups in the PBIEM polyinitiator. The methyl (peak c, from 0.7 ppm to 1.1 ppm) and methylene protons (peak d, 1.75 ppm) of the backbone were also assigned. When the PLMA cylindrical brushes are formed, peak a and a′ disappear, while distinctive peaks from the long alkyl side groups of the PLMA side chains appear: methylene protons (e, 3.85 ppm) connected to the ester group, neighboring methylene

protons (f, 1.5 ppm), the other methylene protons (strong peak g, 1.2 ppm) and the end methyl protons (h, 0.8 ppm). Thus, the ^{1}H NMR spectra indicate the successful grafting of PLMA from the PBIEM backbones.

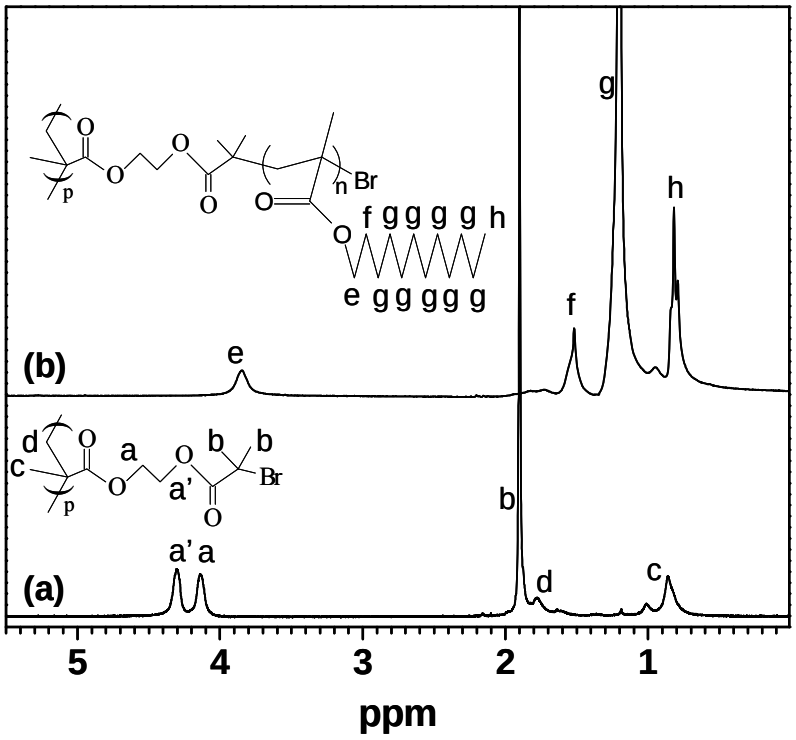

Figure 3. ^{1}H NMR spectra of (a) PBIEM-I and (b) PLMA brush 2 in $CDCl_3$.

2. Initiating efficiencies of the polyinitiators for LMA. The first case of checking the initiating efficiency of the cylindrical brushes prepared by grafting-from strategy was reported by our group[18]. Side chains of PS cylindrical brushes were detached from the backbone by basic hydrolysis of the ester linking groups. Almost 100% initiating efficiency was found for the PS cylindrical brushes. Using base-catalyzed solvolysis, Sumerlin et al.[50] and Neugebauer et al.[51] found low initiating efficiencies for poly(methyl methacrylate) (PMMA) and poly(n-butyl acrylate) (PBA) cylindrical brushes. For the PMMA brushes the initiating efficiencies were lower than 50% even if the

conversion of the monomer was up to 14.5%. Cylindrical brushes prepared from a very bulky sugar-carrying methacrylate also showed initiating efficiencies of less than 40% [34]. The LMA monomer is also very bulky. Thus, the initiating efficiency of the PBIEM backbones is not expected to be very high.

In order to determine the initiating efficiency of the PBIEM polyinitiators towards LMA, base-catalyzed transesterification was employed to cleave the PLMA side chains from the cylindrical brushes. The reaction mechanism is shown in **Scheme 2**.

Scheme 2. Cleavage of side chains from the PLMA brushes

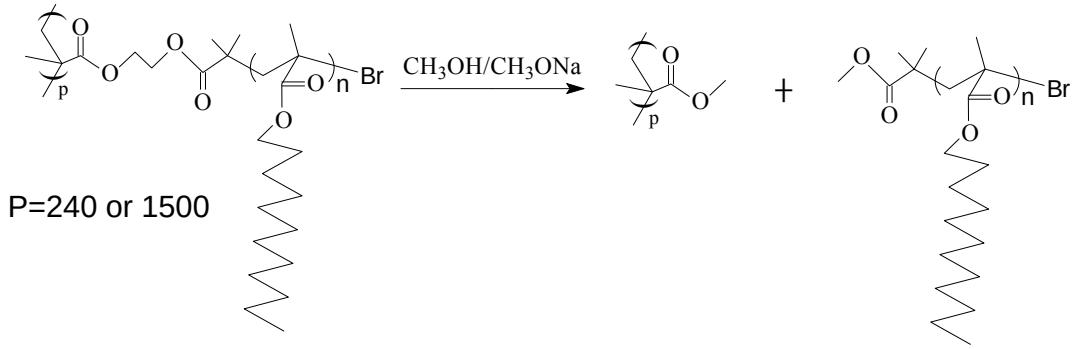

The detached polymers were subjected to ^{1}H NMR and GPC measurements. **Figure 4** shows the ^{1}H NMR spectrum of the side chains cleaved from brush 3. Compared to the ^{1}H NMR spectrum of PLMA cylindrical brushes, there is almost no difference and the distinctive peaks from the PLMA remain. ^{1}H NMR spectrum and GPC trace of linear PLMA polymer, which was subjected to the same reaction conditions of the base catalyzed transesterification, showed no difference from those of the original linear polymers. This suggests the transesterification reactions nearly exclusively occurred to the linking ester groups between the side chains and the backbones, not to the ester groups in the PLMA side chains. Possible reasons could be the high steric strain that the side-chains exert on the backbone or the different polarity of the backbone and the side chains leading to a higher methoxide concentration near to the backbone.

GPC traces of the brush and the cleaved side chains are shown in **Figure 5**. In each case, only one peak was observed in the GPC elution curve, while no high molecular weight peaks were found. This indicates the full detachment of the side chains from the

backbones. Compared to the amount of side chains, the weight fraction of the backbone polymers is very small, and the effect of the backbones can be neglected.

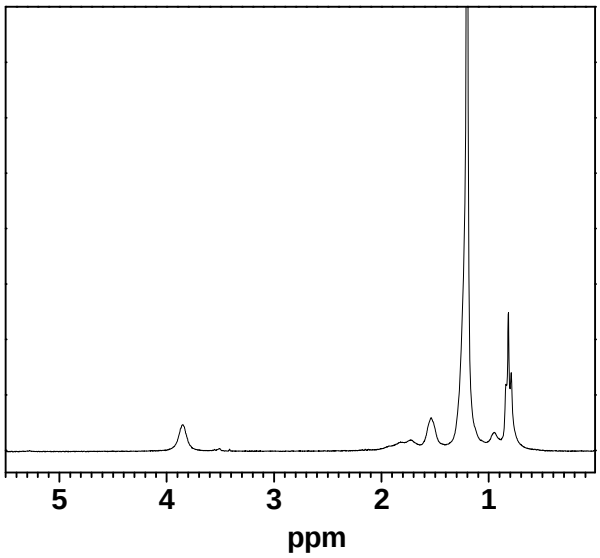

Figure 4. ^{1}H NMR spectrum of cleaved PLMA side chains from brush 3.

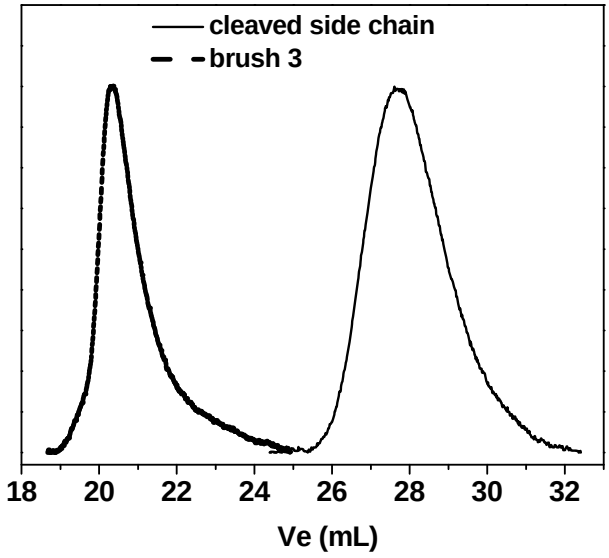

Figure 5. GPC traces of brush 3 and cleaved side chains from brush 3.

To determine the true molecular weight of the cleaved side chains from the PLMA cylindrical brushes, a GPC calibration curve with PLMA linear polymer standards was

used[52]. The results are listed in **Table 2**. From the true molecular weight of the brush, the DP of the backbone and the DP of the side-chains, the number of side chains and thus the initiator efficiency were determined.

Table 2. Characterization of cleaved side-chains from the PLMA cylindrical brushes.

side chain of	10^{-4} x $M_{n,GPC}$ [a]	PDI [a]	$DP_{n,sc,GPC}$ [b]	$DP_{n,sc,calcd}$ [c]	f [d]	N_{sc} [e]	$DP_{n,bb}/DP_{n,sc}$
brush 1	3.40	1.36	130	72	0.55	132	1.8
brush 2	4.24	1.23	162	108	0.67	161	1.5
brush 3	4.31	1.36	164	56	0.34	510	9.1
brush 4	4.83	1.17	184	124	0.67	1005	8.2

[a]Determined by conventional GPC using linear PLMA calibration,. [b]$DP_{n,sc,GPC} = M_{n,GPC}/M_0$, M_0 = 262 g/mol. [c]Calculated from the monomer conversion in table 1, $DP_{n,sc,calcd} = ([M]_0/[I]_0) \times$ conversion. [d]Initiating efficiency of PBIEM, $f = (DP_{n,sc,calcd}/DP_{n,sc,GPC})$; [e]number of side chains per molecule.

As can be seen in Table 2, the initiating efficiencies are quite low, but they increase with conversion, typical for a slow initiation. The polydispersity indices of the cleaved side chains are relatively high, being in the range of the theoretical value for slow initiation, 1.33[53]. This might be attributed to the bulky nature of the LMA monomer and steric hindrance. Also, the incompatibility between the LMA monomer and the polyinitiator could be the partial reason.

3. Characterization of the cylindrical brushes in solution.

Static (SLS) and dynamic light scattering (DLS) were used to characterize the solution properties of the PLMA cylindrical brushes in THF. The corresponding plots are given as Supporting Information. Table 3 summarizes the results obtained from the SLS measurements, namely M_w, the radii of gyration, R_g, and second virial coefficients, A_2. Brush 1 and brush 2 were prepared from the same backbone (DP_n = 240). The R_g of the PLMA brushes increased from 27.8 nm to 51.1 nm. This can be explained by the longer

and denser PLMA side chains attached to the backbones, which leads to the more stretched backbones of the cylindrical brushes. Brush 3 has a much longer backbone (DP_n = 1500), and the R_g value (65.3 nm) is significantly larger than those of the short brushes.

Dilute solutions of the cylindrical brushes in THF were also subjected to DLS measurements. The analysis was supplemented by depolarized DLS measurements. No depolarized signal could be measured indicating that the rotational diffusion times are too small to be measured. Hence, this finding indicates a worm-like semiflexible structure in solution rather than a rod-like one of these systems. **Table 3** shows the hydrodynamic radii obtained by DLS. It is well know that the ratio $\gamma = R_g/R_h$ reflects the polymer architecture[54]. According to theory, for rigid rods is $\gamma > 2$. Thus, the values shown in **Table 3** point to rather small persistence lengths caused by the low grafting density of the side chains.

Table 3. Light scattering characterizations of PLMA cylindrical brushes

Brush	$10^{-6}M_{w,SLS}$ [a]	$10^{6}A_2$ [a]	R_g (nm) [a]	R_h (nm) [b] *(PDI)*	R_g / R_h
1	1.88±0.36	0.39±0.06	27.8±6.3	21.5 (0.10)	1.3
2	9.48±0.49	5.04±0.87	51.1±5.2	42.2 (0.16)	1.2
3	15.80±1.23	5.33±0.77	65.3±4.1	49.4 (0.14)	1.3

[a] Determined by SLS. [b] Determined by DLS unsing the CONTIN procedure, at scattering angle of 90°.

4. Visualization by AFM. Although AFM images can not present the real state of cylindrical brushes in solution because of possible polymer-surface interactions, it is still a powerful tool to reflect the morphologies of cylindrical brushes. Choosing of suitable substrates for the AFM measurements is very important. Mica and silicon wafers were tried as the substrates for the AFM measurement of PLMA cylindrical brushes by dip-coating from THF solutions. Only severe dewetting phenomena were found and no single brushes could be observed. This is due to the poor adsorption of the very hydrophobic PLMA cylindrical brushes to the quite polar mica or silicon wafer surfaces. Thus, freshly

cleaved mica was coated with carbon in order to obtain a more hydrophobic surface, which is more compatible with the nonpolar PLMA brushes.

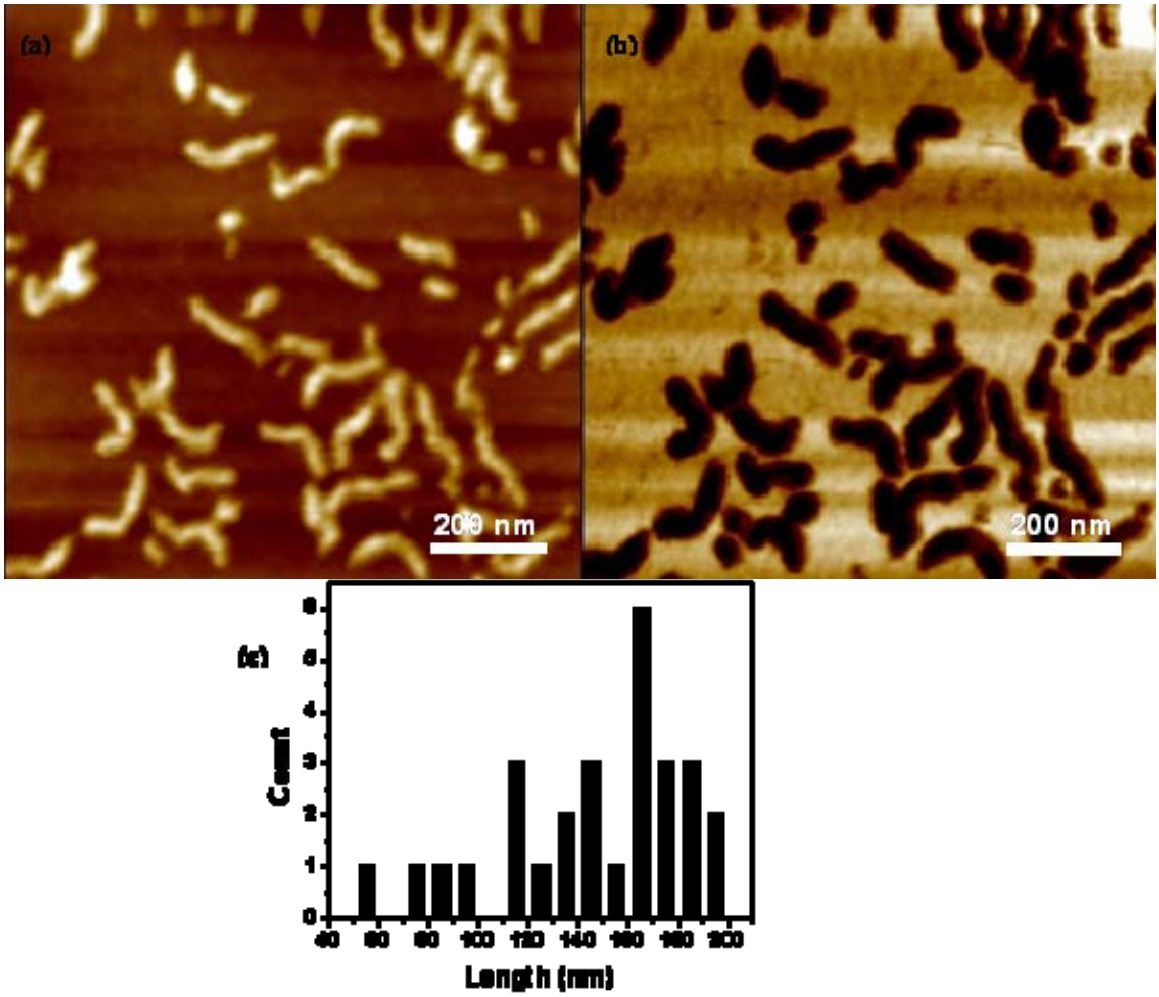

Figure 6. AFM of brush 3: (a) height image (z-range 6 nm), (b) phase image (z range 12°) and (c) histogram of the contour length for 30 molecules.

Figure 6 represents the AFM images of the long brush 3. This long brush 3 exhibits obvious worm-like structures. That is because the backbone (DP_n = 1500) is much longer and the aspect ratio is also much higher. According to the statistical analysis, the number-average length of brush 3 is L_n =151 nm, which is only 40% of the contour length of a fully extended chain, L_c = 0.25 x 1500 nm = 375 nm. This is attributed to rather low grafting density (only 34%) of the side chains. A cross-section analysis of the AFM height and phase images shows that the height of the brushes is around 3 nm while the

width of the brush is approximately 50 nm (not corrected for the tip radius). This indicates the soft PLMA side chains have a good compatibility with the carbon coated mica surface. The side chain length, L_{SC}, can be regarded as half of the width of the brushes in phase image. The ratio of L_n/L_{SC} is calculated to be 6.0, which is comparable to the ratio $DP_{n,bb}/DP_{n,sc}$ shown in **Table 2**.

Additional measurements on the short brush 2 with the DP_n of the backbone with only 240 monomer units show an ellipsoid-like morphology (see Supporting Information, Fig. S5). The number-average length of brush 2 is just L_n = 37 nm, which is 60% of the contour length. Due to the higher grafting density this stretching ratio is higher than for brush 3.

5. Thermal properties of the PLMA cylindrical brushes. It is known that polymers with long alkyl side groups can exhibit sidechain crystallization. Hempel et al.[37] found that poly(*n*-alkyl methacrylates) with $C \geq 12$ of the side chain alkyl carbons, crystalline behaviors were found. In order to check if the PLMA with double-grafted cylindrical structures can form crystals in bulk, DSC measurements were performed.

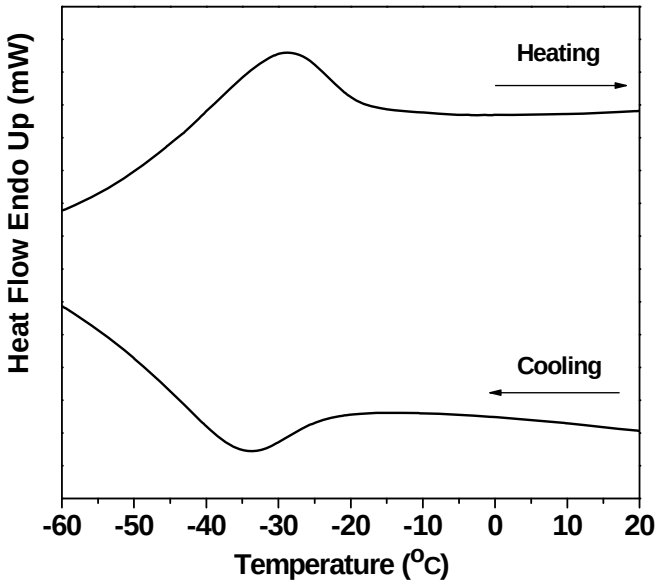

Figure 7. DSC heating and cooling curves of PLMA brush 3.

The DSC measurements show broad apparent melting peaks at -30 °C in the heating curves and crystallization peaks in the cooling curves for all PLMA cylindrical brushes. **Figure 7** shows the heating and cooling traces of brush 3. This demonstrates that the double-grafted cylindrical structures do not affect the crystallization abilities of PLMA.

Conclusions

We successfully synthesized double-grafted cylindrical brushes using the grafting-from technique via ATRP with the CuCl/dNbpy catalyst system. By using polyinitiators with different chain lengths, we obtained relatively narrowly distributed short and long PLMA cylindrical brushes. By detaching the grafted side chains from the backbones using transesterification reactions, we found rather low initiating efficiencies, obviously due to the very bulky nature of the LMA monomer, also possibly due to the incompatibility of the monomer and the polyinitiator. SLS, DLS and AFM results proved the worm-like structure of the brushes in solution and on substrates. DSC measurements showed that the long alkyl side groups in the PLMA side chains are still crystallizable. The highly hydrophobic worm-like PLMA brushes can be dispersed in paraffin oil based ferrofluids and results on the properties of the related inverse magneto-rheological fluids will be published elsewhere.[48]

Acknowledgements

This work was financially supported by the Deutsche Forschungsgemeinschaft (DFG) within SFB 481. We would like to thank Sabine Wunder for the assistance with the GPC measurements, Markus Hund for the help with the AFM measurements, Werner Reichstein for the carbon-coated mica, and Markus Ruppel and Pierre Millard for their constructive discussions. We are also grateful to the referees for their constructive comments and suggestions.

References

[1] W. A. Goddard, III, D. W. Brenner, S. E. Lyshevski, G. J. Iafrate, Eds., *Handbook of Nanoscience, Engineering, and Technology*, CRC Press: Boca Raton, **2003**.

[2] G. M. Whitesides, *Small* **2005**, *1*, 172.

[3] K. J. Klabunde, Editor, *Nanoscale Materials in Chemistry*, John Wiley & Sons: New York, **2001**.

[4] H. Gleiter, *Adv. Mater.* **1992**, *4*, 474.

[5] G. Schmid, Ed., *Nanoparticles: From Theory to Application*, Wiley-VCH: Weinheim, **2004**.

[6] J. A. Schwarz, C. I. Contescu, K. Putyera, *Dekker Encyclopedia of Nanoscience and Nanotechnology-5 Volume Set*, Marcel Dekker: New York, **2004**.

[7] Y. Xia, P. Yang, Y. Sun, Y. Wu, B. Mayers, B. Gates, Y. Yin, F. Kim, H. Yan, *Adv. Mater.* **2003**, *15*, 353.

[8] I. W. Hamley, *Angew. Chem., Int. Ed.* **2003**, *42*, 1692.

[9] S. Bywater, *Adv. Polym. Sci.* **1979**, *30*, 89.

[10] N. Hadjichristidis, *J. Polym. Sci., Part A: Polym. Chem.* **1999**, *37*, 857.

[11] N. Hadjichristidis, M. Pitsikalis, S. Pispas, H. Iatrou, *Chem. Rev.* **2001**, *101*, 3747.

[12] K. Hatada, T. Kitayama, K. Ute, T. Nishiura, *J. Polym. Sci. Polym. Chem.* **2004**, *42*, 416.

[13] F. Vögtle, S. Gestermann, R. Hesse, H. Schwierz, B. Windisch, *Prog. Polym. Sci.* **2000**, *25*, 987.

[14] K. Inoue, *Prog. Polym. Sci.* **2000**, *25*, 453.

[15] J. Pyun, T. Kowalewski, K. Matyjaszewski, *Macro. Rapid Comm.* **2003**, *24*, 1043.

[16] M. Zhang, A. H. E. Müller, *J. Polym. Sci. Polym. Chem.* **2005**, *43*, 3461.

[17] K. L. Beers, S. G. Gaynor, K. Matyjaszewski, S. S. Sheiko, M. Möller, *Macromolecules* **1998**, *31*, 9413.

[18] G. Cheng, A. Böker, M. Zhang, G. Krausch, A. H. E. Müller, *Macromolecules* **2001**, *34*, 6883.

[19] H. G. Börner, K. Beers, K. Matyjaszewski, S. S. Sheiko, M. Möller, *Macromolecules* **2001**, *34*, 4375.

[20] M. Zhang, T. Breiner, H. Mori, A. H. E. Müller, *Polymer* **2003**, *44*, 1449.

[21] C. Cheng, K. Qi, E. Khoshdel, K. L. Wooley, *J. Am. Chem. Soc.* **2006**, *128*, 6808.

[22] H. Lee, W. Jakubowski, K. Matyjaszewski, S. Yu, S. S. Sheiko, *Macromolecules* **2006**, *39*, 4983.

[23] H. G. Boerner, D. Duran, K. Matyjaszewski, M. da Silva, S. S. Sheiko, *Macromolecules* **2002**, *35*, 3387.

[24] H.-I. Lee, K. Matyjaszewski, S. Yu, S. S. Sheiko, *Macromolecules* **2005,** *38*, 8264.

[25] D. Neugebauer, Y. Zhang, T, Pakula, K. Matyjaszewski, *Polymer* **2003**, *44*, 6863.

[26] D. Neugebauer, Y. Zhang, T, Pakula, G. Wegner, K. Matyjaszewski, *Macromolecules* **2005,** *38*, 8687.

[27] D. Neugebauer, M. Theis, T. Pakula, G. Wegner, K. Matyjaszewski, *Macromolecules* **2006**, *39*, 584.

[28] K. Ishizu, J. Satoh, K. Toyoda, A. Sogabe, *J. Mater. Sci.* **2004**, *39*, 4295.

[29] K. Matyjaszewski, S. Qin, J. R. Boyce, D. Shirvanyants, S. S. Sheiko, *Macromolecules* **2003**, *36*, 1843.

[30] J. R. Boyce, D. Shirvanyants, S. S. Sheiko, D. A. Ivanov, S. Qin, H. Boerner, K. Matyjaszewski, *Langmuir* **2004**, *20*, 6005.

[31] M. Schappacher, C. Billaud, C. Paulo, A. Deffieux, *Macromol. Chem. Phys.* **1999**, *200*, 2377.

[32] D. Neugebauer, Y. Zhang, T. Pakula, S. S. Sheiko, K. Matyjaszewski, *Macromolecules* **2003**, *36*, 6746.

[33] J. Rühe, M. Ballauff, M. Biesalski, P. Dziezok, F. Gröhn, D. Johannsmann, N. Houbenov, N. Hugenberg, R. Konradi, S. Minko, M. Motornov, R. R. Netz, M. Schmidt, C. Seidel, M. Stamm, T. Stephan, D. Usov, H. Zhang, *Adv. Polym. Sci.* **2004**, *165*, 79.

[34] C. Li, N. Gunari, K. Fischer, A. Janshoff, M. Schmidt, *Angew. Chem., Int. Ed.* **2004**, *43*, 1101.

[35] S. Muthukrishnan, M. Zhang, M. Burkhardt, M. Drechsler, H. Mori, A. H. E. Müller, *Macromolecules* **2005**, *38*, 7926.

[36] B, Zhang, K. Fischer, M. Schmidt, *Macromol. Chem. Phys.* **2005**, *206*, 157.

[37] E. Hempel, H. Huth, M. Beiner, *Thermochimica Acta* **2003**, *403*, 105.

[38] D. P. Chatterjee, B. M. Mandal, *Macromol. Symp.* **2006**, *240*, 224.

[39] Y. Ma, X. Zheng, F. Shi, Y. Li, S. Sun, *J. Appl. Polym. Sci.* **2003**, *88*, 1622.

[40] J. Jang, B.-S. Kim, *J. Appl. Polym. Sci.* **2000**, *77*, 903.

[41] Y. Feng, C. F. Xiao, *J. Appl. Polym. Sci.* **2006**, *101*, 1248.

[42] M. K. Mishra, J. Bradley, R. G. Saxton, A. Duggal, *J. Polym. Sci. Polym. Chem.* **2001**, *39*, 947.

[43] B. Sannigrahi, S. Sivaram, *Macromol. Chem. Phys.* **1998**, *199*, 463.

[44] W. Xu, X. Zhu, Z. Cheng, J. Chen, *J. Appl. Polym. Sci.* **2003**, *90*, 1117.

[45] V. Raghunadh, D. Baskaran, S. Sivaram, *Polymer* **2004**, *45*, 3149.

[46] D. P. Chatterjee, B. M. Mandal, *Polymer* **2006**, *47*, 1812.

[47] A. T. Skjeltorp, *Phys. Rev. Lett* **1983**, *51*, 2306.

[48] R. Krauss, B. Fischer, Y. Xu, A. H. E. Müller, R. Richter, submitted.

[49] K. Matyjaszewski, D. A. Shipp, J.-L. Wang, T. Grimaud, T. E. Patten, *Macromolecules* **1998**, *31*, 6836.

[50] B. S. Sumerlin, D. Neugebauer, K. Matyjaszewski, *Macromolecules* **2005**, *38*, 702.

[51] D. Neugebauer, B. S. Sumerlin, K. Matyjaszewski, B. Goodhart, S. S. Sheiko, *Polymer* **2004**, *45*, 8173.

[52] H. Becker, A. H. E. Müller, **2006**, unpublished results.

[53] L. Gold, *J. Chem. Phys.* **1958**, *28*, 91.

[54] W. Burchard, *Adv. Polym. Sci.* **1999**, *143*, 113.

Supporting information:

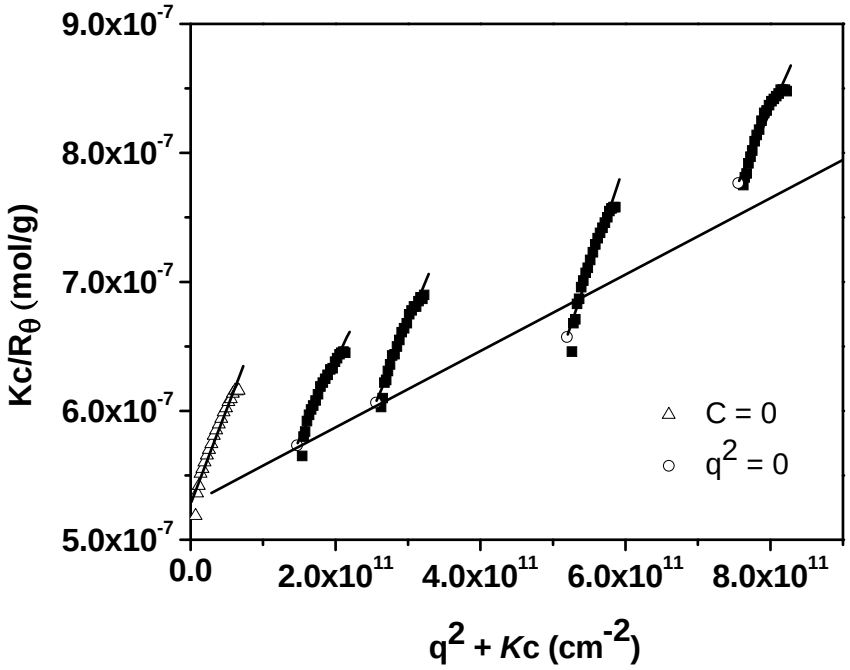

Figure S1. Zimm plot of brush 1 in THF. K = 2.63×10^{14}cm/g.

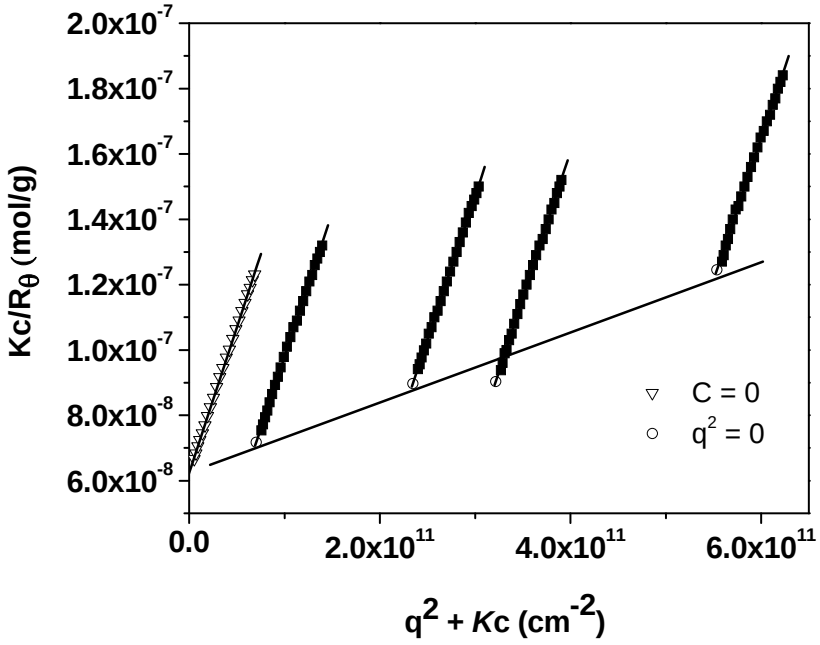

Figure S2. Zimm plot of Brush 3 in THF. K = 1.04×10^{14}cm/g.

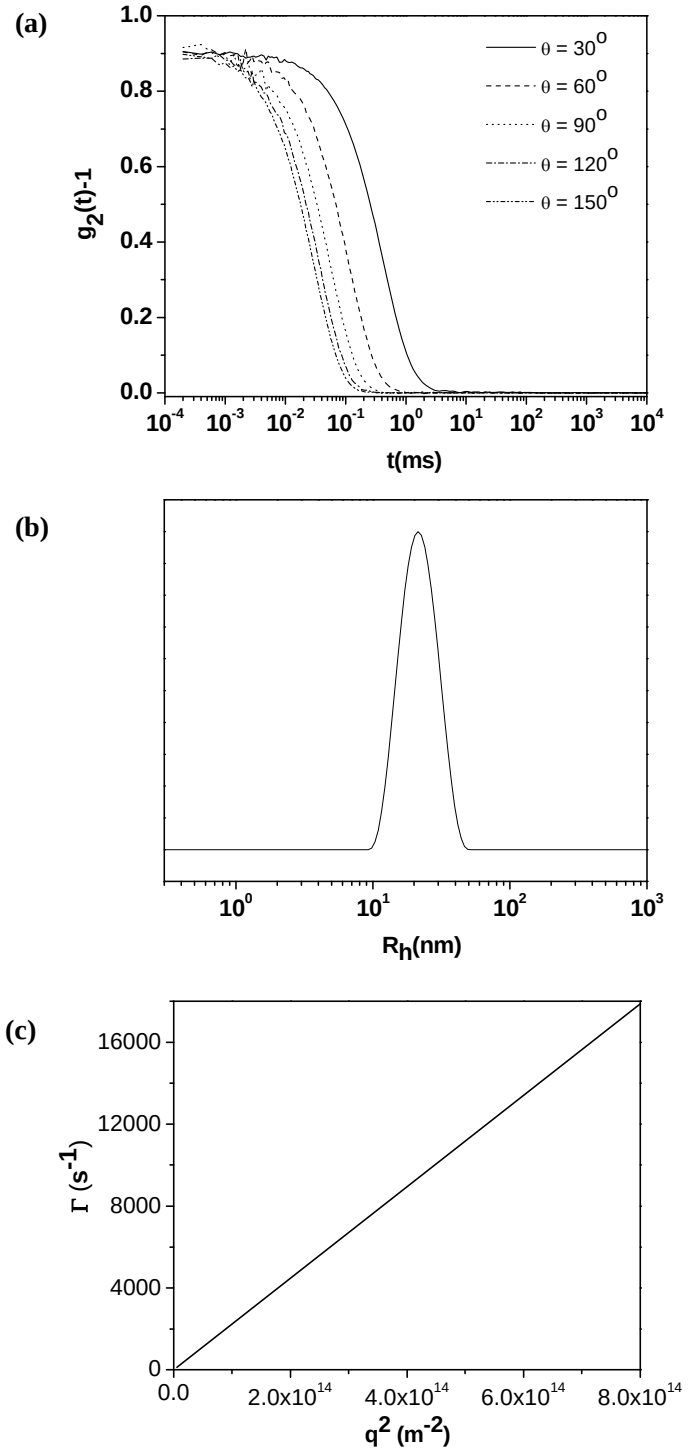

Figure S3. DLS of brush 1: (a) Normalized intensity correlation functions at different scattering angles, (b) hydrodynamic radius distribution at scattering angle of 90°, and (c) dependence of decay rate on the square scattering vector.

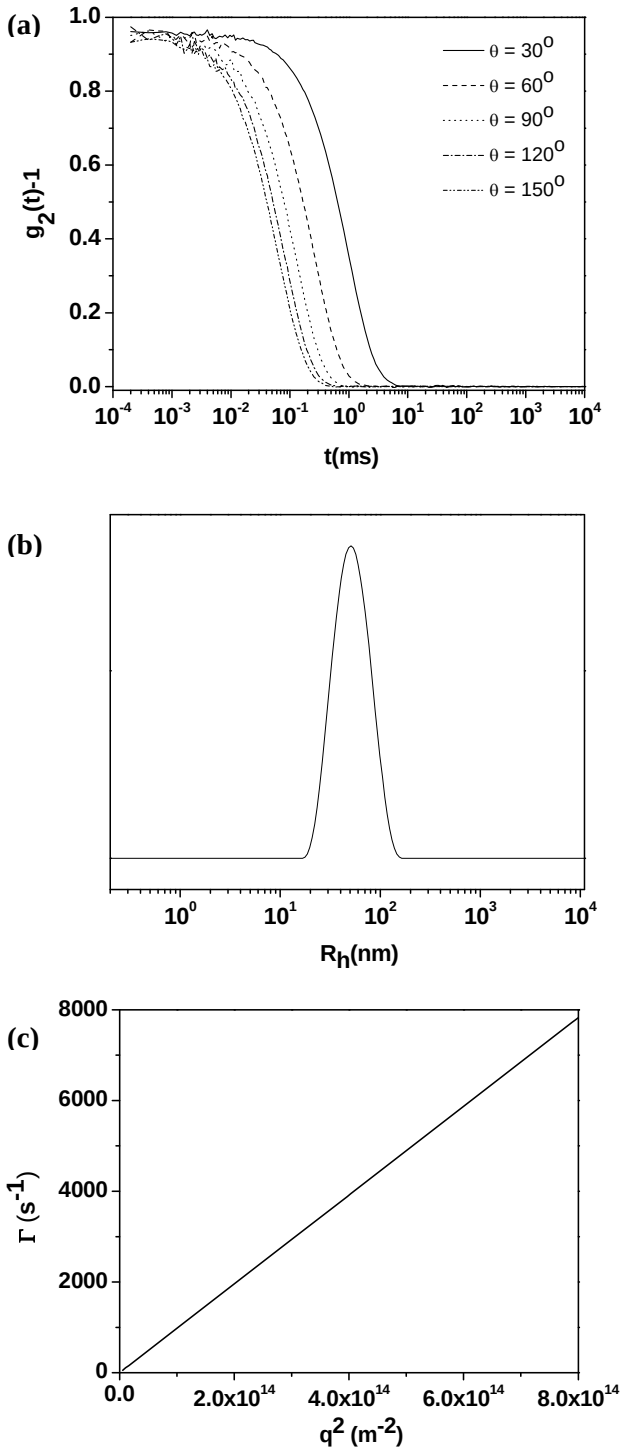

FigureS4. DLS of brush 3: (a) Normalized intensity correlation functions at different scattering angles, (b) hydrodynamic radius distribution at scattering angle of 90°, and (c) dependence of decay rate on the square scattering vector.

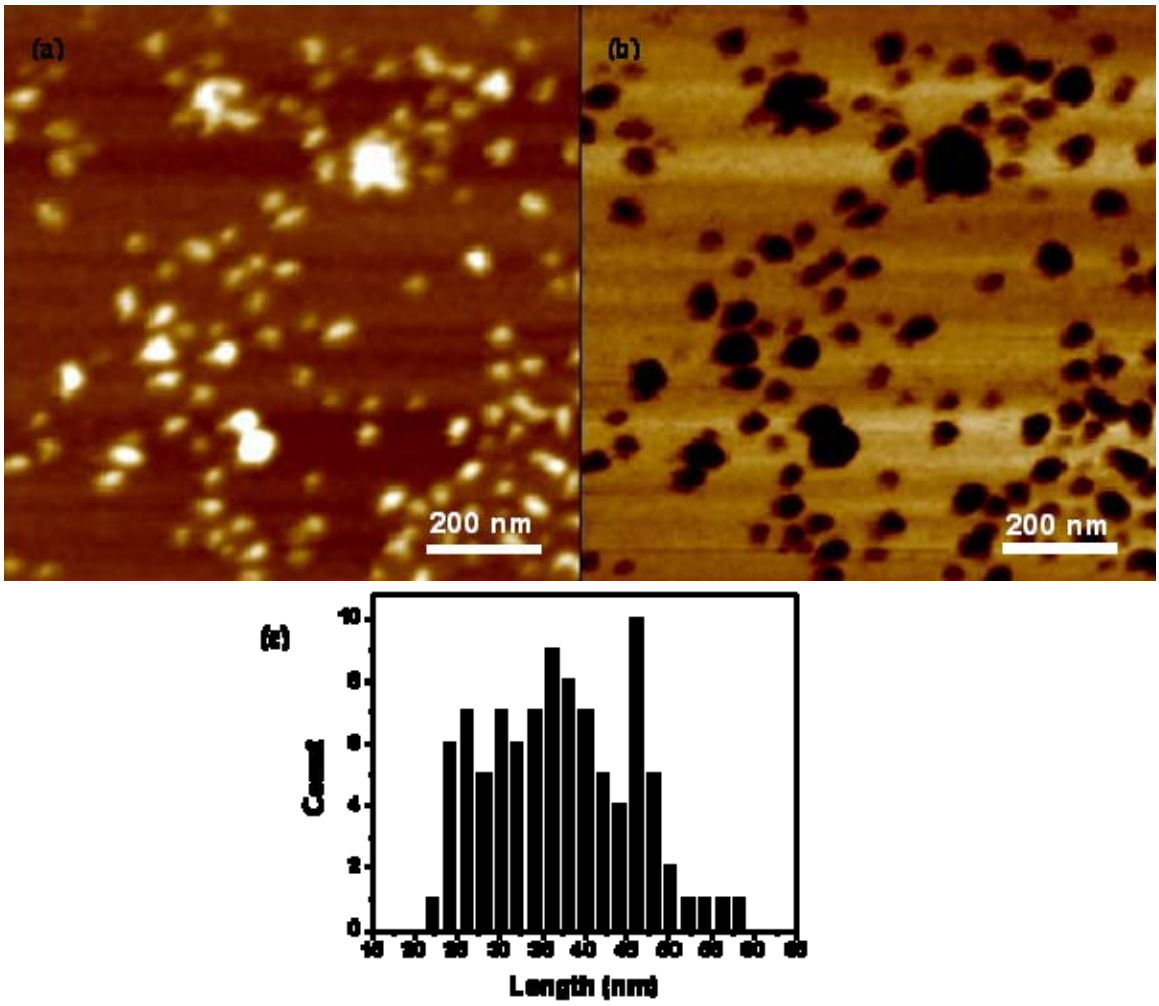

Figure S5. AFM of brush 2: (a) height image (z-range 4 nm), (b) phase image (z range 10^{o}) and (c) histogram of the contour length for 96 molecules

4. pH and Salt Responsive Poly(N,N-dimethylaminoethyl methacrylate) Cylindrical Brushes and their Quaternized Derivatives

Youyong Xu[a], Sreenath Bolisetty[b], Markus Drechsler[a], Bing Fang[a], Jiayin Yuan[a], Matthias Ballauff[b], Axel H. E. Müller*[,a]

[a]Makromolekulare Chemie II , [b]Physikalische Chemie I, and [a,b]Bayreuther Zentrum für Kolloide und Grenzflächen, Universität Bayreuth, D-95440 Bayreuth, Germany

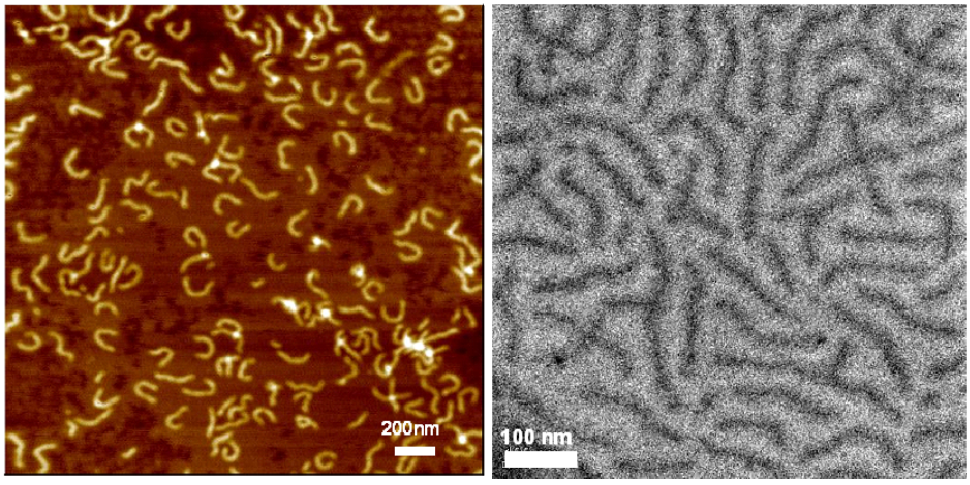

Published in *Polymer* **2008**, 49, 3957-3964

Abstract

We present the synthesis and characterization of poly(N,N-dimethylaminoethyl methacrylate) (PDMAEMA) cylindrical brushes, their pH responsiveness, and the corresponding quaternized poly{[2-(methacryloyloxy)ethyl] trimethylammonium iodide} (PMETAI) brushes. PDMAEMA brushes were prepared by atom transfer radical Polymerization (ATRP) using the grafting-from strategy. Initiating efficiencies of the ATRP processes were determined by cleaving the side-chains and gel permeation chromatography (GPC) analysis. Due to the slow initiation and steric hindrance, the initiating efficiency is only around 50%. PDMAEMA brushes showed worm-like structures and pH responsiveness, as proven by dynamic light scattering (DLS), atomic force microscopy (AFM), and cryogenic transmission electron microscope (cryo-TEM) measurements. Strong cationic polyelectrolyte PMETAI brushes were produced by quaternization of the PDMAEMA brushes. AFM and cryo-TEM images showed similar worm-like morphologies for the PMETAI brushes. The PMETAI brushes collapsed in solution with high concentration of monovalent salt, as proven by DLS and AFM results.

Keywords

PDMAEMA, PMETAI, ATRP, polyelectrolytes, cylindrical polymer brushes, pH responsive, cryo-TEM, AFM, DLS

Introduction

With the rapid development of nano-science and nanotechnology, scientists' attention has been shifting from the preparation of various nanostructures and nano-materials to manipulable nano-devices[1, 2]. Although researchers have long been successful in the microscopic motors, actuators, or sensors, the same concept in the nanometer scale has met great challenges due to the special properties of nano-objects.

In recent years, it became obvious that polymers can play an important role in building smart and controllable nano-objects owing to their natural advantages[3, 4]. Firstly, the size of the polymer chains ranges in the nanometer scale. Secondly, polymers show diversified topologies like linear, star-like, dendritic, comb-shaped and crosslinked structures. Moreover, they can also self-assemble into different structures. Thirdly, because of their vast possibilities of functionalities, polymer can respond to different external or internal stimuli, such as pH, solvent, ions, temperature, radiation, electric or magnetic field [5].

Among polymers of different structures, cylindrical polymer brushes (CPBs) have drawn increasing attention for their potential as single molecular responsive nano-objects. When the grafting density of polymer chains to a much longer linear chain is high enough, a cylindrical polymer brush is formed[6-9]. Because of the anisotropic nature and the worm-like structure, cylindrical brushes demonstrate special solution and bulk properties[10]. So far, three different strategies have been developed for the preparation of CPBs: grafting-onto[11], grafting-from[12, 13] and grafting-through[7]. Every strategy has its own advantages and disadvantages. Different controlled/living polymerization techniques have also been applied to prepare well-defined CPBs: atom transfer radical polymerization (ATRP)[12, 14, 15], nitroxide mediated radical polymerization (NMP)[16, 17], ring-opening polymerization (ROP)[18] and ring-opening metathesis polymerization (ROMP)[19].

There are already several examples of using CPBs as responsive nano-objects. Schmidt et al showed that poly(N-isopropylacrylamide) (PNIPAAm) polymer brushes can transform from worm-like structures into spheres when the temperature is higher than the lower critical soluble temperature (LCST)[20]. Similar brushes with different backbone or side chains were also reported by McCarley et al. [21] and Matyjaszewski et al.[22].

Sheiko et al.[23] and Möller et al.[24] reported the conformational transition of cylindrical polymer brushes on a surface due to lateral pressure stimuli. Matyjaszewski et al. successfully prepared photo-tunable temperature responsive core-shell type cylindrical brushes[25].

Polyelectrolytes are macromolecules carrying covalently bound anions or cationic groups with counterions providing electroneutrality[26, 27]. Due to the Coulombic interactions they demonstrate special solution properties, which are strongly influenced by the type and concentration of salt in aqueous solution.[28] For weak polyacids and –bases the pH value is another important parameter since it controls the ionization degree. Inspired by these special features of polyelectrolytes, the corresponding cylindrical polymer brushes may display totally different responsiveness compared to uncharged cylindrical brushes, which could be used for building smart single-molecular nano-objects. Although there are already several examples of polyelectrolyte cylindrical polymer brushes[29-32], most of the research was concentrated on the synthesis work. Few were conducted on the responsiveness and the transition of the polyelectrolyte cylindrical brushes.

Herein, we describe the synthesis of poly(N,N-dimethylaminoethyl methacrylate) (**PDMAEMA**) cylindrical brushes and their quaternized salts, poly{[2-(methacryloyloxy)ethyl] trimethylammonium iodide} (**PMETAI**) brushes. Previously, our group has reported on the multi-responsive solution properties of PDMAEMA linear and star polymers and their quaternized derivatives[33-35]. Due to the weak polyelectrolyte nature of the PDMAEMA, the corresponding cylindrical polymer brushes are expected to show different properties. Matyjaszewski et al. showed the temperature responsiveness of the PDMAEMA brushes at various concentrations in solution[36]. In this study, we will demonstrate the response of this type of brushes on pH and the concentration of monovalent salt. A detailed study with added di- and trivalent salts will be published elsewhere. The responsiveness of the PDMAEMA and PMETAI brushes could be potentially applied in nano-scale sensor systems or nano-actuator systems[37].

Experimental section:

Materials. CuCl (97%, Aldrich) was purified by stirring with acetic acid overnight. After filtration, it was washed with ethanol and diethyl ether and then dried in vacuum oven. $CuCl_2$ (99%, Acros) was used without purification. 2-dimethylaminoethyl methacrylate (98%, Merck) was purified by passing through basic alumina columns before polymerizations. *N*,*N*,*N*',*N*'',*N*''',*N*''''-hexamethyltriethylenetetraamine (HMTETA, Aldrich) was distilled before use. The synthesis of the macroinitiator poly(2-(2-bromoisobutyryloxy)ethyl methacrylate) (PBIEM) (DP_n = 1500, PDI = 1.08) by anionic polymerization was reported previously[15]. Methyl iodide was purchased from Aldrich and was used as is. All other solvents and chemicals were used as received. Regenerated cellulose membranes were used for the dialysis (ZelluTrans with MWCO = 4000 – 6000 Da from Roth, Karlsruhe, and Spectra/Pore 7 with MWCO = 1000 Da).

Polymerizations. All polymerizations were carried out in round-bottom flasks sealed with rubber septa. A typical example of the synthesis of PDMAEMA cylindrical brushes is described as follows: PBIEM (55.8 mg, 0.2 mmol of initiating α-bromoester groups) and HMTETA (46.1 mg, 0.2 mmol) were dissolved in anisole (31.4 g) in a round-bottom flask and stirred overnight to assure the complete dissolution of the high molecular weight macroinitiator. Then the monomer DMAEMA (15.7 g, 0.1 mol) was injected via a syringe and stirred for 15 min. $CuCl_2$ (5.4 mg, 0.04 mmol) was added, followed by Argon purging for 5 minitues. $CuCl_2$ was dissolved and the color became brown. Then CuCl (19.8 mg, 0.2 mmol) was added and the flask was purged with argon for 15 min. About 0.5 mL of solution was taken out with an argon-purged syringe as an initial sample for conversion measurement by ^{1}H NMR. The round-bottom flask was then inserted into a water bath at room temperature (25 ^{o}C). HMTETA was injected by argon-purged syringe to start the reaction. The solution immediately turned green. Small amounts of samples were taken out at intervals to check the monomer conversion by ^{1}H NMR. After 12.5 h, the reaction solution became viscous and was stopped by opening to the air. Final conversion determined by ^{1}H NMR reached 6.5%. THF was added to dilute the solution. After passing through a basic alumina column, the solution was concentrated by a rotary evaporator. Afterwards, it was precipitated into cold *n*-hexane to remove the residual monomer and other impurities. Then the polymer was re-dissolved in certain amount of

dioxane. A part of the solution was subjected to freeze-drying and the other part was further diluted by dioxane and dialyzed against pure dioxane for 7 days. After the dialysis, a part of the dioxane solution was dialyzed against water for 7 days to switch the solvent from dioxane to water.

Synthesis of poly{[2-(methacryloyloxy)ethyl] trimethylammonium iodide} cylindrical brushes: To quaternize the obtained PDMAEMA brushes, the polymer was dissolved in dioxane. Methyl iodide was added at room temperature at a molar ratio of 2 compared to amino groups. After around 20 min, the solution became turbid. Stirring was kept for 2 days to ensure the full reaction. Then dioxane was decanted and the polymer was washed several times with diethyl ether. Afterwards, the quaternized polymers were dissolved in water and dialyzed against pure water for one week. Finally, it was freeze dried to get white powders.

Cleavage of the side chains from the PDMAEMA brushes: The cleavage of the side chains from the quaternized PDMAEMA brushes was carried out by alkaline hydrolysis. One typical reaction is described as follows: 100 mg of quaternized PDMAEMA brushes and about 10 ml of concentrated NaOH (18 M) aqueous solution were put into a PE vial and heated for 10 days at 90 °C. After one hour at 90 °C, some more drops of water were added to dissolve some suspending polymers. A dark brown precipitate was observed after the reaction and the smell of amine is also quite strong. The mixture was then cooled down and the supernatant solution was removed by syringe to separate it from the precipitate. Concentrated HCl solution was added to the solution to tune the pH to around 4. This solution was freeze-dried and redissolved in water. Dialysis was carried out against pure water by using regenerated membranes (Millipore SpectraPore 7 MWCO 1000) over 3 days. In order to ensure the full protonation of the final product, poly(methacrylic acid) (PMAA), a small amount of HCl was added before freeze-drying the solution. ^{1}H-NMR measurement in D_2O was performed to check the conversion of the ester cleavage. Aqueous GPC was used to check the molecular weight of the final PMAA product with a PMAA calibration.

Characterization. *^{1}H NMR* was measured on a Bruker AC-250 instrument at room temperature with $CDCl_3$ or D_2O as the solvent.

The apparent molecular weights of the PDMAEMA brushes were characterized by conventional *gel permeation chromatography (GPC)* using 0.05 M solution of LiBr in 2-*N*-methylpyrrolidone (NMP) as eluent at a flow rate of 1.0 mL/min at room temperature. PSS GRAM columns (300 mm×8 mm, 7 μm): 10^3, 10^2 Å (PSS, Mainz, Germany) were thermostated at 70 °C. An RI detector and a UV detector (λ = 270 nm) were used. Polystyrene standards (PSS, Mainz) with narrow molecular weight distribution were used to calibrate the columns, and methyl benzoate was used as the internal standard.

An *aqueous GPC* (internal standard, ethylene glycol; additives: 0.1 M NaN_3, 0.01 M NaH_2PO_4) was applied to obtain the molecular weight of PMAA (PMAA standards, PSS, Mainz). Column set: two 8mm PL Aquagel-OH columns (mixed and 30 Å), operated at 35°C and RI detection.

Static light scattering (SLS) was measured on a Sofica goniometer using a He-Ne laser (λ = 632.8 nm). Prior to the light scattering measurements, the sample solutions were filtered 3 times by using Millipore Teflon filters with a pore size of 0.45 μm. Five concentrations of the PLMA cylindrical brush solutions in dioxane were measured at angles in the range from 30 ^{o} to 150 ^{o}. The weight-average molecular weight, M_w, of the PDMAEMA brushes was obtained by the analysis of the Zimm-plots. The refractive index increment of the PDMAEMA cylindrical brushes in dioxane solution at 25 °C was measured to be dn/dc = 0.0543 mL/g using a PSS DnDc-2010/620 differential refractometer.

Dynamic light scattering (DLS) was carried out on an ALV DLS/SLS-SP 5022F compact goniometer system with an ALV 5000/E correlator and a He-Ne laser (λ = 632.8 nm) at an angle of 90^{o}. For the PDMAEMA brush solutions in dioxane, the sample solutions were filtered 3 times by using Millipore Teflon filters with a pore size of 0.45 μm before the light scattering measurements. For the water solution of PDMAEMA brushes at different pH and quaternized brushes at different salt concentration, the sample solutions were filtered by Millipore nylon filters with pore size of 0.45 μm. CONTIN analyses were performed for the measured intensity correlation functions. Apparent hydrodynamic radii, R_h, of the cylindrical brushes were calculated according to the Stokes-Einstein equation.[38] All the measurements were carried out at 25 °C. For the

measurement of quaternized brushes in salt solutions, the change of viscosity of the aqueous solutions was taken into account. For salt concentrations higher than 0.2 M the obtained hydrodynamic radius was divided by the relative viscosity [33].

Atomic force microscopy (AFM) measurements were performed on a Digital Instruments Dimension 3100 microscope operated in tapping mode. The micro-cantilever used for the AFM measurements were from Olympus with resonant frequency between 284.3 kHz and 386.0 kHz, and spring constant ranging from 35.9 to 92.0 N/m. For the PDMAEMA brushes in THF solution, the samples were prepared by dip-coating from very dilute (0.01 g/L) THF solutions of PDMAEMA brushes onto freshly cleaved mica surfaces. For the measurement of the quaternized brushes in water, very dilute aqueous solutions (0.02 g/L) were prepared and were spin-coated on freshly cleaved mica.

For *cryogenic transmission electron microscopy (cryo-TEM)* studies of PDMAEMA brushes and the quaternized brushes, a drop of the sample (aqueous solution, concentration around 0.01 g/L) was put on an untreated bare copper TEM grid (600 mesh, Science Services, München, Germany), where most of the liquid was removed with blotting paper, leaving a thin film stretched over the grid holes. The specimens were instantly shock vitrified by rapid immersion into liquid ethane and cooled to approximately 90 K by liquid nitrogen in a temperature-controlled freezing unit (Zeiss Cryobox, Zeiss NTS GmbH, Oberkochen, Germany). The temperature was monitored and kept constant in the chamber during all the sample preparation steps. After the sample is frozen, it was inserted into a cryo-transfer holder (CT3500, Gatan, München, Germany) and transferred to a Zeiss EM922 EFTEM. Examinations were carried out at temperatures around 90 K at an acceleration voltage of 200 kV. Zero-loss filtered images (ΔE = 0 eV) were taken under reduced dose conditions (100-1000 electrons/nm2). All images were registered digitally by a bottom-mounted CCD camera system (Ultrascan 1000, Gatan) combined and processed with a digital imaging processing system (Gatan Digital Micrograph 3.10 for GMS 1.5).

Results and discussion

Syntheses of PDMAEMA brushes

The PDMAEMA cylindrical brushes were prepared by the combination of anionic polymerization and ATRP using the grafting-from strategy. The synthesis of the backbone of the brushes by anionic polymerization with DP_n = 1500 and a very low polydispersity was reported previously by our group [15]. Scheme 1 shows the synthetic strategy of the PDMAEMA cylindrical brushes.

Scheme 1. Synthetic strategy of the PDMAEMA cylindrical brushes

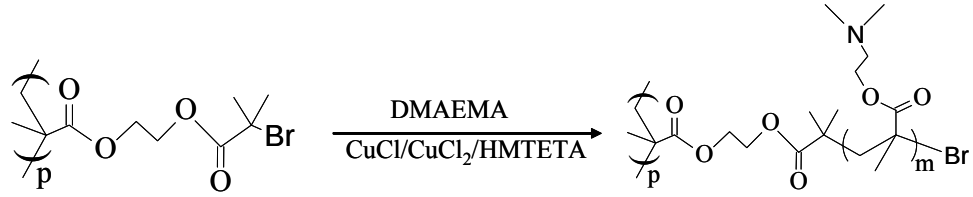

It has been known that the initiating efficiencies of grafting from the backbone for the synthesis of cylindrical brushes are limited due to the steric hindrance[39, 40]. In order to obtain relatively densely grafted cylindrical brushes, some points have to be taken into account. Matyjaszewski et al. have shown that reducing the monomer concentration and increasing the copper amount enhances the grafting efficiency[40]. It is also known that initiation of methacrylates is more efficient when bromine is exchanged to chlorine by the use of CuCl[41]. Using HMTETA as the ligand and anisole as the solvent has proved to work well for the ATRP of linear DMAEMA polymers[42]. Thus, for our system, we chose CuCl as the catalyst, HMTETA as the ligand and anisole as the solvent. Since the monomer DMAEMA is quite reactive, we added 20% $CuCl_2$ to the system to lower the rate of polymerization. Quite low monomer concentrations were used with the weight ratio of DMAEMA to anisole 1:2. Temperature also plays a very important role. Whereas crosslinked polymer was obtained at 70 ^{o}C, soluble polymers were achieved at room temperature. Table 1 lists the results of the polymerizations. It shows relatively low polydispersity for the brushes, considering the extremely high molecular weight. The molecular weights determined by conventional GPC were not true values since the compact structure of the brushes is not comparable with that of the linear polystyrene

standards. However, the calculated molecular weights do not deviate much from the true molecular weight determined by static light scattering in dioxane, indicating that the synthesis of the PDMAEMA brushes was successful.

Table 1. Synthesis, molecular characterization and light scattering measurements of PDMAEMA brushes [a]

Sample	B1	B2
Conversion[b]	6.5%	8.0%
$DP_{sc,calc}$ [c]	32	40
$10^{-5}M_{n,app,GPC}$ [d]	6.26	6.85
PDI_{app} [d]	1.33	1.35
$10^{-6}M_{n,calc}$ [e]	7.95	9.84
$10^{-6}M_{w,SLS}$ [f]	8.64	12.40
R_h [g], nm (PDI)	25 (0.126)	32 (0.165)

[a]ATRP at 25 °C with 33.3 wt % DMAEMA concentration in anisole and constant ratio of $s_0/[I]_0/[CuCl]_0/[CuCl_2]_0/[HMTETA]$ = 500:1:1:0.2:1. $DP_{n,backbone.}$= 1500. [b]Monomer conversion determined by ^1H NMR. [c]calculated DP_n of side-chains, $DP_{sc,calc}$= $([M]_0/[I]_0)\times$conversion. [d]Apparent values determined by conventional GPC with NMP as the eluent and PS calibration. [e]calculated from monomer conversion. $M_{n,calc}$= $(157\times DP_{sc,calc} + 279)\times DP_{n,backbone.}$ [f]determined by SLS in dioxane. [g]Hydrodynamic radius and polydispersity measured by DLS in dioxane.

Although conventional GPC cannot give true molecular weights of the brushes, it still can show the difference of the eluent volume changes between the brushes and the macroinitiator. Figure 1 shows the GPC eluent curves of the PDMAEMA brushes. They both demonstrate monomodal distributions, indicating good control of the ATRP grafting reactions. There is a coupling peak for the macroinitiator PBIEM, which has been reported before[15]. Since the coupling peak covers only a small part of the PBIEM polymer, and the polydispersity of the macroinitiator is very low, it does not influent the final brushes too much.

Solutions of PDMAEMA brushes in dioxane were also subjected to dynamic light scattering analysis. The plots of the decay rates versus the square of the scattering vector are linear and lead to the apparent hydrodynamic radii given in Table 1. The CONTIN plots of both brushes (at 90° scattering angle) are monomodal and the polydispersities, as determined by the cumulant method are below 0.2, demonstrating the narrow distribution of the PDMAEMA brushes.

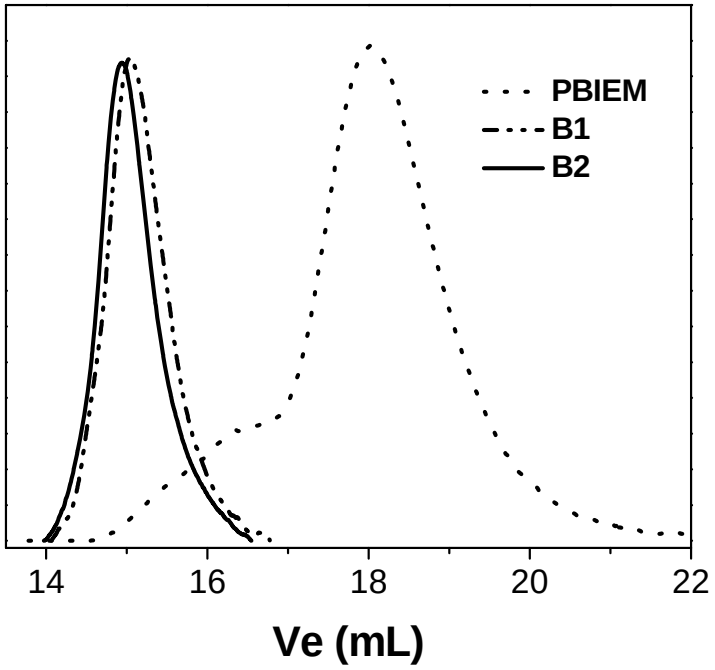

Figure 1. GPC curves of the PDMAEMA brushes in NMP (RI detection)

Figure 2 shows the ^{1}H NMR spectra of the PDMAEMA brushes. The two peaks at 4.1 and 4.3 ppm (a, a′), are assigned to the methylene protons between two ester groups in the PBIEM macroinitiator. When the PDMAEMA cylindrical brushes are formed, peak a and a′ disappear, while distinctive peaks from the dimethyl aminoethyl groups appear: methyl protons (c, 2.2 ppm) connected to the amino group, methylene protons (d, 2.5 ppm) neighboring to the amino groups, and the other methylene protons (e, 3.95 ppm) connected to the ester groups. Thus, the ^{1}H NMR spectra indicate the successful grafting of PDMAEMA from the PBIEM backbones.

Quaternization and grafting densities

The grafting-from strategy does not always provide full initiator efficiency, leading to lower than expected grafting densities. Since the grafting density influences the length, flexibility and other characteristics of the CPBs, its knowledge is important. The ester bonds connecting the side-chains to the backbone are used for the cleavage of the side-chains by a strong base. Because of the LCST behavior of PDMAEMA in aqueous solution at pH > 7, it is not convenient to cleave the PDMAEMA brushes' side chains in basic solutions. Thus, the brushes were quaternized by methyl iodide to their salt form, PMETAI, and subjected to a strong base and heating. This treatment not only cleaves the ester linkage between the side-chains and the backbone, but also the ester groups in the monomer units. Scheme 2 shows the procedures of the quaternization and cleavage reactions.

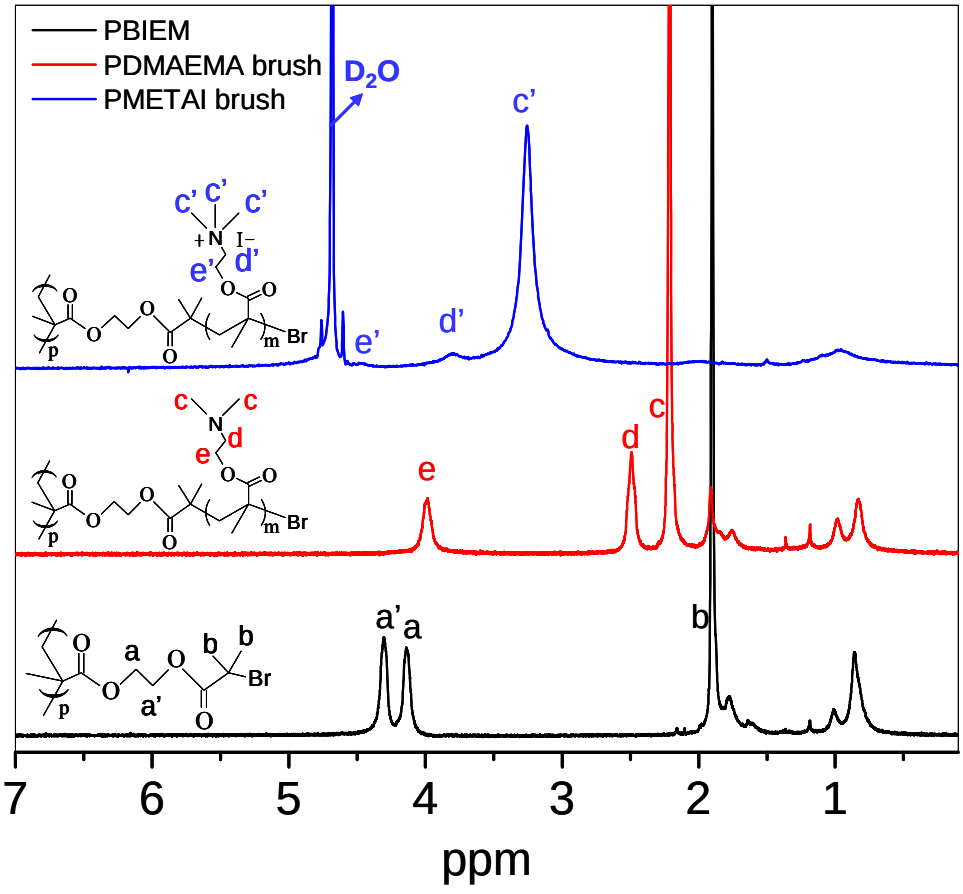

Figure 2. ^{1}H NMR of PBIEM, PDMAEMA brush and PMETAI brush

Scheme 2. Procedure for the quaternization and cleavage reactions

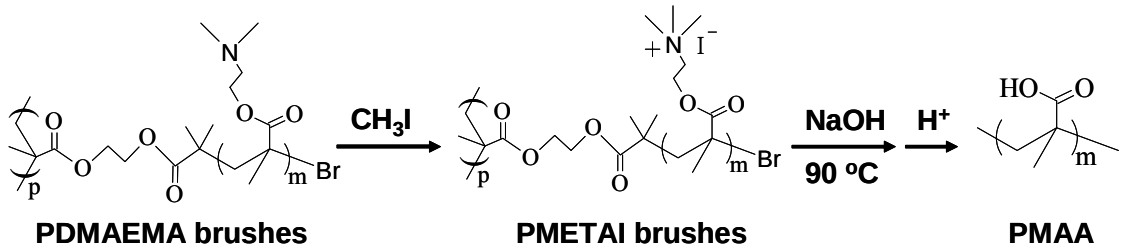

From Figure 2, we can compare the ^{1}H NMR spectra of the PDMAEMA brushes and the quaternized PMETAI brushes. After quaternization, the distinct peaks from the methylaminoethyl groups all shift to higher chemical shift: methyl groups connected to the ammoniums (c', 3.2 ppm), methylene groups adjacent to the ammoniums (d', 3.75 ppm) and the other methylene groups linking to the ester groups (weak peak e', 4.4 ppm). It is also found there are no peaks left at the original peak positions (c, d, e), which indicates quantitative quaternization of the PDMAEMA brushes. Thus, strong cationic polyelectrolyte PMETAI brushes are obtained.

The cleavage of arms from PMETAI star polymers has already been reported by our group[33]. The similar procedure was used to detach the side-chains from the PMETAI brushes. The final product, poly(methacrylic acid) (PMAA), was separated and purified for ^{1}H NMR and aqueous GPC analyses. ^{1}H NMR and water GPC eluent curves of the PMAA cleaved from quaternized B2 sample are shown in the Supporting Information.

The GPC results and calculated initiating efficiencies are listed in Table 2. According to the GPC results, the cleaved PMAA shows mono-modal distribution. However, the polydispersity is relatively high (1.38), which is close to the value 1.33 expected for slow initiation[43]. Since DMAEMA is a quite active monomer and there is remarkable steric hindrance on the backbone, the propagation rate of DMAEMA chains is expected to be much higher than that of initiation. In both brushes the initiating efficiencies are ca. 50%, irrespective of halogen exchange and lower monomer concentration used. Nevertheless, the grafting-from strategy is effective for the preparation of cylindrical brushes despite its inevitable relatively low grafting density.

Thus, both brushes consist of 1500 monomer units in the backbone and carry ca. 750 side chains of DP_n = 65 and 82 for brushes B1 and B2, respectively.

Table 2. GPC results of PMAA arms obtained after cleaving and initiating efficiencies

sample	PDMAEMA brush	PMETAI brush[a]	10^3 $M_{n,GPC}$[b]	PDI[b]	$DP_{sc,calc}$[c]	$DP_{sc,GPC}$[d]	f[e]
PMAA1	B1	Q1	5.6	1.38	32	65	50%
PMAA2	B2	Q2	7.1	1.38	40	82	49%

[a]Q1 and Q2 are the quaternized brushes corresponding to the PDMAEMA brushes B1 and B2. [b]Determined by water GPC using PMAA calibration. [c]from Table 1. [d]$M_{n,GPC}$/86. [e]Initiating efficiencies, $f = DP_{sc,calc}/DP_{sc,GPC}$.

AFM imaging of the PDMAEMA brushes

The morphology of the PDMAEMA brushes is shown by AFM. Figure 3 displays the AFM height images of sample B1 and B2, dip-coated on the freshly cleaved mica surface from THF solution. From Figure 3, we see that the B1 brushes are quite curved while B2 brushes are more stretched, indicating a higher persistence length. Nevertheless, their average lengths are both around 170 nm, which is ca. 45% of the contour length of the totally stretched backbone length (L_c = 1500×0.25 nm = 375 nm), probably due to the low grafting density and the not too long side-chains (65 and 82 monomer units, respectively).

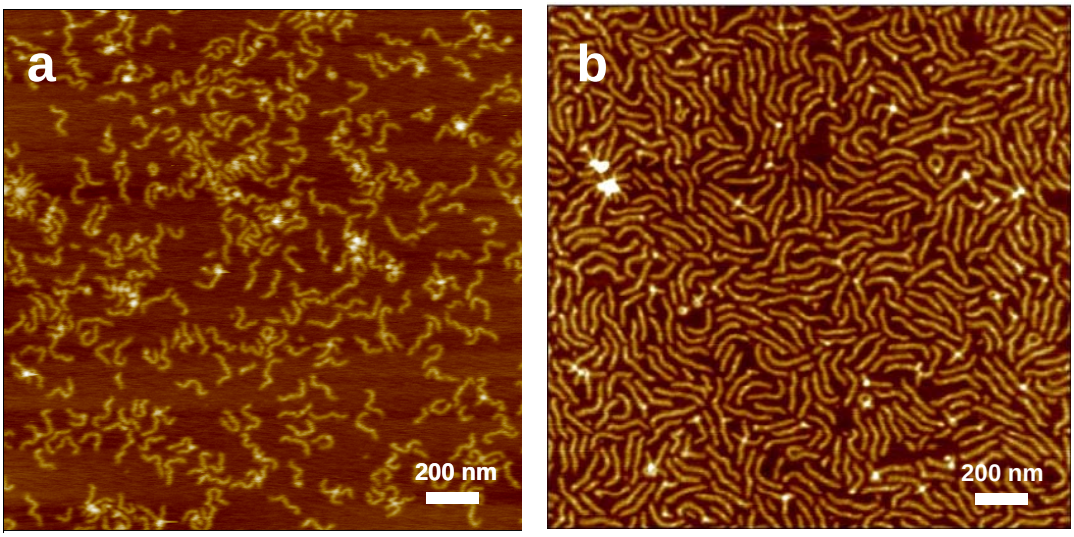

Figure 3. AFM height images of PDMAEMA brushes B1 (a) and B2 (b) obtained by dip-coating from 0.01 g/L THF solutions onto mica. The Z ranges for images (a) and (b) are 4 nm and 5 nm, respectively.

pH responsiveness of PDMAEMA brushes

Since PDMAEMA is a weak cationic polyelectrolyte, its degree of ionization depends on pH. The apparent pK_b value (pK_b = 14 - pH at 50% ionization) for stars with a large number of arms is around 8 [35] and we expect the same behaviour here. In the case of CPBs, a change in ionization is expected to induce structural changes. DLS measurements for the brushes at different pH values were carried out in water at a scattering angle of 90°. Figure 4 shows the hydrodynamic radii of the PDMAEMA brush B2 at different pH values. All measurements were performed in the absence of salt at very low concentration (0.2 g/L) to avoid intermolecular aggregation at high pH values. An obvious pH dependence of the apparent hydrodynamic radii is observed. Wheras R_h at pH 10 is close to the one obtained in dioxane, the values increase by 10 nm between pH 10 and pH 2, which is explained by the stretching of the PDMAEMA brushes at low pH (high ionization) and collapse at high pH.

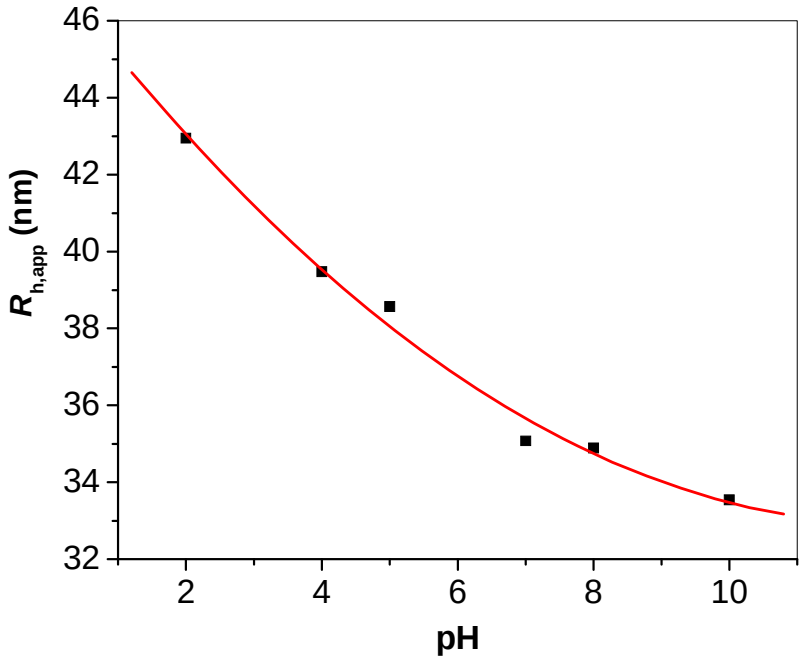

Figure 4. Hydrodynamic radii of PDMAEMA brush B2 in 0.2 g/L aqueous solution at different pH values

In order to see the true morphological changes of the PDMAEMA brushes, cryo-TEM measurements were performed at pH 2, pH 7 and pH 10 in the absence of salt. Figure 5

displays the cryo-TEM images of PDMAEMA brushes in aqueous solution at a concentration as low as 0.01 g/L. It is seen that the length of the PDMAEMA brushes at pH 7 is around 180 nm, which is slightly higher than that measured by AFM. In AFM, the brushes are tightly adsorbed at the mica surface and this surface effect must be taken into account when measuring the size of the brushes. In the cryo-TEM system, the solutions were vitrified in an extremely short time and the images reveal almost the true situations of the brushes in the solution state. At pH 7, the PDMAEMA brushes take a worm like structures and some of them are quite curved. At pH 2, most of the brushes are protonated and ionized, and they show more stretched morphologies. More remarkably, at pH 10, the brushes are strongly contracted with an average length around 110 nm, which is attributed to a collapse of the non-ionized PDMAEMA side chains.

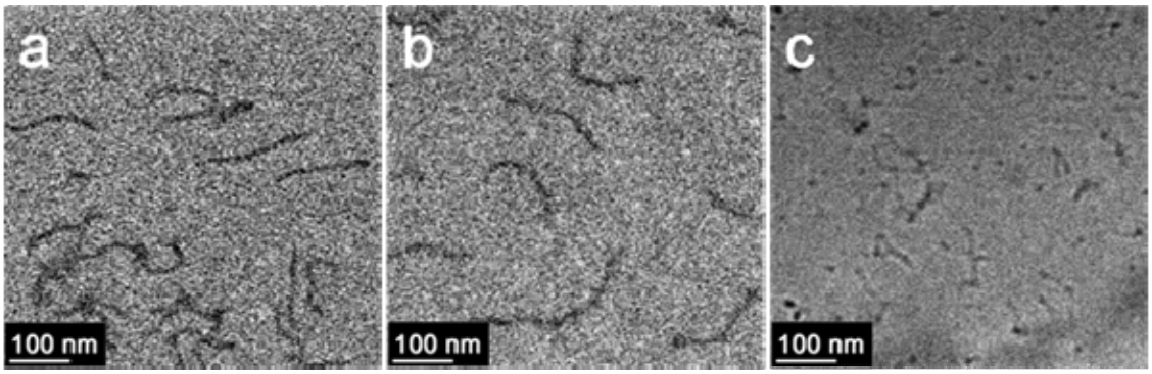

Figure 5. Cryo-TEM images of PDMAEMA brushes in vitrified 0.01 g/L aqueous solution at (a) pH 2, (b) pH 7 and (c) pH 10

Morphology of PMETAI cylindrical brushes

By quaternization with methyl iodide the weak polyelectrolyte PDMAEMA brushes are converted to strong polyelectrolyte brushes, that is, all side chains carry charges irrespective of the pH in the system. From the ^{1}H NMR spectra in Figure 2, the successful conversion was proven. Figure 6 shows typical AFM and cryo-TEM images of PMETAI brush Q2. On mica surface, the PMETAI brushes show a quite curved structure, which again is attributed to the strong interaction of the cationic brushes with negatively charged mica substrate. However, the worm-like structure of the charged CPBs is

immediately obvious. The length of the PMETAI brushes is around 180 nm, similar to that of the PDMAEMA brushes on surface or in solution.

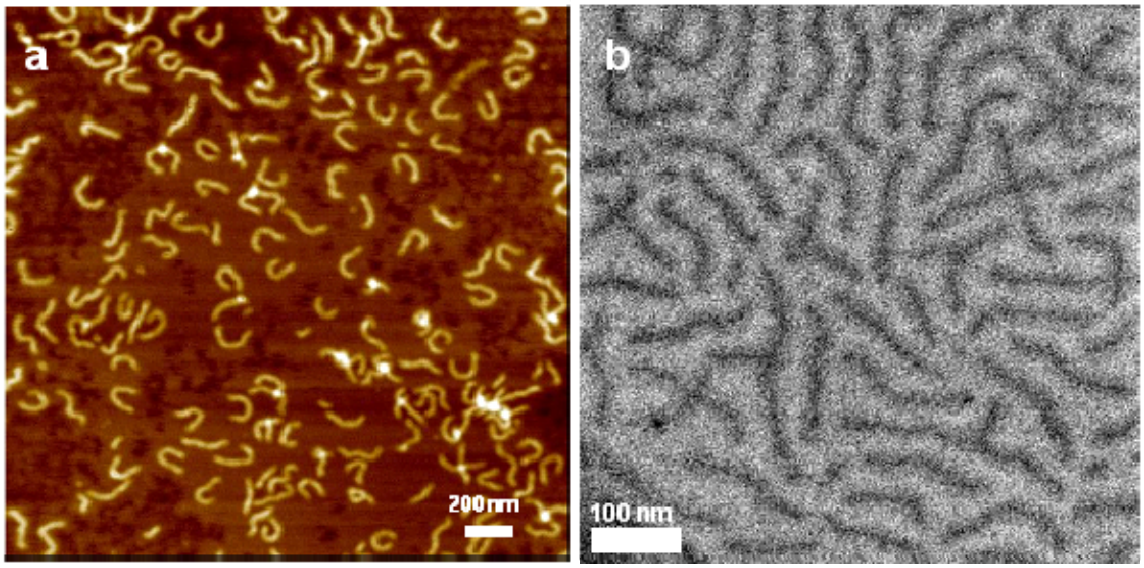

Figure 6. (a) AFM height image (Z range 7 nm) and (b) cryo-TEM image of PMETAI brushes

Effect of monovalent salt

Due to the strong Coulombic repulsion of the charged chains, the strong polyelectrolyte PMETAI brush assumes a rather elongated conformation. Although, due to Manning condensation, the majority of counterions are confined in the brush [44-47], the charge density is still high enough to considerably stretch the brush. Addition of salt to the solution will screen the electrostatic interaction within the polyelectrolyte. Thus, the stretching of the polyelectrolyte chains should be diminished and the conformation should be more collapsed. Figure 7 shows the change of the hydrodynamic radii of the PMETAI Q2 brush with increasing NaBr concentration. There is a remarkable decrease of the apparent R_h when salt is added. Increasing the NaBr concentration from 0 M to 1 M leads to a decrease of 8 nm in R_h. This marked change of the overall shape has already been studied for planar and spherical polyelectrolyte brushes[29, 48]. However, Schmidt et al.[29] reported no significant change of the R_g and R_h for quaternized polyvinylpyridine (PVP) brushes when the concentration of added salt was increased to 0.1 M. Here we performed the DLS measurements at a wider range of salt concentrations (up to 2M of NaBr). Whereas the apparent hydrodynamic radius is equal to the one for

the non-quaternized brush at pH = 2, we indeed find a pronounced decrease of R_h at high salt concentration. The reasons for this discrepancy are not obvious and may be traced back to a difference in grafting density, which is higher for the PVP brushes synthesized by the polymerization of PVP macromonomers.

When the salt concentration is higher than 1 M, the apparent R_h increases again, as has also been found for the spherical polymer brushes[49]. As already pointed out there, bromide ions may have specific interactions with cationic polyelectrolyte chains. Hence, a solution of NaBr of sufficient concentration will lead to an adsorption of bromine ions onto the polyelectrolyte chains which is followed by a re-swelling of the brushes.

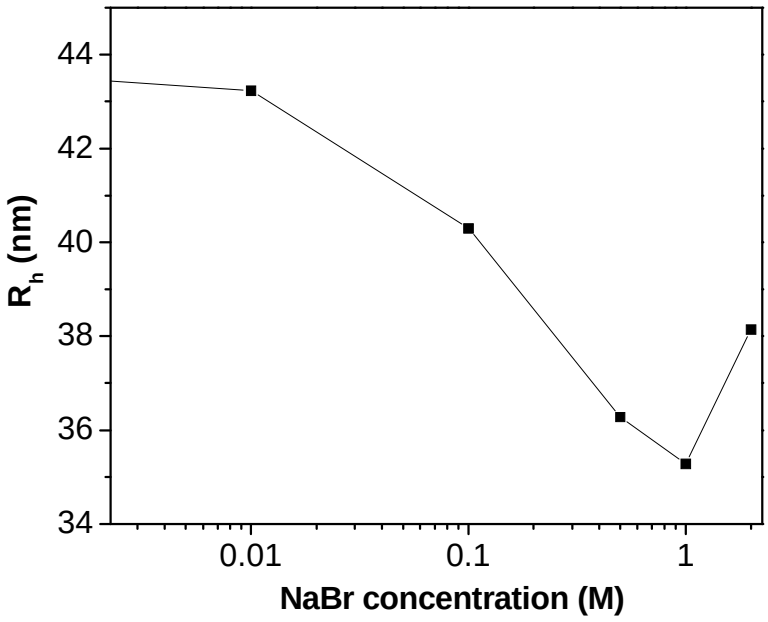

Figure 7. Apparent hydrodynamic radii of the PMETAI brushes as a function of NaBr concentration.

The collapse of the PMETAI brushes at high salt concentration can directly be visualized by AFM. Figure 8 shows the AFM height image of the PMETAI brushes on mica, spin-coated from its 0.5 M NaBr solution. It is clearly seen that most of the brushes show an ellipsoid-like conformation and the length of the brushes is less than 100 nm, which is much lower than that shown in Figure 6.

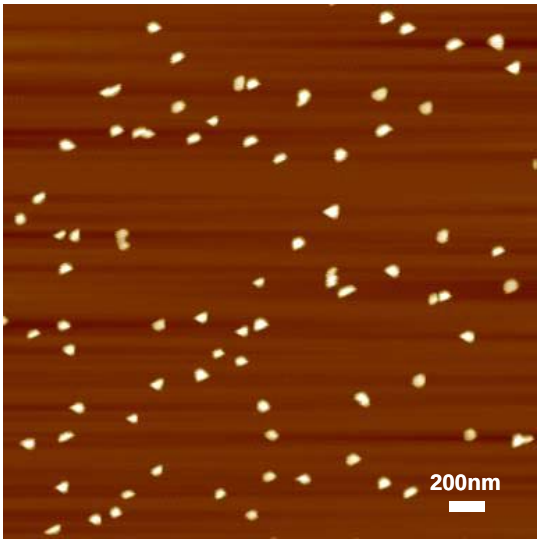

Figure 8. AFM height image of PMETAI brushes on mica spin-coated from 0.5 M NaBr solution. Z range 12 nm

Conclusions

We have demonstrated the successful preparation of PDMAEMA cylindrical brushes using the grafting-from strategy by ATRP. The initiating efficiencies of the ATRP processes were determined by cleaving the side-chains and GPC analysis. The initiating efficiency is around 50%, probably due to slow initiation caused by steric hindrance. DLS, SLS and AFM measurements clearly show the worm-like structure of the PDMAEMA brushes in solution. The brushes also show pH responsiveness as proven by DLS and cryo-TEM at different pH values. ^{1}H NMR confirms the successful quaternization of PDMAEMA brushes to form strong cationic polyelectrolyte PMETAI brushes. The PMETAI brushes collapse in solution with high concentration of monovalent salt, as were evidenced by DLS and AFM.

Acknowledgement

Financial support from Deutsche Forschungsgemeinschaft (DFG) within SFB481 is acknowledged. The authors want to express their gratitude to S. Wunder and M. Hund for their help with the GPC and AFM measurements respectively. Helpful discussions with F. Plamper and P. Millard are appreciated.

References

[1] Schwarz JA, Contescu CI, Putyera K. Dekker Encyclopedia of Nanoscience and Nanotechnology-5 Volume Set. Boca Raton:CRC Press. 2004.

[2] Whitesides GM. Small 2005;1:172-179.

[3] Liu T, Burger C, Chu B. Prog Polym Sci 2002;28:5-26.

[4] Rodriguez-Hernandez J, Checot F, Gnanou Y, Lecommandoux S. Prog Polym Sci 2005;30:691-724.

[5] Minko S. Responsive Polymer Materials: Design and Applications. Oxford:Blackwell Publishing Ltd., 2006.

[6] Tsukahara Y, Mizuno K, Segawa A, Yamashita Y. Macromolecules 1989;22:1546-1552.

[7] Dziezok P, Sheiko SS, Fischer K, Schmidt M, Möller M. Angew Chem Int Ed 1997;36:2812-2815.

[8] Pyun J, Kowalewski T, Matyjaszewski K. Macromol Rapid Comm 2003;24:1043-1059.

[9] Zhang M, Müller AHE. J Polym Sci Pol Chem 2005;43:3461-3481.

[10] Bolisetty S, Airaud C, Xu Y, Müller AHE, Harnau L, Rosenfeldt S, Lindner P, Ballauff M. Phys Rev E 2007;75:040803/040801-040803/040804.

[11] Gao H, Matyjaszewski K. J Am Chem Soc 2007;129:6633-6639.

[12] Beers KL, Gaynor SG, Matyjaszewski K, Sheiko SS, Möller M. Macromolecules 1998;31:9413-9415.

[13] Cheng G, Böker A, Zhang M, Krausch G, Müller AHE. Macromolecules 2001;34:6883-6888.

[14] Börner HG, Beers K, Matyjaszewski K, Sheiko SS, Möller M. Macromolecules 2001;34:4375-4383.

[15] Zhang M, Breiner T, Mori H, Müller AHE. Polymer 2003;44:1449-1458.

[16] Cheng C, Qi K, Khoshdel E, Wooley KL. J Am Chem Soc 2006;128:6808-6809.

[17] Cheng C, Qi K, Germack DS, Khoshdel E, Wooley KL. Adv Mater 2007;19:2830-2835.

[18] Lee H, Jakubowski W, Matyjaszewski K, Yu S, Sheiko SS. Macromolecules 2006;39:4983-4989.

[19] Cheng C, Khoshdel E, Wooley KL. Nano Lett 2006;6:1741-1746.

[20] Li C, Gunari N, Fischer K, Janshoff A, Schmidt M. Angew Chem Int Ed 2004;43:1101-1104.

[21] Balamurugan SS, Bantchev GB, Yang Y, McCarley RL. Angew Chem Int Ed 2005;44:4872-4876.

[22] Yamamoto S-i, Pietrasik J, Matyjaszewski K. Macromolecules 2007;40:9348-9353.

[23] Sun F, Sheiko SS, Moeller M, Beers K, Matyjaszewski K. J Phys Chem A 2004;108:9682-9686.

[24] Gallyamov MO, Tartsch B, Khokhlov AR, Sheiko SS, Boerner HG, Matyjaszewski K, Moeller M. Chem-Eur J 2004;10:4599-4605.

[25] Lee H-i, Pietrasik J, Matyjaszewski K. Macromolecules 2006;39:3914-3920.

[26] Mandel M. Encycl Polym Sci Eng 1987;11:739-829.

[27] Dautzenberg H, Jaeger W, Kötz J, Philipp B, Stscherbina D. Polyelectrolytes: Formation, Characterization and Application. München:Hanser Verlag, 1994.

[28] Manning GS. J Chem Phys 1969;51:924.

[29] Rühe J, Ballauff M, Biesalski M, Dziezok P, Gröhn F, Johannsmann D, Houbenov N, Hugenberg N, Konradi R, Minko S, Motornov M, Netz RR, Schmidt M, Seidel C, Stamm M, Stephan T, Usov D, Zhang H. Adv Polym Sci 2004;165:79-150.

[30] Lienkamp K, Noe L, Breniaux M-H, Lieberwirth I, Gröhn F, Wegner G. Macromolecules 2007;40:2486-2502.

[31] Lienkamp K, Ruthard C, Lieser G, Berger R, Gröhn F, Wegner G. Macromol Chem Phys 2006;207:2050-2065.

[32] Kroeger A, Belack J, Larsen A, Fytas G, Wegner G. Macromolecules 2006;39:7098-7106.

[33] Plamper FA, Schmalz A, Penott-Chang E, Drechsler M, Jusufi A, Ballauff M, Müller AHE. Macromolecules 2007;40:5689-5697.

[34] Plamper FA, Schmalz A, Ballauff M, Müller AHE. J Am Chem Soc 2007;129:14538-14539.

[35] Plamper FA, Ruppel M, Schmalz A, Borisov O, Ballauff M, Müller AHE. Macromolecules 2007;40:8361-8366.

[36] Pietrasik J, Sumerlin BS, Lee RY, Matyjaszewski K. Macromol Chem Phys 2007;208:30-36.

[37] Dai L. Intelligent Macromolecules for Smart Devices: From Materials Synthesis to Device Applications. London:Springer-Verlag, 2003.

[38] Chu B. Laser Light Scattering - Basic Principles and Practise. New York:Academic Press, 1991.

[39] Neugebauer D, Sumerlin BS, Matyjaszewski K, Goodhart B, Sheiko SS. Polymer 2004;45:8173-8179.

[40] Sumerlin BS, Neugebauer D, Matyjaszewski K. Macromolecules 2005;38:702-708.

[41] Matyjaszewski K, Shipp DA, Wang J-L, Grimaud T, Patten TE. Macromolecules 1998;31:6836-6840.

[42] Zhang X, Xia J, Matyjaszewski K. Macromolecules 1998;31:5167-5169.

[43] Gold L. J Chem Phys 1958;28:91-99.

[44] Pincus P. Macromolecules 1991;24:2912-2919.

[45] Borisov OV, Zhulina EB. Eur Phys J B 1998;4:205-217.

[46] Jusufi A, Likos CN, Löwen H. Phys Rev Lett 2002;88:018301.

[47] Jusufi A, Likos CN, Löwen H. J Chem Phys 2002;116:11011-11027.

[48] Ballauff M. Prog Polym Sci 2007;32:1135-1151.

[49] Mei Y, Ballauff M. Eur Phys J E 2005;16:341-349.

Supporting information:

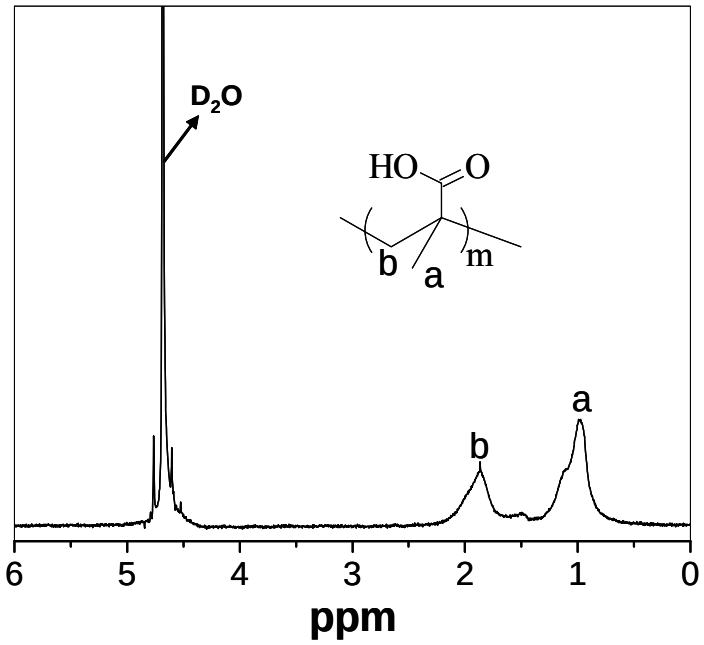

Figure S1. ^{1}H NMR of the linear PMAA cleaved from the PMETAI brushes

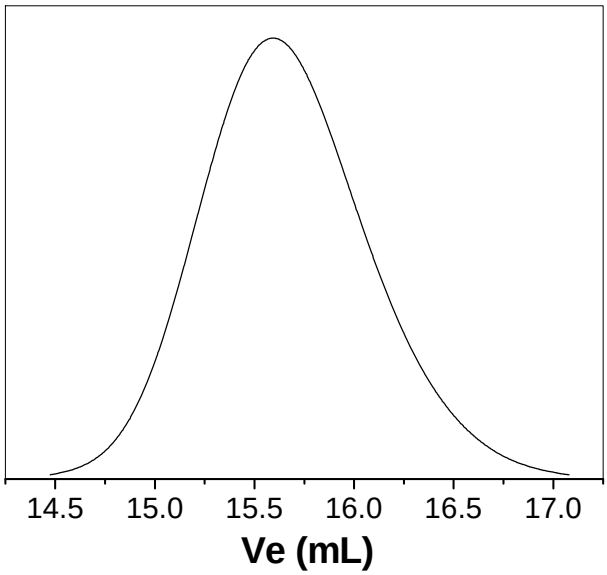

Figure S2. Water GPC eluent curve of the cleaved linear PMAA.

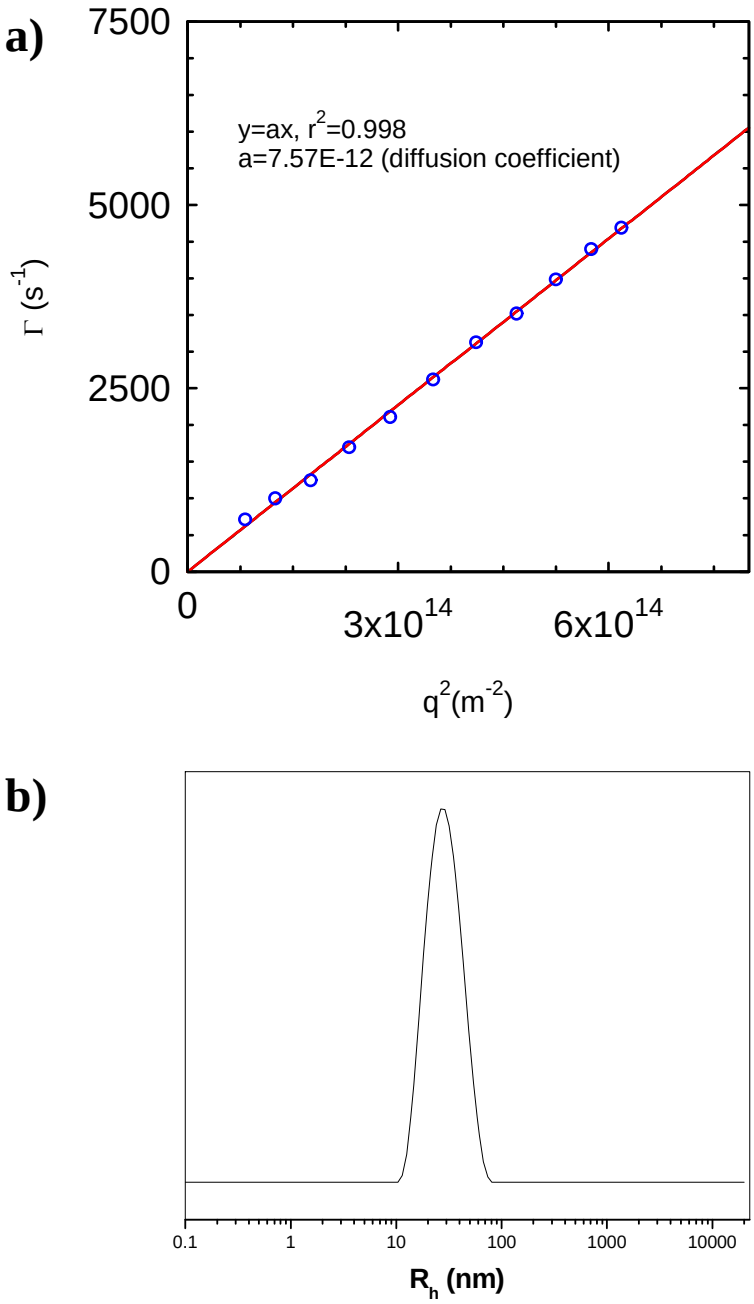

Figure S3. DLS of B1 brush in dioxane solution: a) dependence of decay rate on the square scattering vector; b) hydrodynamic radius distribution at scattering angle of 90°.

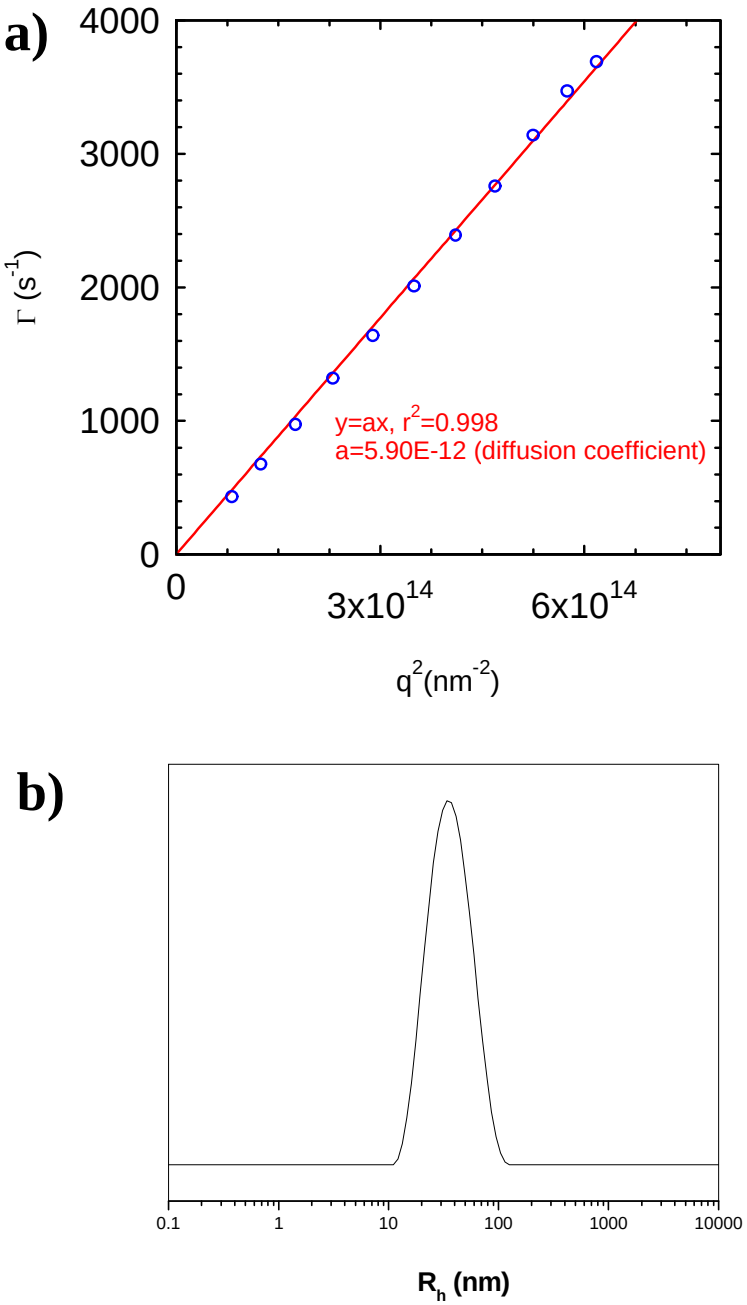

Figure S4. DLS of B2 brush in dioxane solution: a) dependence of decay rate on the square scattering vector; b) hydrodynamic radius distribution at scattering angle of 90°.

5. Manipulating Cylindrical Polyelectrolyte Brushes on the Nanoscale by Counterions: Collapse Transition to Helical Structures

Youyong Xu[a], Sreenath Bolisetty[b], Markus Drechsler[a], Bing Fang[a], Jiayin Yuan[a], Ludger Harnau[c], Matthias Ballauff[b,*], Axel H. E. Müller[a,*]

[a]Makromolekulare Chemie II , [b]Physikalische Chemie I, and [a,b]Bayreuther Zentrum für Kolloide und Grenzflächen, Universität Bayreuth, D-95440 Bayreuth, Germany, [c]Max-Planck-Institut für Metallforschung, Heisenbergstraße 3, D-70569 Stuttgart, Germany, and Institut für Theoretische und Angewandte Physik, Universität Stuttgart, Pfaffenwaldring 57, D-70569 Stuttgart, Germany

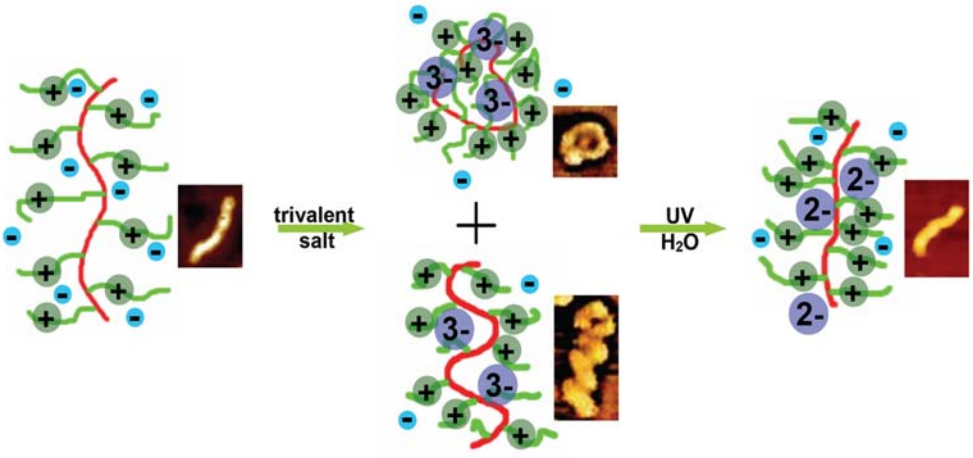

Accepted by *Soft Matter*, **2008**

Abstract

We present a study of the spatial structure of cationic cylindrical polymer brushes in presence of counterions of different valencies. Dynamic Light Scattering (DLS) and Atomic Force Microscopy (AFM) studies demonstrate that the brushes undergo a transition from an extended to a collapsed state when the ionic strength is raised. In the presence of di- or trivalent salt this collapse passes through an intermediate state in which the cylindrical polymer brushes assume a helical conformation. The helical pitch (25 nm) is in the range expected from theoretical considerations. Moreover, we demonstrate that the collapse can be reversed by a photochemical cleavage of the complex trivalent counterion into one monovalent and one divalent ion (photoaquation). All data demonstrate that the spatial structure of cylindrical polymer brushes can be manipulated on the nanoscale in a defined fashion.

Keywords: cylindrical polymer brush, polyelectrolyte brush, AFM, photoaquation, helix.

Introduction

Cylindrical polymer brushes consist of a long main chain onto which flexible side chains are densely grafted.[1-3] These polymers adopt a stretched conformation in dilute solution due to the steric interaction of the side chains.[4,5] Recently, we[6] and others[7] reported on the synthesis of cylindrical polyelectrolyte brushes.[1,8] The most prominent feature of polyelectrolyte brushes in general is the strong confinement of the counterions within the brush layer[9,10]. Hence, virtually all counterions are confined within the brush layer thus creating an enormous osmotic pressure[11]. In case of cylindrical polyelectrolyte brushes, this osmotic pressure should be followed by a strong elongation of the polymers in salt-free solution. Our previous work already demonstrated that adding monovalent salt to solutions of the cylindrical polyelectrolyte brushes leads to a marked decrease of the hydrodynamic radius. This effect is clearly due to the transition of from an osmotic to a salted brush[7a,8,11]. Hence, the side chains that have adopted a highly stretched conformation in the salt-free state (osmotic limit) collapse in presence of a sufficiently high salt concentration. A similar finding was reported for planar[12] and spherical polyelectrolyte brushes[11,13]. Thus, the cylindrical polyelectrolyte brushes behave in the same way as the spherical ones. The obvious difference is related to the fact that the polyelectrolyte chains are not attached to a rigid surface but to a flexible backbone. Hence, the present systems have one more degree of freedom that allows them to react on an external trigger, namely the ionic strength, in a much more pronounced way, as evidenced by the collapse to an unstructured globular state.

Up to now, the dependence of the conformation of cylindrical polymer brushes on ionic strength was only studied in presence of monovalent salt. However, recent work has demonstrated that trivalent counterions lead to a collapse from a stretched to a dense spherical conformation in the case of spherical polyelectrolyte brushes[14] and of polyelectrolyte stars[15]. Moreover, Pochan and colleagues demonstrated that triblock copolymers with acidic coronas can assemble to various structures if multivalent amine is added as counterions[16-20]. In particular, these authors showed that cylindrical micelles with a charged corona may form well-defined helices in presence of triamines and tetraamines. They explained the formation of a helical structure by the combination of a uniaxial pressure along the long axis of the cylinders together with the electrostatic

repulsion of the charged surface of the cylinder. Together with previous work on brushes and polyelectrolyte stars this work suggests that multivalent counterions introduced into cylindrical polyelectrolyte brushes should present a novel way to adjust the conformation within wide limits. Since the charged side chains are appended to the main chains by chemical bonds, it should be possible to explore all states from the full expanded conformation to a fully collapsed state.

Scheme 1: Chemical structure of the cylindrical polyelectrolyte (PMETAI) brush used, **Q2.**

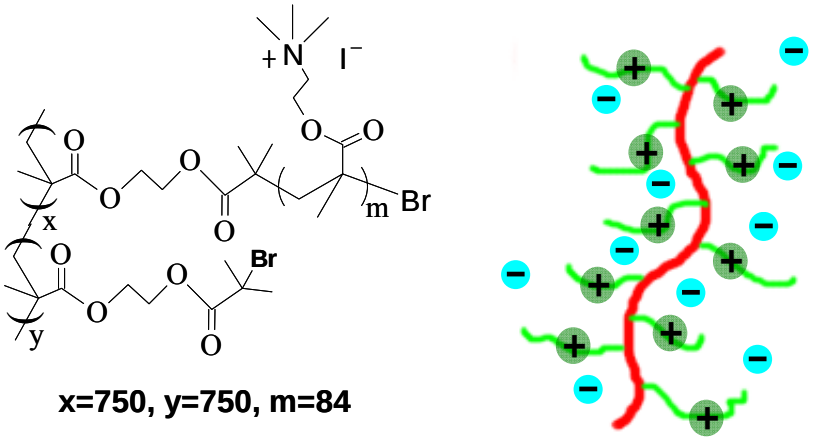

Here we present the first study of the conformation of cylindrical polyelectrolyte brushes in aqueous solution in presence of di- and trivalent counterions. Scheme 1 shows the chemical structure of the polymers under consideration here, having a backbone of 1500 methacrylate units and 750 side-chains of quaternized poly(N,N-dimethylamino methacrylate) (PDMAEMA-Q), also named poly(methacryloylethyl trimethylamino iodide) (PMETAI). Each brush has 6.3×10^4 cationic charges, a number-average molecular weight of 1.9×10^7 g/mol and a polydispersity index of 1.38. The synthesis and the characterization as well as the solution behaviour in presence of monovalent ions are described elsewhere.[6] We investigate the conformation in solution by a combination of dynamic light scattering (DLS) and Atomic Forcs Microscopy (AFM). Moreover, we use photoaquation to convert the complex trivalent ions into a mixture of mono- and divalent ions[21] which is followed by an unfolding of the collapsed chains into an open state again.

The main goal of the present paper is to demonstrate that cylindrical polyelectrolyte brushes can be manipulated on the nanoscale in a well-defined manner.

Experimental

The polyelectrolyte brush **Q2** were synthesized by quaternization of uncharged poly(N,N-dimethylamino methacrylate) (PDMAEMA) brushes, which were prepared by grafting side chains of N,N-dimethylaminoethyl methacrylate (DMAEMA) from a polyinitiator main chain by Atom Transfer Radical Polymerization (ATRP).[22] The details of the synthesis and the characterization are given elsewhere.[6] The quaternized polymer brushes were dissolved in water and dialyzed against pure water for one week. Subsequently, the polymer was obtained by freeze-drying.

Dynamic light scattering (DLS) was carried out on an ALV DLS/SLS-SP 5022F compact goniometer system with an ALV 5000/E correlator and a He-Ne laser (λ = 632.8 nm) at an angle of 90°. Cryogenic transmission electron microscopy (cryo-TEM) was performed as already described. Atomic force microscopy (AFM) measurements were performed on a Digital Instruments Dimension 3100 microscope operated in tapping mode. The micro-cantilevers used for the AFM measurements (Olympus) had resonant frequencies between 284.3 kHz and 386.0 kHz, and spring constants ranging from 35.9 to 92.0 N/m. For the measurement of the quaternized brushes in water, very dilute aqueous solutions (0.02 g/L) were prepared and spin-coated on freshly cleaved mica. For all the quaternized brushes with different salts in water solution, 0.02 g/L aqueous solution of brushes were first prepared and then different amount of salt or salt solutions were introduced by syringe. Then spin-coating was performed on mica surface.

The di- and trivalent salts potassium tetracyanonickelate(II) $K_2[Ni(CN)_4]$ (ABCR) and potassium hexacyanocobaltate(III) $K_3[Co(CN)_6]$ (Aldrich), respectively, were used as received. To transform the trivalent salt into a divalent one, a UV lamp (Honle UVHAND $250_{H1/BL}$, 310 W) was employed. IR radiation was reduced by a water flow cooling system. The glass vials with sample solutions were placed around 7 cm away from the lamp.

Results and discussion

Figure 1 shows typical atomic force microscopy (AFM) and cryogenic transmission electron microscopy (cryo-TEM) images of PMETAI brush **Q2** in salt-free aqueous solution. The extended worm-like structure is evident from both micrographs. On the mica surface, however, the PMETAI brushes seem to adopt a more curved conformation than in solution. This observation must be due to the strong interaction of the cationic brushes with negatively charged mica substrate. The length of the PMETAI brushes is around 180 nm, similar to that of the PDMAEMA brushes on the surface or in the solution. We can hence conclude that the analysis of the cylindrical polyelectrolyte brushes on the mica surface give a reliable information on the solution structure.

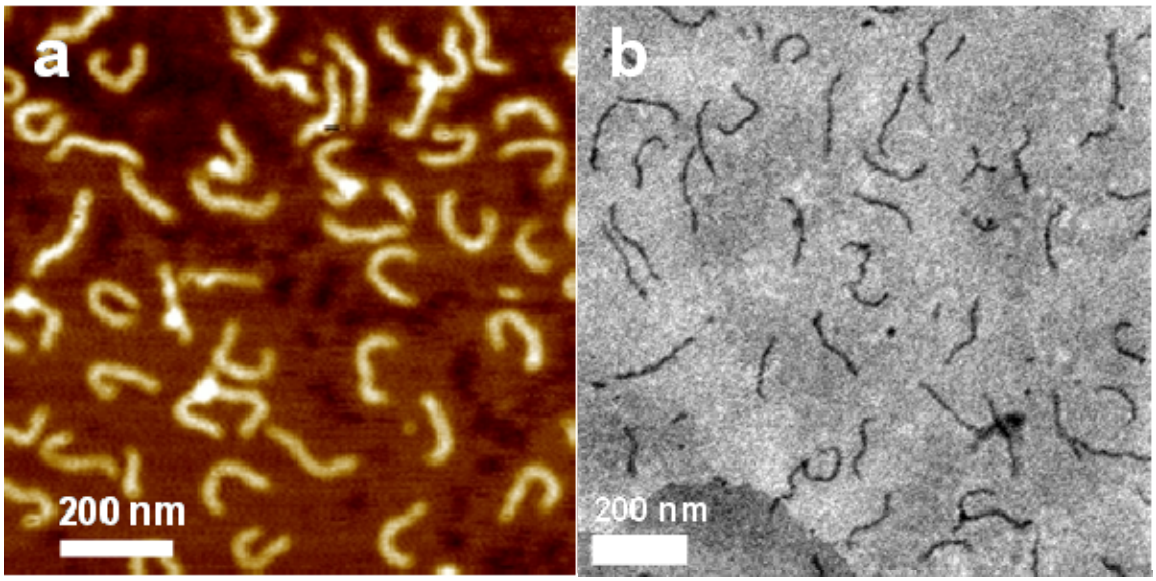

Figure 1. (a) AFM height image (z range 7 nm) of PMETAI brushes spin-coated on freshly cleaved mica from 0.02 g/L aqueous solution and (b) cryo-TEM image of brushes in 0.01g/L aqueous solution.

As shown in our previous report, dynamic light scattering (DLS) is suitable to follow the overall shape of the brushes in solution with great precision although the resulting apparent hydrodynamic radius $R_{H,app}$ gives no direct insight into the overall shape. Fig. 2 summarizes all results obtained on the cylindrical polyelectrolyte brush by DLS. As already discussed in Ref.[6], addition of 0.5 M NaBr leads to a collapse to globular objects. Small salt concentrations have virtually no effect. At highest salt concentration a re-

swelling takes place due to specific interactions of the bromine ions with the cationic charges. If the monovalent counterions are replaced by divalent or trivalent counterions, the osmotic pressure of the polyelectrolyte will decrease due to the much lower ionic strength and a contraction or collapse should be observed at much lower concentration of added salt. Here we chose the two cyanometalates as the divalent and trivalent salt with the quadratic planar tetracyanonickelate(II), $[Ni(CN)_4]^{2-}$, and the octahedral hexacyanocobaltate(III), $[Co(CN)_6]^{3-}$, as the di- and trivalent counterions, respectively.

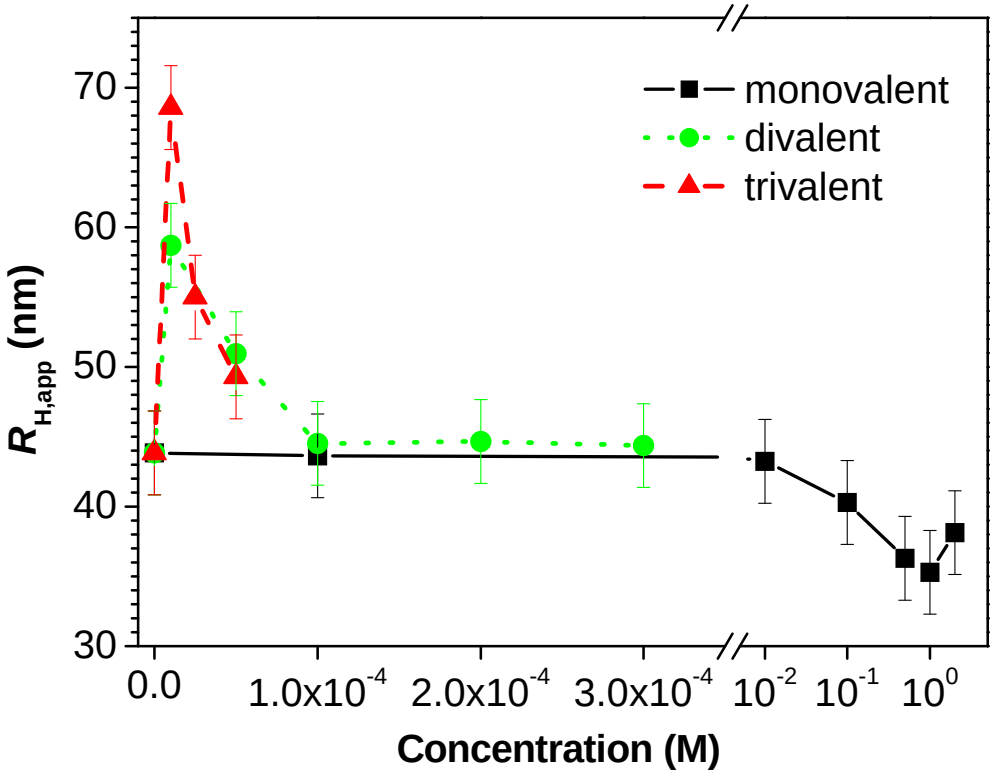

Figure 2. Apparent hydrodynamic radii $R_{H,app}$ as the function of the concentration of monovalent (squares), divalent (circles) and trivalent salt (triangles). The concentration of the brushes is 0.2 g/L in all cases. The data of $R_{H,app}$ in presence of monovalent salt have been taken from Ref.[6].

Fig. 2 demonstrates that this is observed indeed: When a 10 mM solution of the divalent counterions $[Ni(CN)_4]^{2-}$ was added to a 1 g/L solution of the PMETAI brushes (corresponding to 3.3 mM of cationic charges), precipitation was observed immediately. From previous work on spherical polyelectrolyte brushes and polyelectrolyte stars it is

evident that there must be a quick exchange of monovalent counterions by divalent ions.[14,15,21] An excess of divalent ions then can link neighboring brushes which causes intermolecular aggregation of the brushes and precipitation. Hence, the poylmer solutions were diluted to 0.2g/L for all subsequent measurements.

The apparent hydrodynamic radii, $R_{H,app}$, for the brushes in the absence of added salt are around 44 nm. Already at very low concentrations of di- or trivalent salts (10^{-2} mM), the apparent radii increased markedly (58 nm and 68 nm for the divalent and trivalent salt, respectively). Here aggregation takes place too but at a much slower rate. On further addition of the di- and trivalent salts, the $R_{H,app}$ values decrease again, indicating the collapse of the aggregated and/or non-aggregated brushes. Higher concentrations than 0.3 mM and 5×10^{-2} mM for di- and and trivalent salt, respectively, cause precipitation again as is obvious from a stronger raise of the measured hydrodynamic radius (not shown). Even stronger dilutions were not practical due to the much decreased scattering signal.

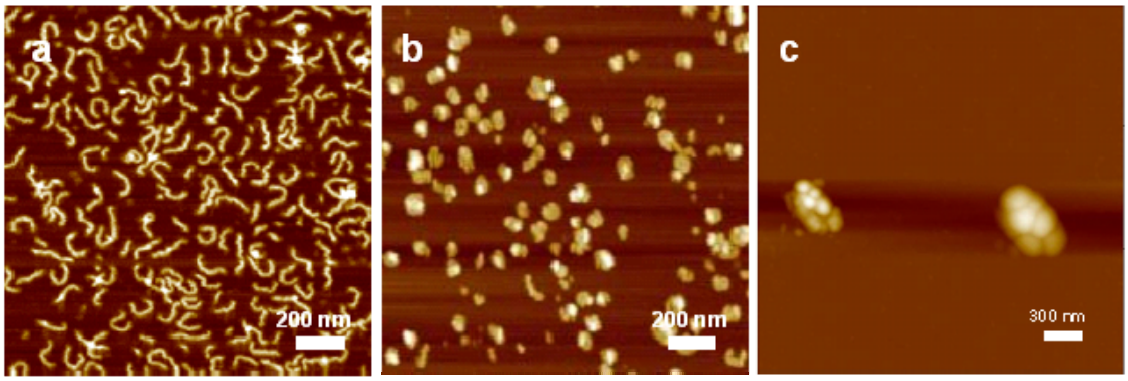

Figure 3. AFM height images of PMETAI brushes spin-coated from divalent salt solutions on mica: (a) $Z_{-/+} = 0.66$, AFM z range 10 nm, brush concentration 0.02 g/L, and the divalent salt concentration 2.2×10^{-2} mM, (b) $Z_{-/+} = 1$, AFM z range 12 nm, brush concentration 0.02 g/L, and the divalent salt concentration 3.3×10^{-2} mM, and (c) $Z_{-/+} = 1$, AFM z range 35 nm, brush concentration 1g/L and divalent salt concentration 1 mM.

To avoid possible complications by aggregation, all AFM-micrograph discussed in the following have been done using polymer concentration that were still lower (0.02g/L). Figure 3 shows typical AFM images of the cylindrical brushes in presence of $[Ni(CN)_4]^{2-}$. The concentration of added salt was 2.2×10^{-2} mM. We chose such a small concentration

to avoid all possible complications by aggregation. Given the small concentration of added salt, a molar charge ratio $Z_{-/+}$ can be defined which is given by the ratio of the added anionic charges and the cationic charges carried by the PMETAI brushes. For the case shown in Fig. 3 $Z_{-/+} = 0.66$. This means that all $[Ni(CN)_4]^{2-}$ ions present in the system would not suffice to neutralize the positive charges of the cylindrical brush. Moreover, there will be a Donnan-equilibrium between the ions inside and outside of the polyelectrolyte brush (see the discussion of this point in Ref.[14]). The previous calculations have shown that the divalent counterions will be taken up by the brush with high preference. Hence, the concentration of the divalent ions remaining in solution must be smaller. In what is to follow, we therefore give only the ratio $Z_{-/+}$ in order to characterize the amount of counterions present in the system.

As is obvious from Fig. 3a, the brushes still kept their worm-like structures. When the charge ratio $Z_{-/+}$ was increased to unity (salt concentration 3.3×10^{-2} mM), most of the brushes collapsed into globular structures, as can be clearly seen in Fig. 3b. The comparison of Fig. 3a and b moreover demonstrates that virtually no aggregates are formed despite the fact that divalent salt is present. Thus, most of the collapsed structures seen in Fig. 3b are still single chains. Figure 3c then demonstrates that there must be a strong attraction due to the presence of divalent salt. Here the polymer concentration was much higher again than in the experiments shown in Fig. 3a and b. The collapsed chains have assumed a nearly spherical shape aggregate and form larger clusters on which the single chains are still visible. These results are in direct agreement with the ones discussed in conjunction with Fig. 2.

An entirely new feature appears at high dilution when $Z_{-/+} = 0.75$. Figure 4 clearly reveals that the collapse can be stopped at an intermediate helical state with a pitch of ca. 25 nm. Obviously, the chains twist in order to relieve a part of the strain caused by the contraction along the long axis of the molecule. In some case this leads to a helix with several turns. Since there is no chiral unit within the chains, both right-handed and the left-handed helices are observed in similar numbers (Figure 4b and c). Figure 4a furthermore demonstrates that the helical conformation is an intermediate state between the stretched and fully collapsed spherical conformation: Some chains are only slightly curved while other are already totally collapsed. Evidently, the helical conformation is

only induced in a small window of salt concentrations in which the charges of the cylindrical brush are not fully balanced by the divalent ions.

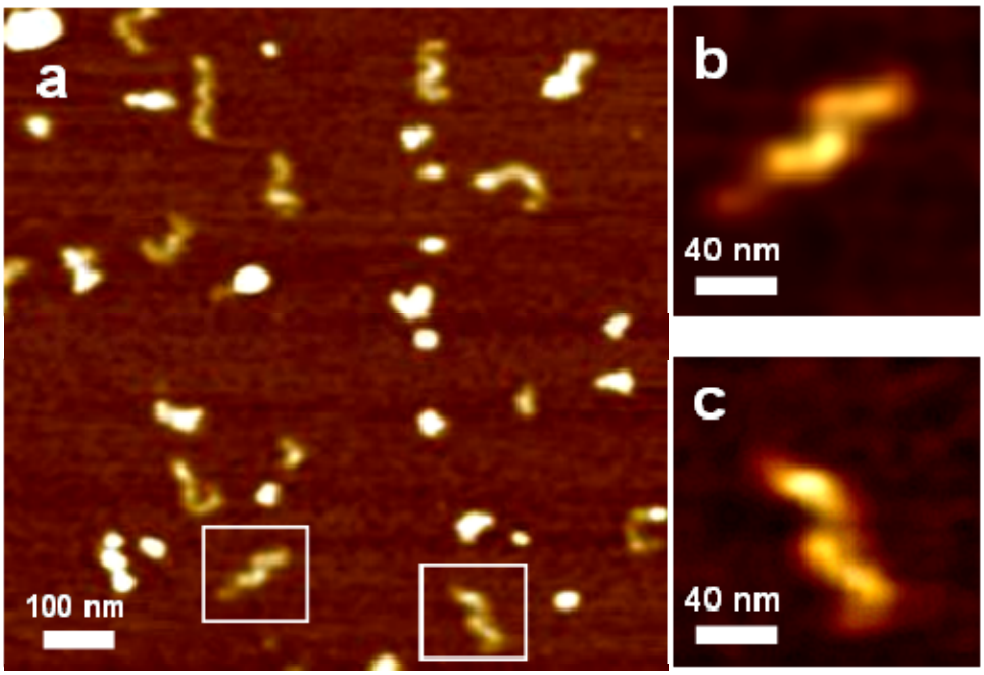

Figure 4. (a) AFM height image of PMETAI brushes with divalent ions $[Ni(CN)_4]^{2-}$ with the ratio $Z_{-/+} = 0.75$. Concentration of the brush was 0.02 g/L and the concentration of the divalent ions 2.5×10^{-2} mM, AFM z range 6 nm; (b) and (c) show a typical right- and left-handed helix, respectively.

Figure 5 depicts the transition of the morphologies of the PMETAI brushes after adding trivalent $[Co(CN)_6]^{3-}$ salt. As already observed in presence of the divalent counterions, helical structures are found (see the enlarged portions of Fig. 5b and 5c). The trivalent counterions lead to very well-defined helices with a pitch of 30 nm. Fig. 5 also demonstrates that the helical structures present again a well-defined intermediate between the stretched and the collapsed globular state.

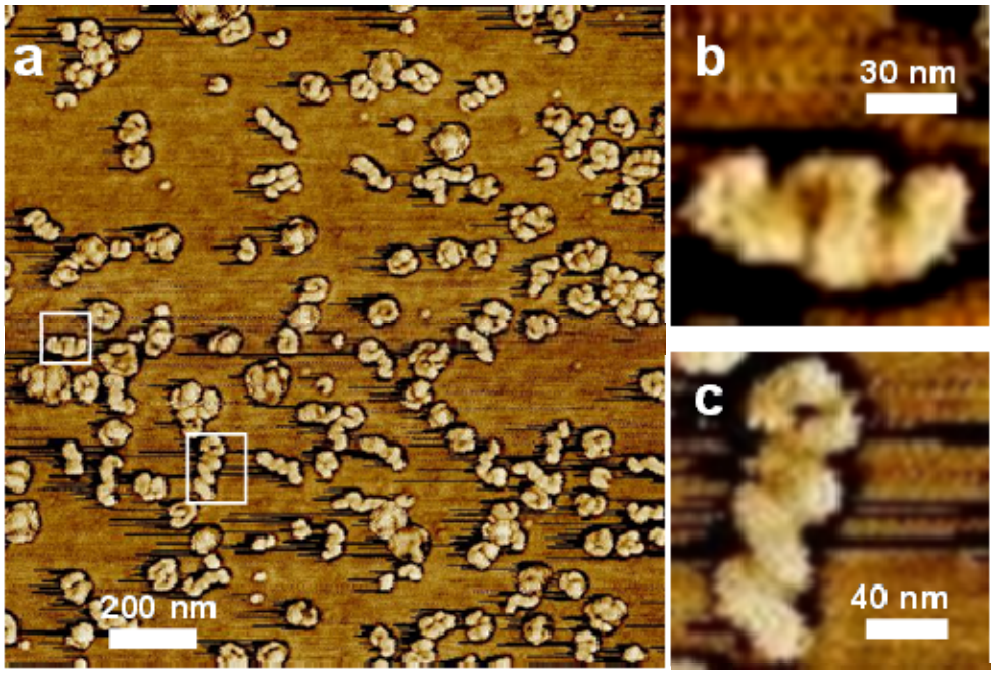

Figure 5. (a) AFM height image of PMETAI brushes with added trivalent salt spin-coated on mica, $Z_{-/+}$ = 1, z range 12 nm, brush concentration 0.02 g/L, and the trivalent salt concentration 2.2×10^{-2} mM; (b) and (c) show a typical right- and left-handed helix, respectively.

One might argue that the helix formation is due to interaction with the substrate. Thus, to see the real conformation of the brushes in solution with added trivalent salt, cryo-TEM measurements were performed. Figure 6 shows the typical structures observed in the vitrified solution with the charge ratio $Z_{-/+}$ = 1 and very low concentration of the brushes (0.02 g/L). The left image shows that the brushes are considerably shortened, which is caused by the collapse with added trivalent salt. The center image shows a helix-like structure with the upper part starting to collapse. The right image shows two typical zigzag morphologies, indicating the transition from extended states to a collapsed structure.

From all results shown in Figures 4, 5 and 6, we conclude the following: Monovalent salt just leads to a collapse from the stretched to the globular conformation as expected from work performed on spherical polyelectrolyte brushes. However, divalent and in particular trivalent ions lead to the formation of a novel intermediate, namely the

formation of helices. In the following section the formation of helices in achiral systems will therefore be discussed in more detail.

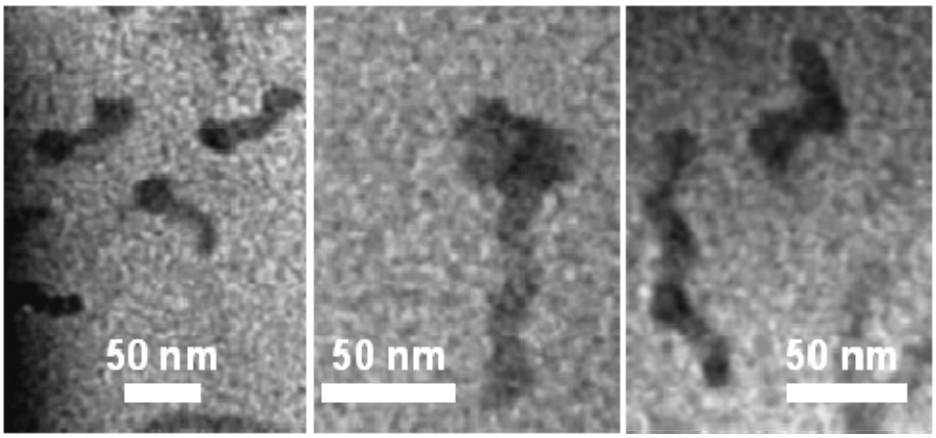

Figure 6. Cryo-TEM images of PMETAI brushes with added trivalent salt, $Z_{-/+} = 1$, brush concentration 0.02 g/L, and the trivalent salt concentration 2.2×10^{-2} mM.

Origin of helical conformations

The above findings fully agree with the results obtained by Pochan et al. on cylindrical micelles.[20] They have demonstrated that helicity may be brought about in achiral systems differing widely in their chemical structure and their overall dimensions. It is hence interesting to discuss the origins of helix formation in more detail. Chain molecules such as proteins and DNA frequently adopt helical conformations. In most cases helicity is caused by chiral main chains or by chiral side groups.[23,24] A different situation arises, however, if a helical structure is brought about solely by packing consideration in achiral systems. Some polymers with bulky side-groups adopt a static or dynamic helical conformation solution; poly(tripenylmethyl methacrylate)[25] and polyhexylisocyanate[26] are examples for the two cases. In a similar manner, polycationic dendronized polymers can form helical double-stranded structures.[27] Modelling proteins as impenetrable flexible tubes of finite thickness reproduces many of the basic building blocks of real proteins.[28] Moreover, purely entropic approaches have been suggested in order to understand the folding of helices. Here the helix arises from an interaction with depleting solvent molecules.[29,30] The effective entropic attraction is due to the extra volume that becomes available to the solvent molecules when chain molecules adopt helical conformations, leading to an overlap of excluded-volume which increases the entropy of the system. The

excluded-volume overlap argument can thus be used as a substitute for the energetic arguments invoked so far.

In general, a helix can be described by a radius R and pitch P, so that the centerline of the helix follows from $\mathbf{r}(s) = (R\cos(2\pi s), R\sin(2\pi s), Ps)$, where s is a parameter that runs from 0 to m, with m being the number of complete turns. The parameters P and R can be varied subject to the constraint that the tube does not self-overlap. The space filling helices shown in Figure 5 are characterized by the ratio $c = P/R \approx 2.8$ which is comparable to the so-called optimal ratio $c^* = 2.5122$ and the ratios of α-helices of common proteins.[28] By creating a helix the cylindrical polymer brushes can generate an overlap of the excluded-volume from successive turns. In the case of small spheres acting as depletion agents the overlap of excluded-volume amounts to two segments of the tube touching. The segments touch along a line because they are aligned. Similarly, there is no overlap of the excluded-volume in the case of a straight tube.

Helices with a particular pitch-radius ratio are selected in the case where boundary effects are not dominant. However, Figures 4 and 5 display cationic cylindrical polymer brushes in contact with a negatively charged mica surface. In the presence of surfaces, the competition between fluid-substrate and fluid-fluid interactions can lead to interesting surface-driven changes of mean local densities, orientations, and conformations of chain molecules.[31] If a tube approaches a substrate, the total volume available to other tubes and solvent molecules increases. The total entropy of the system is increased by an amount proportional the excluded-volume overlap region. Therefore the density of tubes lying with their main body parallel and close to the wall is larger than the density of tubes oriented perpendicular to the wall. The excluded-volume overlap region of a straight tube lying with its main body parallel and in contact with the substrate is proportional to the total length of the tube in the limit of a small size of the solvent molecules. This is due to the fact that the tube touches the substrate along a line. A further increase of the excluded-volume overlap region is possible by forming an overlap of excluded-volume by bending back on itself. Thus, in this case, excluded volumes of distant regions of the tube can overlap. An example of an arc-like tube is shown in Figure 5a below the left-handed helix that is enlarged in Figure 5c. In the case of a helix lying with its main body parallel and in contact with the substrate, the additional excluded-volume overlap region

is considerably smaller, because the contact region of the helix and the substrate is point-like. Hence, the size of the tube-tube excluded-volume overlap region and the tube-substrate excluded-volume overlap region changes considerably when going from the solution to the surface. Therefore a transition from a helical structure of the cylindrical polymer brushes in the bulk to a globular structure close to the substrate may take place.

Real tubes, as opposed to the ideal tubes we have been considering, have a bending rigidity characterized by the persistence length. The bending energy will compete with the entropy and attractive interactions in selecting the ideal tube conformation. However, the strong binding of the trivalent counterions to the polyelectrolyte chains virtually neutralizes the counterions implying a rather small persistence length. Hence the ideal tube model is appropriate in this case and electrostatic repulsion along the long axis of the helix will be of minor importance for the stability of a given conformation.

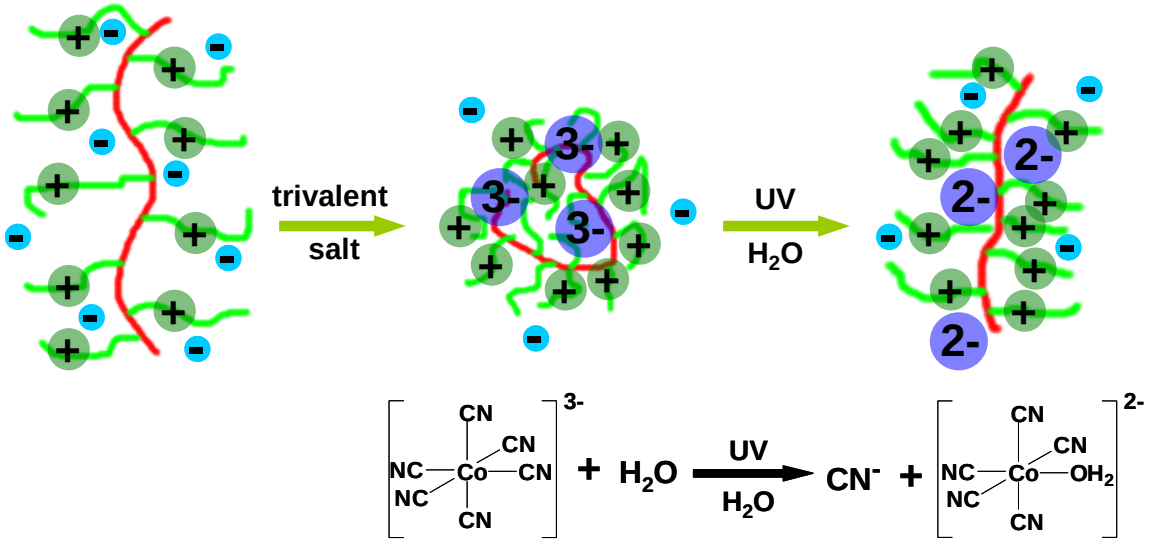

Scheme 2. Transition of the morphology of the PMETAI brushes after adding trivalent salt and subsequent UV radiation: Trivalent counterions lead to a collapse of the cylindrical conformation to a globular structure. Photo-aquation generates one mono- and one divalent counterion from one trivalent ion thus increasing the number of counterions and concomitantly the osmotic pressure in the brush layer. Therefore the brush layer unfolds again and the cylindrical polyelectrolyte brush re-expands and assumes a stretched conformation again.

Unfolding of the globular structure under UV-radiation

From the results shown above, we found that at the concentration of 2.2×10^{-2} mM (with $Z_{-/+}=1$), the trivalent counterions had induced the collapse of the brushes while the same concentration of divalent counterions (leading to $Z_{-/+}=0.66$) the brushes still kept their worm like structures. Now the question arises whether the collapsed state formed in presence of trivalent ions can be reversed by photo-aquation, that is, by conversion of one trivalent counterion into one monovalent and one divalent counterion.[32] This method has recently be used to re-open a polyelectrolyte star polymer collapsed in presence of trivalent ions ("nano-blossoms", see Ref.[21] for further details). When applying UV radiation to a 0.02 g/L solution of the brushes with 2.2×10^{-5} M ($Z_{-/+}=1$) trivalent salt, the trivalent ions are converted to divalent ions via photoaquation and the charge ratio decreases to $Z_{-/+} = 0.66$. This does not suffice anymore to induce the full collapse of the PMETAI brushes and the brushes are expected to return to worm-like structures. Scheme 2 shows this process in a schematic fashion.

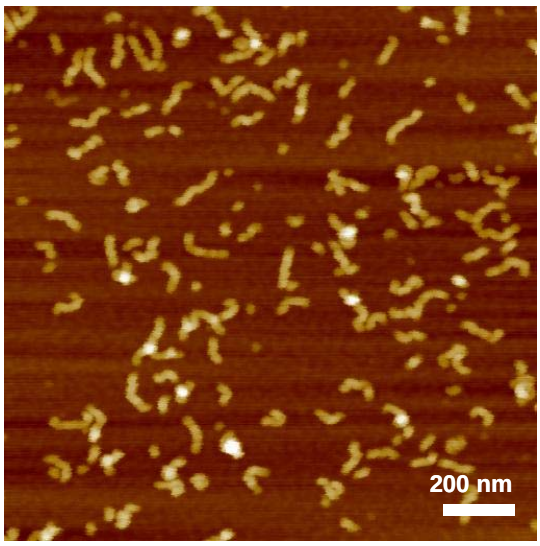

Figure 7. AFM height image of PMETAI brushes with added trivalent salt ($Z_{-/+} = 1$, brush concentration 0.02 g/L, and the trivalent salt concentration 2.2×10^{-2} mM) after UV radiation for 2h; spin-coated on mica, z range 10 nm.

Figure 7 shows the AFM image of the PMETAI brushes with trivalent counterions after UV radiation. It clearly shows that the brushes recovered from their collapsed structure back into a more extended worm-like structure. Hence, the conformation of the

PMETAI cylindrical brushes can be tuned from a worm-like structure to collapsed globular morphology by adding trivalent salt, and finally back to a worm-like conformation by illumination with UV light.

Conclusions

We demonstrated that the collapse of charged cylindrical brushes collapse in presence of divalent or trivalent salt. This collapse goes through an intermediate state where the single bottlebrush polymers assume a helical state. The formation of the helix is prompted by the contraction of the polymer molecules along the long axis by the presence of the multivalent ions. If trivalent ions are converted to a mixture of mono- and divalent ions by light (photo-aquation), the collapse transition can be reversed and the chains are stretched again. All data demonstrate that charged cylindrical brushes can be manipulated by multivalent ions on the nanometric length scale.

Acknowledgement

This work was funded by the Deutsche Forschungsgemeinschaft within SFB 481, project A12. We thank Andreas Walther for the cryo-TEM measurements of the brushes with trivalent counterions.

References

1. M. Wintermantel, M. Gerle, K. Fischer, M. Schmidt, I. Wataoka, H. Urakawa, K. Kajiwara and Y. Tsukahara, *Macromolecules*, 1996, **29**, 978-983.
2. M. Zhang and A. H. E. Müller, *J. Polym. Sci. Polym. Chem.* 2005, **43**, 3461-3481.
3. J. Pyun, T. Kowalewski and K. Matyjaszewski, *Macromol. Rapid Comm.*, 2003, **24**, 1043-1059.
4. B. Zhang, F. Gröhn, J. S. Pederson, K. Fischer and M. Schmidt, *Macromolecules*, 2006**, 39**, 8440-8450.
5. S. Bolisetty, C. Airaud, Y. Xu, A. H. E. Müller, L. Harnau, S. Rosenfeldt, P. Lindner and M. Ballauff, *Phys. Rev. E*, 2007, **75**, 040803(R).
6. Y. Xu, S. Bolisetty, M. Drechsler, B. Fang, J. Yuan, M. Ballauff and A. H. E. Müller, *Polymer*, 2008, **49**, 3957-3964.
7. (a) J. Rühe, M. Ballauff, M. Biesalski, P. Dziezok, F. Gröhn, D. Johannsmann, N. Houbenov, N. Hugenberg, R. Konradi, S. Minko, M. Motornov, R. R. Netz, M. Schmidt, C. Seidel, M. Stamm, T. Stephan, D. Usov and Zhang, H. *Adv. Polym. Sci.*, 2004, **165**, 79-150. (b) K. Lienkamp, L. Noe, M-H. Breniaux, I. Lieberwirth, F. Gröhn and G. Wegner, *Macromolecules*, 2007, **40**, 2486-3502. (c) K. Lienkamp, C. Ruthard, G. Lieser, R. Berger, F. Gröhn and G. Wegner, *Macromol. Chem. Phys.*, 2006, **207**, 2050-2065. (d) A. Kroeger, J. Belack, A. Larsen, G. Fytas and G. Wegner, *Macromolecules*, 2006, **39**, 7098-7106.
8. M. Ballauff and O. Borisov, *Curr. Opinion Colloid Interf. Sci*., 2006, **11**, 316-323.
9. P. Pincus, *Macromolecules*, 1991, **24**, 2912-2919.
10. V. Borisov and E. B. Zhulina, *Eur. Phys. J. B*, 1998, **4**, 205-217.
11. M. Ballauff, *Progr. Polym. Sci*., 2007, **32**, 1135-1151.
12. M. Biesalski, D. Johannsmann and J. Rühe, *J. Chem. Phys.*, 2004, **120**, 8807-8814.
13. Y. Mei and M. Ballauff, *Eur. Phys. J. E*, 2005**, 16**, 341-349.
14. Y. Mei, K. Lauterbach, M. Hoffmann, O. V. Borisov, M. Ballauff and A. Jusufi, *Phys. Rev. Lett.*, 2006, **97**, 158301.
15. F. A. Plamper, M. Ruppel, A. Schmalz, O. Borisov, M. Ballauff and A. H. E. Müller, *Macromolecules*, 2007, **40**, 8361-8366.

16. D. J. Pochan, Z. Chen, H. Cui, K. Hales, K. Qi and K. L. Wooley, *Science*, 2004, **306**, 94-97.
17. Z. Li, Z. Chen, H. Cui, K. Hales, K. Qi, K. L. Wooley and D. J. Pochan, *Langmuir*, 2005, **21**,7533-7539.
18. H. Cui, Z. Chen, K. L. Wooley and D. J. Pochan, *Macromolecules*, 2006, **39**, 6599-6607.
19. Z. Li, Z. Chen, H. Cui, K. Hales, K. L. Wooley and D. J. Pochan, *Langmuir*, 2007, **23**, 4689-4694.
20. S. Zhong,; H. Cui, Z. Chen, K. L. Wooley and D. J. Pochan, *Soft Matter*, 2008, **4**, 90-93.
21. F. A. Plamper, A. Walther, A. H. E. Müller and M. Ballauff, *Nano Lett.*, 2007, **7**, 167-171.
22. M. Zhang, T. Breiner, H. Mori and A. H. E. Müller, *Polymer*, 2003, **44**, 1449-1458.
23. Y. Kamikawa, T. Kato, H. Onouchi, D. Kashiwagi, K. Maeda and E. Yashima, *J. Polym. Sci. Polym. Chem*., 2004, **42**, 4580-4586.
24. N. Gunari, Y. Cong, B. Zhang, K. Fischer, A. Janshoff and M. Schmidt, *Macromol. Rapid Comm.*, 2008, **29**, 821-825.
25. Y. Okamoto, K. Suzuki, K. Ohta, K. Hatada and H. Yuki, *J. Am. Chem. Soc.*, 1979**,** **101**, 4763-4765.
26. S. Lifson, M. M. Green, C. Andreola and N. C. Peterson, *J. Am. Chem. Soc.*, 1989**,** **111**, 8850-8858.
27. C. Böttcher, B. Schade, C. Ecker, J. P. Rabe, L. Shu and A. D. Schlüter, *Chem. Eur. J*., 2005, **11***,* 2923-2928.
28. J. R. Banavar and A. Maritan, *Rev. Mod. Phys*., 2003, **75**, 23-34.
29. Y. Snir, R. Kamien, *Science*, 2005, **307**, 1067.
30. H. Hansen-Goos, R. Roth, K. Mecke and S. Dietrich, *Phys. Rev. Lett*., 2007, **99**, 128101.
31. L. Harnau and S. Dietrich, in *Soft Matter*, ed. G. Gompper and M. Schick, Wiley-VCH, Weinheim, 2007, Vol. 3, pp. 159.

32. (a) A. G. MacDiarmid and N. F. Hall, *J. Am. Chem. Soc.*, 1953, **75**, 5204-5207. (b) M. Wrighton, G. S. Hammond and H. B. Gray, *J. Am. Chem. Soc.*, 1971, **93**, 5254-5255.

6. Switching the Morphologies of Cylindrical Polycation Brushes by Ionic and Supramolecular Inclusion Complexes

Youyong Xu[†], Sreenath Bolisetty[‡], Matthias Ballauff[‡], and Axel H. E. Müller[†],*

[†]*Makromolekulare Chemie II,* [‡]*Physikalische Chemie I, and* [†],[‡]*Bayreuther Zentrum für Kolloide und Grenzflächen, Universität Bayreuth, D-954440 Bayreuth, Germany*

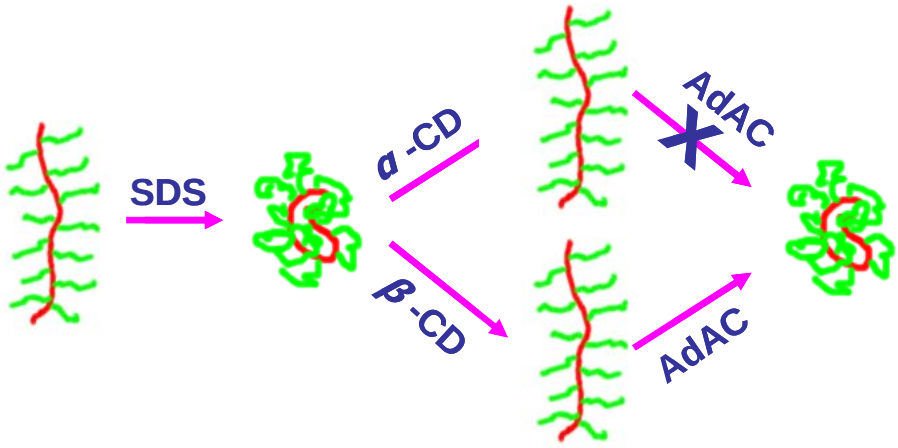

Submitted to *Journal of the American Chemical Society*

Responsive polymers are sensitive to environmental stimuli, which can greatly change their conformations or macro-/microscopic properties[1]. They have drawn more and more attention due to the potential of building smart sensors or actuators based on these intelligent molecules[2]. Smart single-molecular nano-structured polymers are of particular interest for the possibilities of building nanoscopic devices[3]. Among them, cylindrical polymer brushes (CPBs) are good candidates. They are composed of a long linear backbone and densely grafted side-chains[4]. In good solvents, they normally adopt a worm-like conformation owing to the steric hindrance caused by the repelling side-chains, which can be directly observed by atomic force microscopy (AFM) on a suitable substrate[5]. The anisotropic nature provides the brushes with peculiar solution and bulk properties. The chemical properties of the brushes are mainly depending on the side-chains. However, when the backbones are flexible, it provides the CPBs one more degree of freedom, and different morphologies could result from the conformational changes of the backbones caused by the interactions between the side-chains and external stimuli. Worm-to-sphere[6] and worm-to-helix[7] conformational transitions have been evidenced for CPBs with different side-chains and stimuli. These kinds of morphology transitions may give inspirations to creating intelligent nano-devices[8].

Polyelectrolyte CPBs, mimicking some biological macromolecules in nature, contain linear ionic side-chains and show different properties from their neutral counterpart. It is well known that linear polyelectrolytes can form complexes with oppositely charged surfactants and polymers[9]. Although the polyelectrolyte CPBs behave similarly to their linear analogs when forming complexes with surfactants, their distinctive cylindrical nanostructures make it possible to detect the morphology changes directly by microscopy such as AFM. Recently, Schmidt *et al.*[7a] reported helical structures formed by a complex of sodium dodecyl sulfate (SDS) and a cationic polypeptide CPB. When SDS was in excess, a worm-to-sphere transition was observed.

Recently, we reported the synthesis of a new cationic CPB (CCPB) with side-chains of poly(N,N-dimethylaminoethyl methacrylate) (PDMAEMA) and its quaternized analog (PMETAI), and its responsiveness to mono- and multivalent salts[7b,10]. The low initiating efficiency in the synthesis by ATRP led to the chemical structure of the CCPB in scheme 1. Here we present its worm-to-sphere transition by forming ionic complexation with

negatively charged surfactant SDS. More importantly, we are able to switch back to the worm-like morphology by supramolecular inclusion complex between SDS and cyclodextrins (CDs). When β-CD is used for the complex with SDS, we could even make the transition process reversible by using a more competitive inclusion agent, 1-adamantylammonium chloride (AdAC). Scheme 1 depicts the transition process.

Non-polar compounds,[11] linear polymers[12] and polymers with non-polar side groups[13] form stable inclusion complexes with CDs. Figure 1 shows the ^{1}H NMR spectra of SDS and its mixture with α-CD in D_2O. The 3 peaks for the methyl and methylene groups shift to lower field, and the peak for the methylene groups separates into two peaks, indicating that the alkyl chains form an inclusion complex with α-CD with a part of the methylene groups inside the hydrophobic cavity.

Scheme 1: Morphological transitions of CCPB brushes.

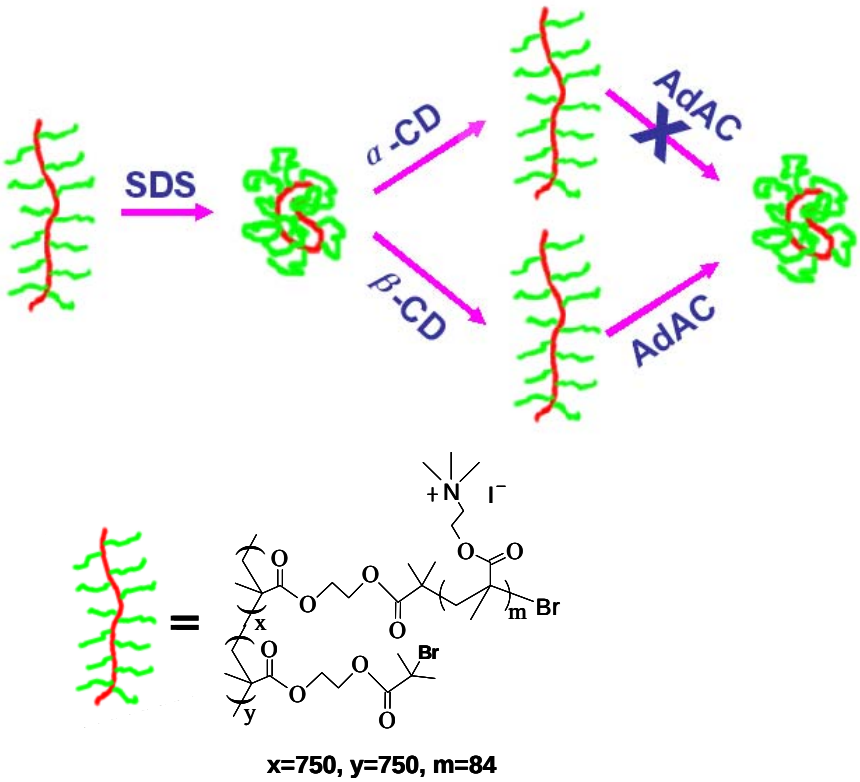

At relatively high concentration (1 g/L) of CCPB, when SDS is added at a charge ratio (ratio of charges of SDS and those carried by the CCPB) $Z_{-/+} = 1$, precipitation appears

immediately, indicating the instantaneous formation of the complex and aggregates (see Supporting Information, Figure S1). Dynamic light scattering (DLS) measurements (Figure 2) show the change of the brush size at c = 0.2 g/L from the CCCB to its complex with SDS, and then with SDS ($Z_{-/+}$ =1) and α-CD, (in equal amounts). For the pure CCPB, the apparent z-average hydrodynamic radius, $R_{h,app}$, is 44 nm. When SDS was added, the solution becomes turbid immediately, but does not precipitate. $R_{h,app}$ increases to ca. 200 nm, indicating the formation of aggregates at this concentration. When α-CD is added to the mixture, the solution becomes clear again and $R_{h,app}$ returns to 53 nm, somewhat higher and more disperse than that of the original brush. This might indicate that the inclusion complex of SDS and α-CD may still form an ionic complex with CCPB, expanding the size of the brushes. (see also Supporting Information, Figure S2).

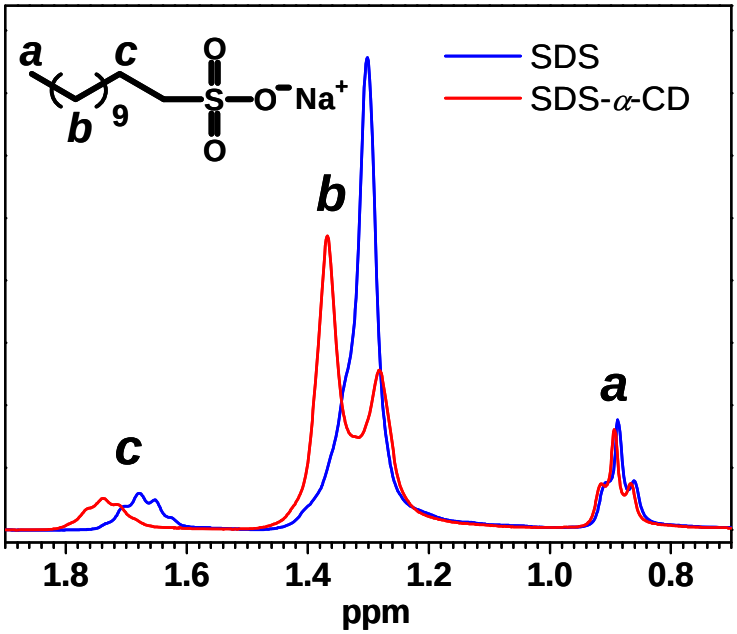

Figure 1. ^{1}H NMR spectra of SDS and its complex with α-CD.

The DLS results demonstrate that it is not possible to avoid aggregates of the CCPB with SDS at brush concentration above 0.2 g/L. To observe the single-molecular morphology changes, AFM measurements from a very low concentration (0.02 g/L) were carried out to diminish the intermolecular aggregates.

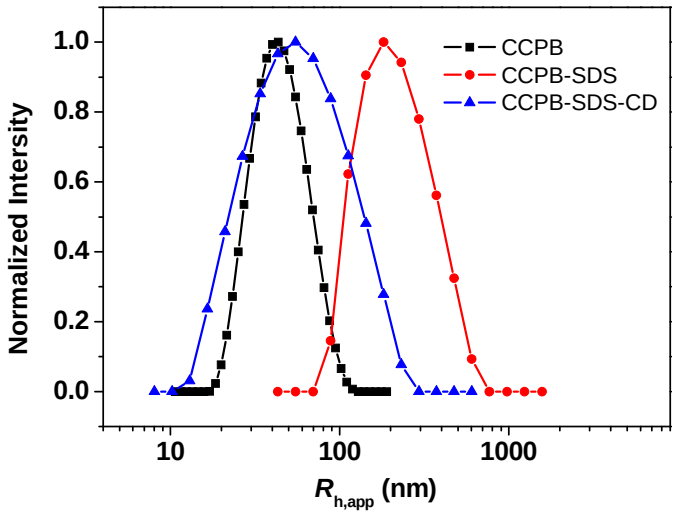

Figure 2. Intensity-weighted hydrodynamic radii distributions of CCPB , and its complexes with SDS, and with SDS + α-CD in aqueous solution, (c_{CCPB} = 0.2 g/L, equimolar amounts).

Figure 3 shows the results of the AFM measurements on mica. The pure CCPB shows typical worm-like structures. When a medium amount of SDS is added, the brush forms pearl-necklace structures, indicating that the SDS forms a complex with cationic side-chains and causes the insoluble part around the backbone of the brush (Figure 3b). Simulations show that pearl-necklace structures form when the inner part of a CPB becomes insoluble.[14] Samokhina *et al.* made a similar observation with spherical polyanion brushes and the cationic surfactant CTAB[15]. The brushes straighten somewhat, probably due to the cross-linking effect of SDS around the backbone. However, when the charge ratio reaches $Z_{-/+}$ = 1, most of the worm-like structures are turned into collapsed spheres (Figure 3c). When α- or β-CD is added to the CCPB-SDS complex ($Z_{-/+}$ = 1), the collapsed spheres return to their worm-like shape (Figures 3d, e), as a result of the inclusion complexes between the dodecyl groups with CDs, which again solubilize the side-chains of the CCPB.

When a more competitive hydrophobe, AdAC, is added to the SDS-β-CD complex, it removes the β-CD from the relatively weak inclusion complex. Then SDS is released, and again forms the insoluble polyelectrolyte-surfactant complex with the CCPB, causing

the collapse of the brush to spheres again (Figure 3f). Due to the unmatched size of AdAC and the cavity of α-CD, the attempt for the re-collapsing with α-CD is not successful.

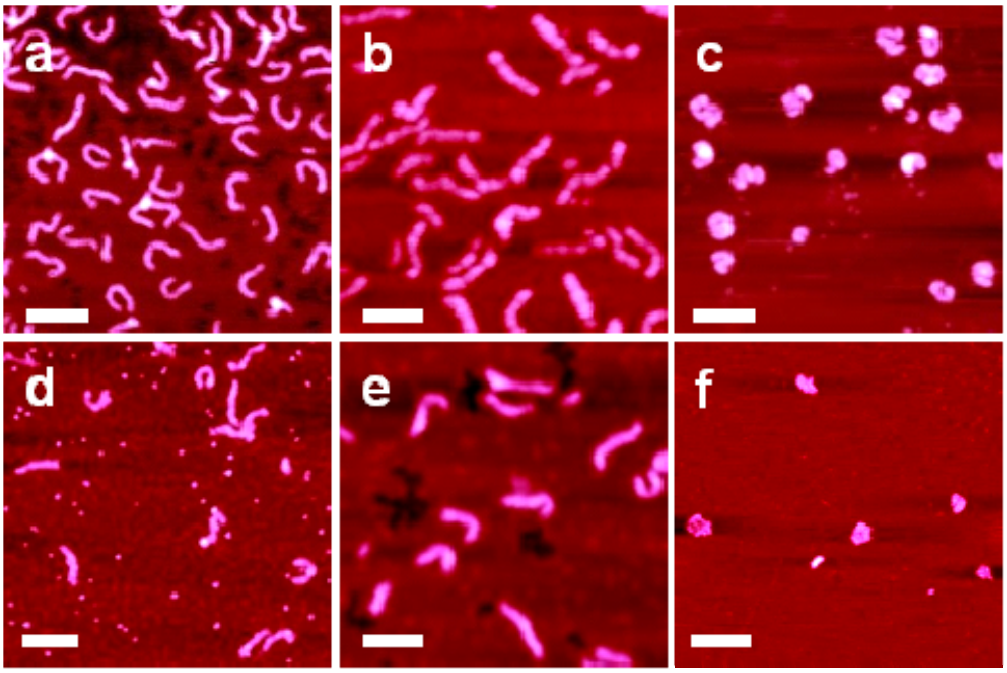

Figure 3. AFM height images of (a) pure CCPB; (b) CCPB with SDS, with $Z_{-/+} = 0.5$; (c) CCPB with SDS, $Z_{-/+} = 1$; (d) CCPB/SDS $Z_{-/+} = 1$ with added α-CD (equimolar with SDS); (e) same, but with added β-CD; (f) sample with β-CD after addition of AdAC (equimolar with β-CD). The scale bars represent 200 nm and the brush concentration is 0.02 g/L. Samples were spin-coated to a freshly cleaved mica surface. AFM height ranges are 5 nm, 12nm, 8nm, 8nm, 8nm, and 4 nm, respectively.

In conclusion, we have shown that the anionic surfactant SDS forms an ionic complex with the cationic CPB, leading to the collapse of the brush from worms to spheres, while both α-CD and β-CD form supramolecular inclusion complexes with SDS, liberating the CCPB, thus again enabling the worm-like conformation. AdAC can remove the β-CD from the SDS-β-CD complex, causing the re-collapse of the brush. This drastic conformation-switching between worms and spheres makes the system a good candidate for sensors or devices on the nano-scale.

ACKNOWLEDGMENT.

This work is financially supported by the Deutsche Forschungsgemeinschaft (DFG) within SFB 481.

Supporting Information Available

Characterization methods and photographs of solutions. This information is available free of charge via the internet at http://pubs.acs.org.

Reference

(1) (a) Chen, G.; Hoffman, A.S. Nature 1995, 373, 49-52. (b) Russell, T. P. Science 2002, 297, 964-967. (c) Yerushalmi, R.; Scherz, A.; Boom, M. E. V. D.; Kraatz, H. –B. J. Mater. Chem. 2005, 15, 4480-4487. (d) Kumar, A.; Srivastava, A.; Galaev, J. Y.; Mattiasson, B. Prog. Polym. Sci 2007, 32, 1205-1237.

(2) Minko, S. Responsive Polymer Materials: Design and Applications; Blackwell Publishing Ltd.: Oxford, 2006.

(3) Dai, L. Intelligent Macromolecules for Smart Devices: From Materials Synthesis to Device Applications; Springer-Verlag: London, 2003.

(4) (a) Zhang, M.; Müller, A. H. E. J. Polym. Sci. Pol. Chem. 2005, 43, 3461-3481. (b) Sheiko, S. S.; Sumerlin, B. S.; Matyjaszewski, K. Prog. Polym. Sci. 2008, 33, 759-785.

(5) Sheiko, S. S.; Möller, M. Chem. Rev. 2001, 101, 4099-4123.

(6) (a) Li, C.; Gunari, N.; Fischer, K.; Janshoff, A.; Schmidt, M. Angew. Chem. Int. Ed. 2004, 43, 1101-1104. (b) Gallyamov, M. O.; Tartsch, B.; Khokhlov, A. R.; Sheiko, S. S.; Boerner, H. G.; Matyjaszewski, K.; Moeller, M. Chem.-Eur. J. 2004, 10, 4599-4605. (c) Sun, F.; Sheiko, S. S.; Moeller, M.; Beers, K.; Matyjaszewski, K. J. Phys. Chem. A 2004, 108, 9682-9686.

(7) (a) Gunari, N.; Cong, Y.; Zhang, B.; Fischer, K.; Janshoff, A.; Schmidt, M. Macromol. Rapid Comm. 2008, 29, 821. (b) Xu, Y.; Bolisetty, S.; Drechsler, M.; Fang, B.; Yuan, J.; Harnau, L.; Ballauff, M.; Müller, A. H. E. Soft Matter 2009, DOI: 10.1039/b812179f.

(8) Xu, H.; Sun, F. C.; Shirvanyants, D. G.; Rubinstein, M.; Shabratov, D.; Beers, K. L.; Matyjaszewski, K.; Sheiko, S. S. Adv. Mater. 2007, 19, 2930-2934.

(9) Thünemann, A. F. Prog. Polym. Sci. 2002, 27, 1473-1572.

(10) Xu, Y.; Bolisetty, S.; Drechsler, M.; Fang, B.; Yuan, J.; Ballauff, M.; Müller, A. H. E. Polymer 2008, 49, 3957-3964.

(11) Rekharsky, M. V.; Inoue, Y. Chem. Rev. 1998, 98, 1875-1917.

(12) Nepogodiev, S. A.; Stoddart, J. F. Chem. Rev. 1998, 98, 1959-1976.

(13) (a) Taura, D.; Hashidzume, A.; Harada, A. Macromol. Rapid Comm. 2007, 28, 2306-2310. (b) Schmitz, S.; Ritter, H. Macromol. Rapid Comm. 2007, 28, 2080-2083.

(14) Polotsky, A.; Charlaganov, M.; Xu, Y.; Leermakers, F. A. M.; Daoud, M.; Müller, A. H. E.; Dotera, T.; Borisov, O. Macromolecules 2008, 41, 4020-4028.

(15) Samokhina, L.; Schrinner, M.; Ballauff, M.; Drechsler, M. Langmuir 2007, 23, 3615-3619.

Supporting information

Materials:

The synthesis of the cationic cylindrical polymer brush (CCPB) with poly{[2-(methacryloyloxy)ethyl] trimethylammonium iodide} (PMETAI) as side-chains was reported previously[1]. Sodium dodecyl sulfonate (SDS) (Aldrich), α-cyclodextrin (α-CD) (Fluka) and β–cyclodextrin (β-CD) (Sigma) were used without further purification. 1-Adamantylammonium chloride was prepared by dropping HCl into the solution of 1-adamantylamine (Aldrich) in water and tuning pH to 4.

Characterization methods:

^{1}H NMR was measured on a Bruker AC-250 instrument at room temperature with D_2O as the solvent.

Dynamic light scattering (DLS) was carried out on an ALV DLS/SLS-SP 5022F compact goniometer system with an ALV 5000/E correlator and a He-Ne laser (λ = 632.8 nm) at an angle of 90^o. The samples were filtered 3 times by using Millipore Nylon filters with a pore size of 1 μm before the light scattering measurements. CONTIN analyses were performed for the measured intensity correlation functions. Apparent hydrodynamic radii, $R_{h,app}$, of the brushes were calculated according to the Stokes-Einstein equation. All measurements were carried out at 25 °C.

Atomic force microscopy (AFM) measurements were performed on a Digital Instruments Dimension 3100 microscope operated in tapping mode. The micro-cantilever used for the AFM measurements were from Olympus with resonant frequencies between 284.3 kHz and 386.0 kHz, and spring constants ranging from 35.9 to 92.0 N/m. The samples were prepared by spin-coating from very dilute (0.02 g/L) solutions onto freshly cleaved mica surfaces.

Figure S1: Photograph of CCPB (1 g/L) with added SDS ($Z_{-/+}$ = 1).

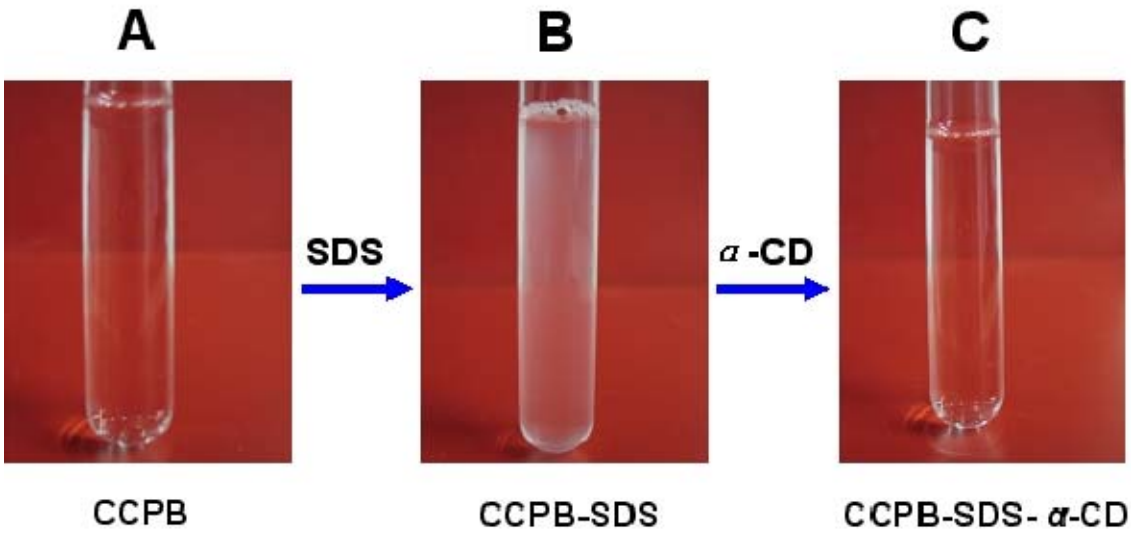

Figure S2: Photographs of (a) pure CCPB (0.2 g/L); (b) complex of CCPB with SDS ($Z_{-/+}$ = 1); and (c) adding α-CD (equal amount to SDS) to sample (b).

Reference

(1) Xu, Y., Bolisetty, S.; Drechsler, M.; Fang, B.; Yuan, J.; Ballauff, M.; Müller, A. H. E. *Polymer* **2008**, *49*, 3957-3964.

7. Manipulating the Morphologies of Cylindrical Polyelectrolyte Brushes by Forming Inter-Polyelectrolyte Complexes with Oppositely Charged Linear Polyelectrolytes: An AFM Study

Youyong Xu, Axel H. E. Müller*

Makromolekulare Chemie II , and Bayreuther Zentrum für Kolloide und Grenzflächen, Universität Bayreuth, D-95440 Bayreuth, Germany

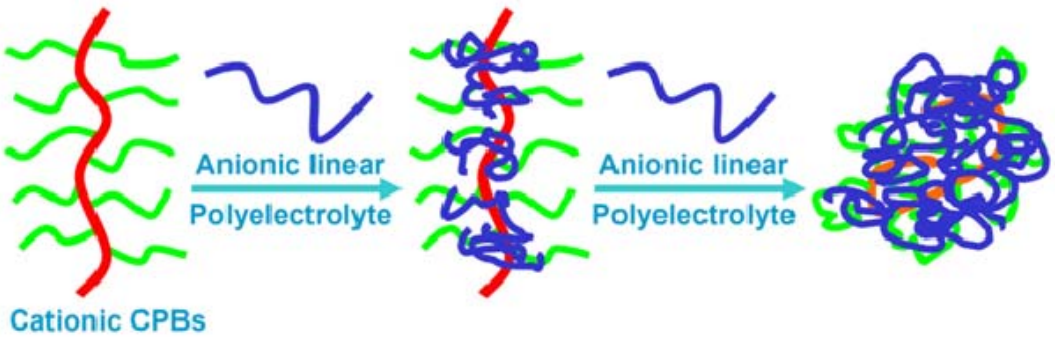

Manuscript to be submitted

Abstract

We present the study of the inter-polyelectrolyte complexes (IPECs) formed by cationic cylindrical brushes (CPBs) and anionic linear poly(sodium styrene sulfonate) (PSS) using AFM measurements on mica surface. The IPECs were mainly prepared by dialysis of the two components from salt solutions. It has been found that the morphologies of the CPBs could be switched by changing the charge ratios between the two polyelectrolytes. For the IPECs with short PSS, the morphologies can be tuned from straight cylinders through intermediate helix-like structures to fully collapsed spheres. Excess of polyanions could stabilize the IPECs and the brushes adopted conformation of twisted worms. When extremely long PSS was used as the polyanions, they can induce the spherical collapse of the brushes at very low $Z_{-/+}$ ratios and no other transition states were found. Interesting micrometer-scale core-shell cylindrical objects were found by directly mixing CPBs with long PSS, which might be the non-equilibrium state caused by the kinetically controlled IPECs formation.

Keyword: Cylindrical polyelectrolyte brushes, PSS, IPECs, AFM

Introduction

Intelligent polymers have drawn more and more attention due to their sensitiveness to various environmental stimuli, which may induce their dramatic morphology transitions or great changes of macro-/micro-scopic properties[1]. Smart nano-structured polymers are of particular importance for the potential of building nano-scopic devices[2]. The research on intelligent polymers of single types has been widely spreading. Recently, the co-assembly processes by multiple-component polymer systems have obtained plenty of interests, owing to their multi-responsiveness and versatilities[3-5]. Among them, inter-polyelectrolyte complexes (IPECs), which can be formed by the interactions of oppositely charged polyelectrolytes, have been applied in different areas like gene transfer[6-9] and capsules as nano-templates[10-12].

Polyelectrolytes carry a large number of covalently-bound charges and surrounding counterions[13]. They can form complexes with oppositely charged polyelectrolytes, surfactants and colloidal particles[14, 15]. There are many factors that influence the structure and properties of IPECs[16]: Molecular natures, such as the type of the ionic groups and molecular weight of the polyelectrolytes; the ratios of the oppositely charged polyelectrolytes; solvent properties, such as pH value, ionic strength and valencies of the counterions; and the preparation methods of the IPECs. Although the studies on the IPECs between linear polyelectrolytes have been active, the IPECs of polyelectrolytes with other topologies are still rare, probably due to the synthetic difficulties. The study on IPECs of non-linear nano-structured polyelectrolytes is highly required by the fast developing nanotechnologies. A few examples of IPECs of spherical polyelectrolytes like dendrimers[17-22], star polymers[23] and micelles[24, 25] were reported. However, studies on the IPECs of one-dimensional nano-structured polyelectrolytes, such as dendronized[26] polymers and cylindrical polymer brushes[27] were rarely reported. Considering the anisotropic nature of these polyelectrolytes, the corresponding IPECs may show different properties and may find their applications in many fields.

Cylindrical polyelectrolyte brushes (CPBs) consist of relatively very long backbones and densely grafted side-chains[28, 29]. One important feature of the CPBs is that most of the counterions are strongly confined within the brush layer[30, 31], which leads to the great osmotic pressure and stretching of the brushes in salt-free solutions[32]. So far, grafting-

from[33] and grafting-through[34, 35] strategies have been adopted to prepare CPBs. But in general, tedious synthetic work to get well-defined CPBs has hindered the further studies of such kind of polyelectrolytes.

We have recently reported the synthesis of cationic CPBs with poly{[2-(methacryloyloxy)ethyl] trimethylammonium iodide} (PMETAI) side-chains by grafting-from via ATRP and further quaternization[33]. These brushes showed responsiveness to different types of counterions, which caused the transition of the morphologies of the brushes from worm-like through helix, to spherical collapsed shapes[33, 36]. We also found that they can form complexes with oppositely charged surfactant sodium dodecyl sulfonate (SDS)[37].

Although Schmidt et al reported the IPECs between cationic brushes with DNA[27], systematic studies of the CPBs with linear polyelectrolytes are still scarce. In this work, we investigate the IPECs formation between the strong cationic PMETAI CPBs and strong anionic linear poly(sodium styrene sulfonate) (PSS). We found that the morphologies of the cationic CPBs could be manipulated by the formation of IPECs with oppositely charged PSS. Scheme 1 shows the morphology changes of the CPBs by the formation of IPECs with linear polyelectrolytes. This provides an additional way of controlling the morphologies of the CPBs, which might find its applications for some sensors or devices in nano-scale. Different mole ratios between the cations carried by the CPBs and the anions of the PSS were investigated, which controls the formation of the IPECs and the morphologies of the CPBs. Influence of the molecular weight of PSS to the formed IPECs are also discussed.

In the study of the IPECs, different characterization methods have been applied to determine the macro-scopic properties of the formed IPECs. Atomic force microscopy (AFM) is a robust tool, which can directly observe the nano-structured polymers on different substrates[38]. Since we are interested in the conformation changes of the single brushes, most of the experiments were carried out in highly diluted solutions to avoid the inter-molecular aggregates. However, most characterization methods are not available in this concentration range. So in this work, AFM measurements were mostly employed to directly examine the IPECs formed by the cationic CPBs with linear polyelectrolytes.

Scheme 1. Schematic morphology changes of cationic CPBs by forming IPECs.

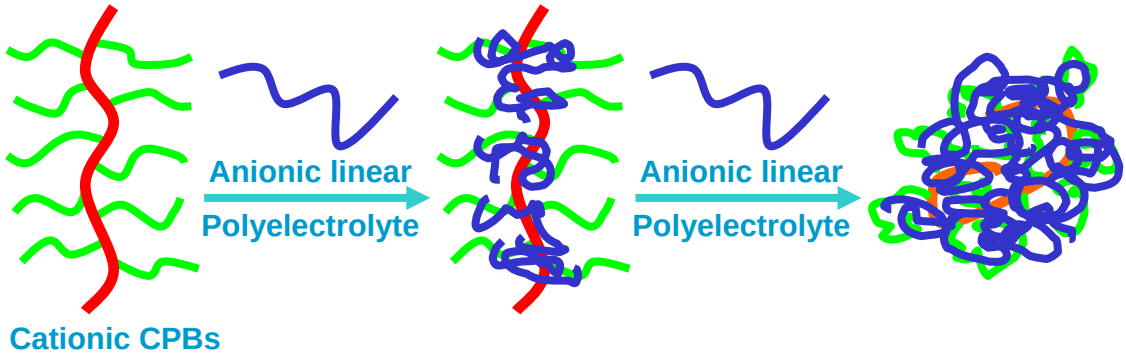

Experimental

Materials

Cationic cylindrical polymer brush with side-chain of poly{[2-(methacryloyloxy)ethyl] trimethylammonium iodide} (PMETAI) has been prepared in previous work[33]. The brushes have backbone of *DP* 1500. Grafting density of the side-chain is 50% and the *DP* of the side-chains is 84. The number-average molecular weight (M_n) of the brushes is 1.9×10^7 g/mol.

Narrowly distributed linear poly(sodium styrene sulfonate) (PSS) with two different molecular weights were purchased from Fluka and were used as received (standard for GPC, sample 1: $M_n = 1.32\times10^4$, *DP* = 64, PDI < 1.2; sample 2: $M_n = 2.26\times10^6$, *DP* = 11000, PDI < 1.2).

NaCl was used as it is. Millipore water was used for the preparation of samples and dialysis.

Preparation of IPECs by direct mixing

Stock solutions of PSS (10 mM of anionic charges) were first prepared by dissolving them in de-ionized water. PMETAI brush dilute solutions (0.02g/L, 6.67 mM of cationic charges) were then prepared. Different amount of PSS was injected by micro-syringe according to the charge ratios between the cations and anions.

Preparation of IPECs by dialysis

Stock solutions of PSS (10 mM of anionic charges) were first prepared by dissolving them in de-ionized water. PMETAI brush dilute solutions (0.02g/L, 6.67 mM of cationic charges) with 0.2 M NaCl were then prepared. Different amount of PSS was injected by micro-syringe according to the charge ratios between the cations and anions. Then the solutions were subjected to dialysis against de-ionized water for 4 days.

Characterizations

Dynamic light scattering (DLS) was carried out on an ALV DLS/SLS-SP 5022F compact goniometer system with an ALV 5000/E correlator and a He-Ne laser (λ = 632.8 nm) at an angle of 90^{o}. In each case, the concentration of the PMETAI brush is 0.2 g/L and concentration of NaCl is 0.1 M. Different amount of PSS was added directly according to the charge ratios. The samples were filtered 3 times by using Millipore Nylon filters with a pore size of 1 μm before the light scattering measurements. CONTIN analyses were performed for the measured intensity correlation functions. All measurements were carried out at 25 °C.

Atomic force microscopy (AFM) measurements were performed on a Digital Instruments Dimension 3100 microscope operated in tapping mode. The micro-cantilever used for the AFM measurements were from Olympus with resonant frequencies between 284.3 kHz and 386.0 kHz, and spring constants ranging from 35.9 to 92.0 N/m. The samples were prepared by spin-coating from very dilute (0.02 g/L) solutions onto freshly cleaved mica surfaces.

Results and discussions

Strong cationic PMETAI brushes and strong anionic linear PSS were employed in this work for the formation of IPECs. Since they are all strong polyelectrolytes, their ionization behaviors are not dependent on the pH value. Nevertheless, all the experiments were performed at pH 7. The formation of IPECs is a process of electrostatic interaction of charged polymer chains and subsequent release of counterions[39, 40]. Thus ionic strength may play an important role to the formation and properties of IPECs. We prepared the IPECs by two different methods: direct mixing and mixing in salt solutions with

following dialysis in pure water. The length of the linear polyelectrolyte may also have influence on the IPECs, so short linear PSS and extremely long PSS are used for the comparison of the IPECs formation with PMETAI brushes.

At relative high concentration of the PMETAI CPBs(0.2 g/L), IPECs samples were prepared by directly mixing PSS with CPBs with different charge ratios $Z_{-/+}$ (the mole ratio between the charges carried by the anionic PSS and those by cationic CPBs) in the solutions with 0.1 M NaCl. For the IPECs of CPBs with short PSS, turbid solution was obtained when $Z_{-/+}$ reached 0.4, indicating formation of big aggregates in the solution. When the charge ratio was as high as 0.5, precipitation appeared. DLS measurements revealed that at charge ratio $Z_{-/+}$ as low as 0.1, big aggregates were already seen. So, at this concentration of the brushes, the aggregates of the brushes are unavoidable. Since we are more interested in the single-molecular morphologies of the CPBs, very low concentration (0.02 g/L) of the CPBs was used for the following studies to diminish the inter-molecular aggregates. Unfortunately, at this concentration, the signals for the DLS were too weak for reliable measurements. So AFM measurements of the spin-coated samples on mica surfaces were mainly performed for the direct observation of the CPBs' morphology changes.

IPECs prepared by dialysis

It has been reported that adding salt weakens the formation of IPECs[15]. In order to acquire IPECs with well-defined structures, relative high concentration of salt (0.2 M) was added to the systems when mixing cationic CPBs with PSS. Slow dialysis process was followed to remove the excess counterions for the IPECs formation. IPECs with well-defined single-molecular structures were observed by this process.

For the IPECs by short PSS and CPBs (concentration of 0.02 g/L), when the charge ratio $Z_{-/+}$ is 0.5 or lower, the solutions were clear, while at $Z_{-/+}$ of 0.75, some precipitation was observed. At $Z_{-/+}$ of 1, more precipitation appeared and it was hard to find any objects in the AFM measurement, suggesting most of the polymers were phase segregated from the solution. When $Z_{-/+}$ reached 2, the solution became transparent again. Similar behavior was found for the IPECs with the long PSS. The only difference is that the precipitation happened at even lower charge ratio (full precipitation at $Z_{-/+}$ 0.75). The

change of the solubilities at such low concentration of brushes showed that the charge ratio $Z_{-/+}$ might have great influence on the morphologies of the IPECs. Detailed AFM measurements provided the micro-scopic information of the IPECs.

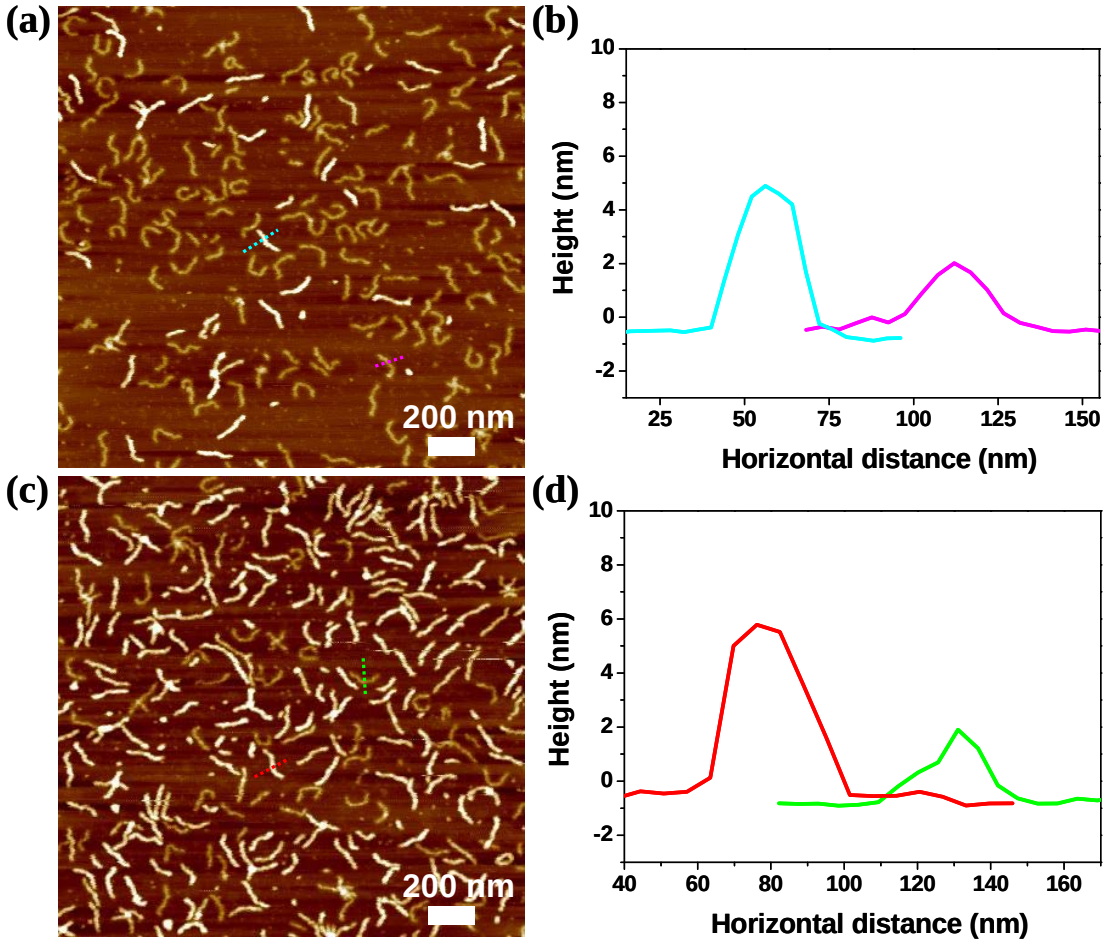

Figure 1. (a) AFM height image of IPECs by CPBs and short PSS, charge ratio $Z_{-/+}$ 0.1, AFM Z range 10 nm; (b) Section analyses of the cursors displayed in (a); (c) AFM height image of IPECs by CPBs and short PSS, charge ratio $Z_{-/+}$ 0.5, AFM Z range 10 nm; (d) Section analyses of the cursors displayed in (c).

Figure 1 shows the height images and section analyses of IPECs by short PSS and CPBs with $Z_{-/+}$ of 0.1 and 0.5. When the charge ratio $Z_{-/+}$ is 0.1, it is clearly shown in figure 1a, there are some brushes are much higher than the others. Quantitative section analysis in figure 1b revealed that most of the brushes are around 1.8 nm, which is within the error of the original brushes (1.6 nm)[33]. But some brushes have height of around 5 nm,

which is significantly higher than the original brushes, indicating the formation of the IPECs of the cationic CPBs with PSS. From figure 1a, we can also find that the original brushes adopt quite curvy morphologies (the bending angle sometimes even reaches 180^{o}, probably due to the strong electrostatic interaction between the positively charged CPBs and negatively charged mica surfaces), while those IPECs are mostly more straight than the original brushes, but kept the same length of the original brushes (around 180 nm). Explanation for this is that the linear PSS formed IPECs with the brush and partially crosslinked the brushes, which increased the rigidity of the brushes. In the IPECs formed between linear polyelectrolytes and stars or micelles, the linear polyelectrolytes normally go to the core or around the core area due the hydrophobicity of the formed IPECs. Here no direct core-shell structures were recorded by the AFM height image and section analysis, suggesting that the distribution of the linear PSS in the brush is random, which raised the rigidity of the brushes. Interestingly, the formation of the IPECs with brushes was inhomogeneous and the question why brushes did not form IPECs in a homogeneous way with similar size and height in the solutions remain difficult to answer. Similar phenomena were also found for IPECs of cationic CPBs with DNA, where kinetics and diffusion controlled formation of IPECs in the solution was reckoned as the reason[27].

When the charge ratio $Z_{-/+}$ reached 0.5, similar finding was shown in figure 1c. Species of different heights were recorded in the AFM height image. But it is clear that the portion of the higher brushes is significantly increased, while some part of the brushes remained unchanged. Section analysis in figure 1d demonstrates that the heights of some brushes kept their original ones (around 1.8 nm), while the heights of those who formed IPECs were raised to 6 nm. Similarly, these IPECs adopted more straight conformation than original brushes on the substrate.

From the results discussed above, with the increasing charge ratio $Z_{-/+}$, the proportion of the non-complexed brushes is decreasing. When $Z_{-/+}$ is as high as 0.75, the original brushes could not be found any more in the AFM images, shown in figure 2a. Most of the brushes have similar heights of around 8 nm, as evidence by the section analysis in figure 2d. New conformation of the brushes was detected, displayed in the AFM height and phase images (figure 2a and 2b). The surface of the CPBs became uneven with some tubers. Enlarged part of figure 2a displayed in figure 2c shows that the brush took helical-

like structures with a pitch of around 30 nm. Also it is found that the average length of the formed IPECs is around 140 nm, which is lower than that of the original CPBs.

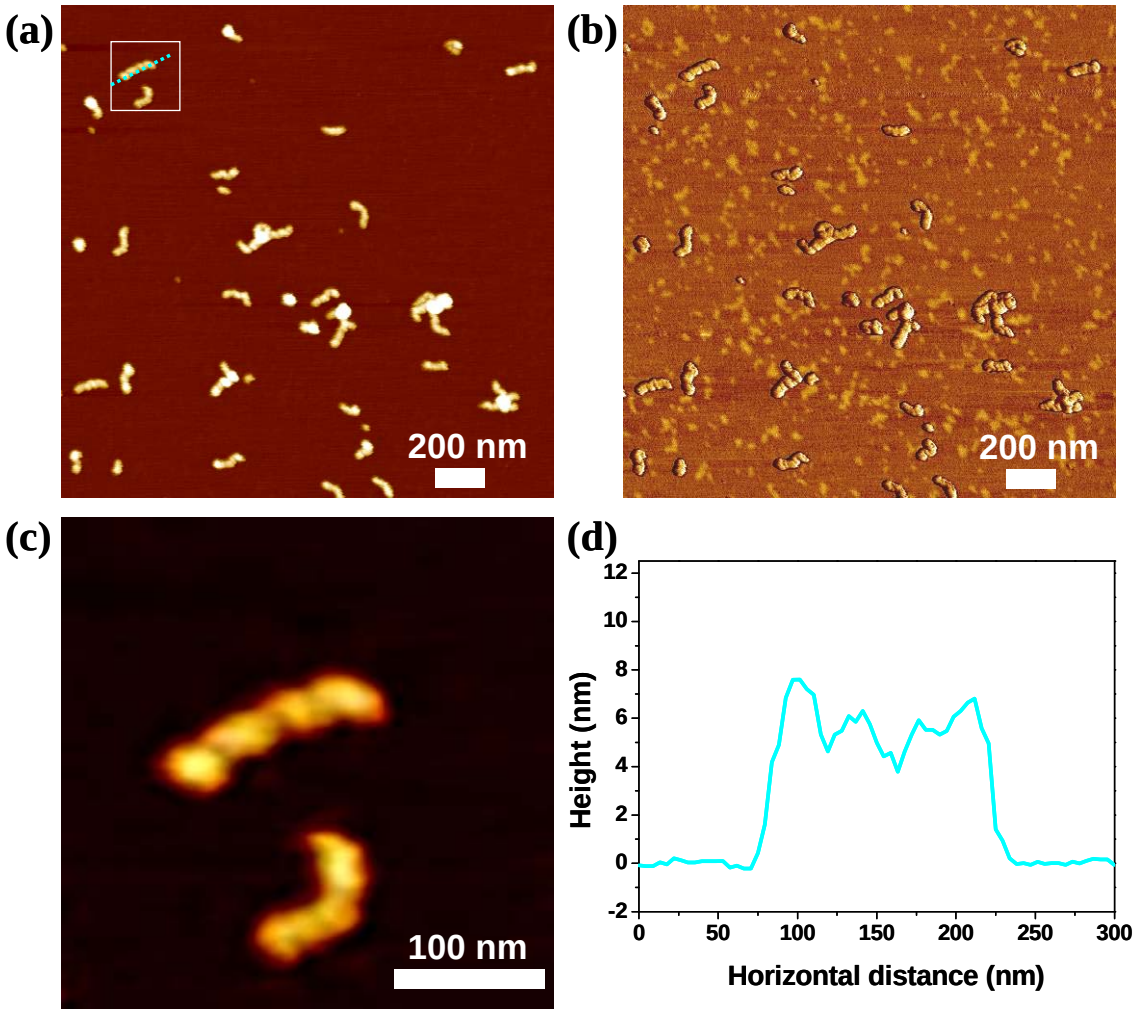

Figure 2. (a) AFM height image of IPECs by CPBs and short PSS, charge ratio $Z_{-/+}$ 0.75, AFM Z range 20 nm; (b) AFM phase image of IPECs by CPBs and short PSS, charge ratio $Z_{-/+}$ 0.75, AFM Z range 25°; (c) Magnified image of selected area in (a); (d) Section analysis of the cursors displayed in (a).

When the number of the charges carried by the cationic CPBs and anionic PSS equals, most of the polymers precipitated from the solution, and only very few objects could be observed in the AFM measurements. In some area, some spherical objects (diameter of 80 nm) were detected, while no worm-like structure could be found. Section analysis of these spherical objects indicated that they were just a little higher (2.2 nm) than the

original brushes. They might be the IPECs of those much smaller brushes with PSS. In order to get more information of the IPECs with $Z_{-/+}$ of 1, 0.1 M NaCl solution was prepared with the IPECs precipitation. After vigorous stirring overnight, most of the precipitation was re-dissolved and it was possible to prepare the AFM samples using this solution. More ellipsoid and spherical objects (size around 90 nm) were shown in figure 3c. Section analysis showed they have an average height of 9 nm, which is higher than those described above for $Z_{-/+}$ 0.1, 0.5 and 0.75. These results indicates that when $Z_{-/+}$ reaches 1, the positive charges of the CPBs and the negative charges of PSS compensate each other and lead to the phase separation of the IPECs from the solution. Adding salt weakened the IPECs and brought the IPECs back to the solution again.

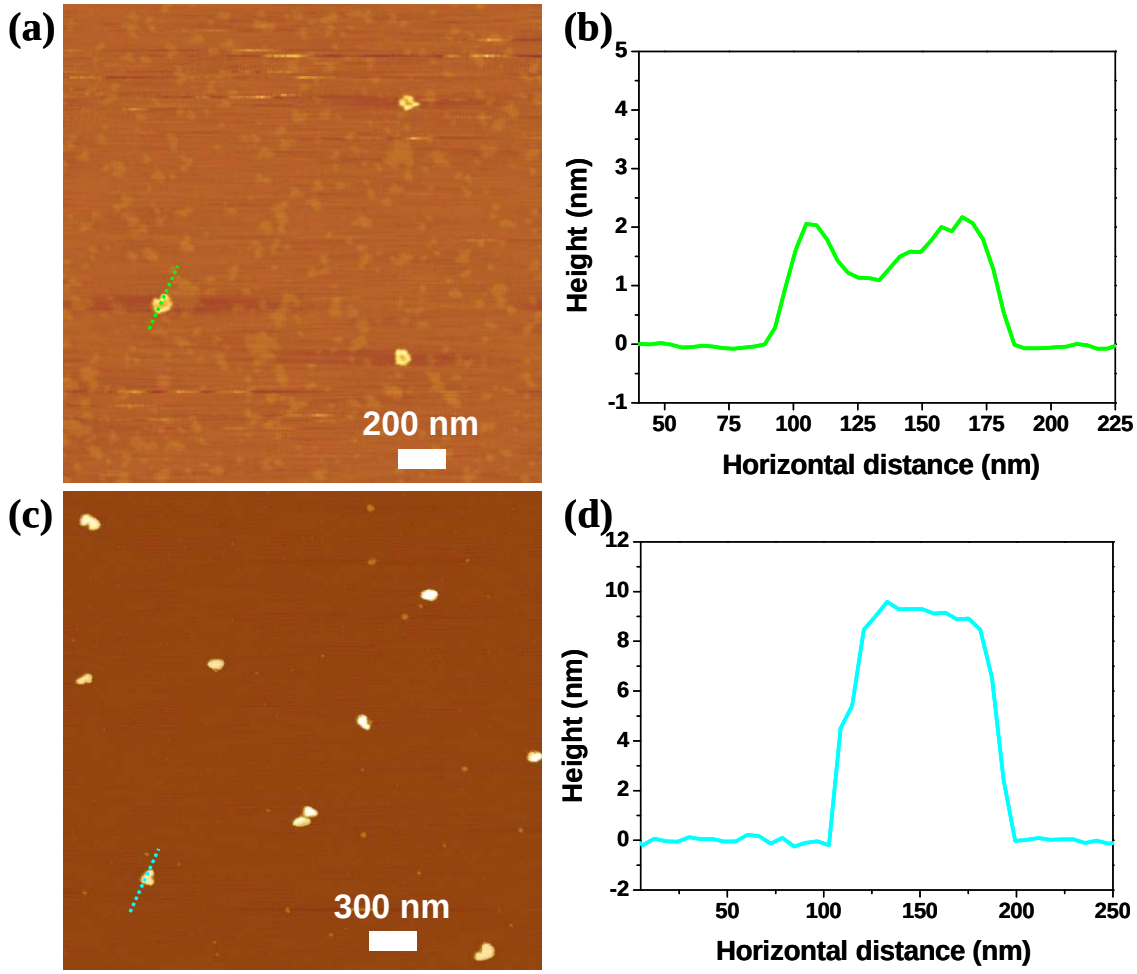

Figure 3. (a) AFM height image of IPECs by CPBs and short PSS, charge ratio $Z_{-/+}$ 1, AFM Z range 7 nm; (b) Section analysis of the cursors displayed in (a); (c) AFM height

image of IPECs by CPBs and short PSS in 0.1 M NaCl solution, charge ratio $Z_{-/+}$ 1, AFM Z range 30 nm; (d) Section analysis of the cursors displayed in (c).

When CPBs were mixed with excess linear PSS ($Z_{-/+} = 2$), worm-like structures could be found again. Figure 4a shows the co-existence of spheres and twisted worms. Since the negatively charges of PSS is in excess, the CPBs were wrapped by the linear polyanions, which make the IPECs still soluble in the solution. Section analysis shows the height of the IPECs was increased to 12 nm.

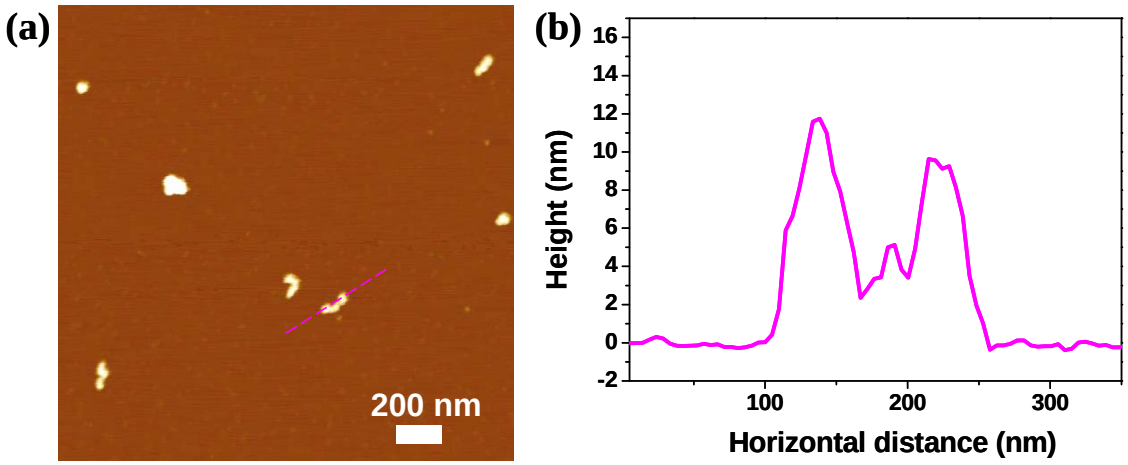

Figure 4. (a) AFM height image of IPECs by CPBs and short PSS, charge ratio $Z_{-/+}$ 2, AFM Z range 25 nm; (b) Section analysis of the cursors displayed in (a).

For the comparison, extremely long PSS (*DP*>10000) was used for the formation of IPECs with CPBs. Figure 5a shows the AFM image of the IPECs by CPBs and long PSS with charge ratio $Z_{-/+}$ of 0.2. Worm-like brushes are observed and some collapsed globular brushes co-exist. Different from the IPECs formed by CPBs and short PSS, no worm-like brushes with greater height could be found. Section analysis in figure 5b indicates that the globular IPEC is as high as 6.5 nm. This means that when long PSS was added to the CPBs, those brushes that formed IPECs with PSS immediately became collapsed spheres and no intermediate transition states were detected, which were found for the IPECs by CPBs and short PSS with $Z_{-/+}$ 0.1, 0.5 and 0.75. A good reason for this is that the PSS with extremely high molecular weight carries a huge amount of negative

charges (11000 negative charges for every molecule) and can induce the collapse of the single brush molecules in the solution.

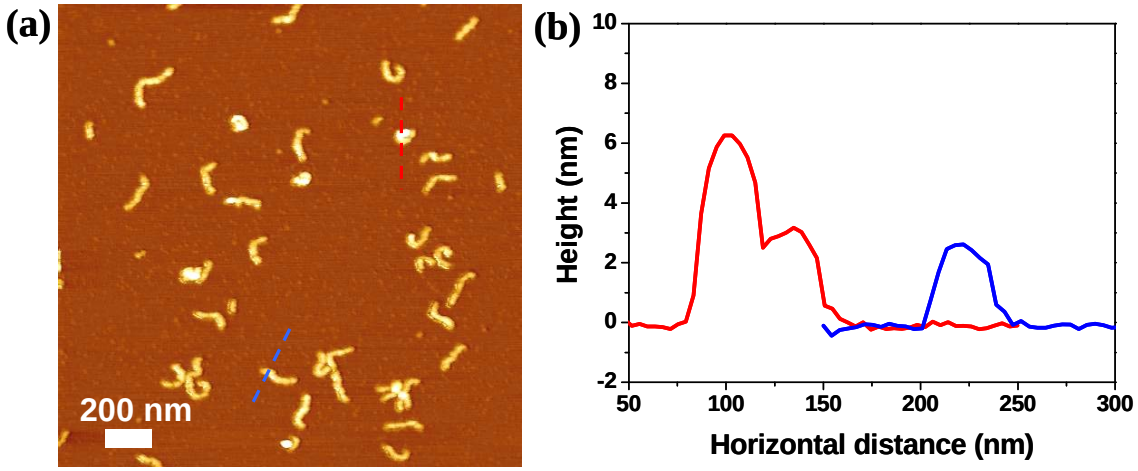

Figure 5. (a) AFM height image of IPECs by CPBs and long PSS, charge ratio $Z_{-/+}$ 0.2, AFM Z range 10 nm; (b) Section analysis of the cursors displayed in (a).

Further investigation on the IPECs formed by CPBs and long PSS with charge ratio 0.5 was carried out. Completely soluble solution was obtained. Figure 6a shows the AFM height image of the IPECs. Obviously, no worm-like structures can be observed any more and only some spherical objects with diameter of 90 nm are clearly seen. Phase image shown in figure 6b revealed that the brushes adopted twisted morphologies to form the spherical IPECs, obviously induced by the extremely long linear PSS. It is surprising that at charge ratio $Z_{-/+}$ as low as 0.5, most of the brushes were already collapsed into spheres. Section analysis displayed in figure 6e shows that the height of the spheres is only around 3.5 nm, which is quite lower than that of the IPECs with short PSS ($Z_{-/+}$ of 1). Interestingly, when NaCl was added to the soluble IPECs (0.1 M NaCl), the size of the spheres turned smaller (around 60 nm), and clear core-shell structures were observed both in the height and phase images, displayed in figure 6c and 6d. Section analysis shows that the height of the core reaches 12 nm. Since the cationic charges carried by the CPBs are still in excess to the negative charges by the PSS, the shell is probably non-complexed PMETAI side-chains and core is the IPECs between PMETAI and PSS. This suggests that without adding salt, the IPECs formed by the long PSS and CPBs were

quite loose. When salt is added, re-arrangement happened and denser IPECs were formed in the inner part and the non-complexed PMETAI side-chains remain outside.

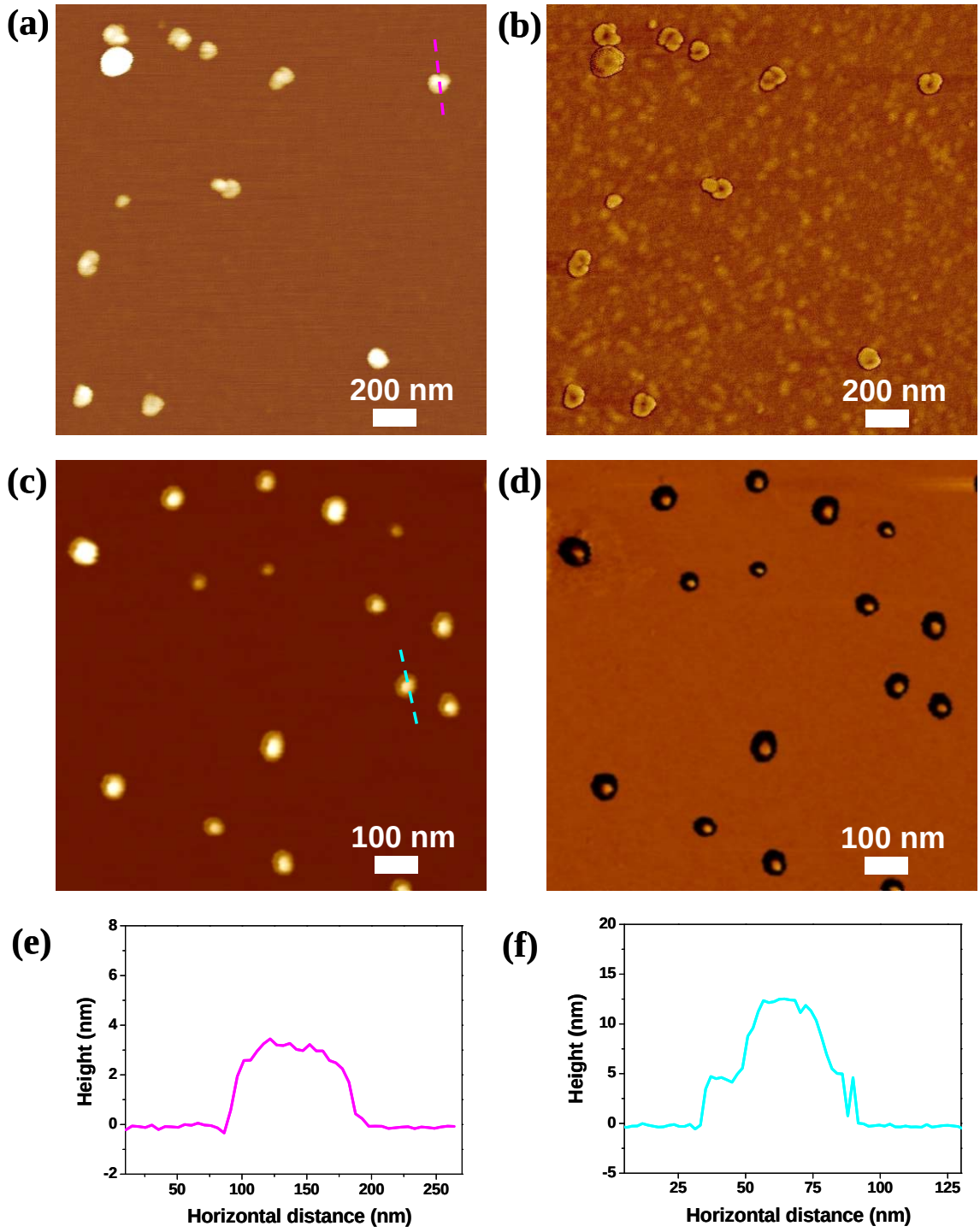

Figure 6. (a) AFM height image of IPECs by CPBs and long PSS, charge ratio $Z_{-/+}$ 0.5, AFM Z range 8 nm; (b) AFM phase image of IPECs by CPBs and long PSS, charge ratio

$Z_{-/+}$ 0.5, AFM Z range 12°; (c) AFM height image of IPECs by CPBs and long PSS from 0.1 M NaCl solution, charge ratio $Z_{-/+}$ 0.5, AFM Z range 35 nm; (d) AFM phase image of IPECs by CPBs and long PSS from 0.1 M NaCl solution, charge ratio $Z_{-/+}$ 0.5, AFM Z range 20°; (e) Section analysis of the cursors displayed in (a); and (f) Section analysis of the cursors displayed in (c).

IPECs by CPBs and PSS with charge ratio $Z_{-/+} > 0.5$ (0.75 and 1), most of the polymers precipitated from the solution and no objects were observed in the AFM measurements.

IPECs with excess long PSS ($Z_{-/+} = 2$) was also prepared for the comparison to those with short linear PSS. Very less objects were found on the substrate, probably due to the incompatibility of the negatively charged IPECs with the negatively charged mica surface. Ellipsoidal structures could be seen in figure 7a. Quantitative section analysis shows the IPECs are as high as 17 nm, which is higher than all the IPECs described above, probably due to the high molecular weight of the complex PSS.

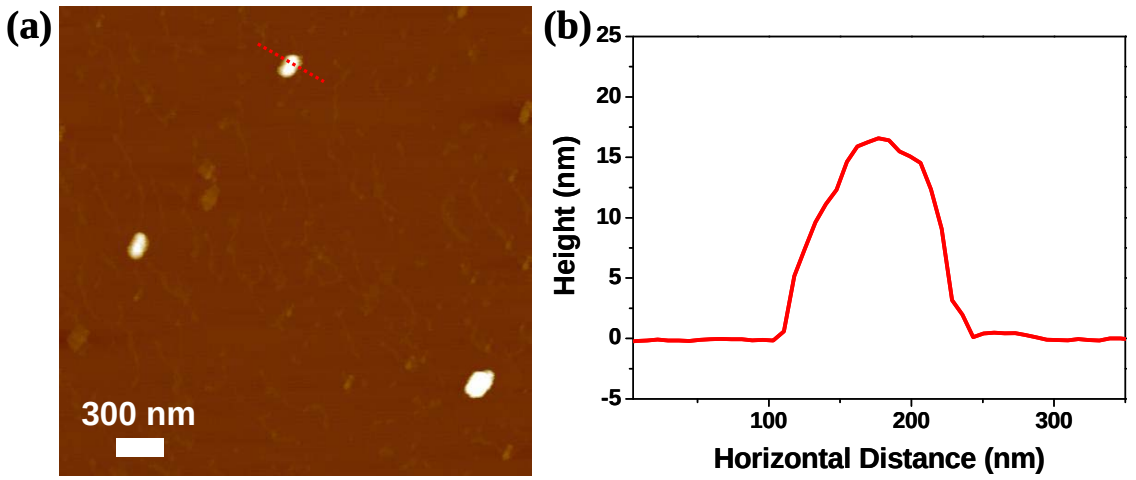

Figure 7. (a) AFM height image of IPECs by CPBs and long PSS, charge ratio $Z_{-/+}$ 2, AFM Z range 30 nm; (b) Section analysis of the cursors displayed in (a).

IPECs prepared by direct mixing

IPECs were also prepared by direct mix the two polymers. It was found that in this case, the inter-molecular aggregates were still dominating. Figure S1 in the supporting information shows the AFM height image of the IPECs formed by CPBs with short PSS

via direct mixing ($Z_{-/+}$ = 0.75). Big aggregates were clearly exhibited even at such a low concentration of brushes (0.02 g/L), and no single brushes were found.

Surprisingly, when long PSS was directly mixed with CPBs with charge ratio 2, in addition to the random big aggregates (supporting information Figure S2), micrometer-scale cylindrical objects were recorded by AFM measurements, demonstrated in figure 8a. The diameter of the cylinders is around 900 nm and the length varies from 1 μm to 5 μm. Due to the toxicity of the cationic CPBs to most of the bacteria[41], these objects are excluded as bacteria. From figure 8a, we can see the cylinders have non-continuous narrow cores and relatively long shells. Section analysis in figure 8b shows that the height of the core is around 1.8 nm, which is close to that of the pure brushes. The length of the fully stretched long PSS was calculated as 2.75 μm (11000×0.25 nm), which is longer than the cylinders' diameters. So the shell could be the extremely long PSS.

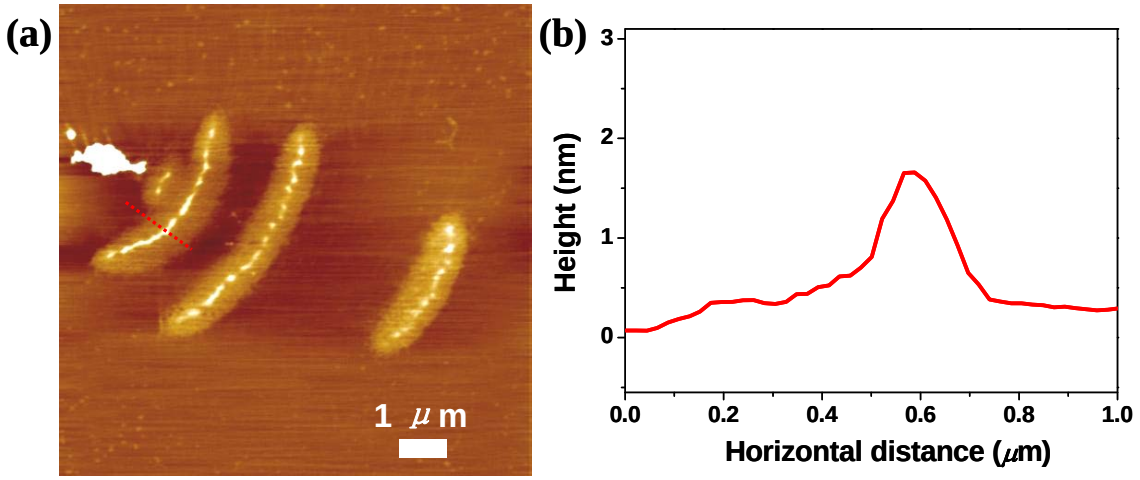

Figure 8. (a) AFM height image of IPECs by CPBs and long PSS via direct mixing, charge ratio $Z_{-/+}$ = 2, AFM Z range 3 nm; (b) Section analysis of the cursors displayed in (a).

In summary, we have investigated the IPECs formed by cationic CPBs and anionic linear PSS using AFM measurements. The IPECs were prepared either by dialysis of the salt solutions or by direct mixing the two components. When they are prepared by dialysis process, more well-defined structures were observed. It has been found that changing the charge ratios between the two polyelectrolytes, the morphologies of the CPBs could be tuned. For the IPECs with short PSS, two species were observed at the

charge ratio $Z_{-/+}$ of 0.1 and 0.5 and the brushes which formed IPECs became more straight on the substrates. When $Z_{-/+}$ reached 0.75, most of the brushes formed IPECs with PSS and helix-like transition states were found. If the amount of charges were equal, the brushes collapsed into sphere-like objects. Excess of polyanions stabilized the IPECs and the brushes adopted conformation of twisted worms. When extremely long PSS was used as the polyanions, they can induce the spherical collapse of the brushes at very low $Z_{-/+}$ ratios and no other transition states were detected. Full collapse of the brushes was demonstrated for $Z_{-/+} = 0.5$. Similarly, excess of the long linear polyanions kept the IPECs in solution. Interesting micrometer-scale core-shell cylinders were found by directly mixing CPBs with long PSS, which might be the non-equilibrium state caused by the kinetically controlled IPECs formation.

Conclusions

It has been demonstrated in this paper that the morphologies of the cationic CPBs could be tuned by the formation with linear anionic polyelectrolyte PSS. By using different charge ratios between the CPBs and PSS, the morphologies can be changed from straight cylinders through helix-like structures to fully collapsed spheres. The length of the linear polyanions has great impact to the formation of the IPECs. The findings could provide better understandings of the IPECs formed by polyelectrolytes or bio-macromolecules, and might be useful for the building of smart nano-sensors.

Acknowledgement

We thank Sreenath Bolisetty (PC I, Universität Bayreuth) for the DLS measurements. Financial support by Deutsche Forschungsgemeinschaft within SFB 481 is gratefully acknowledged.

Reference

1. Minko, S., *Responsive Polymer Materials: Design and Applications*. Blackwell Publishing Ltd.: Oxford, 2006.

2. Dai, L., *Intelligent Macromolecules for Smart Devices: From Materials Synthesis to Device Applications*. Springer-Verlag: London, 2003.

3. Wang, X.; Guerin, G.; Wang, H.; Wang, Y.; Manners, I.; Winnik, M. A. *Science* **2007,** 317, 644-647.

4. Yamamoto, Y.; Fukushima, T.; Saeki, A.; Seki, S.; Tagawa, S.; Ishii, N.; Aida, T. *J. Am. Chem. Soc.* **2007,** 129, 9276-9277.

5. Voets, I. K.; Van der Burgh, S.; Farago, B.; Fokkink, R.; Kovacevic, D.; Hellweg, T.; De Keizer, A.; Cohen Stuart, M. A. *Macromolecules* **2007,** 40, 8476-8482.

6. Kabanov, A. V.; Kabanov, V. A. *Bioconjugate Chem.* **1995,** 6, 7-20.

7. Wolfert, M. A.; Dash, P. R.; Nazarova, O.; Oupicky, D.; Seymour, L. W.; Smart, S.; Strohalm, J.; Ulbrich, K. *Bioconjugate Chem.* **1999,** 10, 993-1004.

8. Goffeney, N.; Bulte, J. W. M.; Duyn, J.; Bryant, L. H., Jr.; van Zijl, P. C. M. *J. Am. Chem. Soc.* **2001,** 123, 8628-8629.

9. Bronich, T.; Kabanov, A. V.; Marky, L. A. *J. Phys. Chem. B* **2001,** 105, 6042-6050.

10. Ariga, K.; Hill, J. P.; Ji, Q. *Phys. Chem. Chem. Phys.* **2007,** 9, 2319-2340.

11. Quinn, J. F.; Johnston, A. P. R.; Such, G. K.; Zelikin, A. N.; Caruso, F. *Chem. Soc. Rev.* **2007,** 36, 707-718.

12. Wang, Y.; Angelatos, A. S.; Caruso, F. *Chem. Mater.* **2008,** 20, 848-858.

13. Mandel, M. *Encycl. Polym. Sci. Eng.* **1987,** 11, 739-829.

14. Thünemann, A. F. *Prog. Polym. Sci.* **2002,** 27, 1473-1572.

15. Thünemann, A. F.; Müller, M.; Dautzenberg, H.; Joanny, J.-F.; Löwen, H. *Adv. Polym. Sci.* **2004,** 166, 113-171.

16. Philipp, B.; Dautzenberg, H.; Linow, K. J.; Koetz, J.; Dawydoff, W. *Prog. Polym. Sci.* **1989,** 14, 91-172.

17. Miura, N.; Dubin, P. L.; Moorefield, C. N.; Newkome, G. R. *Langmuir* **1999,** 15, 4245-4250.

18. Zhang, H.; Dubin, P. L.; Ray, J.; Manning, G. S.; Moorefield, C. N.; Newkome, G. R. *J. Phys. Chem. B* **1999,** 103, 2347-2354.

19. Welch, P.; Muthukumar, M. *Macromolecules* **2000,** 33, 6159-6167.

20. Leisner, D.; Imae, T. *J. Phys. Chem. B* **2003,** 107, 13158-13167.

21. Leisner, D.; Imae, T. *J. Phys. Chem. B* **2004,** 108, 1798-1804.

22. Kabanov, V. A.; Zezin, A. B.; Rogacheva, V. B.; Panova, T. V.; Bykova, E. V.; Joosten, J. G. H.; Brackman, J. *Faraday Discuss.* **2004,** 128, 341-354.

23. Pergushov, D. V.; Babin, I. A.; Plamper, F. A.; Zezin, A. B.; Müller, A. H. E. *Langmuir* **2008,** 24, 6414-6419.

24. Pergushov, D. V.; Remizova, E. V.; Feldthusen, J.; Zezin, A. B.; Müller, A. H. E.; Kabanov, V. A. *J. Phys. Chem. B* **2003,** 107, 8093-8096.

25. Pergushov, D. V.; Remizova, E. V.; Gradzielski, M.; Lindner, P.; Feldthusen, J.; Zezin, A. B.; Müller, A. H. E.; Kabanov, V. A. *Polymer* **2004,** 45, 367-378.

26. Gössl, I.; Shu, L.; Schlüter, A. D.; Rabe, J. P. *J. Am. Chem. Soc.* **2002,** 124, 6860-6865.

27. Störkle, D.; Duschner, S.; Heimann, N.; Maskos, M.; Schmidt, M. *Macromolecules* **2007,** 40, 7998-8006.

28. Zhang, M.; Müller, A. H. E. *J. Polym. Sci. Polym. Chem.* **2005,** 43, 3461-3481.

29. Sheiko, S. S.; Sumerlin, B. S.; Matyjaszewski, K. *Prog. Polym. Sci.* **2008,** 33, 759-785.

30. Pincus, P. *Macromolecules* **1991,** 24, 2912-19.

31. Borisov, O. V.; Zhulina, E. B. *Eur. Phys. J. B* **1998,** 4, 205-217.

32. Ballauff, M. *Prog. Polym. Sci.* **2007,** 32, 1135-1151.

33. Xu, Y.; Bolisetty, S.; Drechsler, M.; Fang, B.; Yuan, J.; Ballauff, M.; Müller, A. H. E. *Polymer* **2008,** 49, (18), 3957-3964.

34. Rühe, J.; Ballauff, M.; Biesalski, M.; Dziezok, P.; Gröhn, F.; Johannsmann, D.; Houbenov, N.; Hugenberg, N.; Konradi, R.; Minko, S.; Motornov, M.; Netz, R. R.; Schmidt, M.; Seidel, C.; Stamm, M.; Stephan, T.; Usov, D.; Zhang, H. *Adv. Polym. Sci.* **2004,** 165, 79-150.

35. Hua, F.; Kita, R.; Wegner, G.; Meyer, W. *ChemPhysChem* **2005,** 6, (2), 336-343.

36. Xu, Y.; Bolisetty, S.; Drechsler, M.; Fang, B.; Yuan, J.; Harnau, L.; Ballauff, M.; Müller, A. H. E. *Soft Matter* **2008**, in press.

37. Xu, Y.; Bolisetty, S.; Ballauff, M.; Müller, A. H. E. **2008,** submitted.

38. Sheiko, S. S.; Möller, M. *Chem. Rev.* **2001,** 101, 4099-4123.

39. Hofs, B.; Voets, I. K.; de Keizer, A.; Cohen Stuart, M. A. *Phys. Chem. Chem. Phys.* **2006,** 8, 4242-4251.

40. Gummel, J.; Cousin, F.; Boue, F. *J. Am. Chem. Soc.* **2007,** 129, 5806-5807.

41. Panarin, E. F.; Solovskii, M. V.; Zaikina, N. A.; Afinogenov, G. E. *Makromol. Chem., Supplement* **1985,** 9, 25-33.

Supporting information:

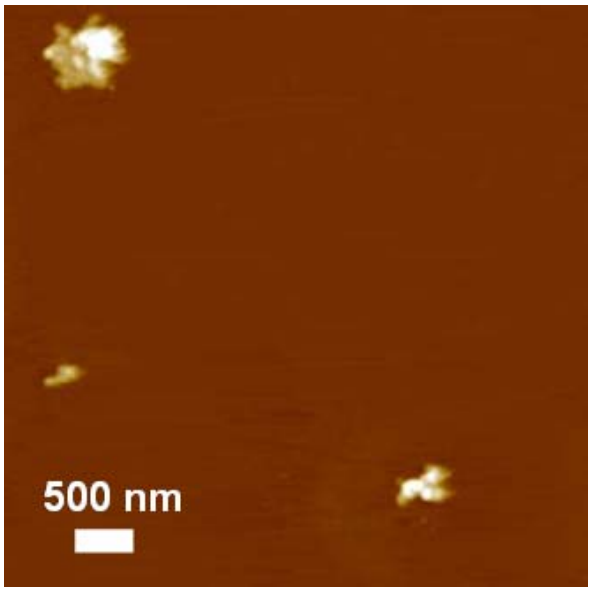

Figure S1. AFM height image of the IPECs formed by CPBs and short PSS with charge ratio $Z_{-/+}$ 0.75. AFM Z range 40nm.

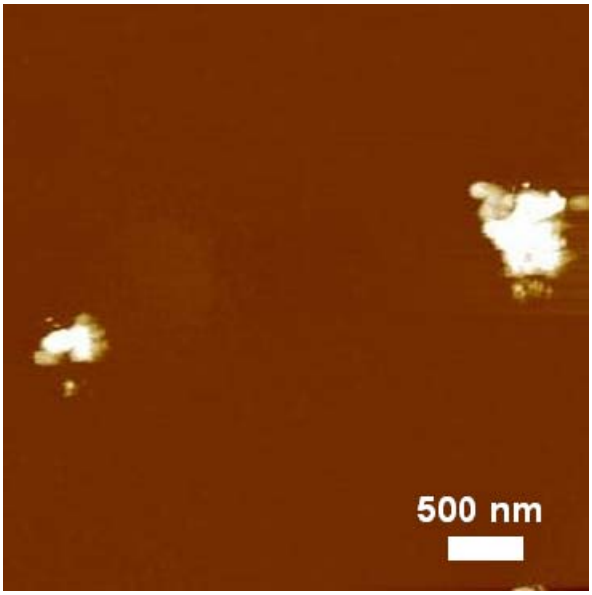

Figure S2. AFM height image of the IPECs formed by CPBs and long PSS with charge ratio $Z_{-/+}$ 2. AFM Z range 30nm.

8. Direct Synthesis of Poly(potassium 3-sulfopropyl methacrylate) Cylindrical Polymer Brushes via ATRP using Supramolecular Complex with Crown Ether

Youyong Xu[a], Andreas Walther[a], Sreenath Bolisetty[b], Matthias Ballauff[b], Axel H. E. Müller[a,*]

[a]*Makromolekulare Chemie II* , [b]*Physikalische Chemie I, and Bayreuther Zentrum für Kolloide und Grenzflächen, Universität Bayreuth, D-95440 Bayreuth, Germany*

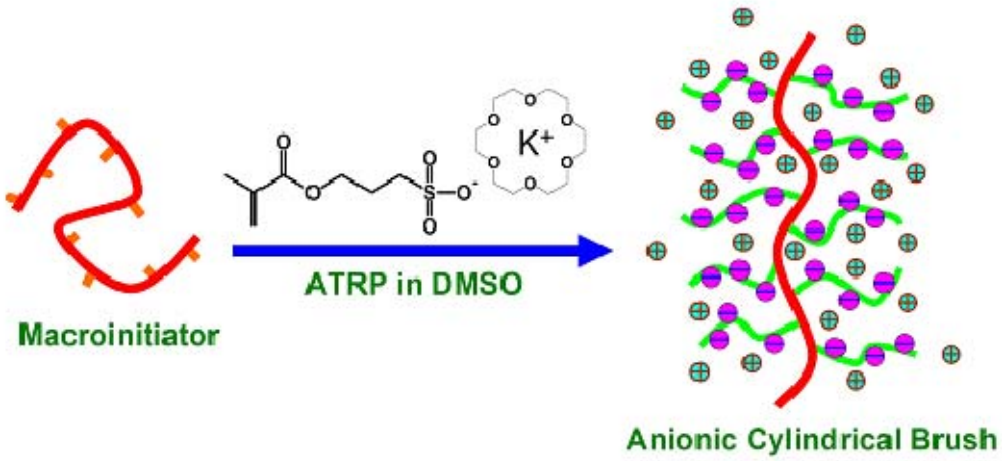

Manuscript to be submitted

Polyelectrolytes are polymers which carry a large number of charges and surrounding counterions[1]. Research on them has revealed their vital role in nature, and has promoted their wide applications in industry processes and our daily life[2]. Their conformations can be varied dramatically with added salt due to the strong Coulomb forces between the closely bound charges. When they are weak polyelectrolytes, the degree of ionization highly depends on the pH. Polyelectrolytes can form complex with oppositely charged polyelectrolytes, surfactants and colloidal particles[3, 4]. Extensive studies on linear polyelectrolytes have been carried out, while with the rapid development of nanotechnologies, more and more well-defined nanostructured polyelectrolytes are demanded for different cases of applications[5]. Cylindrical polyelectrolyte brushes (**CPB**s), which have relatively very long backbones and densely grafted side-chains, have drawn a lot of attention owing to their anisotropic nature, and special solution properties[6]. But the difficulties of preparing such kind of polymers have hindered the study on their properties and further applications. So far, very few examples of CPBs have been reported[6-11].

Both grafting-from[7, 8, 12] and grafting-through[6, 11] strategies have been used for the preparation of CPBs. In order to get CPBs with well-defined structures, living/controlled polymerizations were adopted to make either the backbone or the side-chains. For example, for the grafting-through method, anionic polymerization[6] and atomic transfer radical polymerization (ATRP)[11] have been used to prepare the side-chains. One limiting point for these polymerization methods is that the initiating or catalyst systems are very sensitive to different functional groups like hydroxyl, carboxylic or ionic groups, and maybe paralyzed by impurities like water. So generally, monomers with protected functional groups are needed. This complicated the synthesis process and more tedious synthetic steps, such as deprotection[7, 8, 11] and functionalization like quaternization[6, 12] and sulfonation[6], are required to get water-soluble CPBs. In some cases, it is very hard to reach full de-protection and functionalization due to the very high molecular weight of the CPBs. Side reactions, such as the cross-linking caused by sulfonation of polystyrene, happen occasionally[6]. Most ionic monomers are soluble in water and related living/controlled radical polymerizations have showed the possibilities of preparing polymers in aqueous or mixed solvents[13-15]. But another problem has to be addressed in

this case. Controlled radical polymerizations like ATRP are generally used for the preparation of CPBs by grafting-from strategy. Thus, macro-initiators, generally hydrophobic, have to be employed, which makes it impossible to carry out the polymerizations in water due to the low solubility of the macro-initiators. To solve the problem, good solvents for both macro-initiators and ionic monomers are badly needed.

In our continuous efforts of preparing different anionic and cationic CPBs, we mostly used ATRP for the grafting-from process[7, 8, 12]. More and more interests have now been shifted to strong polyelectrolytes due to their attractive solution and counterion properties. Previously, we reported the synthesis of a new strong cationic CPB and its responsiveness to counterions of different valencies[12, 16]. Strong anionic CPBs have also drawn our attention, since they may serve as a model for the study of the counterion distribution, and possible complexes with oppositely charged polyelectrolytes and even proteins[17]. Although Wegner et al has reported the synthesis of anionic CPBs by using protected sulfonated monomer, the further de-protections were somehow problematic and it was hard to get fully ionized CPBs[9, 10]. So we turned to non-protected sulfonated monomers. Solubility of two commercial sulfonated monomers, styrene-4-sulfonic acid sodium salt (**SSNa**) and potassium 3-sulfopropyl methacrylate (**SPMA**), have been tried in different solvents and they are soluble (or partially soluble) with high dilution in very polar solvent dimethyl sulfoxide (**DMSO**). This makes it possible to graft them from the macro-initiator, poly{2-(2-bromoisobutyryloxy)ethyl methacrylate} (**PBIEM**), which we have employed for the other brushes. However, direct ATRP of these monomers in DMSO caused precipitation 10 to 15 min after the reaction started, probably due to the low solubility of the high molecular weight strong ionic CPBs.

In this communication, we solved the problems mentioned above by forming supramolecular complexes between the monomer SPMA and crown ether 18-crown-6 (18-C-6), which not only improved the solubility of SPMA, but also stabilized the anionic CPBs in the polar organic solvent DMSO. Due to the improved solubility, narrowly distributed anionic CPBs with extremely high molecular weights (higher than 2×10^7 Da) were prepared. According to our knowledge, this is the first time that ionic monomer/crown ether supramolecular complex has been used for the ATRP process to directly prepare CPBs. The case described here not only shows the robustness of the

method for the synthesis of CPBs, it provides possibilities of building well-defined polyelectrolyte topologies such as ionic block copolymers, stars, spherical brushes, dendritic and hyperbranched polyelectrolytes, where hydrophobic (macro)initiators or precursors might be used.

Scheme 1 displays the synthetic procedures. Monomer SPMA first formed complex with 18-C-6, since it has been reported that 18-C-6 preferentially forms supramolecular complex with potassium ion[18, 19]. Then ATRP was employed to graft the SPMA/18-C-6 complex from macro-initiator PBIEM. After the polymerizations, dialysis was applied to purify the anionic poly(potassium 3-sulfopropyl methacrylate) cylindrical brushes (**BSPMA**).

Scheme 1. Synthetic procedures for anionic BSPMA.

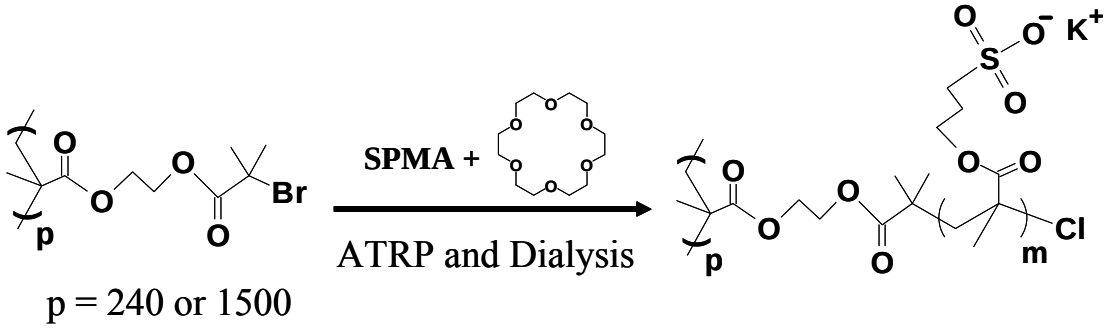

To prove the formation of the complex between SPMA and 18-C-6, ^{1}H NMR measurements were carried out. Figure 1a shows the ^{1}H NMR spectra of pure 18-C-6 and mixture of SPMA with 18-C-6 in DMSO. The inset clearly shows that the peak assigned to the methylene groups of 18-C-6 shifted from 3.51 to 3.55, which indicates the formation of supramolecular complex between 18-C-6 and potassium ions in monomer SPMA.

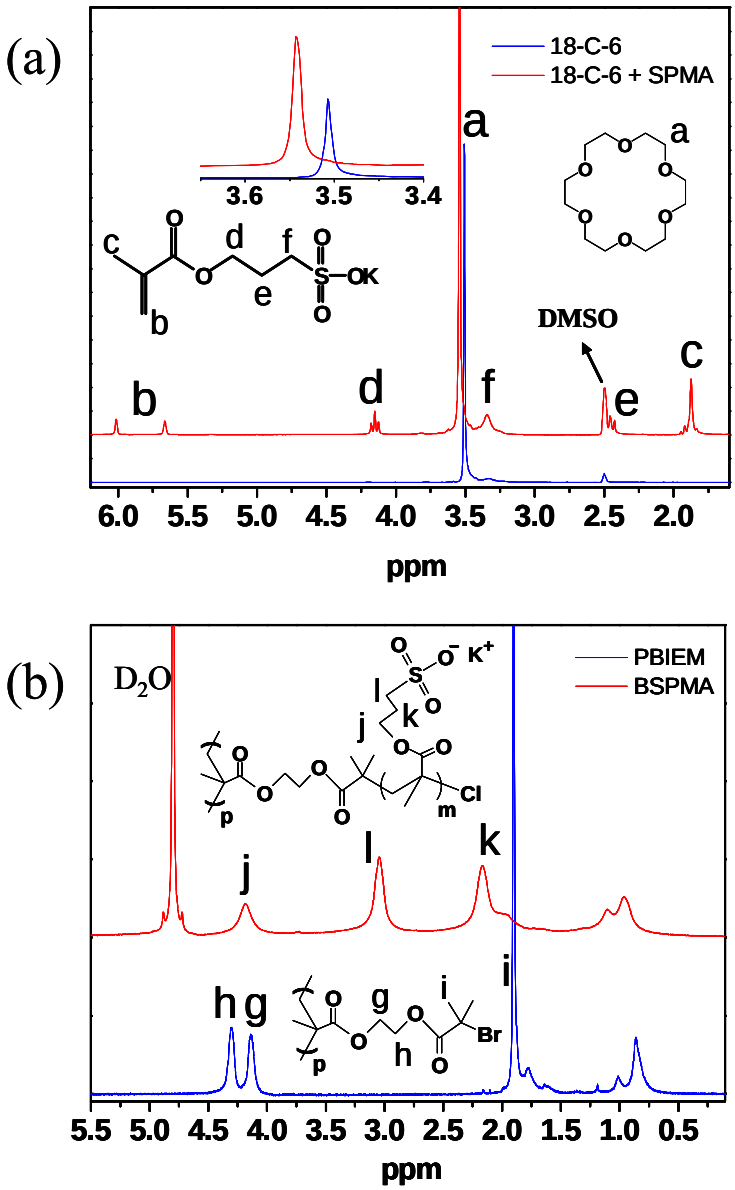

Figure 1. (a) ^{1}H NMR spectra of pure 18-C-6 and the mixture of SPMA with 18-C-6. The inset shows the magnified part between 3.4 ppm and 3.65 ppm; (b) ^{1}H NMR spectra of macro-initiator PBIEM and final anionic brush BSPMA.

For the preparation of anionic BSPMA, PBIEM with DP_n 240 and 1500 were employed, which has been reported previously by us[8]. The resulted brushes are termed as BSPMA1 and BSPMA2, respectively. In order to improve the initiating efficiency,

halogen exchange and high dilution (10 wt% of monomer) were adopted. The details of the ATRP process and molecular characterization was shown in table 1 and supporting information. After the polymerizations, the dark blue solution are miscible with water and various organic solvents like acetone, dioxane, THF, methanol and so on, which further proved that the 18-C-6 also forms complex with the as-prepared anionic BSPMA since without the 18-C-6, these highly ionic polymers are not soluble in those organic solvent and should precipitate. Dialysis against dioxane was first carried out to remove 18-C-6, internal standard anisole and ligand HMTETA. After 5 days' dialysis, the polymers precipitated in the dialysis tubes. Then the dialysis media was changed to 0.2 M KCl solution for 7 days to remove copper inside and the color turned transparent and colorless. Final product BSPMA was obtained by further dialysis in pure water for 5 days. And after the freeze-drying, white powders were obtained, indicating no copper remains in the BSPMA brushes. The brushes are well soluble in water.

Table1. ATRP of SPMA in DMSO and molecular characterizations.

sample	Conv.[b]	$DP_{sc,calc}$[c]	$10^7 * M_{n,calc}$[d]	$10^7 * M_{w,sls}$[e]	$R_{h,app}$[f] *(PDI)*	$M_{n,PMAA}$[g]	$DP_{sc,exp}$[h]	f[i]
BSPMA1	17.8%	89	0.53	NA	34nm *(0.140)*	NA	NA	NA
BSPMA2	12.7%	64	2.40	2.63	74nm *(0.173)*	15700	182	0.35

[a]10 wt % of monomer in DMSO and 10 wt% anisole as internal standard. 18-crown-6 was added with the same mole amount to monomer. ATRP at R. T. with constant ratio of $[M]_0/[I]_0/[CuCl]_0/[HMTETA]_0$ = 500:1:2:2. [b]Monomer conversion determined by ^{1}H NMR. [c]Calculated *DP* of side-chains, $DP_{sc,calc} = ([M]_0/[I]_0) \times$conversion. [d]Calculated from monomer conversion. $M_{n,calc}$= (Monomer molecular weight $\times DP_{sc,calc}$ + 234.5)$\times$ $DP_{backbone}$. [e]determined by SLS in 0.1 M NaCl solutions. dn/dc was determined to be 0.1157 mL/g. [f]Apparent hydrodynamic radius and polydispersity measured by DLS in 0.1 M NaCl solutions. [g]Number averaged molecular weight of PMAA obtained from the hydrolysis of the brushes, determined by water GPC using linear PMAA calibration. [h]*DP* of the PMAA obtained from the hydrolysis of the brushes. [i]Initiating efficiency $f = DP_{sc,calc}/DP_{sc,exp}$.

Figure 1b shows the ^{1}H NMR spectra of PBIEM and BSPMA2. It is observed that the sharp peak for the methyl groups neighboring the bromide (peak i, 1.9 ppm) and two peaks for the methylene groups between two ester bonds (peak g and h, 4.1 ppm and 4.3

ppm, respectively) in PBIEM disappeared, while distinct peaks j, k, l (4.2 ppm, 2.2 ppm, and 3.1 ppm, respectively) appears in the brush BSPMA (assigned to the three methylene groups linking ester bond and sulfonate group). This verifies the successful grafting of the SPMA from macro-initiator PBIEM.

Conventional aqueous gel permeation chromatography (GPC) was measured for BSPMA2, although it is not able to determine the true molecular weight and polydispersity of the CPBs (see supporting information, figure S1). The Mono-modal peak also revealed the formation of the BSPMA brush.

In order to determine the true molecular weight of the brush, static light scattering (SLS) measurement was performed for BSPMA2 in 0.1 M NaCl solution. Absolute weight averaged molecular weight (M_w) shown in table 1 is in accordance with the calculated number averaged molecular weight (M_n), suggesting the accurate realization of brush BSPMA with extremely high molecular weight (more than 2×10^7 Da).

Brushes with two different backbones were subjected to dynamic light scattering measurements in 0.1 M NaCl solutions. CONTIN plots show narrow mono-modal peaks for both brushes. As shown in table 1, the apparent hydrodynamic radius of BSPMA2 (74 nm) is much higher than that of BSPMA1 (34 nm), due to the DP_n of the macro-initiator for BSPMA2 is much larger than that for BSPMA1. The polydispersities for both brushes are quite narrow (<0.2), demonstrating the well-defined structures of the BSPMA brushes.

Considering the new ATRP process with complexed ionic monomer with crown ether in very polar solvent, it is interesting to know the initiating efficiency for these brushes. Brush BSPMA2 was subjected to cleavage reaction in strong base and heating environment. The procedure was described in supporting information scheme S1. The side-chains were cleaved from the backbone and were finally transformed into linear poly(methacrylic acid) (PMAA) (evidenced by the ^{1}H NMR spectrum shown in supporting information figure S3). Further aqueous GPC measurement using linear PMAA as calibration was carried out to determine the real *DP* of the side-chains in the brush BSPMA2. As listed in table 1, there is a great difference between the *DP* of the cleaved side-chains and that calculated from monomer conversion, and the initiating efficiency was only 0.35, which is much lower than that for other monomers reported by us[7, 12], although measures like halogen exchange and high dilution were taken. The reason

probably lies in three points: first, the incompatibility of the hydrophobic macro-initiator and the ionic monomer, even if it has formed complex with crown ether; second, the steric hindrance raised by the complex formation between the monomer and crown ether; and third, the high polarity of DMSO, which boosted the rate of the side-chain growth and relatively make the initiating process slower[20]. Nevertheless, the low initiating efficiencies for the grafting-from process in preparing cylindrical polymer brushes have been pointed out by Matyjaszewski *et al* before,[21, 22] and our case is just another example to show that.

Direct evidence for the successful preparation of BSPMA brushes was provided by atomic force microscopy (AFM) measurements shown in figure 2. For BSPMA1, the backbone is relatively short and its length is comparable with the side-chains. Thus it mainly shows spherical or ellipsoid morphologies, with average diameter around 40 nm (see figure 2b). When it comes to BSPMA2, which has a very long backbone, worm-like structures can be clearly observed in figure 2a. The average length for BSPMA2 is around 120 nm, which is considerably lower than that of other brushes grafting from the same backbone[8, 12]. This may be attributed to the much lower grafting density of the side-chains.

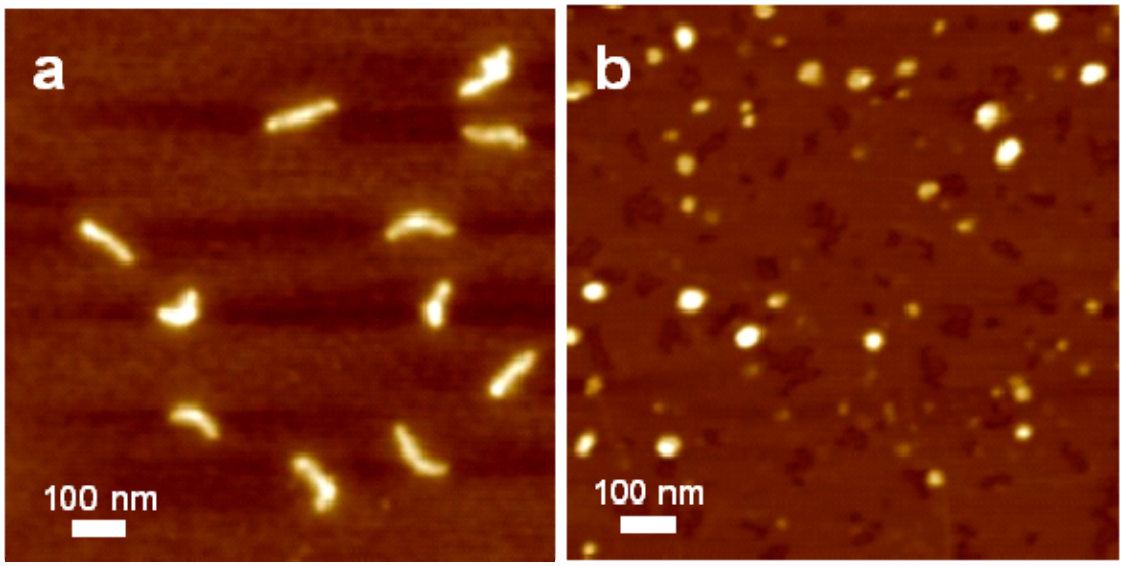

Figure 2. AFM height images of (a) BSPMA2 and (b) BSPMA1 dip-coated on mica surface from 0.01 g/L solutions in water without added salt. AFM Z ranges are 10 nm and 15 nm, respectively.

The real morphologies of BSPMA brush in solution were revealed by cryogenic transmission electron microscopy (cryo-TEM) measurement. Figure 3 shows the cryo-TEM images of BSPMA2 (1g/L) in 0.1 M CsCl solution, which can enhance the contrast of the brush in solution. Clear worm-like structures are found in large scale and the average length of BSPMA2 obtained from the cryo-TEM image is around 130 nm, a little higher than that by AFM measurement. Interestingly, some black dots of 2 to 3 nm were found around the brushes, as displayed in figure 3b. This might be a good evidence for the condensation of counterions around the strong anionic CPBs[23, 24].

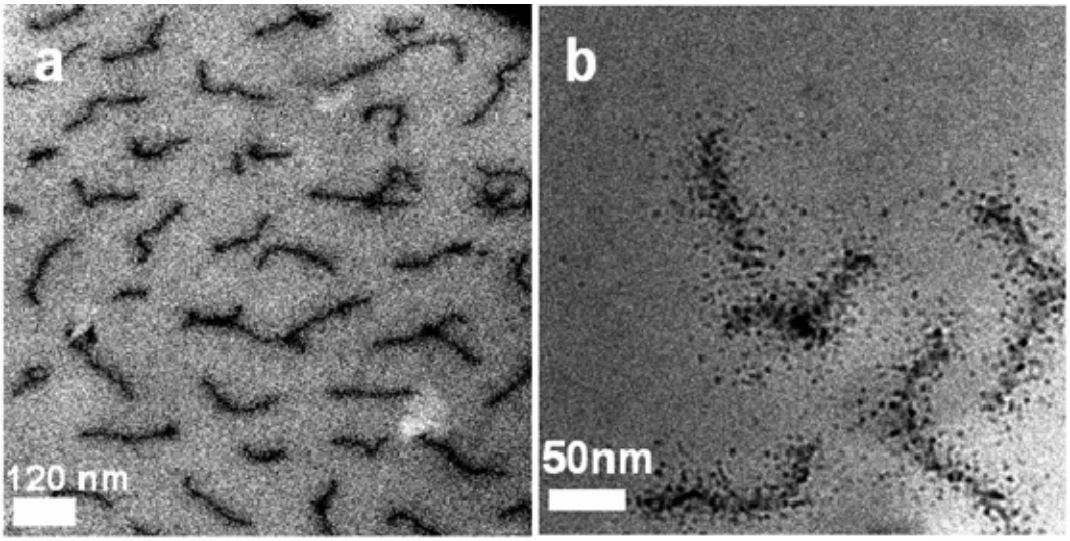

Figure 3. Cryo-TEM images of BSPMA2 (1g/L) in 0.1 M CsCl solutions (a), and at a higher magnification.

In conclusion, we have demonstrated the successful preparation of strong anionic CPBs by direct grafting of SPMA/crown ether complex in DMSO. Measurements of ^{1}H NMR, aqueous GPC, DLS and SLS proved the formation of the BSPMA brushes with backbones of different lengths. Cleavage of the side-chains revealed the low initiating efficiency for the ATRP of such systems. AFM and cryo-TEM measurements displayed the worm-like structures of BSPMA either on surface or in solution. The method by forming supramolecular complex with crown ether not only provides a straightforward and convenient way in preparing CPBs, but also could be extended to the building of other polyelectrolytes with different topologies, such as block copolymers, stars,

spherical brushes with different cores, dendritic and hyperbranched polymers. Study of the solution properties of the prepared strong anionic CPBs is in progress. Detailed kinetic investigations into the ATRP process of SPMA/crown ether system in different solvents are also going on, and the results will be published elsewhere.

Acknowledgement

The authors are grateful to the financial support by Deutsche Forschungsgemeinschaft (DFG) within SFB 481.

Supporting information available

Experimental details, characterization methods, aqueous GPC of BSPMA2, DLS CONTIN plots of BSPMA1 and BSPMA2, scheme of cleavage reaction, ^{1}H NMR and aqueous GPC of cleaved PMAA.

References

1. Dautzenberg, H.; Jaeger, W.; Kötz, J.; Philipp, B.; Seidel, C.; Stscherbina, D., *Polyelectrolytes: Formation, Characterization and Application*. Carl Hanser Verlag: Munich, 1994.

2. Mandel, M. *Encycl. Polym. Sci. Eng.* **1987,** 11, 739-829.

3. Thünemann, A. F. *Prog. Polym. Sci.* **2002,** 27, 1473-1572.

4. Thünemann, A. F.; Müller, M.; Dautzenberg, H.; Joanny, J.-F.; Löwen, H. *Adv. Polym. Sci.* **2004,** 166, 113-171.

5. Bohrisch, J.; Eisenbach, C. D.; Jaeger, W.; Mori, H.; Müller, A. H. E.; Rehahn, M.; Schaller, C.; Traser, S.; Wittmeyer, P. *Adv. Polym. Sci.* **2004,** 165, 1.

6. Rühe, J.; Ballauff, M.; Biesalski, M.; Dziezok, P.; Gröhn, F.; Johannsmann, D.; Houbenov, N.; Hugenberg, N.; Konradi, R.; Minko, S.; Motornov, M.; Netz, R. R.; Schmidt, M.; Seidel, C.; Stamm, M.; Stephan, T.; Usov, D.; Zhang, H. *Adv. Polym. Sci.* **2004,** 165, 79-150.

7. Cheng, G.; Böker, A.; Zhang, M.; Krausch, G.; Müller, A. H. E. *Macromolecules* **2001,** 34, 6883-6888.

8. Zhang, M.; Breiner, T.; Mori, H.; Müller, A. H. E. *Polymer* **2003,** 44, 1449-1458.

9. Lienkamp, K.; Ruthard, C.; Lieser, G.; Berger, R.; Gröhn, F.; Wegner, G. *Macromol. Chem. Phys.* **2006,** 207, 2050-2065.

10. Lienkamp, K.; Noe, L.; Breniaux, M.-H.; Lieberwirth, I.; Gröhn, F.; Wegner, G. *Macromolecules* **2007,** 40, 2486-2502.

11. Hua, F.; Kita, R.; Wegner, G.; Meyer, W. *ChemPhysChem* **2005,** 6, 336-343.

12. Xu, Y.; Bolisetty, S.; Drechsler, M.; Fang, B.; Yuan, J.; Ballauff, M.; Müller, A. H. E. *Polymer* **2008,** 49, 3957-3964.

13. Ashford, E. J.; Naldi, V.; O'Dell, R.; Billingham, N. C.; Armes, S. P. *Chem. Comm.* **1999**, 1285-1286.

14. Wang, X. S.; Jackson, R. A.; Armes, S. P. *Macromolecules* **2000,** 33, 255-257.

15. Masci, G.; Bontempo, D.; Tiso, N.; Diociaiuti, M.; Mannina, L.; Capitani, D.; Crescenzi, V. *Macromolecules* **2004,** 37, 4464-4473.

16. Xu, Y.; Bolisetty, S.; Drechsler, M.; Fang, B.; Yuan, J.; Harnau, L.; Ballauff, M.; Müller, A. H. E. *Soft Matter* **2008**, in press.

17. Wittemann, A.; Haupt, B.; Ballauff, M. *Phys. Chem. Chem. Phys.* **2003,** 5, 1671-1677.

18. Pedersen, C. J. *J. Am. Chem. Soc.* **1967,** 89, 7017-36.

19. Pedersen, C. J.; Frensdorff, H. K. *Angew. Chem. Int. Ed.* **1972,** 11, 16-25.

20. Matyjaszewski, K.; Xia, J. *Chem. Rev.* **2001,** 101, 2921-2990.

21. Neugebauer, D.; Sumerlin, B. S.; Matyjaszewski, K.; Goodhart, B.; Sheiko, S. S. *Polymer* **2004,** 45, 8173-8179.

22. Sumerlin, B. S.; Neugebauer, D.; Matyjaszewski, K. *Macromolecules* **2005,** 38, 702-708.

23. Pincus, P. *Macromolecules* **1991,** 24, 2912-19.

24. Borisov, O. V.; Zhulina, E. B. *Eur. Phys. J. B* **1998,** 4, 205-217.

Supporting information

Experimental details:

Materials. CuCl (97%, Aldrich) was purified by stirring with acetic acid overnight. After filtration, it was washed with ethanol and diethyl ether and then dried in vacuum oven. *N*,*N*,*N*',*N*'',*N*''',*N*'''-hexamethyltriethylenetetraamine (HMTETA, Aldrich) was distilled before use. Potassium 3-sulfopropyl methacrylate (98%, Aldrich) was used directly. All the other solvents and chemicals were used as received. Regenerated cellulose membranes were used for the dialysis (Spectra/Pore 7 with MWCO = 12000 Da).

Polymerizations. All polymerizations were carried out in round-bottom flasks sealed with rubber septa. A typical example of the synthesis of BSPMA2 is described as follows: PBIEM (27.9 mg, 0.1 mmol of initiating α-bromoester groups), SPMA (12.3 g, 0.05 mol) and 18-crown-6 (13.2 g, 0.05 mol) were dissolved in DMSO (100 g) in a round-bottom flask and stirred overnight to assure the complete dissolution of the complex and macro-initiator. Then anisole (12 g) was injected via a syringe and stirred for 15 min. Afterwards, CuCl (19.8 mg, 0.2 mmol) was added and the flask was purged with argon for 15 min. About 0.5 mL of solution was taken out with an argon-purged syringe as an initial sample for conversion measurement by ^{1}H NMR. The round-bottom flask was then inserted into a water bath at room temperature (25 ^{o}C). HMTETA (46mg, 0.2 mmol) was injected by argon-purged syringe to start the reaction. Small amounts of samples were taken out at intervals to check the monomer conversion by ^{1}H NMR. After 45 min, the reaction solution was stopped by opening to the air. Final conversion determined by ^{1}H NMR reached 12.7%. The solution was first dialyzed against dioxane for 5 days to remove 18-C-6, internal standard anisole and ligand HMTETA. The polymers precipitated in the dialysis tubes. Then the dialysis media was changed to 0.2 M KCl solution for 7 days to remove copper inside and the color turned transparent and colorless. Final product BSPMA was obtained by further dialysis in pure water for 5 days. After freeze-drying, white powders were obtained.

Cleavage of the side chains: The cleavage of the side chains was carried out by alkaline hydrolysis. The reaction is described as follows: 100 mg of BSPMA2 and about

20 ml of concentrated NaOH (18 M) aqueous solution were put into a PE vial and heated for 14 days at 90 °C. Concentrated HCl solution was added to the solution to tune the pH to around 4. This solution was freeze-dried and re-dissolved in water. Dialysis was carried out against pure water by using regenerated membranes (Millipore SpectraPore 7 MWCO 1000) over 3 days. In order to ensure the full protonation of the final product, poly(methacrylic acid) (PMAA), a small amount of HCl was added before freeze-drying the solution. ^{1}H-NMR measurement in D_2O was performed to check the conversion of the ester cleavage. Aqueous GPC was used to check the molecular weight of the final PMAA product with a PMAA calibration.

Characterization. *^{1}H NMR* was measured on a Bruker AC-250 instrument at room temperature.

An *aqueous GPC* (internal standard, ethylene glycol; additives: 0.1 M NaN_3, 0.01 M NaH_2PO_4) was applied to determine the elution curve of BSPMA2 and the molecular weight of PMAA (PMAA standards, PSS, Mainz). Column set: two 8mm PL Aquagel-OH columns (mixed and 30 Å), operated at 35°C and RI detection.

Static light scattering (SLS) was measured on a Sofica goniometer using a He-Ne laser (λ = 632.8 nm). Prior to the light scattering measurements, the sample solutions were filtered 3 times by using Millipore Nylon filters with a pore size of 1 μm. Four concentrations of the BSPMA2 solutions in 0.1 M NaCl were measured at angles in the range from 30 ^{o} to 150 ^{o}. The weight-average molecular weight, M_w was obtained by the analysis of the Zimm-plots. The refractive index increment in 0.1 M NaCl solution at 25 °C was measured to be dn/dc = 0.1157 mL/g using a PSS DnDc-2010/620 differential refractometer.

Dynamic light scattering (DLS) was carried out on an ALV DLS/SLS-SP 5022F compact goniometer system with an ALV 5000/E correlator and a He-Ne laser (λ = 632.8 nm) at an angle of 90^{o}. The sample solutions were filtered 3 times by using Millipore Nylon filters with a pore size of 1 μm before the light scattering measurements. CONTIN analyses were performed for the measured intensity correlation functions. Apparent hydrodynamic radii, $R_{h,app}$, were calculated according to the Stokes-Einstein equation.

Atomic force microscopy (AFM) measurements were performed on a Digital Instruments Dimension 3100 microscope operated in tapping mode. The micro-cantilever used for the AFM measurements were from Olympus with resonant frequency between 284.3 kHz and 386.0 kHz, and spring constant ranging from 35.9 to 92.0 N/m. The samples were prepared by dip-coating on freshly cleaved mica from 0.01 g/L brush solutions.

For cryogenic transmission electron microscopy (cryo-TEM) studies of BSPMA2, a drop of the sample (aqueous solution with 0.1 M CsCl, concentration around 1 g/L) was put on an untreated bare copper TEM grid (600 mesh, Science Services, München, Germany), where most of the liquid was removed with blotting paper, leaving a thin film stretched over the grid holes. The specimens were instantly shock vitrified by rapid immersion into liquid ethane and cooled to approximately 90 K by liquid nitrogen in a temperature-controlled freezing unit (Zeiss Cryobox, Zeiss NTS GmbH, Oberkochen, Germany). The temperature was monitored and kept constant in the chamber during all the sample preparation steps. After the sample is frozen, it was inserted into a cryo-transfer holder (CT3500, Gatan, München, Germany) and transferred to a Zeiss EM922 EFTEM. Examinations were carried out at temperatures around 90 K at an acceleration voltage of 200 kV. Zero-loss filtered images (ΔE = 0 eV) were taken under reduced dose conditions (100-1000 electrons/nm2). All images were registered digitally by a bottom-mounted CCD camera system (Ultrascan 1000, Gatan) combined and processed with a digital imaging processing system (Gatan Digital Micrograph 3.10 for GMS 1.5).

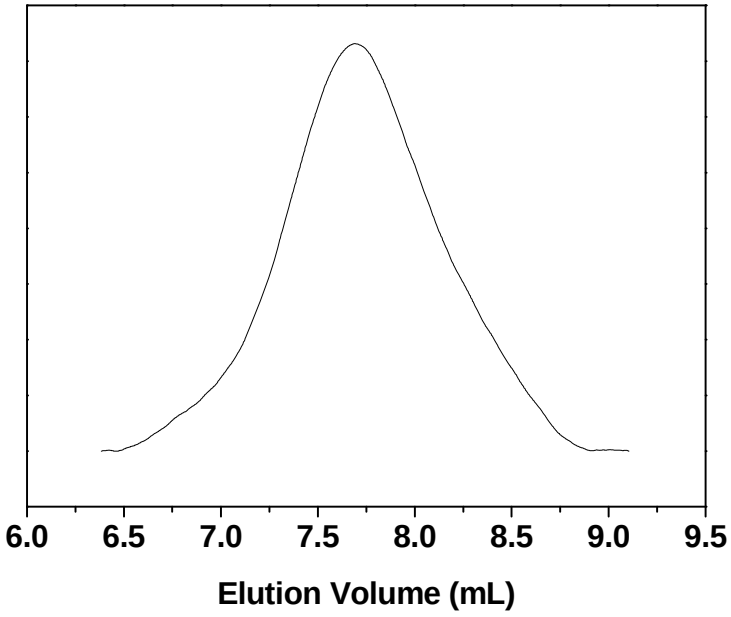

Figure S1: Aqueous GPC elution curve of BSPMA2.

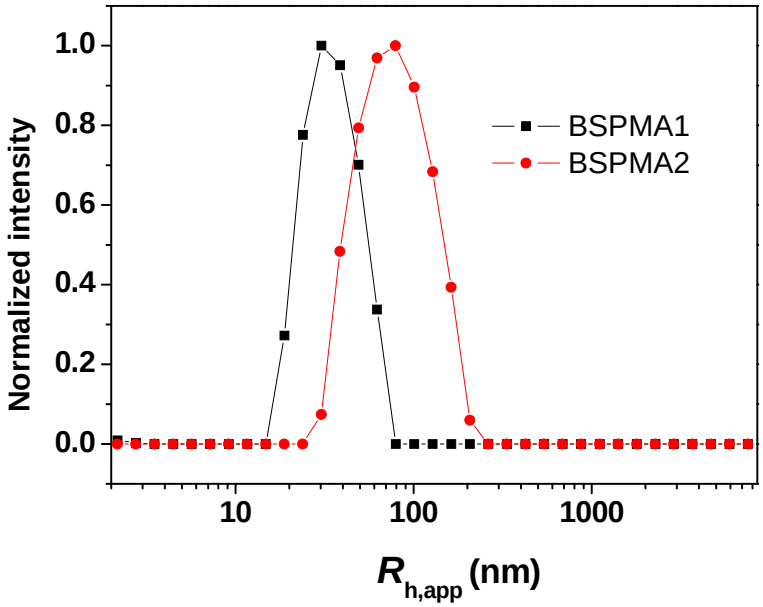

Figure S2: DLS CONTIN plot of BSPMA1 and BSPMA2 in 0.1 M NaCl solutions.

Scheme S1: Cleavage reaction of BSPMA2.

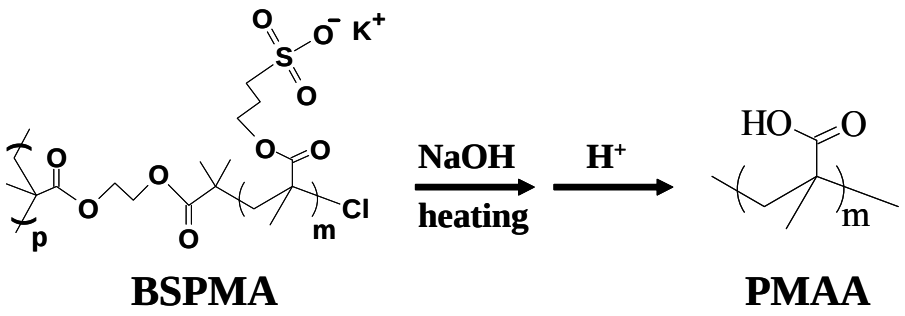

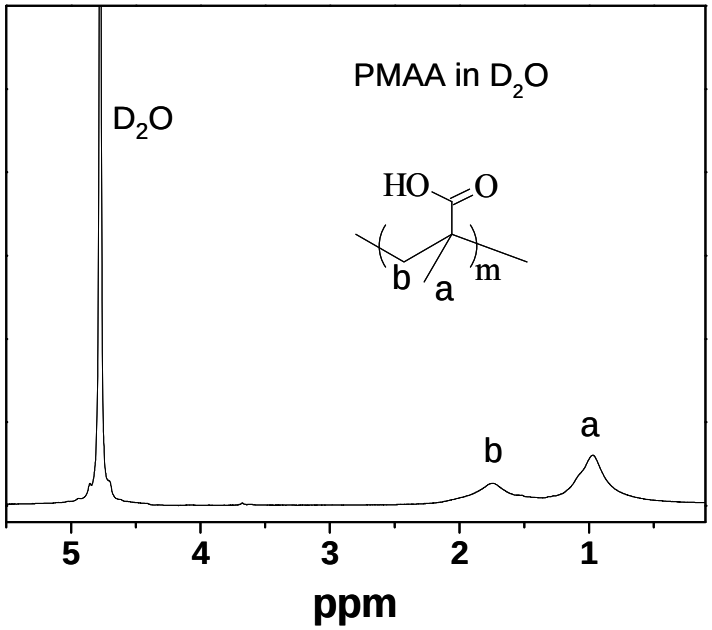

Figure S3. ^{1}H NMR spectrum of the cleaved PMAA.

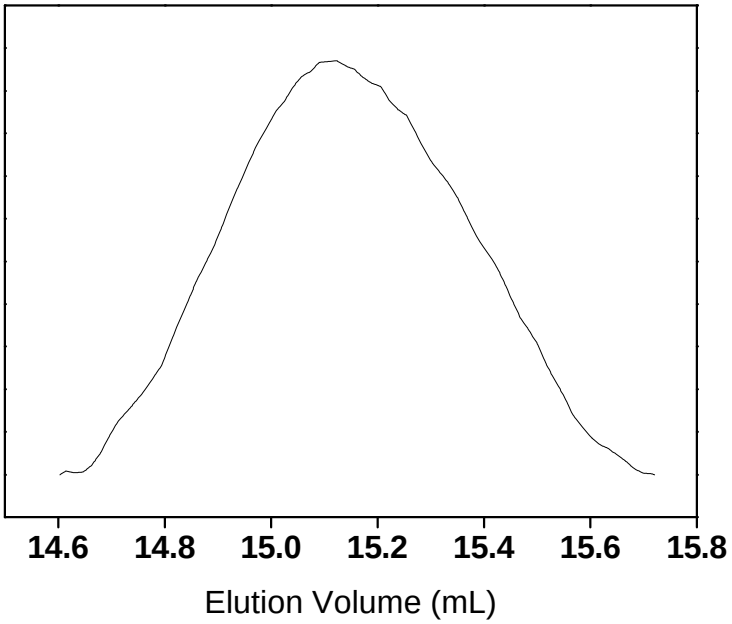

Figure S4. Aquesous GPC elution curve of the cleaved PMAA.

9. Hybrids of Magnetic Nanoparticles with Double-hydrophilic Core-shell Cylindrical Polymer Brushes and their Alignment in Magnetic Field

Youyong Xu[1], Jiayin Yuan[1], Bing Fang[1], Markus Drechsler[1], Sreenath Bolisetty[2], Matthias Ballauff[2], and Axel H. E. Müller[1,*]

[1]*Makromolekulare Chemie II* , [2]*Physikalische Chemie I, and Bayreuther Zentrum für Kolloide und Grenzflächen, Universität Bayreuth, D-95440 Bayreuth, Germany*

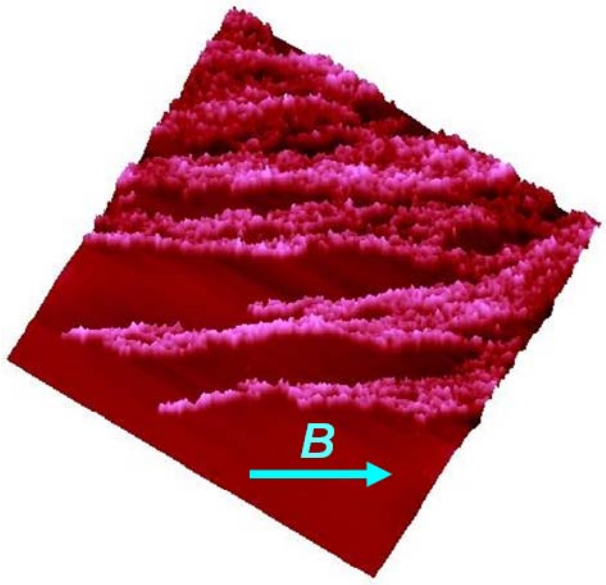

Manuscript to be submitted

Abstract

We demonstrate in this paper the synthesis of double-hydrophilic core-shell cylindrical polymer brushes (CPBs), their hybrids with magnetite nanoparticles using introducing-into strategy, and the directed alignments of the magnetic hybrid cylinders by magnetic fields. Consecutive grafting from a macro-initiator poly(2-(2-bromoisobutyryloxy)ethyl methacrylate) (PBIEM) by *tert*-butyl methacrylate (tBMA) and oligoethyleneglycol methacrylate (OEGMA) using ATRP technique was performed and further de-protection yielded core-shell CPBs with poly(methacrylic acid) (PMAA) as the core and POEGMA as the shell, which was evidenced by ^{1}H NMR, GPC, DLS and SLS. The resulted core-shell brush is well soluble in water and shows pH responsiveness due to the weak polyelectrolyte core. Pearl-necklace structures were observed in the cryo-TEM image at pH 4, while at pH 7, these structures disappeared owing to the ionization of the core. Similar morphology was also found for the polychelate of the core-shell CPBs with Fe^{3+}. Superparamagnetic magnetite nanoparticles were parepared and introduced into the core-shell brushes. The hybrid material retained the superparamagnetic property of the magnetite particles, verified by the SQUID. Large-scale alignments of the hybrid cylinders in relatively low magnetic fields were performed on surface, clearly clarified by AFM and TEM measurements.

Key words:

Double-hydrophilic, cylindrical polymer brushes, magnetic nanoparticles, alignment, pH responsive, polychelate

Introduction

Stimulus-responsive polymers have gained a lot of research interests due to their potential applications in many intelligent devices[1]. In the past years, polymers sensitive to different stimuli such as solvent, temperature, pH and salt have been widely developed. With the advances in the nanotechnologies and living/controlled polymerization techniques[2-4], nano-structured polymer systems with mono- and multi-responsiveness have also been well established. Although people have long been intrigued by the self-assembly of natural or synthetic polymers[5-9], the attention has been shifted to directed or controlled assembly of the polymers or their hybrids for specific demands[10-12]. Rational utilization of the sensitiveness of the polymers and other materials for the building of smart devices has been a hot topic[13]. Controlled assembly of the polymers or hybrids to form patterned or aligned structures is an especially important example[14, 15], which has found its practical applications in the micro-electronics and liquid crystal displays. External forces are required to drive the formation of the ordered structures. Mechanical forces like shear flow[16-20] have proven to be successful in the orientation of polymer systems. Recently, electric field[21, 22] has been thriving in the alignment of block copolymers. Controlled alignment of polymers or their hybrids by magnetic field is also emerging in many aspects[23-27]. The non-contacting alignment by magnetic field is easier to handle and safer than that by electric field. But many challenges are still remaining. In most cases, very high magnetic fields are necessary to orient the organic polymers[23, 24, 27]. Inorganic magnetic materials have been incorporated into different polymers to generate better responses to magnetic field[28]. With the development of nanotechnologies and demands for smaller nano-objects, many contributions have been made to the synthesis of magnetic nanoparticles and their hybrids with polymers or other materials[29-36]. Pyun et al[37-39] showed the preparation of polymer grafted ferromagnetic cobalt nanoparticles and their alignment in magnetic fields. Minko et al[40] made the complex of magnetite nanoparticles with polyelectrolytes and their orientation in magnetic fields. Correa-Duarte et al[41] obtained magnetically alignable hybrids of magnetic nanoparticles with carbon nanotubes using layer-by-layer assembly. Gao et al[42] and Greiner et al[43] even showed the micro-manipulations of the magnetic hybrid cylinders by magnetic fields.

Continuous efforts have been made in our group for the making of different magnetic nano-hybrids of magnetic nanoparticles with cylindrical polymer brushes (**CPBs**)[44]. CPBs are composed of a relatively long backbone with densely grafted side-chains[45-47]. Due to their stretched and anisotropic nature, they exhibit different solution and bulk properties. Three different strategies, grafting-onto[48], grafting-through[49], and grafting-from[50], have been adopted to synthesize the CPBs. Recent progress in controlled/living polymerizations made it possible to prepare well-defined CPBs by grafting-from strategy, using atom transfer radical polymerization (ATRP)[50, 51], nitroxide mediated radical polymerization (NMRP)[52] and ring opening polymerization (ROP)[53, 54]. Based on these techniques, CPBs with various architectures have been prepared. Core-shell CPBs[51, 52, 55, 56], brushes with a grafting density gradient[57, 58], hetero-grafted brushes[59-61], brush block copolymers[54, 62], star brushes[63, 64], ring brushes[65] and double-grafted brushes[66, 67] have been prepared. CPBs with various functionalities were also available. CPBs responsive to stimuli such as solvent[68], temperature[69], light[70], pH[71] and salt[71] are the novel examples.

Our group has reported the hybrids of core-shell CPBs with different inorganic nanomaterials like CdS[72], CdSe[73] and silica[74]. In our previous work, superparamagnetic maghemite nanoparticles were also successfully *in situ* incorporated in amphiphilic core-shell CPBs[44]. Because of the amphiphilic nature of the CPBs, organic solvent mixtures were used to disperse the hybrids, which were not so stable for long time and were not convenient for the applications. The magnetic nanoparticles generated in situ in the core of the CPBs were only 3 to 4 nm and the magnetic response was very weak.

In this work, we made crucial improvements and prepared water soluble double-hydrophilic core-shell CPBs, which is sensitive to pH and ions. More importantly, we employed a new strategy, introducing-into, to improve the magnetic responsiveness of the hybrid. Pre-made magnetite nanoparticles were introduced to the core of the core-shell CPBs and the hybrids were aligned in a large scale by relatively low magnetic fileds. This provided a novel example for the alignment and directed assembly of polymer hybrid systems and applications are possible in many potential areas.

Experimental

Materials. CuCl (97%, Aldrich) was purified by stirring with acetic acid overnight. After filtration, it was washed with ethanol and diethyl ether and then dried in vacuum oven. Oligoethyleneglycol methacrylate (**OEGMA**) (MW350, Bisomer, Germany) and *tert*-butyl methacrylate (**tBMA**) (kindly donated by BASF) were purified by passing through basic alumina columns before polymerizations. Trifluoroacetic acid (Aldrich) was used as received. *N*,*N*,*N*',*N*'',*N*''',*N*'''-hexamethyltriethylenetetraamine (HMTETA, Aldrich) was distilled before use. The synthesis of the macroinitiator poly(2-(2-bromo-isobutyryloxy)ethyl methacrylate) (**PBIEM**) (DP_n = 1500, PDI = 1.08) by anionic polymerization was reported previously by our group[56]. All other solvents and chemicals were used as received. Regenerated cellulose membranes were used for the dialysis (from Spectra/Pore 7 with MWCO = 12 kDa).

Preparation of PtBMA brush. The polymerization for the preparation of poly(*tert*-butyle methacrylate) brush (Abbreviated as brush **BT**) was carried out in a round-bottom flask sealed with a rubber septum. The procedures are described as follows: PBIEM (55.8 mg, 0.2 mmol of initiating α-bromoester groups) was dissolved in anisole (14 g) in a round-bottom flask and stirred overnight to assure the complete dissolution of the high molecular weight macro-initiator. After that, the monomer tBMA (14.2 g, 0.1 mol) was injected via a syringe and stirred for 15 min. Then CuCl (20 mg, 0.2 mmol) was added and the flask was purged with argon for 15 min. About 0.5 mL of solution was taken out with an argon-purged syringe as an initial sample for conversion measurement by ^{1}H NMR. The round-bottom flask was then inserted into a water bath at room temperature (25 ^{o}C). HMTETA (23 mg, 0.1 mmol) was injected by argon-purged syringe to start the reaction. Small amounts of samples were taken out at intervals to check the monomer conversion by ^{1}H NMR. After 2.5 h, the reaction was stopped by opening to the air. Final conversion determined by ^{1}H NMR reached 11.9%. THF was added to dilute the solution. After passing through a basic alumina column, the solution was concentrated by a rotary evaporator. Afterwards, it was precipitated into mixture of methanol and water (4:1 v/v) to remove the residual monomer and other impurities. Then the polymer was re-dissolved in certain amount of dioxane and followed by freeze-drying overnight.

Preparation of PtBMA-b-POEGMA brush. The synthesis of core-shell PtBMA-b-POEGMA brush (abbreviated as brush **BTO**) was carried out in a similar way as it was described above. The ATRP was performed at R. T. using methyl ethyl ketone as the solvent instead of anisole. Brush BT was used as the macro-initiator (88 mg, 0.01 mmol of initiating groups). Monomer OEGMA (3.5 g, 0.01 mol), CuCl (2mg, 0.02 mmol) and HMTETA (4.6 mg, 0.02 mmol) were used in the process. The final monomer conversion determined by ^{1}H NMR was 20.0%. After the polymerization, it was precipitated into cold *n*-Hexane, dissolved in dioxane and dialyzed against dioxane for one week to remove the residual monomer and other impurities. Then it was freeze-dried for further use.

Preparation of PMAA-b-POEGMA brushes. Brush BTO was subjected to hydrolysis to transform the PtBMA core into PMAA (poly(methacrylic acid)), which resulted in PMAA-b-POEGMA brush (abbreviated as brush **BMO**). Brush BTO was dissolved in dichloromethane and 10 fold excess of trifluoroacetic acid was injected, which was kept at R. T. for 48 h for the full reaction. After the reaction, solvent was evaporated and re-dissolved in dioxane for the freeze-drying. It was dialyzed against water for 7 days and part of it was freeze-dried.

Polychelate of brush BMO with Fe^{3+}. Brush BMO was first dissolved in water and the pH was tuned to 7 by adding NaOH solutions. Then suitable amount of $FeCl_3$ solution was added. The solution was stirred overnight for further use.

Synthesis of magnetite nanoparticles. Magnetite nanoparticles (**MNP**) was prepared by the co-precipitation procedures described in the literatures using citric acid as the protecting agent[40, 75].

Preparation of hybrid of MNP and brush BMO. First, 20 mL solution of BMO brush (0.1g/L) was prepared and the pH was adjusted to 7 by NaOH solutions. Then 2 mL MNP solution (10 g/L) was added to the solution. The mixture was dialyzed against water for 7 days. Some precipitation was observed on the wall of the dialysis tube. After the dialysis, the solution was filtered to remove the precipitation. Then it was subjected to ultra-filtration using a membrane with pore size 50 nm.

Characterization. ^{1}H NMR was measured on a Bruker AC-250 instrument at room temperature with $CDCl_3$ or D_2O as the solvent.

The apparent molecular weights of the brushes were characterized by conventional gel permeation chromatography (GPC) using 0.05 M solution of LiBr in 2-*N*-methylpyrrolidone (NMP) as eluent at a flow rate of 0.72 mL/min at room temperature. PSS GRAM columns (300 mm×8 mm, 7 μm): 10^3, 10^2 Å (PSS, Mainz, Germany) were thermostated at 70 °C. An RI detector and a UV detector (λ = 270 nm) were used. Polystyrene standards (PSS, Mainz) with narrow molecular weight distribution were used to calibrate the columns, and methyl benzoate was used as the internal standard.

Static light scattering (SLS) was measured on a Sofica goniometer using a He-Ne laser (λ = 632.8 nm). Prior to the light scattering measurements, the sample solutions were filtered 3 times by using Millipore Teflon filters with a pore size of 1 μm. Five concentrations of the brushes solutions in dioxane were measured at angles in the range from 30 ^{o} to 150 ^{o}. The weight-average molecular weight, M_w, of the brushes was obtained by the analysis of the Zimm-plots. The refractive index increments of the brush BT and BTO in dioxane solution at 25 °C were measured to be dn/dc = 0.0537 and 0.0422 mL/g respectively, using a PSS DnDc-2010/620 differential refractometer.

Dynamic light scattering (DLS) was carried out on an ALV DLS/SLS-SP 5022F compact goniometer system with an ALV 5000/E correlator and a He-Ne laser (λ = 632.8 nm) at an angle of 90^{o}. For the brush solutions in dioxane, the samples were filtered 3 times by using Millipore Teflon filters with a pore size of 1 μm before the light scattering measurements. CONTIN analyses were performed for the measured intensity correlation functions. Apparent hydrodynamic radii, R_h, of the cylindrical brushes were calculated according to the Stokes-Einstein equation. All the measurements were carried out at 25 °C.

Atomic force microscopy (AFM) measurements were performed on a Digital Instruments Dimension 3100 microscope operated in tapping mode. The micro-cantilever used for the AFM measurements were from Olympus with resonant frequency between 284.3 kHz and 386.0 kHz, and spring constant ranging from 35.9 to 92.0 N/m. For the brush BT and brush BTO, the samples were prepared by dip-coating from very dilute

(0.01 g/L) THF solutions of brushes onto freshly cleaved mica surfaces. For the measurement of the hybrid of BMO brush with magnetite nanoparticles, very dilute aqueous solutions (0.02 g/L) were prepared and were spin-coated on freshly cleaved mica. For the alignment of the hybrid on surface, 3 drops of the solution of the magnetic hybrid (0.05 g/L) was put on the freshly cleaved mica surface. A magnet was put parallel to the mica surface with distance of 3 cm. Then the sample was kept overnight to evaporate the water in the solution.

Transmission electron microscopy (TEM) measurements of the hybrid of BMO brush with MNP were carried out on Zeiss CEM 902, which was operated at 80 kV. The samples were prepared by putting one drop of the solution (0.05 g/L) on the carbon coated copper grid (200 mesh, Science Services, München, Germany). For the alignment of the magnetic hybrid, one drop of the sample solution was put on the carbon coated copper grid in a magnetic field (0.2 Tesla) and dried overnight. Then the sample was measured by a Zeiss EM 922 EFTEM with an acceleration voltage of 200 kV.

For cryogenic transmission electron microscopy (cryo-TEM) studies of brush BMO and its polychelate with Fe^{3+}, a drop of the sample (aqueous solution, concentration around 0.01 g/L) was put on an untreated bare copper TEM grid (600 mesh, Science Services, München, Germany), where most of the liquid was removed with blotting paper, leaving a thin film stretched over the grid holes. The specimens were instantly shock vitrified by rapid immersion into liquid ethane and cooled to approximately 90 K by liquid nitrogen in a temperature-controlled freezing unit (Zeiss Cryobox, Zeiss NTS GmbH, Oberkochen, Germany). The temperature was monitored and kept constant in the chamber during all the sample preparation steps. After the sample is frozen, it was inserted into a cryo-transfer holder (CT3500, Gatan, München, Germany) and transferred to a Zeiss EM 922 EFTEM. Examinations were carried out at temperatures around 90 K at an acceleration voltage of 200 kV. Zero-loss filtered images (ΔE = 0 eV) were taken under reduced dose conditions (100-1000 electrons/nm2). All images were registered digitally by a bottom-mounted CCD camera system (Ultrascan 1000, Gatan) combined and processed with a digital imaging processing system (Gatan Digital Micrograph 3.10 for GMS 1.5).

Magnetic properties of the hybrid of brush BMO and MNP was determined by superconducting quantum interference device (SQUID) using Quantum Design, MPMS-7.

Results and discussions

Syntheses of CPBs

Different CPBs prepared by grafting-from using ATRP have been reported by our group previously[51, 56, 67, 71, 74]. PBIEM with high molecular weights and narrowly distributions served as the macro-initiators and different side-chains grew from the backbone. In this work, we prepared double-hydrophilic core-shell CPBs by consecutive grafting by ATRP and further reactions. Scheme 1 shows the procedures of the synthetic work. First, PtBMA brush (BT) was prepared by grafting from macro-initiator PBIEM (DP=1500). Continued grafting of second monomer OEGMA using the brush BT as the precursor was performed resulted in the PtBMA-b-POEGMA brush (brush BTO). Finally, cleavage of the *t*-butyl groups of the PtBMA core was realized by trifluoroacetic acid catalyst. Thus, core-shell structured CPBs with core containing large number of carboxylic groups and shell composed of considerable short ethylene glycol units were fabricated. The as-prepared CPBs are well soluble in water.

Scheme 1. Synthetic procedures of the double-hydrophilic core-shell CPBs.

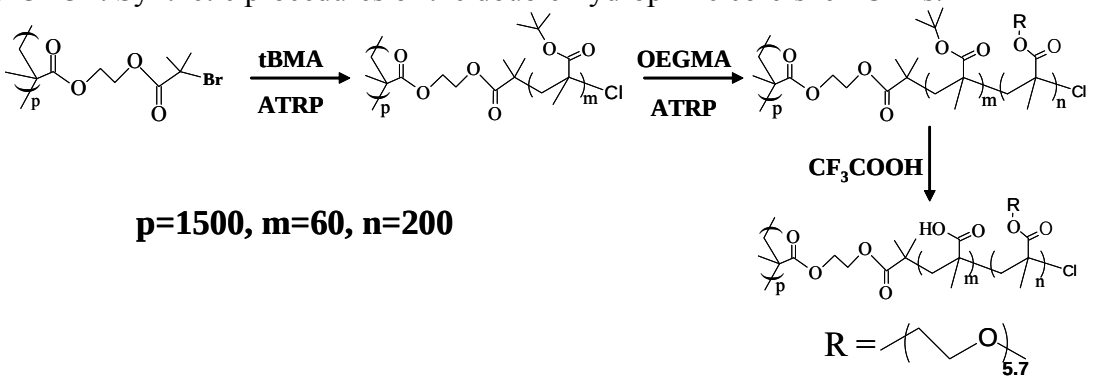

Conventional GPC measurements with NMP as the eluents were performed for macro-initiator PBIEM, brush BT, brush BTO. Although the normal GPC cannot give the true

molecular weights and distributions of the brushes because of the difference of the hydrodynamic radii between the brushes and linear polymer standards, it is still able to show the difference of the eluent volume changes between the formed brushes and the macroinitiator. Figure 1 shows the GPC eluent curves of the CPBs. A coupling peak for the macroinitiator PBIEM exists, which covers only a small portion of the macro-initiator. But the overall polydispersity of the macro-initiator is very low, and the coupling peak has very minor effect on the final brushes, which has been evidenced by our previous works[56, 67, 71]. It is clearly shown that brush BT and BTO both demonstrate monomodal distributions, and BTO peak shifts to higher molecular weight direction, indicating good control of the ATRP grafting reactions.

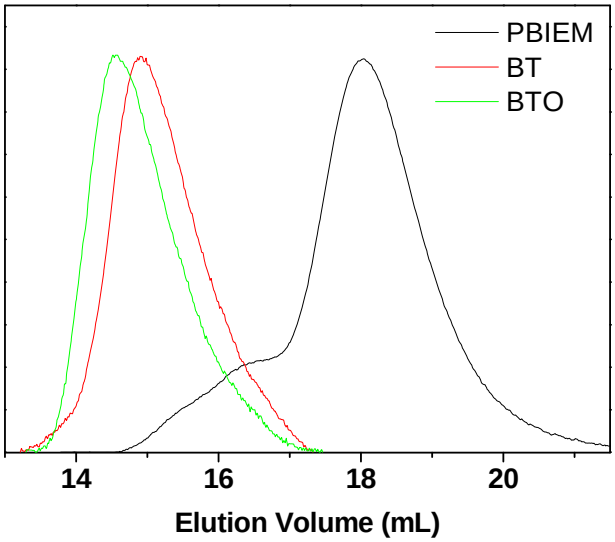

Figure 1. GPC eluent curves of the PBIEM, brush BT and BTO.

Comparison of ^{1}H NMR spectra of the brushes is displayed in Figure 2. The two peaks at area a (4.1 and 4.3 ppm for the methylene protons between two ester groups in the PBIEM macro-initiator) and the peak at area c (1.9 ppm for the methyl groups neighboring the bromide group in PBIEM) disappeared when brush BT was formed, while at the same time, the distinctive peak for the *t*-butyl groups (1.4 ppm at area d) of PtBMA rose. After the blocking of POEGMA shell, intrinsic peaks for the short ethylene glycol units were shown at area b (between 3.0 ppm to 4.0 ppm). In the mean time, the peak for the *t*-butyl groups at 1.4 ppm remained, indicating the successful grafting of the

di-block side-chains. After the treatment with trifluoroacetic acid, the peak at 1.4 ppm for the *t*-butyl groups vanished, demonstrating the completing of the de-protection of the carboxylic groups. Thus, the ^{1}H NMR spectra clearly confirmed the successful synthesis of the double-hydrophilic core-shell CPBs with PMAA core and POEGMA shell.

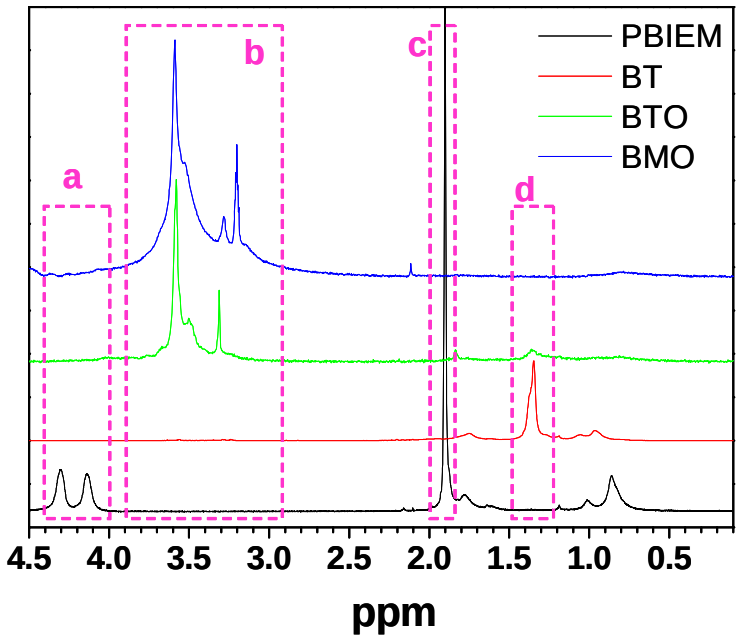

Figure 2. ^{1}H NMR Spectra of macro-initiator PBIEM, brush BT, BTO and BMO.

Table1. Molecular characterizations and light scattering analyses of brush BT and BTO.

sample	conversion[a]	$DP_{sc,calc}$ [b]	$10^{-7}M_{n,calc}$ [c]	$10^{-7}M_{w,SLS}$ [d]	$R_{h,app}$ [e], nm (PDI)
BT	11.9%	60	1.31	1.50	48 (0.22)
BTO	20.0%	200	10.5	10.9	170 (0.32)

[a]Monomer conversion determined by ^{1}H NMR. [b]Calculated DP of side-chains, $DP_{sc,calc} = ([M]_0/[I]_0)\times$conversion, for sample BT and BTO, the ratios of $[M]_0/[I]_0$ are 500 and 1000, respectively. [c]Calculated from monomer conversion. $M_{n,calc}$ = (Monomer molecular weight $\times DP_{sc,calc}$ + 234.5) $\times DP_{n,backbone}$. [d]determined by SLS in dioxane. [e]Apparent hydrodynamic radius and polydispersity measured by DLS in dioxane.

In order to know the true molecular weights of the brush BT and BTO, solutions of them in dioxane were subjected to SLS analyses. DLS measurements were also carried out. The results are listed in table 1. Absolute weight averaged molecular weights (M_w) of the brushes shows very little deviations from the calculated number averaged molecular weights (M_n), again proving the success of the brush syntheses. The CONTIN plots of both brushes (at 90° scattering angle) are monomodal (see supporting information: S1). The apparent hydrodynamic radii ($R_{h,app}$) for the brush BT and BTO are 48 nm and 170 nm, respectively, displaying significant increase of the size of the brushes.

pH responsiveness of BMO brush

The double-hydrophilic core-shell brush BMO is composed of a shell of POEGMA and a core of PMAA. The weak polyelectrolyte nature of PMAA leads to the pH responsiveness of the BMO brush. Cryo-TEM measurements of BMO brush showed their true solution morphologies at different pH values in Figure 3. It was reported by literature[76] that the p*K*a value of PMAA is around 4.71. So at pH 4, most of the carboxylic groups are protonated and are not well soluble in water, while at pH 7, most of them are ionized and well soluble in water. This was indeed observed from Figure 3. In Figure 3a, an interesting structure, pearl-necklace structure, was clearly observed due to the association of the PMAA core in the brushes. This was also predicted by simulation work and explained theoretically by Oleg et al recently[77]. However, at pH 7, these special morphologies disappeared, owing to the mostly dissociated carboxylic groups in the core.

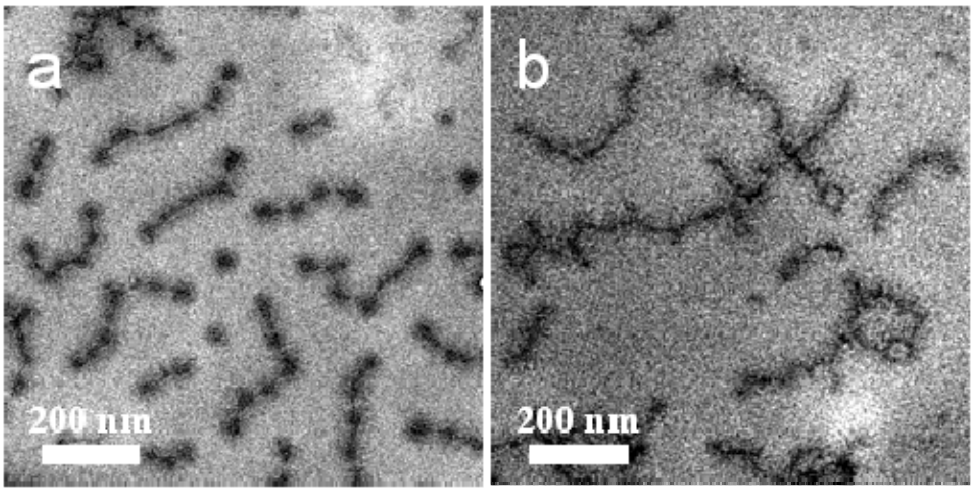

Figure 3. cryo-TEM images of BMO brush at a) pH=4 and b) pH=7.

From Figure 3, we also found that the brushes are mostly around 300 nm long. This length is much higher than that of other brushes prepared by the same macro-initiator (normally around 150 nm to 180 nm)[56, 67, 71]. This could be explained by the bulk nature of the OEGMA monomer. As shown in Table 1, the $R_{h,app}$ values of the brushes increased from 48 nm to 170 nm, indicating great expansion of the brushes. Although the length of 300 nm is still shorter than that of the fully stretched backbone (375 nm), it has showed the stretching effect of the bulky side-chains.

Polychelate of BMO brush with Fe^{3+}

Since the PMAA in the core of the BMO brush is a polyelectrolyte, it is able to uptake different counterions around it. At pH 7, the carboxylic groups are ionized and mono-valent counterions should be mostly around the brush core. When trivalent counterions, in this case, Fe^{3+} ions are put into the solution, fast exchange of counterions would drive the moving of Fe^{3+} ions into the core of the brush[78-80]. This would cause the collapse of PMAA around the core. Figure 4 shows the pearl-necklace structures clearly. Similar findings were also reported previously by our group[44, 81, 82] for the polychelates of amphiphilic brushes with Cd^{2+} and Fe^{3+}.

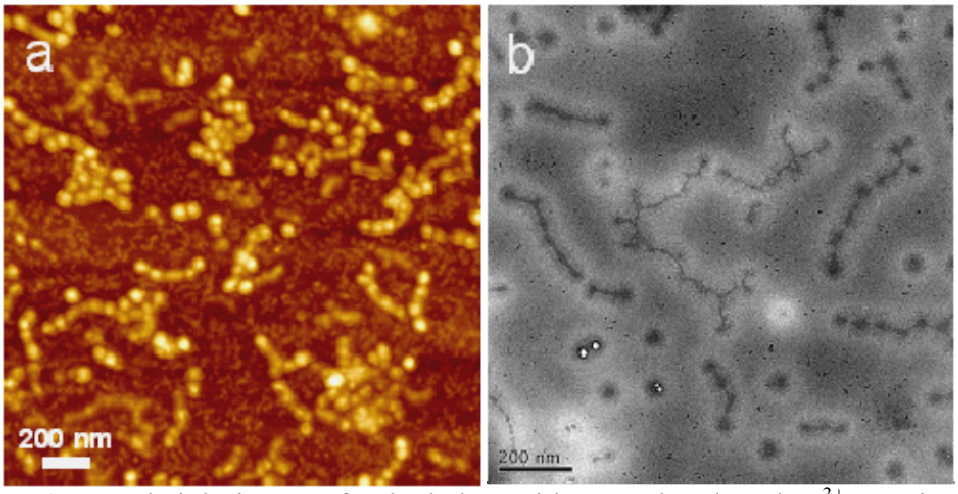

Figure 4. a) AFM height image of polychelate with BMO brush and Fe^{3+} on mica surface, Z range 35nm; and b) cryo-TEM image of polychelate with BMO brush and Fe^{3+} at pH=7.

Hybrid of brush BMO with magnetite nanoparticles

In order to prepare the cylindrical magnetic nano-hybrids, magnetite nanoparticles were first produced by co-precipitation procedures reported in literatures[40, 75]. The magnetite nanoparticles were protected by citric acid and were stable in water. Figure 5 demonstrates the TEM image of the as-prepared magnetite nanoparticles. Analysis indicates that the average diameter of the particles is around 10 nm, which is quite typical for the nanoparticles prepared by this process. SQUID measurement (see supporting information: S2) revealed that the particles are superparamagnetic without magnetic hysteresis at temperature 200 K.

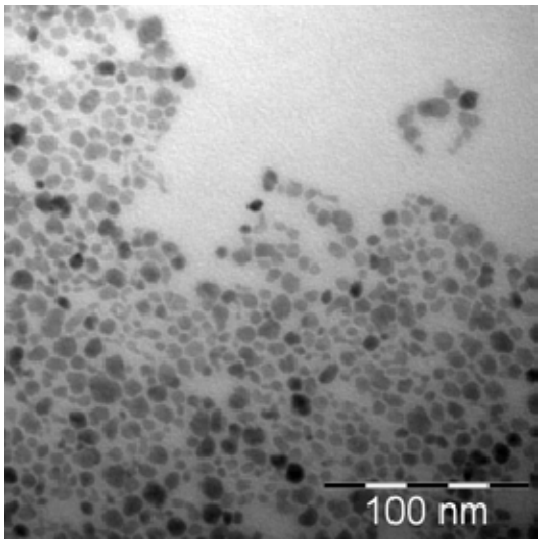

Figure 5. TEM image of the magnetite nanoparticles.

The hybrid of magnetic nanoparticles with brush BMO was prepared in the procedure illustrated in Scheme 2. Excess of magnetite nanoparticles were mixed with BMO brush solution (pH tuned to 7) first, which was followed by dialysis. Citric acid was dialyzed away through the pores of the membrane and ligand exchange happened since there were large number of carboxylic groups in the core of the BMO brushes, which have strong interaction with the surfaces of the magnetite nanoparticles. The excess particles lost their protection and aggregated to form precipitations. Some particles were still free in the solutions. By filtration, the precipitation was removed. And ultra-filtration using a membrane with pore size 50 nm could remove the free magnetite particles while keeping the magnetic hybrid in the solutions.

The formation of the magnetic hybrid was evidenced by non-stained TEM portrayed in Figure 6. Chain-like structures are visible and Figure 6b further displayed the particles are arranged in a linear way. The size of the chains fit that of the brush BMO, as shown previously. This demonstrates that the construction of the hybrid of magnetite nanoparticles with brush BMO was achieved successfully. AFM images also evidenced the formation of the magnetic hybrid and no free particles were observed (see supporting information: S3).

Scheme 2. the introducing-into strategy for the preparation of magnetic nano-hybrid.

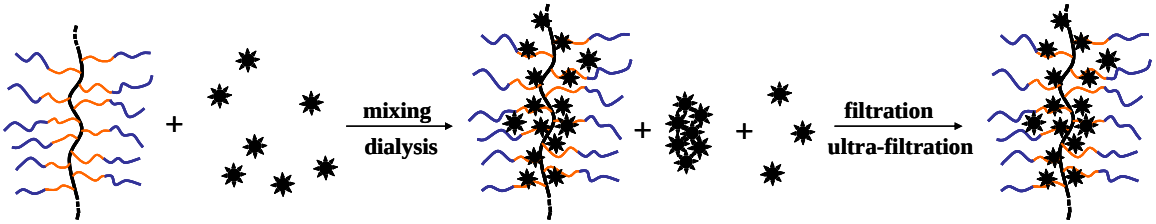

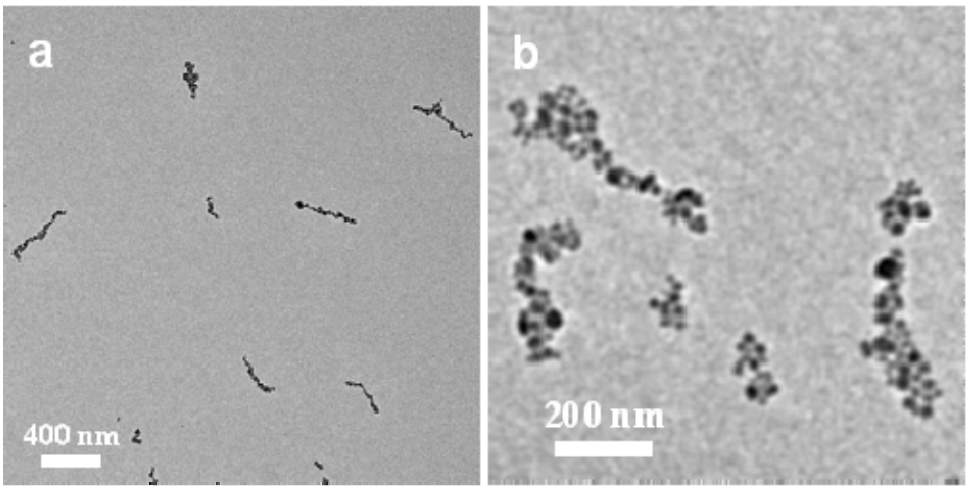

Figure 6. Non-stained TEM of the purified hybrid of brush BMO and magnetite nanoparticles.

The magnetic properties of the hybrid of brush BMO and magnetite nanoparticles were characterized by SQUID. Figure 7 shows the magnetization curve of the hybrid in different magnetic field at 200 K. No apparent magnetic hysteresis was found for the hybrid material, indicating that the hybrid of the brush BMO with the magnetite nanoparticles retained the superparamagnetic property of the original particles. This made

it possible to study the responses of the hybrid cylinders in the magnetic field and further alignment experiments.

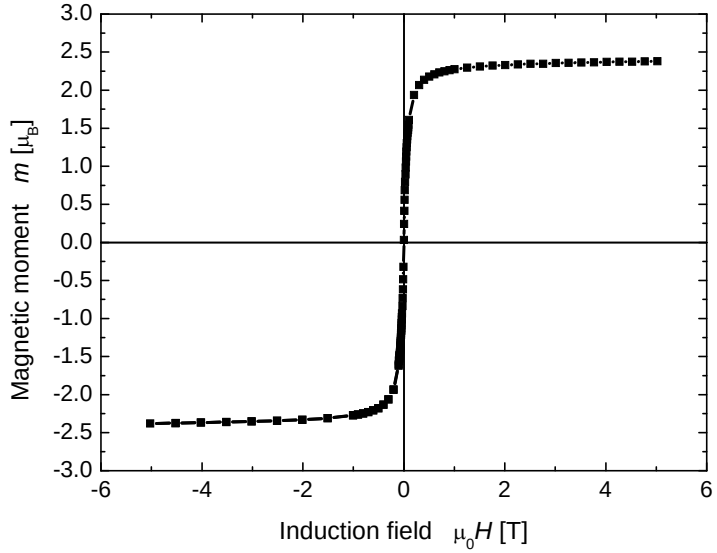

Figure 7. Magnetization curve of the hybrid of brush BMO and MNP at 200 K.

Alignment of the hybrid in magnetic fields

In the literatures[23, 24, 26, 27], most examples of alignments required high magnetic field. In our case, we have shown that magnetite nanoparticles are enriched around the core of the brush BMO, which increased the local concentration of magnetic particles around the brushes, and made it possible to align the hybrid cylinders in relatively low magnetic fields.

It is indeed shown in Figure 8 that the hybrid cylinders formed aligned morphologies in a low field (40 mT) and in a scale of tens of microns, individual or aggregated chains were clearly observed. In Figure 8b, we can even see the end-to-end organization of single hybrid materials in the magnetic field direction.

Similar experiment with higher magnetic field (0.3 T) was also carried out on the TEM grid. Analogous alignment was also obtained in a larger scale (several hundred micron scale). In Figure 9a and 9b, aligned stripes are clearly observed. Analysis of single stripe indicates that the width is much larger than the width of single hybrid cylinders, indicating the densely aggregated state of those cylinders. More detailed measurements in

the non-stained TEM shows that these stripes are made up of large number of magnetic nanoparticles (see supporting information: S4).

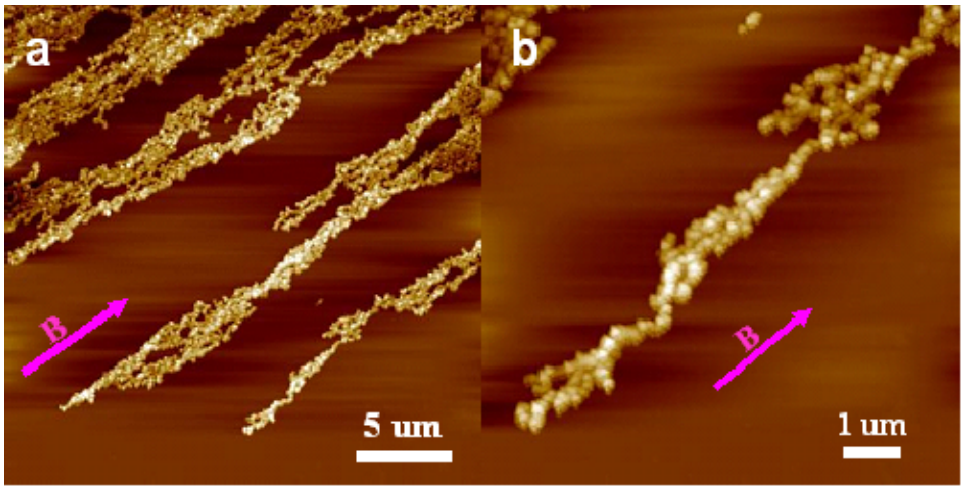

Figure 8. a) AFM height image of Aligned magnetic hybrid on mica surface in a magnetic field of 40 mT, Z range 50 nm; and b) Magnification of one aligned chain of the magnetic hybrid cylinders.

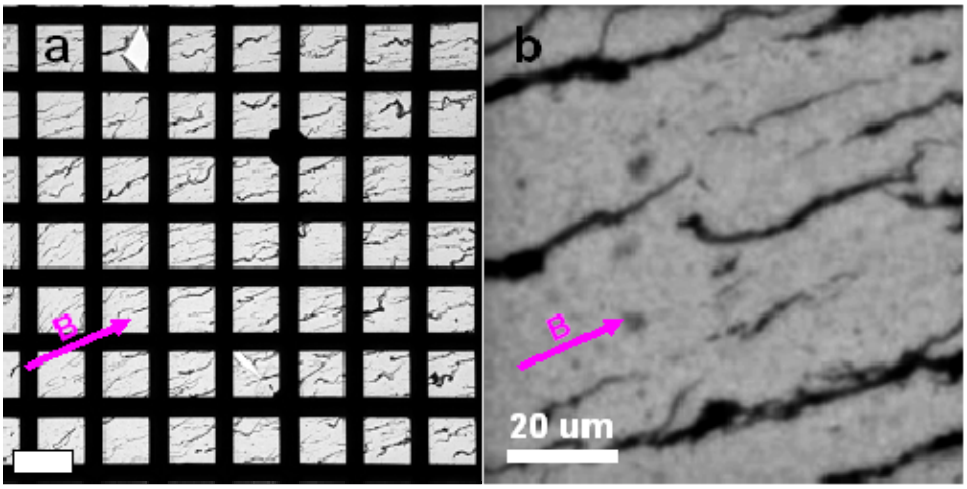

Figure 9. a) and b): non-stained TEM images of the aligned structures of the hybrid cylinders in a magnetic field of 0.3 T. Scale bar in the left image represents 100 micron.

Conclusions

We have successfully prepared double-hydrophilic core-shell CPBs with PMAA as the core and POEGMA as the protecting shell, by grafting-from strategy using ATRP technique, which was evidenced by different characterization methods like ^{1}H NMR,

GPC, DLS and SLS. The as-prepared core-shell brush is soluble in water and shows pH responsiveness due to the weak polyelectrolyte characteristic of PMAA in the core. At pH 4, distinct pearl-necklace structures were observed in the cryo-TEM images. However, at pH 7, these structures disappeared owing to the ionization of the PMAA in water. The polychelate of the brush BMO with Fe^{3+} also showed similar pearl-necklace structures, as was demonstrated by AFM and cryo-TEM measurements. Superparamagnetic magnetite nanoparticles with average diameter of 10 nm were parepared and were introduced into the core-shell brushes. The hybrid material retained the superparamagnetic property of the magnetite particles, which was verified by the SQUID measurement. Micron-scale alignments of the hybrid cylinders in magnetic field were performed on mica surface and on TEM grid. Oriented stripes of the cylinders or the aggregated hybrids were observed from the AFM and TEM images. The successful preparation of the magnetic nano-hybrid cylinders and their convenient alignments in relatively low magnetic fields provided a novel example of directed assembly of polymer/inorganic nanoparticle hybrid materials by external field. They could be potentially applied in preparing well-patterned surfaces or in the micro-electronics.

Acknowledgements

The authors thank Mr. Benjamin Balke from Johannes Gutenberg-Maniz Universität for the great help with the SQUID measurements. Financial support by the Deutsche Forschungsgemeinschaft (DFG) within SFB 481 is apprecited.

References

1. Minko, S., *Responsive Polymer Materials: Design and Applications*. Blackwell Publishing Ltd.: Oxford, 2006.

2. Matyjaszewski, K.; Xia, J. *Chem. Rev.* **2001,** 101, 2921-2990.

3. Hawker, C. J.; Bosman, A. W.; Harth, E. *Chem. Rev.* **2001,** 101, 3661-3688.

4. Barner-Kowollik, C.; Davis, T. P.; Heuts, J. P. A.; Stenzel, M. H.; Vana, P.; Whittaker, M. *J. Polym. Sci. Polym. Chem.* **2003,** 41, 365-375.

5. Whitesides, G. M.; Mathias, J. P.; Seto, C. T. *Science* **1991,** 254, 1312-19.

6. Fendler, J. H. *Chem. Mater.* **1996,** 8, 1616-1624.

7. Ulman, A. *Chem. Rev.* **1996,** 96, 1533-1554.

8. Greig, L. M.; Philp, D. *Chem. Soc. Rev.* **2001,** 30, 287-302.

9. Xia, Y.; Gates, B.; Li, Z.-Y. *Adv. Mater.* **2001,** 13, 409-413.

10. Vossmeyer, T.; DeIonno, E.; Heath, J. R. *Angew. Chem. Int. Ed.* **1997,** 36, 1080-1083.

11. Huang, Y.; Duan, X.; Wei, Q.; Lieber, C. M. *Science* **2001,** 291, 630-633.

12. Smay, J. E.; Gratson, G. M.; Shepherd, R. F.; Cesarano, J., III; Lewis, J. A. *Adv. Mater.* **2002,** 14, 1279-1283.

13. Dai, L., *Intelligent Macromolecules for Smart Devices: From Materials Synthesis to Device Applications*. Springer-Verlag: London, 2003.

14. Lee, B.-w.; Clark, N. A. *Science* **2001,** 291, 2576-2580.

15. Nie, Z.; Kumacheva, E. *Nat. Mater.* **2008,** 7, 277-290.

16. Xue, W.; Grest, G. S. *Phys. Rev. Lett.* **1990,** 64, 419-22.

17. Kempe, M. D.; Kornfield, J. A. *Phys. Rev. Lett.* **2003,** 90, 115501.

18. Angelescu, D. E.; Waller, J. H.; Register, R. A.; Chaikin, P. M. *Adv. Mater.* **2005,** 17, 1878-1881.

19. Xu, H.; Sheiko, S. S.; Shirvanyants, D.; Rubinstein, M.; Beers, K. L.; Matyjaszewski, K. *Langmuir* **2006,** 22, 1254-1259.

20. Pozzo, D. C.; Walker, L. M. *Macromolecules* **2007,** 40, 5801-5811.

21. Böker, A.; Elbs, H.; Hansel, H.; Knoll, A.; Ludwigs, S.; Zettl, H.; Urban, V.; Abetz, V.; Müller, A. H. E.; Krausch, G. *Phys. Rev. Lett.* **2002,** 89, 135502/1-135502/4.

22. Thurn-Albrecht, T.; DeRouchey, J.; Russell, T. P.; Kolb, R. *Macromolecules* **2002,** 35, 8106-8110.

23. Osuji, C.; Ferreira, P. J.; Mao, G.; Ober, C. K.; Vander Sande, J. B.; Thomas, E. L. *Macromolecules* **2004,** 37, 9903-9908.

24. Boamfa, M. I.; Lazarenko, S. V.; Vermolen, E. C. M.; Kirilyuk, A.; Rasing, T. *Adv. Mater.* **2005,** 17, 610-614.

25. Piao, G.; Kimura, F.; Kimura, T. *Langmuir* **2006,** 22, 4853-4855.

26. Tao, Y.; Zohar, H.; Olsen, B. D.; Segalman, R. A. *Nano Lett.* **2007,** 7, 2742-2746.

27. Hill, R. J. A.; Sedman, V. L.; Allen, S.; Williams, P. M.; Paoli, M.; Adler-Abramovich, L.; Gazit, E.; Eaves, L.; Tendler, S. J. B. *Adv. Mater.* **2007,** 19, 4474-4479.

28. Filipcsei, G.; Csetneki, I.; Szilagyi, A.; Zrinyi, M. *Adv. Polym. Sci.* **2007,** 206, 137-189.

29. Huber, D. L. *Small* **2005,** 1, 482-501.

30. Sun, S. *Adv. Mater.* **2006,** 18, 393-403.

31. Yavuz Cafer, T.; Mayo, J. T.; Yu William, W.; Prakash, A.; Falkner Joshua, C.; Yean, S.; Cong, L.; Shipley Heather, J.; Kan, A.; Tomson, M.; Natelson, D.; Colvin Vicki, L. *Science* **2006,** 314, 964-967.

32. Lu, A. H.; Salabas, E. L.; Schueth, F. *Angew. Chem. Int. Ed.* **2007,** 46, 1222-1244.

33. Salgueirino-Maceira, V.; Correa-Duarte, M. A. *Adv. Mater.* **2007,** 19, 4131-4144.

34. Jun, Y.-w.; Choi, J.-s.; Cheon, J. *Chem. Comm.* **2007**, 1203-1214.

35. Laurent, S.; Forge, D.; Port, M.; Roch, A.; Robic, C.; Vander Elst, L.; Muller, R. N. *Chem. Rev.* **2008,** 108, 2064-2110.

36. Latham, A. H.; Williams, M. E. *Acc. Chem. Res.* **2008,** 41, (3), 411-420.

37. Korth, B. D.; Keng, P.; Shim, I.; Bowles, S. E.; Tang, C.; Kowalewski, T.; Nebesny, K. W.; Pyun, J. *J. Am. Chem. Soc.* **2006,** 128, 6562-6563.

38. Benkoski, J. J.; Bowles, S. E.; Korth, B. D.; Jones, R. L.; Douglas, J. F.; Karim, A.; Pyun, J. *J. Am. Chem. Soc.* **2007,** 129, 6291-6297.

39. Keng, P. Y.; Shim, I.; Korth, B. D.; Douglas, J. F.; Pyun, J. *ACS Nano* **2007,** 1, 279-292.

40. Sheparovych, R.; Sahoo, Y.; Motornov, M.; Wang, S.; Luo, H.; Prasad, P. N.; Sokolov, I.; Minko, S. *Chem. Mater.* **2006,** 18, 591-593.

41. Correa-Duarte, M. A.; Grzelczak, M.; Salgueirino-Maceira, V.; Giersig, M.; Liz-Marzan, L. M.; Farle, M.; Sierazdki, K.; Diaz, R. *J. Phys. Chem. B* **2005,** 109, 19060-19063.

42. Gao, C.; Li, W.; Morimoto, H.; Nagaoka, Y.; Maekawa, T. *J. Phys. Chem. B* **2006,** 110, 7213-7220.

43. Kriha, O.; Becker, M.; Lehmann, M.; Kriha, D.; Krieglstein, J.; Yosef, M.; Schlecht, S.; Wehrspohn, R. B.; Wendorff, J. H.; Greiner, A. *Adv. Mater.* **2007,** 19, 2483-2485.

44. Zhang, M.; Estournes, C.; Bietsch, W.; Müller, A. H. E. *Adv. Funct. Mater.* **2004,** 14, 871-882.

45. Pyun, J.; Kowalewski, T.; Matyjaszewski, K. *Macromol. Rapid Comm.* **2003,** 24, 1043-1059.

46. Zhang, M.; Müller, A. H. E. *J. Polym. Sci. Polym. Chem.* **2005,** 43, 3461-3481.

47. Sheiko, S. S.; Sumerlin, B. S.; Matyjaszewski, K. *Prog. Polym. Sci.* **2008,** 33, 759-785.

48. Gao, H.; Matyjaszewski, K. *J. Am. Chem. Soc.* **2007,** 129, 6633-6639.

49. Dziezok, P.; Sheiko, S. S.; Fischer, K.; Schmidt, M.; Möller, M. *Angew. Chem. Int. Ed.* **1997,** 36, 2812-2815.

50. Beers, K. L.; Gaynor, S. G.; Matyjaszewski, K.; Sheiko, S. S.; Möller, M. *Macromolecules* **1998,** 31, 9413-9415.

51. Cheng, G.; Boeker, A.; Zhang, M.; Krausch, G.; Müller, A. H. E. *Macromolecules* **2001,** 34, 6883-6888.

52. Cheng, C.; Qi, K.; Khoshdel, E.; Wooley, K. L. *J. Am. Chem. Soc.* **2006,** 128, 6808-6809.

53. Lee, H.; Jakubowski, W.; Matyjaszewski, K.; Yu, S.; Sheiko, S. S. *Macromolecules* **2006,** 39, 4983-4989.

54. Lee, H.-i.; Matyjaszewski, K.; Yu-Su, S.; Sheiko, S. S. *Macromolecules* **2008,** 41, 6073-6080.

55. Börner, H. G.; Beers, K.; Matyjaszewski, K.; Sheiko, S. S.; Möller, M. *Macromolecules* **2001,** 34, 4375-4383.

56. Zhang, M.; Breiner, T.; Mori, H.; Müller, A. H. E. *Polymer* **2003,** 44, 1449-1458.

57. Boerner, H. G.; Duran, D.; Matyjaszewski, K.; da Silva, M.; Sheiko, S. S. *Macromolecules* **2002,** 35, 3387-3394.

58. Lee, H.-I.; Matyjaszewski, K.; Yu, S.; Sheiko, S. S. *Macromolecules* **2005,** 38, 8264-8271.

59. Neugebauer, D.; Zhang, Y.; Pakula, T.; Matyjaszewski, K. *Polymer* **2003,** 44, 6863-6871.

60. Neugebauer, D.; Zhang, Y.; Pakula, T.; Matyjaszewski, K. *Macromolecules* **2005,** 38, 8687-8693.

61. Neugebauer, D.; Theis, M.; Pakula, T.; Wegner, G.; Matyjaszewski, K. *Macromolecules* **2006,** 39, 584-593.

62. Ishizu, K. *Polym. J.* **2004,** 36, 775-792.

63. Matyjaszewski, K.; Qin, S.; Boyce, J. R.; Shirvanyants, D.; Sheiko, S. S. *Macromolecules* **2003,** 36, 1843-1849.

64. Boyce, J. R.; Shirvanyants, D.; Sheiko, S. S.; Ivanov, D. A.; Qin, S.; Boerner, H.; Matyjaszewski, K. *Langmuir* **2004,** 20, 6005-6011.

65. Schappacher, M.; Deffieux, A. *Science* **2008,** 319, 1512-1515.

66. Neugebauer, D.; Zhang, Y.; Pakula, T.; Sheiko, S. S.; Matyjaszewski, K. *Macromolecules* **2003,** 36, 6746-6755.

67. Xu, Y.; Becker, H.; Yuan, J.; Burkhardt, M.; Zhang, Y.; Walther, A.; Bolisetty, S.; Ballauff, M.; Müller, A. H. E. *Macromol. Chem. Phys.* **2007,** 208, 1666-1675.

68. Fischer, K.; Schmidt, M. *Macromol. Rapid Comm.* **2001,** 22, 787-791.

69. Pietrasik, J.; Sumerlin, B. S.; Lee, R. Y.; Matyjaszewski, K. *Macromol. Chem. Phys.* **2007,** 208, 30-36.

70. Lee, H.-i.; Pietrasik, J.; Matyjaszewski, K. *Macromolecules* **2006,** 39, 3914-3920.

71. Xu, Y.; Bolisetty, S.; Drechsler, M.; Fang, B.; Yuan, J.; Ballauff, M.; Müller, A. H. E. *Polymer* **2008,** 49, 3957-3964.

72. Zhang, M.; Drechsler, M.; Müller, A. H. E. *Chem. Mater.* **2004,** 16, 537-543.

73. Yuan, J.; Drechsler, M.; Xu, Y.; Zhang, M.; Müller, A. H. E. *Polymer* **2008,** 49, 1547-1554.

74. Yuan, J.; Xu, Y.; Walther, A.; Bolisetty, S.; Schumacher, M.; Schmalz, H.; Ballauff, M.; Müller, A. H. E. *Nat. Mater.* **2008,** 7, 718-722.

75. Massart, R. *IEEE Trans. Magn.* **1981,** MAG-17, 1247-1248.

76. Nagasawa, M.; Murase, T.; Kondo, K. *J Phys. Chem.* **1965,** 69, 4005-12.

77. Polotsky, A.; Charlaganov, M.; Xu, Y.; Leermakers, F. A. M.; Daoud, M.; Müller, A. H. E.; Dotera, T.; Borisov, O. *Macromolecules* **2008,** 41, 4020-4028.

78. Mei, Y.; Lauterbach, K.; Hoffmann, M.; Borisov, O. V.; Ballauff, M.; Jusufi, A. *Phys. Rev. Lett.* **2006,** 97, 158301/1-158301/4.

79. Plamper, F. A.; Walther, A.; Müller, A. H. E.; Ballauff, M. *Nano Lett.* **2007,** 7, 167-171.

80. Mei, Y.; Ballauff, M. *Eur. Phys. J. E* **2005,** 16, 341-349.

81. Zhang, M.; Drechsler, M.; Müller, A. H. E. *Chem. Mater.* **2004,** 16, 537-543.

82. Zhang, M.; Teissier, P.; Krekhova, M.; Cabuil, V.; Müller, A. H. E. *Prog. Colloid Polym. Sci.* **2004,** 126, 35-39.

Supporting Information

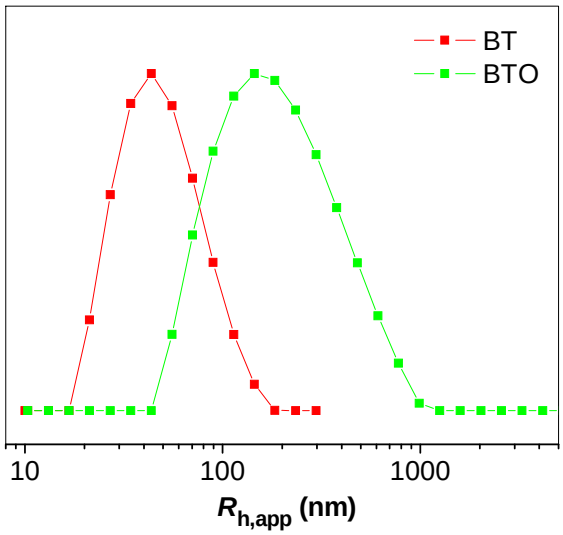

S1. CONTIN plot of brush BT and BTO in dioxane.

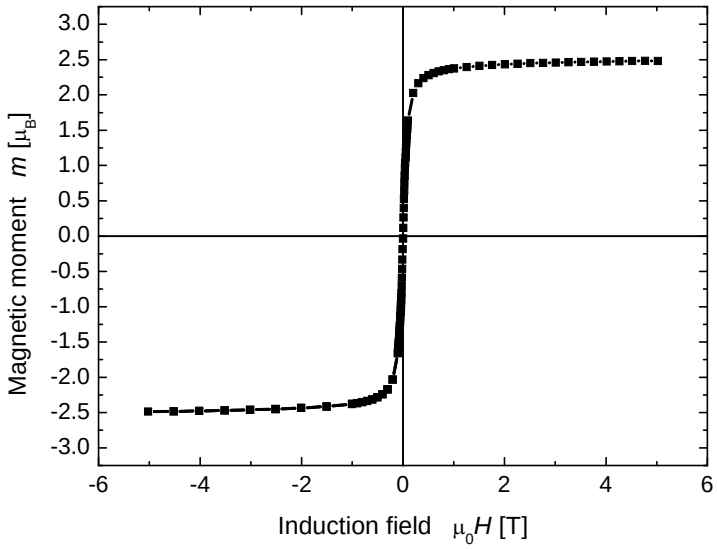

S2. Magnetization curve of magnetite nanoparticles at 200 K.

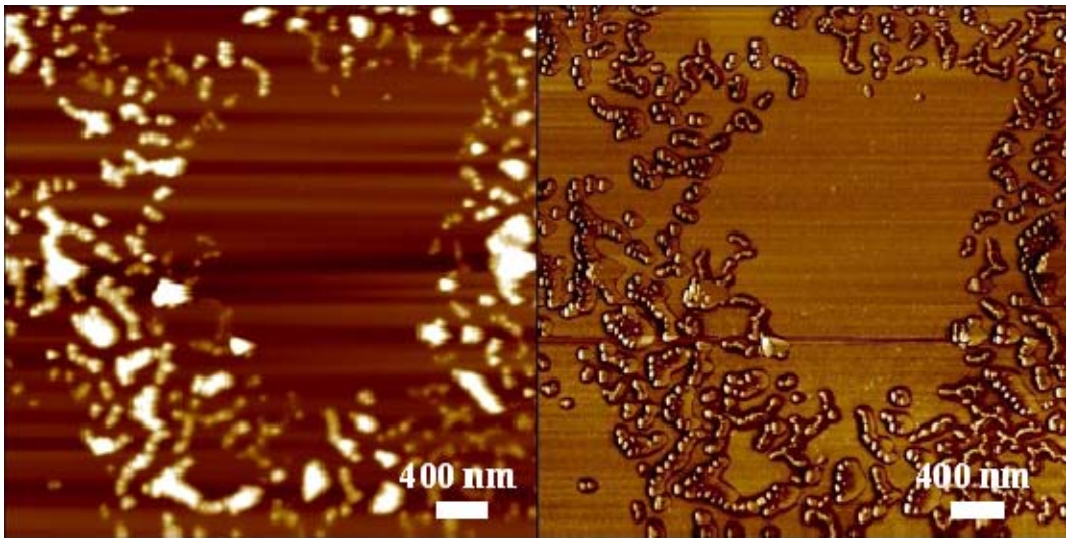

S3. AFM height (left) and Phase (right) images of the magnetic hybrid of brush BMO and magnetite nanoparticles.

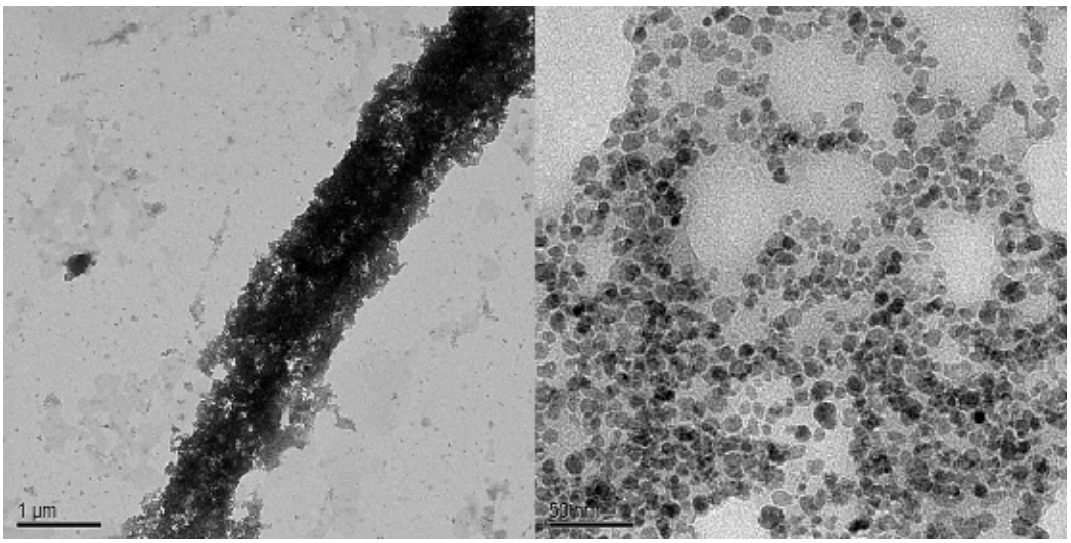

S4. Non-stained TEM images of the aligned stripes of the hybrids in a magnetic field of 0.2 T. Scale bars in the left and right images stand for 1 um and 50 nm, respectively.

10. Single-molecular Hybrid Nano-cylinders: Attaching Polyhedral Oligomeric Silsesquioxane Covalently to Poly(glycidyl methacrylate) Cylindrical Brushes

Youyong Xu, Jiayin Yuan, Axel H. E. Müller*

Makromolekulare Chemie II , and Bayreuther Zentrum für Kolloide und Grenzflächen, Universität Bayreuth, D-95440 Bayreuth, Germany

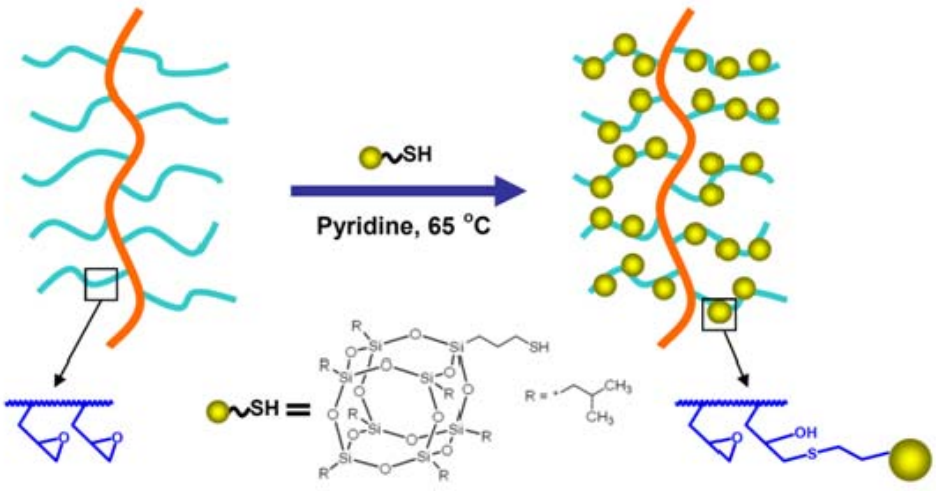

Manuscript to be submitted

Abstract:

We present the preparation of novel single-molecular hybrid nano-cylinders by covalently attaching the mono-thiol-functionalized polyhedral silsesquioxane (POSS-SH) to poly(glycidyl methacrylate) cylindrical brushes (BGMA). Grafting of GMA from a long macro-initiator poly(2-(2-bromoisobutyryloxy)ethyl methacrylate) (PBIEM) via ATRP was first carried out. Gel permeation chromatography (GPC), ^{1}H NMR, dynamic light scattering (DLS), static light scattering (SLS) and atomic force microscopy (AFM) measurements confirmed the well-defined worm-like structures of BGMA brushes. Then POSS-SH was covalently linked to BGMA brushes by reacting with the large number of epoxy groups. The fulfillment of the hybrid materials BGMA-POSS were demonstrated by Fourier transform infrared spectroscopy (FTIR), DLS, SLS, energy dispersive X-ray spectroscopy (EDX) and thermal gravimetric analysis (TGA) measurements. Due to the high steric hindrance, the attaching efficiency of POSS-SH only reached 20%. Nevertheless, size increases for the length and diameter were shown by AFM and non-stained transmission microscopy (TEM) measurements. Residual SiO_2 left from the TGA measurement of BGMA-POSS in air displayed interesting porous structures, as were revealed by scanning electron microscopy (SEM) and TEM characterizations.

Keywords: poly(glycidyl methacrylate), cylindrical polymer brush, POSS, nano-composite

Introduction

With the rapid development of nanotechnologies, tremendous materials with different functionalities on nano-scale have been fabricated[1]. Combining inorganic materials' outstanding mechanical, optical, electric and magnetic properties, with the soft organic materials' excellent processibilities, functionalities and biocompatibilities, nano-composite materials have demonstrated their advanced performances, which exceed the simple addition of their every single component's characteristics, due to the special surface and quantum effects on nano-scale. Polymer based nano-composites have been widely investigated and a large category of inorganic materials, such as carbon materials, ceramics, clays, metals, metal oxides and silica, have been incorporated into different polymeric materials[2]. One advantage of such kind of composite materials is that very small amount of the added inorganic nano-materials can remarkably improve the mechanical, thermal and other properties of the polymer matrix[3]. To prepare the polymer-based nano-composites with inorganic materials, two general strategies have been applied. The easiest way is to directly dispersing the nanometer-sized inorganic materials into the polymer by mechanical blending, melting or solution treatments. In order to improve the compatibilities of the inorganic materials with the polymer matrix, surface functionalizations are sometimes necessary. Recent research revealed the size of the blending materials is a key factor for the dispersing process[4]. Due to the non-covalent blending, the forces between the additive and the matrix are weak, and the improvement of the properties and the stabilities are poor. The other method is to prepare the nano-composites via covalent linking, either by direct polymerization of functional monomers attached with inorganic groups, or by post-polymerization reactions. Thanks to the strong covalent linking of the inorganic part to the organic polymer chains, better performances of these materials are expected.

Recent progresses have been achieved in the making of nano-composite materials on molecular level, which find their promising micro-electronic, optic and magnetic applications. Suitable nano-structured polymer matrices are greatly demanded. Spherically-shaped polymers like star polymers[5, 6], dendrimer[7] and hyperbranched polymers[8] can meet the requirements to some extent. Demands on anisotropic polymer molecules are increasing, owing to their interesting properties and potential applications.

One-dimensional polymers like dendronized polymers[9] and cylindrical polymer brushes (CPBs)[10, 11] can play the roles. Tedious synthetic procedures for dendronized polymers have limited their uses. Relatively easier preparations of CPBs make them more attractive.

CPBs, comprising very long backbones and densely grafted side-chains, adopt worm-like morphologies in good solvents. Owing to their anisotropic nature, special solution and bulk properties have been displayed[12, 13]. So far, grafting-to[14], grafting-through[15] and grafting-from[16, 17] strategies have been explored to prepare CPBs. Generally, well-defined CPBs can be obtained by using grafting-from method, since both the backbones and the side-chains could be grown by well-established living/controlled polymerization techniques.

In the past years, a lot of attention has been paid to polyhedral silsesquioxanes (POSS), which have special cage structures[18]. They are made up of inner silicon/oxygen $(SiO_{1.5})_n$ cages and outside organic substituents. Sized between 1 to 3 nm, they can be viewed as the smallest silica nanoparticles. Unlike the pure inorganic silica materials, the outside organic substituents provide them many possibilities for further functionalizations, organo-cmopatibilities, and even bio-compatibilities. Incorporating POSS into polymers can dramatically improve their thermal and mechanical properties[18-21]. To prepare the composite of POSS with polymers, different methods have been developed. When the shell of POSS is deigned to be reactive, polymers can be connected covalently to them, either by grafting-from[22] or grafting-to[23] procedures. Another convenient way is to prepare monomers carrying POSS units and further polymerizations. Controlled radical polymerizations, such as atomic transfer radical polymerizations (ATRP) have been used successfully to prepare the homo-polymers or block-copolymers of POSS containing methacrylates[24-26].

In our groups' persistent efforts, single-molecular nano-composites with semi-conducting[27, 28] and magnetic nanoparticles[29] non-covalently incorporated in core-shell CPBs have been achieved. Very recently, we have reported the preparation of CPBs with silsesquioxanes as the cores and poly(oligoethyleneglycol methacrylate) (POEGMA) as the water soluble shells, by consecutive ATRP of a siloxane containing monomer and OEGMA and further sol-gel process[30]. They could be derived into silica nanowires by pyrolysis on substrates.

In this work, we employed another strategy to prepare silsequioxane containg single-molecular cylindrical nano-hybrids. By attaching thiol-functionalized POSS to the preformed poly(glydidyl methacrylate) CPBs (termed as BGMA), we successfully obtained nano-cylinders (termed as BGMA-POSS) which contain the cage-like inorganic materials and organic cylindrical matrix. They might be used as building blocks for some nano-devices.

Experimental

Materials

CuCl (97%, Aldrich) was purified by stirring with acetic acid overnight. After filtration, it was washed with ethanol and ether and then dried in vacuum oven. $CuCl_2$ (99%, Acros) was used without purification. *N*,*N*,*N*',*N*'',*N*''',*N*'''-hexamethyltriethylenetetraamine (HMTETA, Aldrich) was distilled before use. 4,4′-Dinonyl-2,2′-dipyridyl (dNbpy) was purchased from Aldrich and used without further purification. Glycidyl methacrylate (GMA) (97%, Aldrich) was purified by passing through basic alumina columns before polymerization. Macro-initiator poly(2-(2-bromoisobutyryloxy)ethyl methacrylate) (PBIEM) (DP_n = 1500, PDI = 1.08) was reported previously[31]. Mercaptopropyl-isobutyl-POSS (POSS-SH) (from Aldrich, molecular weight: 892 Da) was used as it is. All the other solvents and chemicals were used as received.

Preparation of BGMA

The grafting of GMA was carried out in a round-bottom flask sealed with a rubber septum. PBIEM (55.8 mg, 0.2 mmol of initiating α-bromoester groups) and dinonylbipyridyl (dNbpy) (163.5 mg, 0.4 mmol) were dissolved in anisole (28 g) in a pear-shaped flask and stirred overnight to assure the complete dissolution of the high molecular weight polyinitiator. Then the monomer GMA (14.2 g, 0.1 mol) was injected via a syringe and stirred for 15 min. The flask was purged with argon for 15 min. About 0.5 mL of solution was taken out with an argon-purged syringe as an initial sample for conversion measurement by ^{1}H NMR. A round-bottom flask with CuCl (20 mg, 0.2 mmol) and $CuCl_2$ (1.4 mg, 0.01 mmol) was also deoxygenated by argon flow. Then the solution in the pear-shaped flask was transferred into the round-bottom flask by a cannula.

The solution immediately turned brown. The round-bottom flask was then inserted into a water-bath at 25 °C. Small amount of samples were taken out at intervals to check the monomer conversion. After 32 hours, the conversion determined by ^{1}H NMR reached 24.9%. The round-bottom flask was then opened to air. THF was added to dilute the solution and the color of the solution turned green. After passing through a basic alumina column, it was precipitated into cold hexane. Then it was re-dissolved in dioxane. White powders were obtained after freeze-drying.

Preparation of BGMA-POSS

BGMA was dissolved in THF in a bottle and POSS-SH was added (2-fold to the glycidyl groups in BGMA) and followed by vigorous stirring. Then small amount of pyridine was added to the solution. It was subjected to heating at 65 ^{o}C. The reaction was kept for 7 days. Afterwards, it was cooled to room temperature and was purified by ultrafiltration through a membrane with the pore size of 200 nm using THF as the eluent.

Characterizations

^{1}H NMR was measured on a Bruker AC-250 instrument at room temperature using $CDCl_3$ as the solvent.

Conventional GPC using THF as eluent at a flow rate of 1.0 mL/min at room temperature was performed for BGMA brush. Column set: 5 μm p SDV gel, 10^2, 10^3, 10^4, and 10^5 Å, 30 cm each (PSS, Mainz). Detectors used are RI and UV operated at 254 nm. Polystyrene standards (PSS, Mainz) with narrow molecular weight distribution were used for the calibration of the column set.

Fourier transform infrared (FTIR) spectra were recorded at room temperature using a Bruker FTIR EQUINOX 55/S spectrometer at a resolution of 4 cm^{-1}. The samples were prepared by casting sample solutions onto NaCl plates.

Dynamic light scattering (DLS) was carried out on an ALV DLS/SLS-SP 5022F compact goniometer system with an ALV 5000/E correlator and a He-Ne laser (λ = 632.8 nm) at angle of 90^o. Before the light scattering measurements, the sample solutions were filtered 3 times by using Millipore Teflon filters. CONTIN analyses were taken for the

measured intensity correlation functions. Apparent hydrodynamic radii, R_h, of the brushes were calculated according to the Stokes-Einstein equation. All the measurements were carried out at 25°C.

Static light scattering (SLS) was measured on a Sofica goniometer using a He-Ne laser (λ = 632.8 nm). Prior to the light scattering measurements, the sample solutions were filtered 3 times. Five concentrations of the brush solutions were measured at angles in the range from 30 ^{o} to 150 ^{o}. Absolute weight-average molecular weights, M_w, and radii of gyration, R_g, were obtained by the analysis of the Zimm-plots. The refractive index increments of the BGMA in dioxane and BGMA-POSS in THF at 25 °C were measured to be dn/dc = 0.07361 mL/g and 0.08092 mL/g, respectively, using a PSS DnDc-2010/620 differential refractometer.

Atomic force microscopy (AFM) measurement in liquid was carried out on a Digital Instruments Nanoscope Multimode using anisole as the solvent. The measurements were performed at room temperature.

Atomic force microscopy (AFM) measurement of BGMA-POSS on dry state was performed on a Digital Instruments Dimension 3100 microscope operated in tapping mode. The micro-cantilever used for the AFM measurements were from Olympus with resonant frequency between 284.3 kHz and 386.0 kHz, and spring constant ranging from 35.9 to 92.0 N/m. Carbon-coated mica substrates were prepared using a Balzers MED 010 mini-deposition system. Carbon with a thickness of approximately 10 nm was deposited on the freshly cleaved mica surfaces by evaporation. The samples were prepared by dip-coating from very dilute (0.01 g/L) THF solution of BGMA-POSS onto carbon coated mica surface.

Scanning electron microscopy (SEM) and energy dispersive X-ray spectroscopy (EDX) were measured on a Zeiss, LEO 1530 FESEM.

Non-stained transmission microscopy (TEM) measurements were performed on a LEO 922 OMEGA, operated at 200 kV.

Thermal gravimetric analyses (TGA) were performed on Netzsch 409C, in air atmosphere, with the temperature ranging from 25 ^{o}C to 65 ^{o}C and heat rate of 10 ^{o}C/min.

Results and discussions

Synthesis of BGMA

To prepare the hybrid materials BGMA-POSS, precursor CPBs with poly(glycidyl methacrylate) side-chains were first synthesized by grafting from a narrowly distributed macro-initiator PBIEM[31] (DP_n = 1500, PDI = 1.08) using ATRP technique. Scheme 1 depicts the synthetic process of BGMA.

Scheme1. Synthetic procedure of brush BGMA.

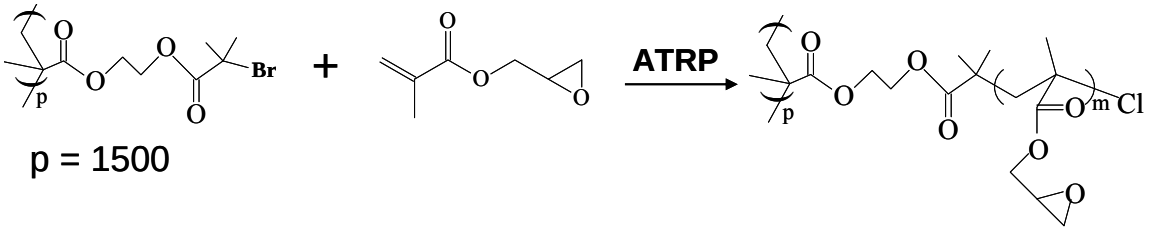

It has been known that the initiating efficiency for the grafting-from by ATRP is low[32, 33]. Some measures were taken to improve it. $CuCl/CuCl_2$ catalysts were used instead of CuBr, to enhance the initiating process and lower the rate of growth, utilizing the halogen exchange phenomenon[34]. In addition, concentration of monomer was kept very low (around 30 wt%). Preliminary polymerizations using HMTETA as the ligand led to insoluble materials, suggesting too fast polymerization rate. So, weaker ligand dNbPy was used to slow down the polymerization. Due to the existence of very reactive epoxy groups in the monomer, the polymerization was carried out at room temperature to avoid possible side-reactions at high temperatures.

Figure 1 shows the ^1H NMR spectra of macro-initiator PBIEM and as-prepared BGMA. Disappearing of the distinctive peaks from the PBIEM (methylene groups linking the ester groups at 4.1 ppm and 4.3 ppm; and methyl groups neighboring bromide groups at 1.9 ppm), and rising of the specific peaks for BGMA (methylene group linking the ester bond and epoxy, at 3.7 ppm and 4.2 ppm; and hydrogens in the epoxy ring, at 2.6 ppm, 2.8 ppm and 3.2 ppm) indicating the success of the grafting reaction.

Conventional GPC measurements were performed for the comparison of PBIEM and BGMA. Although they can not provide the true molecular weights and polydispersities of CPBs, the elution curves can be used to reflect the shift of the molecular weights. Figure 2 displays the GPC elution curves of PBIEM and BGMA. A small shoulder peak for

PBIEM has been reported before, which does not influence the preparation of CPBs, due to the very trivial portion in the whole polymer. It can be clearly seen that the mono-modal peak for BGMA was shifted in the direction of higher molecular weight. There is almost no intersection for the two peaks, which suggests the full grafting to the macro-initiator.

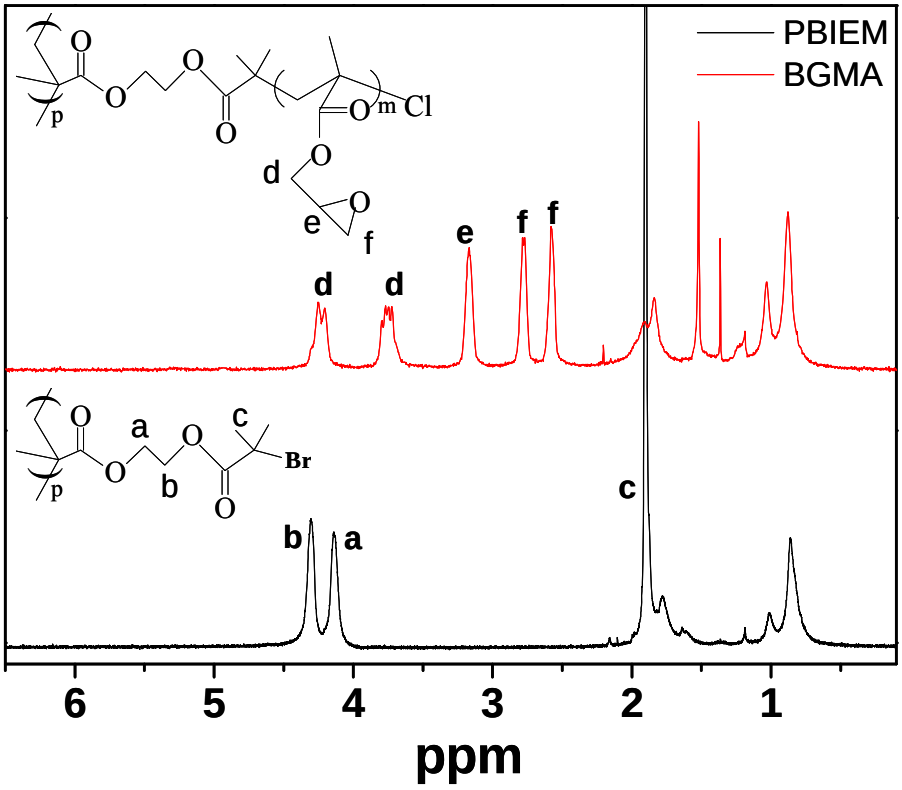

Figure 1. ^{1}H NMR spectra of PBIEM and BGMA in $CDCl_3$.

In order to get the true molecular weight and size of the brush BGMA, the solutions of GMA in dioxane were subjected to SLS and DLS measurements. Table 1 listed the results. The calculated number average molecular weight (M_n) is comparable to the weight average molecular weight (M_w), indicating the successful preparation of the brush. DLS measurement shows that the apparent hydrodynamic radius of BGMA in dioxane is around 57 nm, and the PDI is about 0.24, which is relatively low for brush of such high molecular weight.

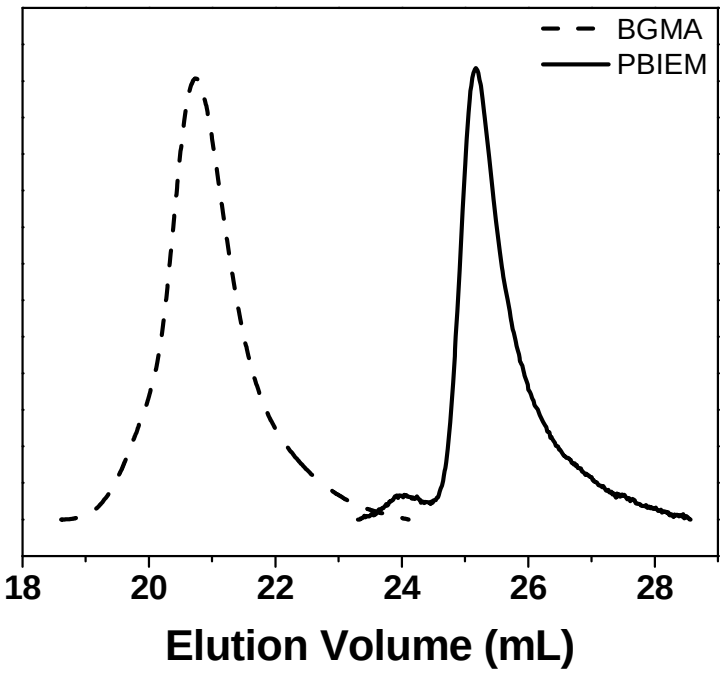

Figure 2. GPC elution curves of PBIEM and BGMA in THF.

Table1. Light scattering measurements of BGMA in dioxane and B-GMA-POSS in THF.

sample	Conver.[a]	$DP_{sc,calc}$[b]	$10^7 * M_{n,calc}$[c]	$10^7 * M_{w,sls}$[d]	R_g[e]	$R_{h,app}$[f] (*PDI*)
BGMA	24.9 %	125	2.70	3.26	104 nm	57 nm (*0.24*)
BGMA-POSS	NA	NA	NA	8.12	112 nm	62 nm (*0.17*)

[a]Monomer conversion determined by ^{1}H NMR. [b]Calculated *DP* of side-chains, $DP_{sc,calc}$= $([M]_0/[I]_0)\times$conversion. [c]Calculated from monomer conversion. $M_{n,calc}$= (Monomer molecular weight$\times DP_{sc,calc}$ + 234.5)$\times DP_{backbone.}$ [d]determined by SLS in dioxane or THF solutions for BGMA and BGMA-POSS, respectively. [e]Radii of gyration measured by SLS. [f]Apparent hydrodynamic radii and polydispersities measured by DLS in dioxane or THF solutions for BGMA and BGMA-POSS, respectively.

True morphologies of the brush BGMA were recorded by AFM measurements in solution. Figure 3a shows the AFM height image of BGMA on mica surface in anisole, a

good solvent for BGMA. Clear worm-like structures can be observed, and the average length of the brushes is about 130nm, which is shorter than the other brushes prepared by the same macro-initiator[35, 36]. Section analysis in figure 3b indicates that the height of the brushes is around 2.5 nm.

The results illustrated above evidenced that well-defined BGMA brush was successfully prepared by grafting the epoxy containing monomer to a long linear macro-initiator.

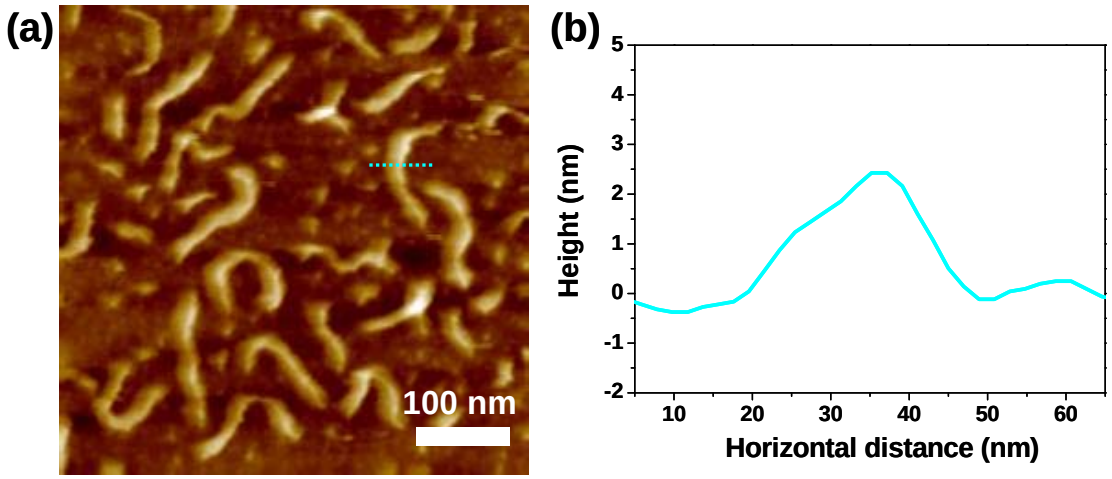

Figure 3. (a) AFM height image of BGMA on mica in anisole, Z rang 7 nm; and (b) section analysis of the cursor shown in (a).

Preparation of the hybrid cylinder BGMA-POSS

It has been reported that the highly active epoxy groups can react with mercaptans in the presence of base[37]. Thus, by attaching a mono-thiol functionalized POSS to the epoxy containing BGMA brushes, hybrid nano-cylinders were obtained. Scheme 2 shows the process for the reaction.

The as-prepared hybrid can be well dispersed in diluted THF solutions. When it was dried, it could not be dissolved again. So it is hard to make ^{1}H NMR measurements for such kind of materials. In stead, FTIR measurements of the solution-casted samples on NaCl plates were performed. Figure 4 shows the FTIR spectra of the POSS-SH, BGMA and hybrid BGMA-POSS. It can be observed that there were almost no absorption around 3500 cm^{-1} for the precursor POSS-SH and BGMA, indicating no hydroxyl groups in them.

However, a strong and broad peak around 3500 cm^{-1} was clearly seen for the hybrid material BGMA-POSS, indicating the abundance of hydroxyl groups in it, as depicted in scheme 2. The spectrum of BGMA-POSS also shows the coexistence of the strong peaks attributing to the ester groups (around 1720 cm^{-1}) from the BGMA precursor and Si-O (around 1100 cm^{-1}), demonstrating the success of the fabrication of the hybrid materials.

Scheme 2. Procedure for the preparation of nano-hybrid BGMA-POSS.

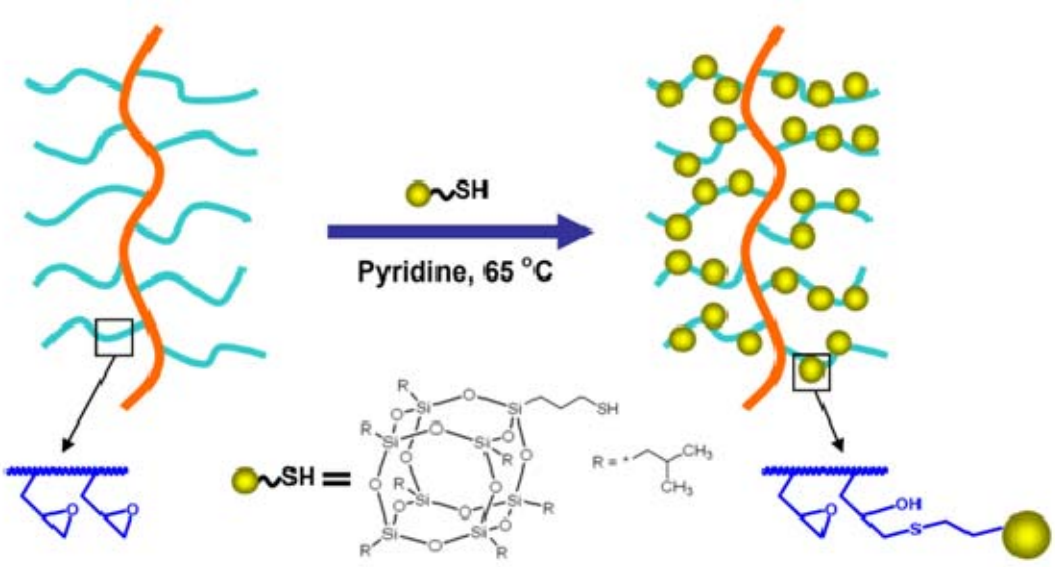

Light scattering measurements were also carried out for the hybrid BGMA-POSS. From the results listed in table 1, we can see the M_w has been significantly increased from 3.26×10^7 to 8.12×10^7 when POSS-SH was attached to BGMA. Apparent rises of R_g and $R_{h,app}$ are also observed. According to the molecular weight values, the grafting efficiency of POSS-SH to BGMA was calculated to be 19.2%, which indicates quite low attaching efficiency, probably due to the high steric hindrance inside the BGMA brush.

To see the morphologies of the hybrid materials, non-stained TEM measurements were performed for both BGMA and BGMA-POSS. From the image of BGMA (see supporting figure S1), no clear objects could be identified, due to the low contrast of the pure polymer brush BGMA. Figure 5 displayed the non-stained TEM image of BGMA-POSS. Clear nano-cylinders can be observed and their lengths are around 150 nm, which is a little higher than that of BGMA brushes on mica surface, likely caused by the stretching effect of the attached POSS-SH. The increase of the contrast in the TEM

measurements provided another proof that the high contrast material POSS-SH nanoparticles have been attached to the brushes.

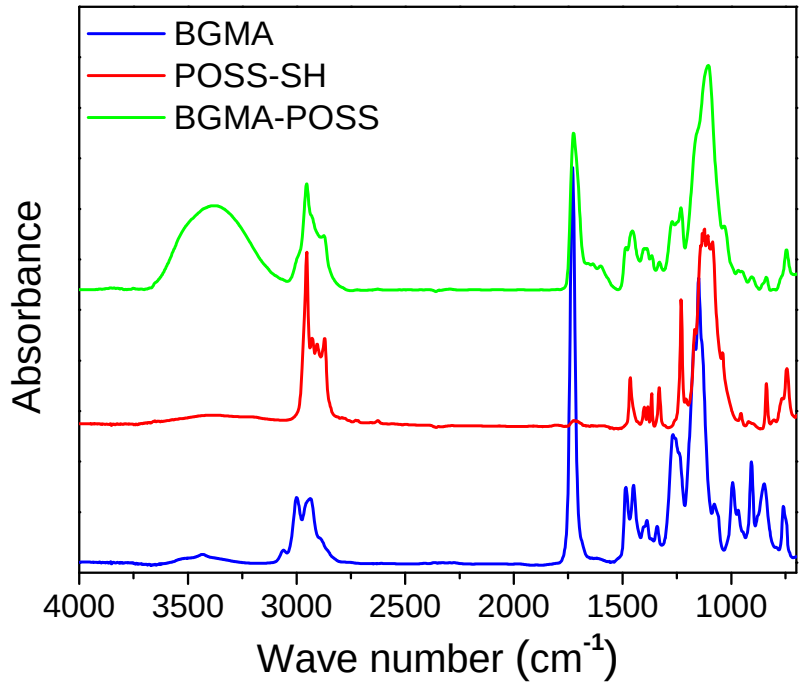

Figure 4. FTIR spectra of POSS-SH, BGMA and BGMA-POSS on NaCl plates.

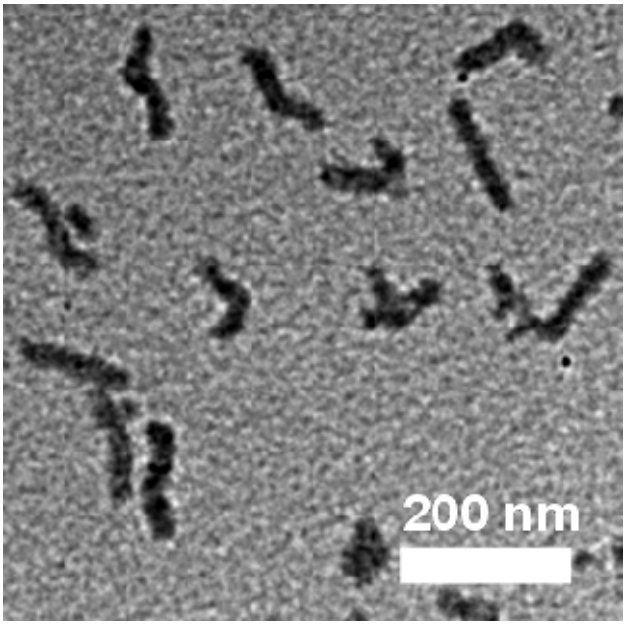

Figure 5. Non-stained TEM image of BGMA-POSS on carbon-coated TEM grid.

The same sample on the carbon-coated grid for the TEM measurement was directly subjected EDX measurement on an aluminum sample holder. In addition to apparent peaks for copper, aluminum and carbon from the TEM grid and sample holder, clear peak for silicon at 1.75 keV is observed in figure 6. This has qualitatively proved the existence of silicon element, thus POSS-SH in the BGMA-POSS hybrid.

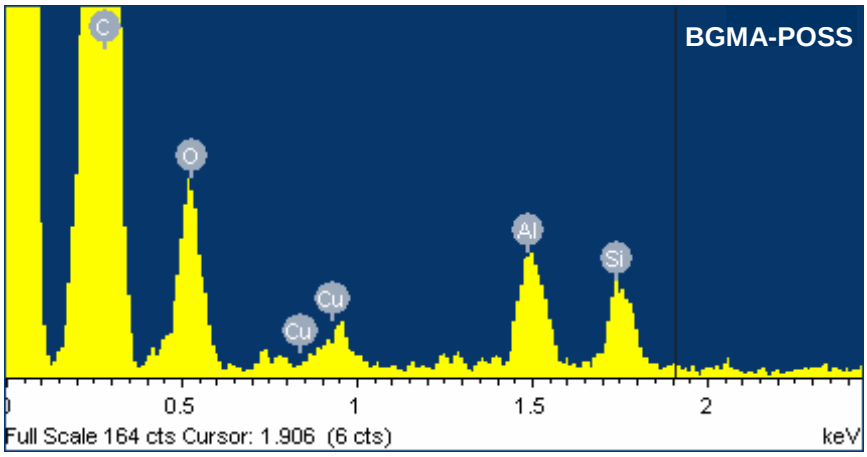

Figure 6. EDX spectrum of BGMA-POSS on the carbon coated TEM grid.

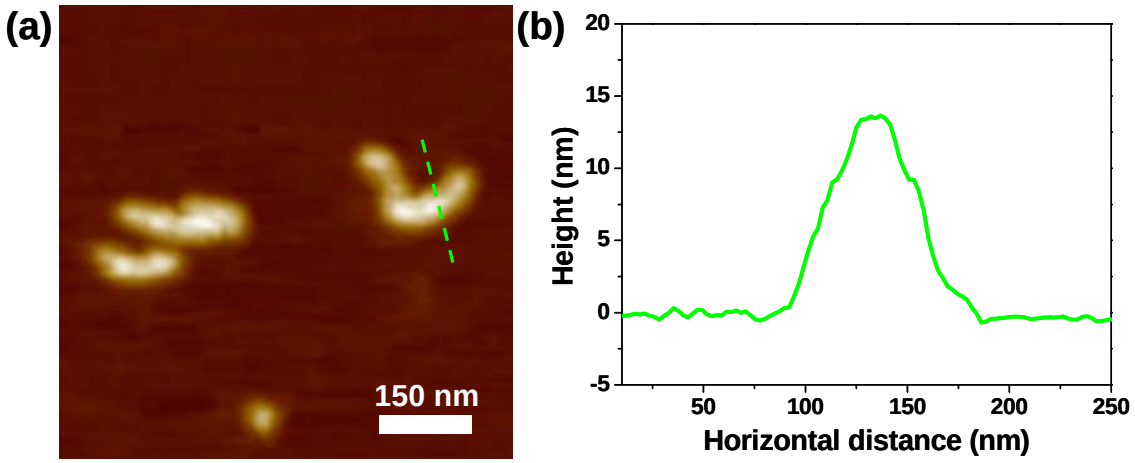

Figure 7. (a) AFM height image of BGMA-POSS on carbon coated mica surface, Z range 30 nm; and (b) section analysis of the cursors present in (a).

AFM measurement of the BGMA-POSS supplied more information of the hybrid. Figure 7 shows the AFM height image of BGMA-POSS on carbon-coated mica surface. It can be seen that some brushes' length has exceeded 150 nm, suggesting the effect of

the attached POSS-SH. Further section analysis discloses that the height of these hybrid cylinders is around 14 nm, which is much higher than that of the pure BGMA in solution.

Pyrolysis and resulted materials

The hybrid material BGMA-POSS was subjected to TGA measurements. Figure 8 displays the TGA results of pure brush BGMA, POSS-SH, and BGMA-POSS in air. It can be found that the degradation temperature for BGMA-POSS hybrid is a little lower than those of the precursor BGMA and POSS-SH, probably a result of the epoxy groups' ring-opening and formation of large number of hydroxyl groups. After the heating process, almost nothing was left for pure brush BGMA, while some residuals are observed for POSS-SH and BGMA-POSS. EDX analysis (see supporting figure S2) of these residuals shows the main components of the residuals are silicon and oxygen, suggesting their nature of SiO_2. According to calculations, if all the silicon element in the POSS-SH was turned into SiO_2, then the theoretical residual percent in the TGA measurement should be 41%. The measured value is only 26%, which is much less than the calculated value. This might be because considerable amount of SiO_2 dust was flushed away by the air flow in the TGA measurement. The same thing could have happened to the hybrid BGMA-POSS. The efficiency of the POSS-SH attaching was only 9.0% according to the calculation from the residuals percent in TGA measurements, which is much lower than that calculated by SLS measurements. A big proportion of formed trivial SiO_2 dust must have been brought away by the flowing air, which caused the discrepancy of the attaching efficiency values.

The residual SiO_2 was collected for the SEM measurement, as shown in figure 9. Loosely distributed layers are observed. More detailed analysis of these materials was done by TEM measurement. As is displayed in figure 10, a lot of white dots were found on the layered structures, indicating the formation of small pores with diameter 3 to 4 nm, due to the degradation of the organic part in the hybrid materials.

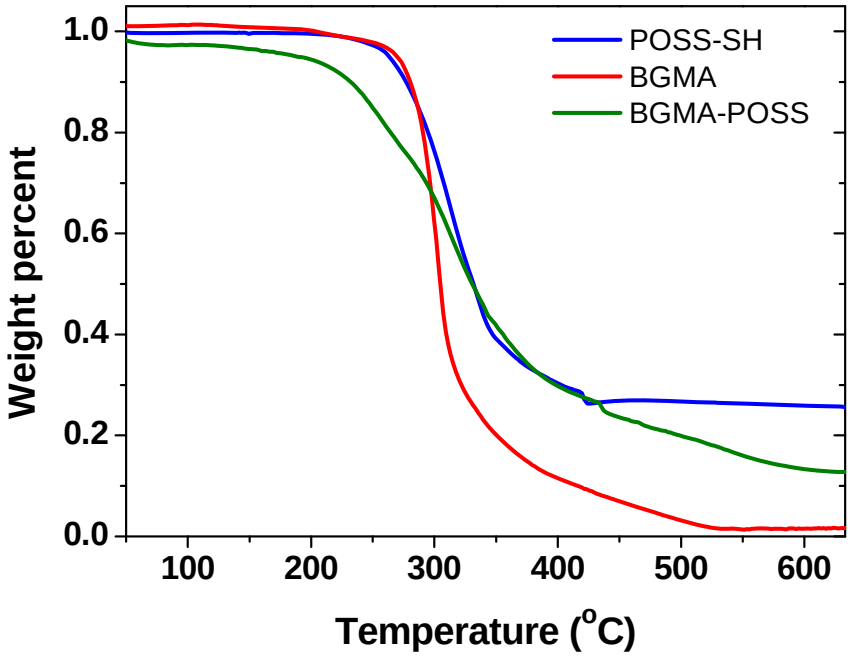

Figure 8. TGA measurements of BGMA, POSS-SH and BGMA-POSS in air.

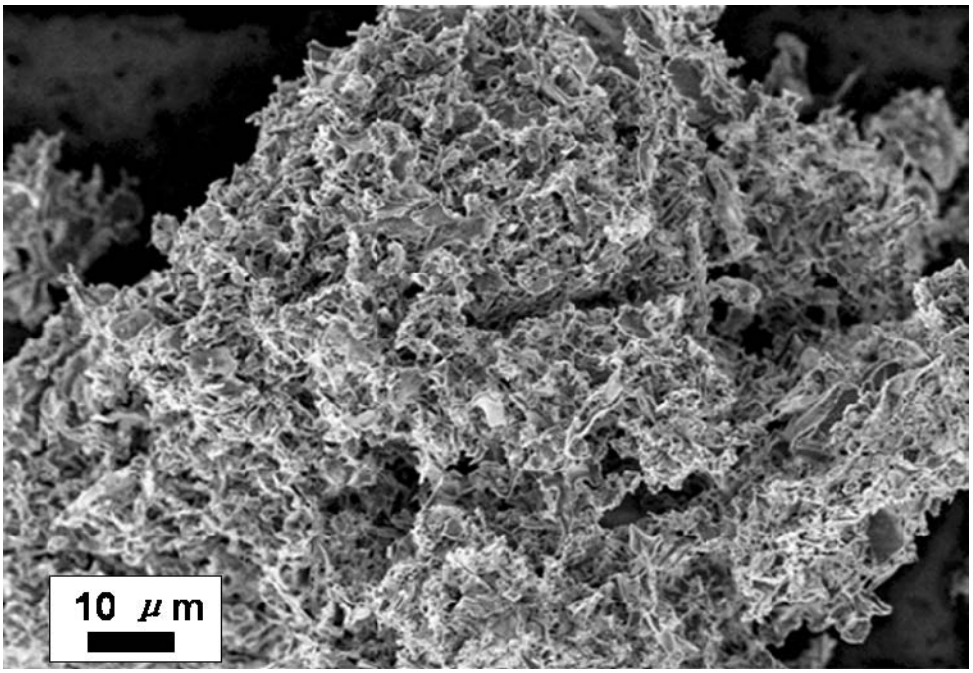

Figure 8. SEM image of the residual SiO_2 collected from TGA measurement of BGMA-POSS in air.

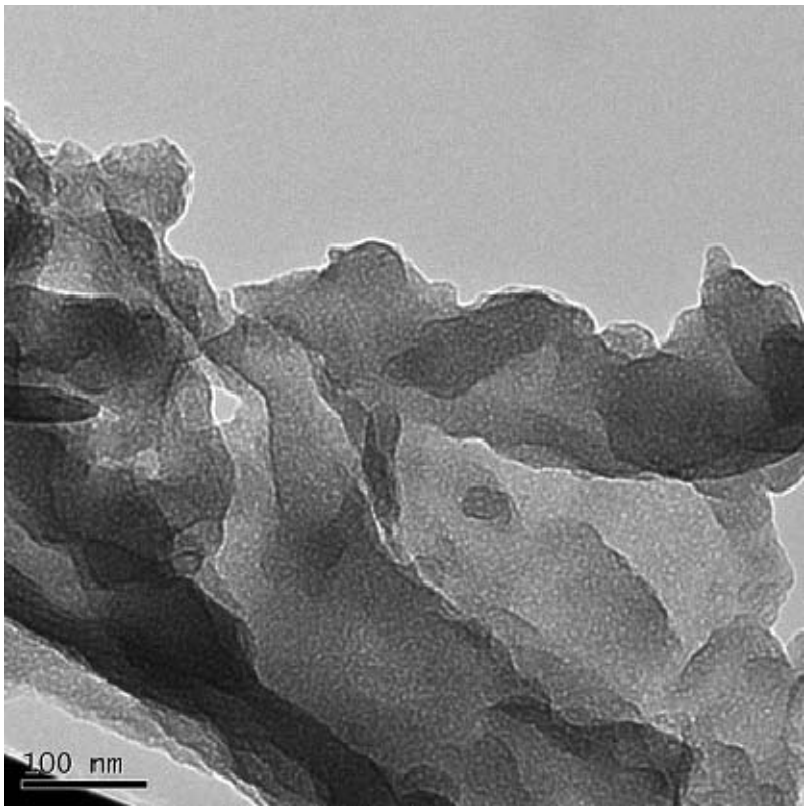

Figure 8. TEM image of the residual SiO_2 collected from TGA measurement of BGMA-POSS in air.

Conclusions

We have demonstrated the successful fabrication of single-molecular nano-hybrid cylinders by attaching the thiol-functionalized POSS to matrix CPBs with poly(glycidyl methacrylate) as the side-chains. Brush BGMA was first prepared by grafting of GMA from a long macro-initiator PBIEM via ATRP. ^{1}H NMR, GPC, DLS, SLS and AFM measurements confirmed the well-defined worm-like structures of BGMA brushes. Then POSS-SH was covalently attached to BGMA brushes by reacting with the epoxy groups. FTIR, DLS, SLS, EDX and TGA measurements evidenced the achievement of the hybrid materials BGMA-POSS. Due to the steric hindrance, only 20% of the epoxy groups reacted with POSS-SH. Slight size increases for the length and diameter were indicated by AFM and non-stained TEM measurements. The residual SiO_2 obtained from the pyrolysis of BGMA-POSS in TGA measurement showed interesting porous structures, which might find its applications in areas such as catalyst carrier or molecular sieves.

Acknowledgements

The authors want to express their gratitude to Mr. Benjamin Gössler for the quick SEM and EDX measurements. Help from Christina Löffler and Sandra Ganzleben (MCI, Universität Bayreuth) with the Measurements of TGA is appreciated. Constructive discussions with Prof. Dr. Weian Zhang are gratefully acknowledged. We thank Deutsche Forschungsgemeinschaft (DFG) for the financial support (within SFB 481).

References

1. Gross, M., *Springer Handbook of Nanotechnology*. Springer-Verlag: Berlin, 2005.
2. Schaefer, D. W.; Justice, R. S. *Macromolecules* **2007,** 40, 8501-8517.
3. Paul, D. R.; Robeson, L. M. *Polymer* **2008,** 49, 3187-3204.
4. Mackay, M. E.; Tuteja, A.; Duxbury, P. M.; Hawker, C. J.; Horn, B. V.; Guan, Z.; Chen, G.; Krishnan, R. S. *Science* **2006,** 311, 1740-1743.
5. Hadjichristidis, N.; Pispas, S.; Pitsikalis, M.; Iatrou, H.; Vlahos, C. *Adv. Polym. Sci.* **1999,** 142, 71-127.
6. Hadjichristidis, N. *J. Polym. Sci. Polym. Chem.* **1999,** 37, 857-871.
7. Vögtle, F.; Gestermann, S.; Hesse, R.; Schwierz, H.; Windisch, B. *Prog. Polym. Sci.* **2000,** 25, 987-1041.
8. Inoue, K. *Prog. Polym. Sci.* **2000,** 25, (4), 453-571.
9. Schlüter, A. D.; Rabe, J. P. *Angew. Chem. Int. Ed.* **2000,** 39, 864-883.
10. Zhang, M.; Müller, A. H. E. *J. Polym. Sci. Polym. Chem.* **2005,** 43, 3461-3481.
11. Sheiko, S. S.; Sumerlin, B. S.; Matyjaszewski, K. *Prog. Polym. Sci.* **2008,** 33, 759-785.
12. Wintermantel, M.; Fischer, K.; Gerle, M.; Ries, R.; Schmidt, M.; Kajiwara, K.; Urakawa, H.; Wataoka, I. *Angew. Chem. Int. Ed.* **1995,** 34, 1472-1474.
13. Bolisetty, S.; Airaud, C.; Xu, Y.; Müller, A. H. E.; Harnau, L.; Rosenfeldt, S.; Lindner, P.; Ballauff, M. *Phys. Rev. E* **2007,** 75, 040803/1-040803/4.
14. Gao, H.; Matyjaszewski, K. *J. Am. Chem. Soc.* **2007,** 129, 6633-6639.
15. Dziezok, P.; Sheiko, S. S.; Fischer, K.; Schmidt, M.; Möller, M. *Angew. Chem. Int. Ed.* **1997,** 36, 2812-2815.
16. Beers, K. L.; Gaynor, S. G.; Matyjaszewski, K.; Sheiko, S. S.; Möller, M. *Macromolecules* **1998,** 31, 9413-9415.
17. Börner, H. G.; Beers, K.; Matyjaszewski, K.; Sheiko, S. S.; Möller, M. *Macromolecules* **2001,** 34, 4375-4383.
18. Li, G.; Wang, L.; Ni, H.; Pittman, C. U., Jr. *J. Inorg. Organomet. Polym.* **2002,** 11, 123-154.
19. Kannan, R. Y.; Salacinski, H. J.; Butler, P. E.; Seifalian, A. M. *Acc. Chem. Res.* **2005,** 38, 879-884.

20. Pielichowski, K.; Njuguna, J.; Janowski, B.; Pielichowski, J. *Adv. Polym. Sci.* **2006,** 201, 225-296.

21. Phillips, S. H.; Haddad, T. S.; Tomczak, S. J. *Curr. Opin. Solid State Mater. Sci.* **2004,** 8, 21-29.

22. Ohno, K.; Sugiyama, S.; Koh, K.; Tsujii, Y.; Fukuda, T.; Yamahiro, M.; Oikawa, H.; Yamamoto, Y.; Ootake, N.; Watanabe, K. *Macromolecules* **2004,** 37, (23), 8517-8522.

23. Pyun, J.; Matyjaszewski, K. *Chem. Mater.* **2001,** 13, 3436-3448.

24. Pyun, J.; Matyjaszewski, K. *Macromolecules* **2000,** 33, 217-220.

25. Pyun, J.; Matyjaszewski, K.; Kowalewski, T.; Savin, D.; Patterson, G.; Kickelbick, G.; Huesing, N. *J. Am. Chem. Soc.* **2001,** 123, 9445-9446.

26. Pyun, J.; Matyjaszewski, K.; Wu, J.; Kim, G.-M.; Chun, S. B.; Mather, P. T. *Polymer* **2003,** 44, 2739-2750.

27. Zhang, M.; Drechsler, M.; Müller, A. H. E. *Chem. Mater.* **2004,** 16, 537-543.

28. Yuan, J.; Drechsler, M.; Xu, Y.; Zhang, M.; Müller, A. H. E. *Polymer* **2008,** 49, 1547-1554.

29. Zhang, M.; Estournes, C.; Bietsch, W.; Müller, A. H. E. *Adv. Funct. Mater.* **2004,** 14, 871-882.

30. Yuan, J.; Xu, Y.; Walther, A.; Bolisetty, S.; Schumacher, M.; Schmalz, H.; Ballauff, M.; Müller, A. H. E. *Nat. Mater.* **2008,** 7, 718-722.

31. Zhang, M.; Breiner, T.; Mori, H.; Müller, A. H. E. *Polymer* **2003,** 44, 1449-1458.

32. Neugebauer, D.; Sumerlin, B. S.; Matyjaszewski, K.; Goodhart, B.; Sheiko, S. S. *Polymer* **2004,** 45, 8173-8179.

33. Sumerlin, B. S.; Neugebauer, D.; Matyjaszewski, K. *Macromolecules* **2005,** 38, 702-708.

34. Matyjaszewski, K.; Shipp, D. A.; Wang, J.-L.; Grimaud, T.; Patten, T. E. *Macromolecules* **1998,** 31, 6836-6840.

35. Xu, Y.; Becker, H.; Yuan, J.; Burkhardt, M.; Zhang, Y.; Walther, A.; Bolisetty, S.; Ballauff, M.; Müller, A. H. E. *Macromol. Chem. Phys.* **2007,** 208, 1666-1675.

36. Xu, Y.; Bolisetty, S.; Drechsler, M.; Fang, B.; Yuan, J.; Ballauff, M.; Müller, A. H. E. *Polymer* **2008,** 49, 3957-3964.

37. Carioscia, J. A.; Stansbury, J. W.; Bowman, C. N. *Polymer* **2007,** 48, 1526-1532.

Supporting information:

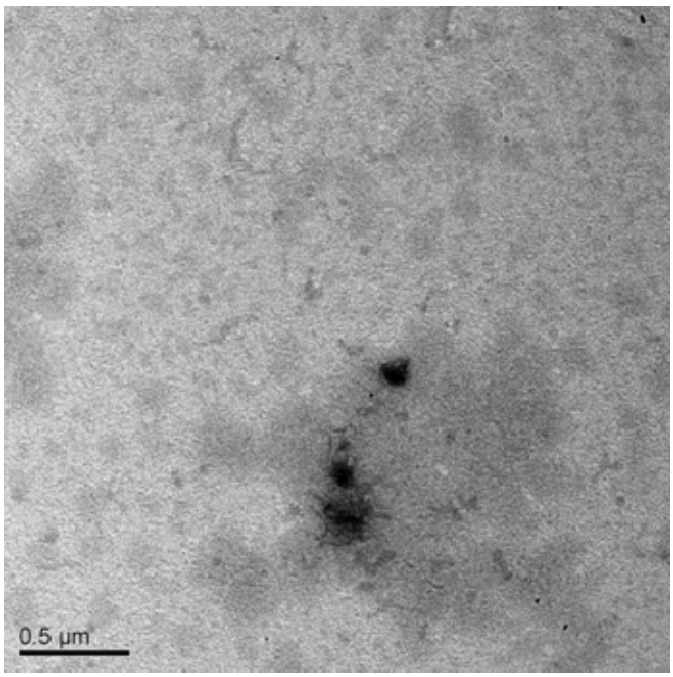

Figure S1. Non-stained TEM of BGMA.

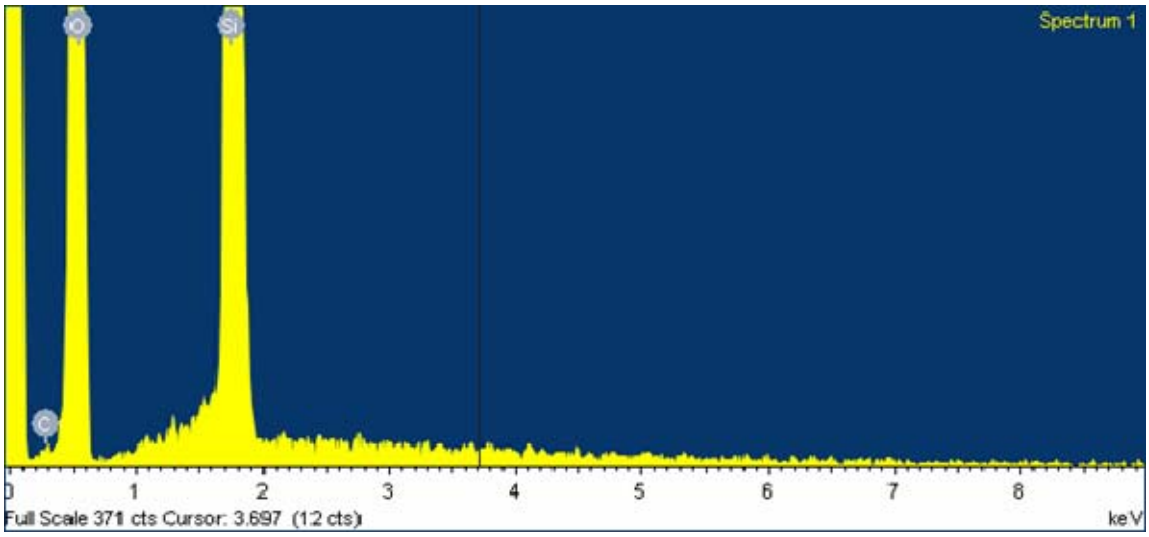

Figure S2. EDX spectrum of the residual from the TGA measurement of BGMA-POSS in air.

11. List of publications

- Youyong Xu, Sreenath Bolisetty, Matthias Ballauff, Axel H. E. Müller, Switching the Morphologies of Cylindrical Polycation Brushes by Ionic and Supramolecular Inclusion Complexes, ***Journal of the American Chemical Society***, 2008, Submitted.
- Youyong Xu, Sreenath Bolisetty, Markus Drechsler, Bing Fang, Jiayin Yuan, Ludger Harnau, Matthias Ballauff, Axel H. E. Müller, Manipulating Cylindrical Polyelectrolyte Brushes on the Nanoscale by Counterions: Collapse Transition into Helical Structrures, ***Soft Matter***, 2008, accepted.
- Youyong Xu, Sreenath Bolisetty, Markus Drechsler, Bing Fang, Jiayin Yuan, Matthias Ballauff, and Axel H. E. Müller, pH and Salt Responsive Poly(N,N-dimethylaminoethyl methacrylate) Cylindrical Brushes and their Quaternized Derivatives, ***Polymer***, 2008, 49, 3957-3964.
- Jiayin Yuan, Youyong Xu, Andreas Walther, Sreenath Bolisetty, Manuela Schumacher, Holger Schmalz, Matthias Ballauff, and Axel H. E. Müller, Water-Soluble Organo-Silica Hybrid Nanowires, ***Nature Materials***, 2008, 7, 718-722.
- Alexei Polotsky, Marat Charlaganov, Youyong Xu, Frans A. M. Leermakers, Mohamed Daoud, Axel H. E. Müller, Tomonori Dotera, and Oleg Borisov, Pearl-necklace structures in core-shell molecular brushes: Experiments, Monte-Carlo Simulations, and Self-consistent Field Modeling, ***Macromolecules***, 2008, 41, 4020-4028.
- Jiayin Yuan, Youyong Xu, Manuela Schumacher, Holger Schmalz, Axel H. E. Müller, Core-shell Cylindrical Polymer Brushes with Silica Nanowire Core, ***Polymer Preprint*** *(Am. Chem. Soc., Div. Polym. Chem.)*, 2008, 49(1), 21-22.
- Youyong Xu, Markus Drechsler, Jiayin Yuan, Axel H. E. Müller, Hybrids of Magnetic Nanoparticles with Double-hydrophilic Core-shell Cylindrical Polymer Brushes, ***Polymer Preprint*** *(Am. Chem. Soc., Div. Polym. Chem.)*, 2008, 49(1), 338-339.
- Jiayin Yuan, Markus Drechsler, Youyong Xu, Mingfu Zhang, and Axel H. E. Müller, Cadmium Selenide Nanowires within Core-shell Cylindrical Polymer Brushes: Synthesis, Characterization and the Double-loading Process, ***Polymer***, 2008, 49,

1547-1554.

- Jiayin Yuan, Holger Schmalz, Youyong Xu, Nobuyoshi Miyajima, Markus Drechsler, Michael W. Möller, Felix Schacher, Axel H. E. Müller, Room-temperature Growth of Uniform Tellurium Nanorods and the Assembly of Tellurium or Fe_3O_4 Nanoparticles on the Nanorods, ***Advanced Materials***, 2008, 20, 947-952.
- Youyong Xu, Harald Becker, Jiayin Yuan, Markus Burkhardt, Yong Zhang, Andreas Walther, Sreenath Bolisetty, Matthias Ballauff, Axel H. E. Müller, Double-grafted Cylindrical Brushes: Synthesis and Characterization of Poly(lauryl methacrylate) Brushes, ***Macromolecular Chemistry and Physics,*** 2007, 208, 1666-1675.
- Chao Gao, Sharmila Muthukrishnan, Wenwen Li, Jiayin Yuan, Youyong Xu, Axel H. E. Müller, Linear and Hyperbranched Glycopolymer-Functionalized Carbon Nanotubes: Synthesis, Kinetics, and Characterization, ***Macromolecules***, 2007, 40, 1803-1815.
- Sreenath Bolisetty, Cedric Airaud, Youyong Xu, Axel H. E. Müller, L. Harnau, Sabine Rosenfeldt, P. Lindler, Matthias Ballauff, Softening of the Stiffness of Bottle-brush Polymers by Mutual Interaction, ***Physical Review E***, 2007, 75, 040803 (R).
- Lu Zhu, Youyong Xu, Weizhong Yuan, Jingyu Xi, Xiaobin Huang, Xiaozheng Tan, Sixun Zheng, One-pot Synthesis of Poly(cyclotriphosphazene-co-4,4′-sulfonyldiphenol) Nanotubes via an in situ Template Approach, ***Advanced Materials***, 2006, 18, 2997-3000.
- Youyong Xu, Chao Gao, Hao Kong, Deyue Yan, Yi Zheng Jin, Paul C. P. Watts, Growing Multihydroxyl Hyperbranched Polymers on the Surfaces of Carbon Nanotubes by in situ Ring-opening Polymerization, ***Macromolecules***, 2004, 37, 8846-8853.
- Youyong Xu, Chao Gao, Hao Kong, Deyue Yan, Ping Luo, Wenwen Li, Yiyong Mai, One-pot Synthesis of Amphiphilic Core-shell Suprabranched Macromolecules, ***Macromolecules***, 2004, 37, 6264-6267.

Acknowledgements

First of all, I would like to thank Prof. Dr. Axel H. E. Müller for giving me the opportunity to study and to do research in such a nice team MC II. He provided me very interesting topics and easy-going working atmosphere here. Although in most of time, he is quite busy for all kinds of things, I benefited a lot from his supervision, constructive discussions and kindness. More importantly, I appreciate the freedom of research he gave, by which I got chances to try different scientific ideas. Some just did not work, and some are exciting! Such experience will definitely encourage me to perform better in the future work. I am really proud of having a "Doktorvater" like him.

I also want to thank Prof. Dr. Matthias Ballauff for many fruitful discussions and suggestions. I was impressed by his knowledge and efficiency. Owing to our joint project, I got chances to know that he is actually a nice person. Without his help, it will be very difficult for me to deal with some physical and theoretical things.

I am grateful to Dr. Reinhard Richter and Robert Krauß for their broadening my knowledge of magnetic materials and interesting ferrofluids. Although we had a tough time in the collaboration project, the outcome is not that bad. Some short, but useful discussions with Prof. Dr. Alexander Böker are appreciated.

Many thanks go to Sreenath Bolisetty for his help in many measurements and discussions. Such close collaborations contributed to my sense of teamwork and cooperation.

I would also like to use this opportunity to express my gratitude to many colleagues in MCII for their helps in not only chemistry but also many other things. Thanks to Dr. Mingfu Zhang for his excellent previous works and introducing me the ATRP and AFM techniques. Special thanks go to Andreas Walther for his useful suggestions and cryo-TEM measurements. Without his translation of the "zusammenfassung", I cannot finish this thesis so smoothly. Felix Schacher's help for correcting part of the thesis is greatly appreciated. I am indebted to Dr. Xavier André and Sabine Wunder for introducing the GPC instruments to me. I will always be grateful to many people: Jiayin Yuan, Bing Fang, Dr. Markus Drechsler, Dr. Markus Burkhardt, Dr. Yong Zhang, Sandrine Tea, Manuela Schumacher, Evis Penott-Chang, Benjamin Gössler, Astrid Göpfert, for their time and patience in measuring many of my samples. Specially, I would like to thank

Annette Krökel for her help in many things in the lab. I would like to extend my thanks to many other people: Harald Becker, Dr. Holger Schmalz, Alexander Schamlz, Pierre Millard, Sergey Nosov, Anja Goldmann, Markus Ruppel, Dr. Felix Plamper, Dr. Marina Krekhova, Dr. Olivier Colombani, Dr. Alexandre Terrenoire, Dr. Weian Zhang, Dr. Chao Gao, Dr. Petar Petrov, Dr. Dmitry V. Pergushov, Dr. Sharmila Muthukrishnan, Dr. Girish Behera, Dr. Saikat Mandal, Dr. Michael Witt, Andreas Hanisch, and André Gröschel, for a lot of scientific discussions and suggestions. I also appreciate the nice working atmosphere from the other group members: Güther Jutz, wolf Andrea, Stephan Weiß, Stefan Reinicke, Joachim Schmelz, Alexandra Sperschneider, André Pfaff, Markus Müllner, Hans-Joachim Voigtländer, Marli Tebaldi de Sordi, Dr. Andrew Ah Toy, Susanne Edinger, Kerstin Matussek, Cornelia Rettig, Melanie Förtsch, Annika Ochs, Denise Danz, Karina Möller, and Jeannine Rockser.

During my study, I received many helps from other groups. I thank Markus Hund and Dr. Kristin Schmidt of PCII for their support in the AFM measurements. I appreciate the kind help and discussions from Dr. Yu Mei, Dr. Sabine Rosenfeldt, Dr. Yan Lu, and Dr. Alexander Wittemann of PCI. I want to express my thanks to Dr. Christian Neuber, Dr. Klaus Kreger, Christina Löffler, and Sandra Ganzleben of MCI for their help. Special thank goes to Bejamin Balke of Mainz University, who measured the SQUID for me.

I must say a lot of thank you to Gaby Oliver for her great help in many many things. Without her help and kindness, I would have run in too many troubles in the sea of bureaucracies.

For sure, without the financial support from Deutsche Forschungsgemeinschaft, nothing could have been done in my research works.

Specially, I want to express my gratitude to some of my Chinese colleagues: Dr. Chih-Cheng Peng, Jiayin Yuan, Bing Fang, Dr. Weian Zhang, Dr. Li-Tang Yan, and Xinjun Zhang. With them around, life is much easier and enjoyable.

Finally, my special thanks go to my parents and Jiazhen, for their continuous support and love during all these years. I appreciate everything you have done for me. Without your encouragements, it would be very difficult for me to finish this thesis smoothly.

Erklärung

Die vorliegende Arbeit wurde von mir selbstständig verfasst und ich habe keine anderen als die angegebenen Hilfsmittel benutzt.

Ferner habe ich nicht versucht, anderweitig mit oder ohne Erfolg eine Dissertation einzureichen oder mich der Doktorprüfung zu unterziehen.

Bayreuth, 06.10.2008

(Youyong Xu)